TA7
W34
No. M-73-4
Cop 2

US-CE-C Property of the United States Government

TECHNICAL REPORT M-73-4

A MATHEMATICAL MODEL FOR PREDICTING MICROSEISMIC SIGNALS IN TERRAIN MATERIALS

by

J. R. Lundien, H. Nikodem

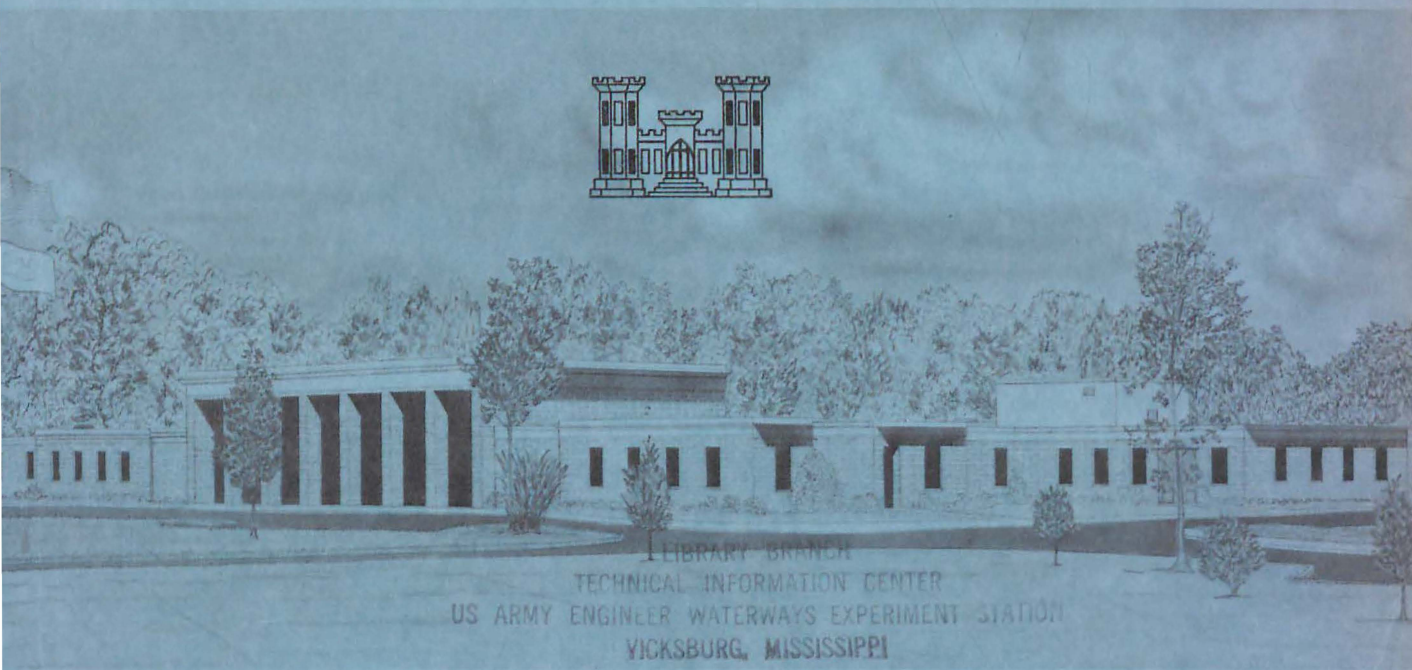

LIBRARY BRANCH
TECHNICAL INFORMATION CENTER
US ARMY ENGINEER WATERWAYS EXPERIMENT STATION
VICKSBURG, MISSISSIPPI

June 1973

Sponsored by Defense Special Projects Group and U. S. Army Materiel Command

Conducted by U. S. Army Engineer Waterways Experiment Station
Mobility and Environmental Systems Laboratory
Vicksburg, Mississippi

APPROVED FOR PUBLIC RELEASE; DISTRIBUTION UNLIMITED

Destroy this report when no longer needed. Do not return it to the originator.

The findings in this report are not to be construed as an official Department of the Army position unless so designated by other authorized documents.

This program is furnished by the Government and is accepted and used by the recipient with the express understanding that the United States Government makes no warranties, expressed or implied, concerning the accuracy, completeness, reliability, usability, or suitability for any particular purpose of the information and data contained in this program or furnished in connection therewith, and the United States shall be under no liability whatsoever to any person by reason of any use made thereof. The program belongs to the Government. Therefore, the recipient further agrees not to assert any proprietary rights therein or to represent this program to anyone as other than a Government program.

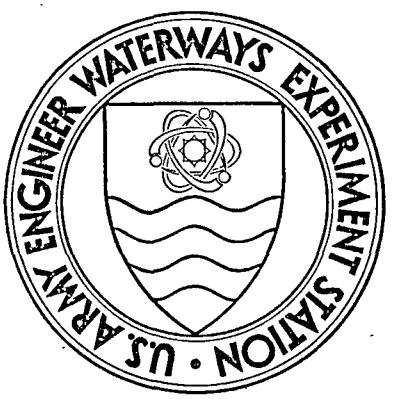

TECHNICAL REPORT M-73-4

A MATHEMATICAL MODEL FOR PREDICTING MICROSEISMIC SIGNALS IN TERRAIN MATERIALS

by

J. R. Lundien, H. Nikodem

June 1973

Sponsored by Defense Special Projects Group, Task TM 700A-71-030, and
U. S. Army Materiel Command, Project 1T162112A131

Conducted by U. S. Army Engineer Waterways Experiment Station
Mobility and Environmental Systems Laboratory
Vicksburg, Mississippi

ARMY-MRC VICKSBURG MISS

APPROVED FOR PUBLIC RELEASE; DISTRIBUTION UNLIMITED

TA7
W34
no. 91-12-4
Engr.

THE CONTENTS OF THIS REPORT ARE NOT TO BE USED FOR ADVERTISING, PUBLICATION, OR PROMOTIONAL PURPOSES. CITATION OF TRADE NAMES DOES NOT CONSTITUTE AN OFFICIAL ENDORSEMENT OR APPROVAL OF THE USE OF SUCH COMMERCIAL PRODUCTS.

75128

FOREWORD

The study reported herein was conducted at the U. S. Army Engineer Waterways Experiment Station (WES) during 1971-1972. It was sponsored by the Defense Special Projects Group (DSPG) under DSPG Task TM 700A-71-030, "Seismic Detection Study," and by the Directorate of Research, Development and Engineering, U. S. Army Materiel Command, under Department of the Army Project No. 1T162112A131, "Environmental Constraints on Materiel."

The study was under the general supervision of Messrs. W. G. Shockley, Chief of the Mobility and Environmental Systems Laboratory (MESL), and W. E. Grabau, Chief of the Environmental Systems Division (ESD), MESL. Mr. B. O. Benn, Chief of the Environmental Research Branch (ERB), ESD, directed the study with the assistance of Mr. J. R. Lundien and Dr. H. Nikodem of ERB. The computer programs were prepared by Mr. E. A. Baylot, ERB, and Dr. G. Y. Baladi, Research Group, Soil Dynamics Division, Soils and Pavements Laboratory (SPL). The information for the macrogeometry coefficients was compiled by Mr. F. K. Chang, Research Group, Earthquake Engineering and Vibrations Division, SPL. This report was prepared by Mr. Lundien and Dr. Nikodem.

The Director of WES during this investigation was COL Ernest D. Peixotto, CE. Mr. F. R. Brown was Technical Director.

CONTENTS

	Page
FOREWORD	v
NOTATION	ix
SUMMARY	xiii
PART I: INTRODUCTION	1
Background	1
Approach	3
Purpose and Scope	5
PART II: DEVELOPMENT OF THE MATHEMATICAL MODEL	6
Wave Interactions	6
Derivation of Equations	10
PART III: SIGNAL PREDICTIONS	35
Computation of Site Coefficients	36
Signal Transformation	45
PART IV: EXAMPLE OUTPUTS OF THE MODEL	48
Coefficients for WES Study Site 319	48
Signal Predictions for WES Study Site 319	52
Measured and Predicted Signals for WES Study Site 341	67
PART V: CONCLUSIONS AND RECOMMENDATIONS	77
LITERATURE CITED	79
TABLE 1	
APPENDIX A: EFFECTS OF SURFACE MACROGEOMETRY ON PROPAGATION OF RAYLEIGH WAVES	A1
Literature Survey	A1
Some Results from the Literature.	A5
APPENDIX B: COMPUTER PROGRAM TO PREDICT MICROSEISMIC SIGNALS IN TERRAIN MATERIALS	B1
Function and Methods	B1
Input	B1
Output	B1
Program Listings	B2
Flow Charts	B2

CONTENTS

Page

TABLES B1-B4

APPENDIX C: RAYLEIGH WAVE DISPERSION CURVE PROGRAM C1

Function and Method C1
Input C2
Output C2
Program Listing C2
Flow Charts C2

TABLES C1-C4

NOTATION

$a_{m_{ab}}$	Element of A_m
$a^{-1}_{m_{ab}}$	Element of A_m^{-1}
a_i	i^{th} layer variable
A	Arbitrary solution variable
A_i	4×4 matrix of coefficients of equations 14a-14d
A_i^{-1}	Inverse matrix of A_i
$A(r,z)$	General solution variable
$\vec{b}$	Vector for describing stresses at the surface
C	Specialized matrix
$d_{m_{ab}}$	Element of D_m
d_i	Thickness of the ith layer
D_i	4×4 matrix to relate solutions on the top of a particular layer to the bottom of a particular layer
$\mathrm{Det}(A_i)$	Determinant of A_i
E	4×4 unit matrix
f	Frequency
f_{ab}	Element of F (1 number)
$f(\kappa)$	Arbitrary function of κ
F	4×4 matrix relates displacement solution of top layer to stresses in top layer
G	4×4 matrix relates solution at 1st layer to n^{th} layer
H_i	Depth of bottom of ith layer
$H_\ell^1(\kappa r)$	Hankel function, 1st kind
$H_\ell^2(\kappa r)$	Hankel function, 2d kind

i	$\sqrt{-1}$
$I(r)$	Arbitrary function of r
J_m	Bessel function
ℓ	Order of Bessel function
L	Source force amplitude frequency component
m	Arbitrary integer
n	Number of layers
N	Bessel function
p_{zr}	Vertical radial component of stress tensor
p_{zz}	Vertical vertical component of stress tensor
P	A point within a body; also particle motion coefficient
q_i	Radial component of displacement
$Q(\kappa)$	Amplitude coefficient, radial component
$Q_i''(\kappa), Q_i'(\kappa)$ $S_i''(\kappa), S_i'(\kappa)$	general solutions of equation 6; same as A values for layer number i
r	Range or radius
$\vec{S}$	Displacement vector
t	Time
T_i	4×4 matrix
u,v,w	Components of particle displacement
V_R	Velocity of propagation for a Rayleigh wave
w_i	Vertical component of displacement
$W(\kappa)$	Amplitude coefficient, vertical component
x,y,z	Cartesian coordinates, distance
X,Y,Z	Cartesian components of body forces
$\vec{X}_i$	Solution vector (1 by 4)
$\vec{y}$	Solution at the surface (i.e. X_1 for $z = 0$)
y_s	s^{th} component of the vector y
z	Depth from surface amplitude of incident Rayleigh wave
α	Velocity of propagation of an irrotational disturbance (P-wave velocity)
β	Velocity of propagation of an equivoluminal disturbance (S-wave velocity)
δ	Arbitrary variable; logarithmic decrement

Δ	Determinant of F
$\Delta_{\ell s}$	ℓ - s subdeterminant of Δ
η	Arbitrary variables
Θ	Cubical dilatation
κ	Wave number of propagating wave
κ_R	Wave number for a Rayleigh wave
κ_α	Wave number for P-wave
κ_β	Wave number for S-wave
λ, μ	Lamé's constants
ν_i, ν_i'	z-component of wave number for layer number i
ξ	Damping factor
ρ	Mass density
σ	Poisson's ratio
τ	Arbitrary variable
ϕ	Scalar potential
$\vec{\emptyset}$	Zero vector
χ	Angle
$\vec{\psi}$	Vector potential
ω	Circular frequency = $2\pi f$
$\vec{\Omega}$	Rotation
$\vec{\nabla}$	Nabla or del operator

SUMMARY

The mathematical model presented herein allows the user to make predictions for the wave amplitude and frequency content of microseismic signals that would interact with a seismic intrusion detection device at the surface of the ground. These signals are propagated as a result of a force applied to the surface of a medium (stress) which in turn causes a corresponding motion to travel away from the source. Efforts were made to keep the operation of the model as general as possible such that little restriction is placed on either the source of the seismic signal or the ground media through which the signal propagates. As a result, the source signal is needed in the form of a time domain stress signal at the points of contact on the ground. The ground media can have any seismic profile that can be approximated by a layered viscoelastic structure.

Examples are given of two sites to illustrate the variation in predicted signals due to multiple mode Rayleigh wave propagation, varying damping factors, varying ranges from the source, and input stress signal shapes.

A MATHEMATICAL MODEL FOR PREDICTING MICROSEISMIC SIGNALS IN TERRAIN MATERIALS

PART I: INTRODUCTION

Background

1. The successful use of seismic intrusion detectors in Vietnam has emphasized their potential value in battlefields throughout the world. Unfortunately, this experience has also highlighted some dramatic shortcomings in the present family of seismic sensors. Perhaps the most serious limitations involve their inability to discriminate among target classes, i.e. wheeled vehicles, tracked vehicles, personnel, fixed-wing aircraft, etc. The present sensors indicate only activations of the sensor; therefore, an operator must interpret the class of target from the number and frequency of the activations.

2. The difficulty in designing a sensor logic capable of discriminating among targets lies in the problem of identifying signal features that are consistently associated with a particular target. If correlations between signal features and specific targets can be made, then criteria for sensor logic design can be stated. The present approach to sensor design can be summarized in the following steps.

a. Assemble a data base of signals from all classes of targets. Ideally the data base should be statistically representative, i.e. it should contain a statistically valid sample of all target and environmental conditions in which the sensor is intended to operate.

b. Measure the properties of selected features that are hypothesized to be uniquely associated with a specific target class. Examples of these features include: (1) ratio of high- to low-frequency energy, (2) time between occurrences of a specified amplitude, (3) number of zero crossings, and (4) others.

c. Select the features that can be correlated with the target class.

d. Design and build circuits to extract the features from the analog signals.

3. Because the correlations are sought from a specific data base, the results are limited in applicability. This limitation is in direct proportion to the extent to which the signal population in the data base represents the totality of possible signals. It is well known that the frequency and amplitude characteristics of a seismic signal are functions of the source and its interaction with the road or ground surface (including the travel rate of the source energy) and the seismic propagation conditions between the source and sensor. The question then arises: In a seismic signal, is it possible to identify a feature (or features) that is relatively unaffected by variables introduced by the source-ground interactions and the propagating medium?

4. The design of experiments to provide data that allow isolation of discriminate features (that is, signal characteristics that are uniquely associated with a specific target) is by no means clear-cut. Attempts to empirically generate a data base of a size sufficient to permit the isolation, by existing data analysis techniques, of the variables introduced by the generation and propagation of seismic energy have not been entirely successful. To simply increase the size of the data base would be uneconomical. For this reason a more systematic approach is now being attempted at the U. S. Army Engineer Waterways Experiment Station (WES) wherein mathematical modeling is used to simulate the generation and propagation of the seismic signal. If the simulation models are sufficiently accurate in their representation of the source, the ground or road surface, and the propagating medium, then systematic studies of the persistency of the derived discriminate features in various test and site conditions can be established.

5. The foregoing discussion therefore indicates that the design of the sensor's "discrimination logic" must be established on a very basic procedure; i.e., attributes of the signal that are essentially unchanged by either distance or environment must be sought and the decision-making analysis must be based upon them. Also, improvement in sensor design involves the prediction of kinds and magnitudes of change in signal characteristics to be expected in the "deployment environment," and the discrimination logic should be adjusted to evaluate the

expected signal configuration at a selected distance. It should be noted that both procedures require a quantitative understanding of what might be called "signal degradation." The ideal, of course, would be an understanding of the causes of signal degradation so thorough that the characteristics of the original signal could be reconstructed from consideration of the recorded wave train plus the characteristics of the intervening terrain. This report addresses the problem of quantitatively describing the total seismic signal as it propagates through a complex medium.

Approach

6. The most general and useful solution to the problem of quantitatively describing the total seismic signal would be one that faithfully simulates the generation, coupling, propagation, and decoupling of the seismic signal from the target to the sensor. Fig. 1 illustrates these phenomena. Stress from a target (walking man, moving vehicle, etc.) applied over a finite time causes the surface of the ground to deflect. This "forcing function" coupled to the ground initiates particle motion, which, in turn, generates a seismic wave. Seismic waves can propagate in a number of modes and show a decrease in amplitude due to geometric attenuation and viscous damping. The seismic wave amplitude may be further reduced if the wave travels near the surface of a macrogeometry feature. For example, macrogeometry features such as trenches, wedges, or steps in elevation can cause part of the wave traveling along the surface to be reflected in a new direction of travel or converted to body waves, which may or may not travel in the same direction as the original wave. The waves finally arrive at a measurement point (a geophone) in a pattern entirely different from their initial pattern. This change is a function of site properties and range and path of propagation.

7. To develop the mathematics to simulate the phenomena in fig. 1, it is convenient to consider the earth as a homogeneous medium, but such a generalization does not allow a prediction of seismic waves

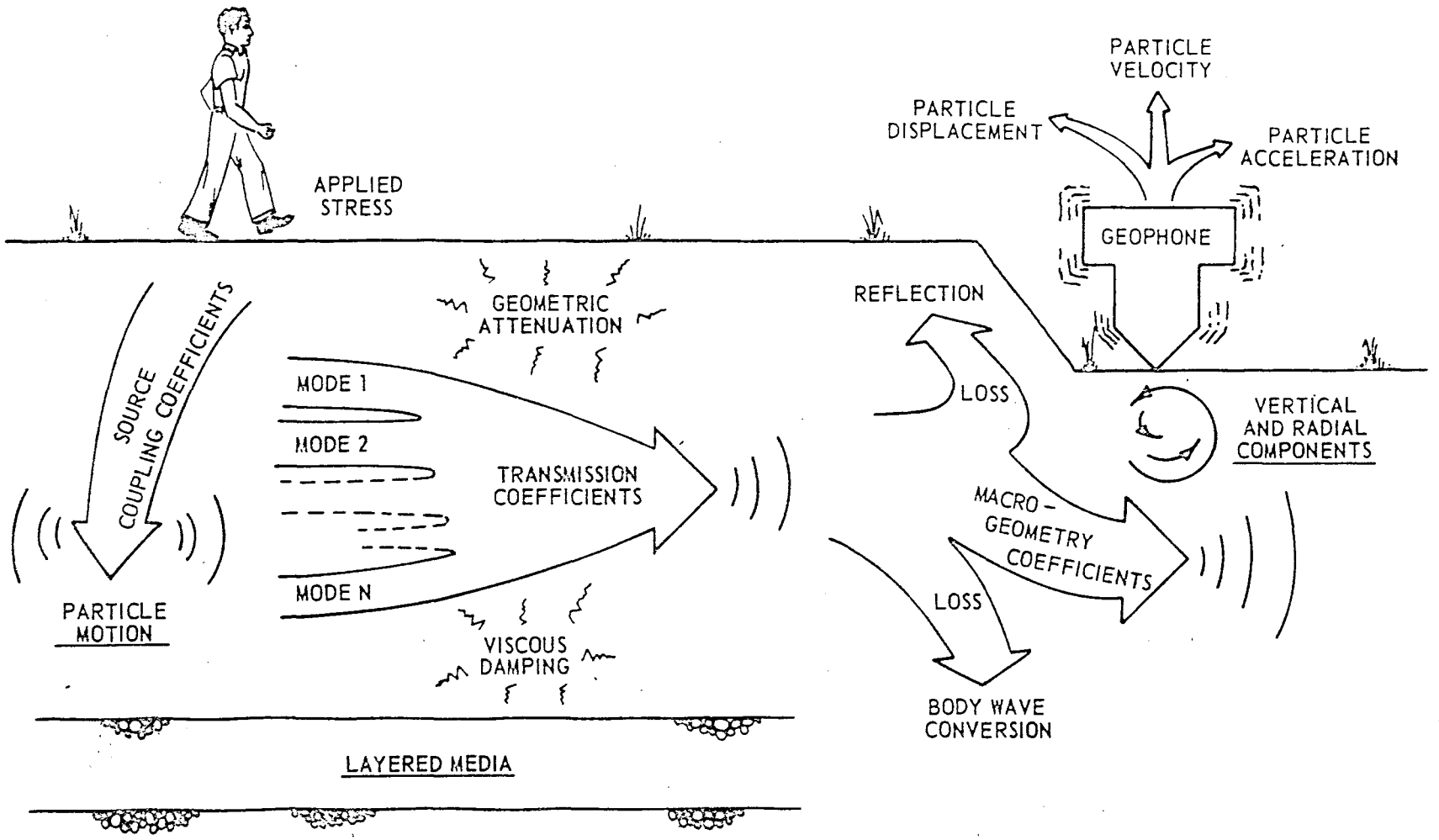

Fig. 1. Seismic wave propagation

comparable to those observed on seismic records measured in the field. A more realistic and useful assumption is one in which the earth is considered to be a layered medium with each layer considered homogeneous. The approach taken in the study reported herein is one that attempts to develop the mathematics within the framework of theoretical mechanics to simulate the phenomena described above.

Purpose and Scope

8. The purpose of this report is to describe the model (or method) developed for computing the amplitude and frequency contents of seismic waves (given the source signal from a specific target, i.e. vehicles, men, aircraft, etc.) as functions of substrate conditions, surface macrogeometry, and distance from the seismic source. Inputs to this model include the source signal, the soil properties, the surface configuration, and the range from the source to the point of prediction.

9. The model was developed to aid in the design of discriminating logic for seismic sensors; however, there are many additional applications such as those listed below that appear practicable (though not within the scope of this report):

a. Preparation of military geographic intelligence products for existing and prototype seismic sensors.

b. Establishing trade-offs between sensor design complexity and terrain data requirements for deployment.

c. Development of sensor deployment criteria.

d. Design of sensor fields against specific threats.

e. Evaluation of concepts for artillery ranging using seismic techniques.

PART II: DEVELOPMENT OF THE MATHEMATICAL MODEL

Wave Interactions

10. In an unbounded isotropic solid, there are only two types of elastic waves that can be propagated: the longitudinal, or compressional, wave and the traverse, or shear, wave. When there is a bounding surface, however, elastic surface, or Rayleigh, waves may also occur. The particle motion of a Rayleigh wave is elliptically retrograde in a plane perpendicular to the bounding surface and parallel to the direction of propagation (fig. 2). The Rayleigh wave velocity of propagation

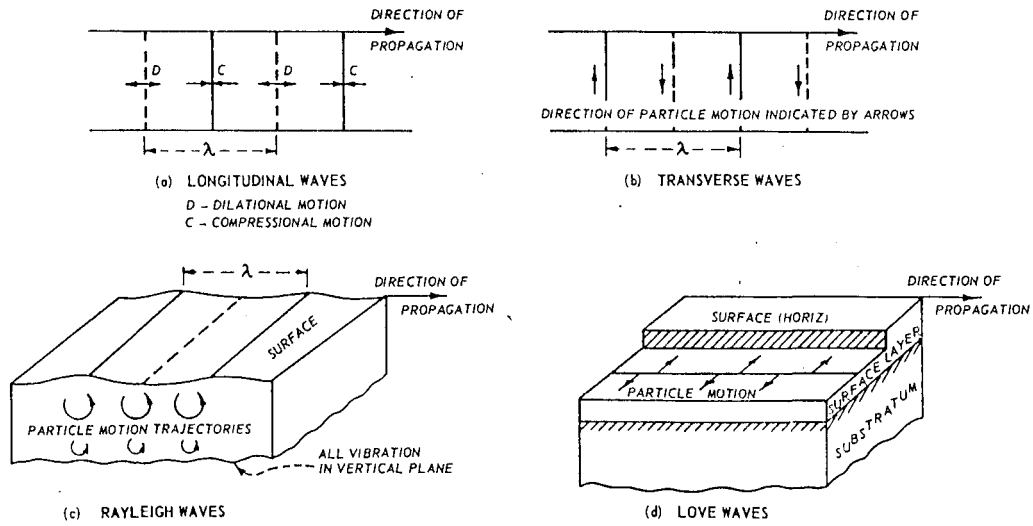

Fig. 2. Characteristics of elastic waves in a solid

is smaller than that of compression or shear waves, as shown in fig. 3 where wave velocities are plotted against Poisson's ratio.[1] An additional wave, i.e. a Love wave, can be propagated if horizontal layers exist. This wave is a horizontally polarized shear wave trapped in a superficial layer and propagated by multiple total reflections.[2,3]

Geometric damping

11. The energy per unit area of a wave front in a homogeneous half-space decreases as the wave travels away from its source since the energy must be distributed over an area that increases with increasing

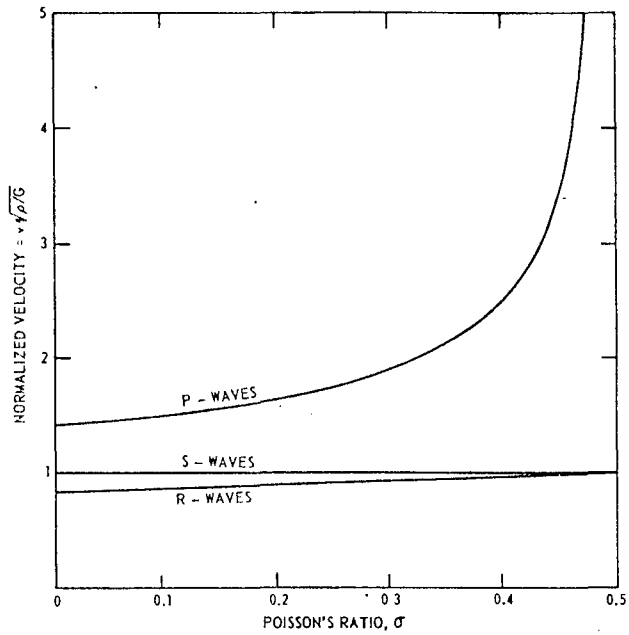

Fig. 3. Relation between Poisson's ratio, σ, and velocities of propagation of compression (P), shear (S), and Rayleigh (R) waves in a semi-infinite elastic medium (from reference 1)

range. At a relatively great distance (i.e. approximately 2.5 wavelengths or more) from the source, the shear and compression waves propagate radially outward from the source along a hemispherical wave front, and the Rayleigh wave propagates radially outward along a cylindrical wave front. The decrease in displacement amplitude associated with energy decrease is termed geometric attenuation. For shear and compression waves it is proportional to $1/r$ (r is the range from the seismic source), except along the surface of the half-space where it is proportional to $1/r^2$. The decrease in amplitude of a Rayleigh wave due to geometric attenuation is proportional to $1/\sqrt{r}$.

12. For a vertically oscillating, uniformly distributed, circular energy source on the surface of a homogeneous, isotropic, elastic half-space, the distribution of total input energy among the three elastic waves has been determined to be 67 percent Rayleigh wave, 26 percent shear wave, and 7 percent compression wave.[2] Because approximately

two-thirds of the total input energy is transmitted away from a vertically oscillating source by a Rayleigh wave, and a Rayleigh wave decays much more slowly with distance at the surface than compression or shear waves, the Rayleigh wave has been considered to be the proper one to exploit in developing a seismic intrusion detection system.

Internal damping

13. In addition to the loss of energy due to geometric attenuation, there is also a certain loss from internal friction in which some of the mechanical energy is converted into heat. The total loss from this mechanism increases with distance and frequency (i.e. approximately exponentially at far ranges). This internal damping is often described by the logarithmic decrement δ, which is the natural logarithm of the ratio of the excursions during two successive oscillations when no external forces are applied to maintain the oscillation. This measurement of decay of free vibration for a given soil sample can be derived from resonant frequency tests. It is often convenient to describe the internal damping of soils in terms of an equivalent damping factor D that is related to the logarithmic decrement by the relation:

$$D = \frac{\delta}{\left(4\pi^2 + \delta^2\right)^{1/2}}$$

Some typical values of this internal damping in soils are tabulated below.[2]

Type Soil	Equivalent Damping Factor	Reference
Dry sand and gravel	0.03-0.07	Weissmann and Hart[4]
Dry and saturated sand	0.01-0.03	Hall and Richart[5]
Dry sand	0.03	Whitman[6]
Dry and saturated sands and gravels	0.05-0.06	Barkan[7]
Clay	0.02-0.05	Barkan[7]
Silty sand	0.03-0.10	Stevens[8]
Dry sand	0.01-0.03	Hardin[9]

14. Rayleigh waves with short wavelengths (high-frequency waves) are attenuated more rapidly with depth than those with long wavelengths (low-frequency waves)(see fig. 4); the behavior is analogous to the skin

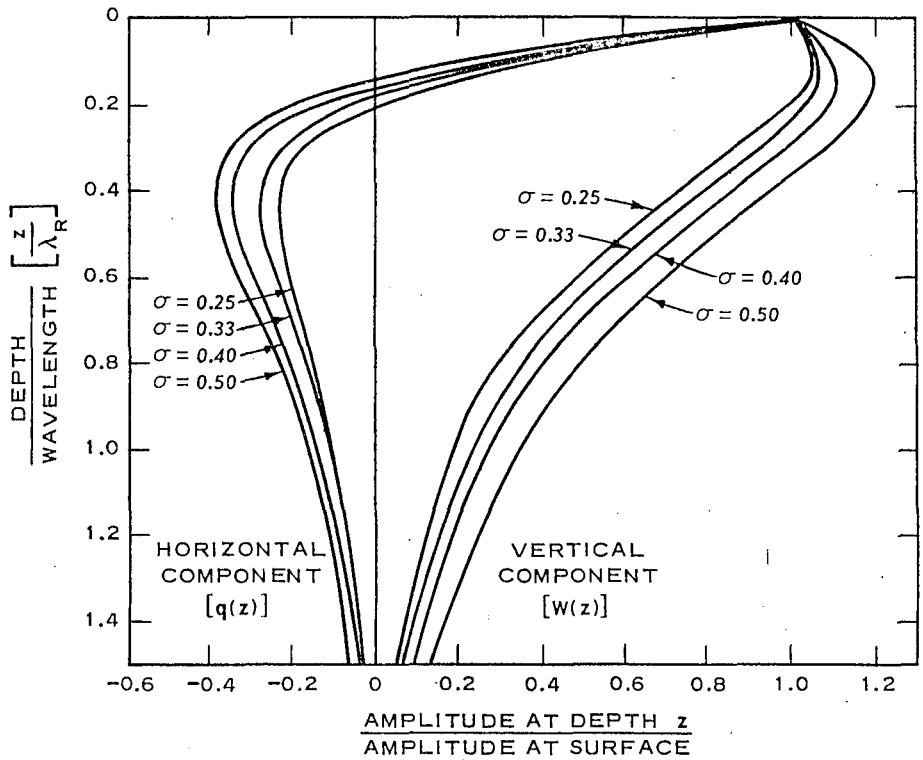

Fig. 4. Amplitude ratio versus dimensionless depth for Rayleigh wave (from reference 2)

effect in the transmission of high-frequency alternating electric currents in conductors.[10] The majority of the energy is carried at depths equivalent to less than one wavelength of the propagating wave. Thus when waves travel through a horizontally layered material (i.e. a material in which wave velocity is constant within a layer, but different from layer to layer), the Rayleigh wave velocity will vary with wavelength causing the Rayleigh wave to become dispersed as it propagates in a layered medium. For example, Rayleigh wave energy whose wavelength is significantly less than the first-layer depth travels in the first layer at a velocity slightly less than the shear wave velocity. Rayleigh wave energy whose wavelength is significantly greater than surface-layer depths travels in the basement or foundation material with a velocity

slightly less than the shear wave velocity of that material. For energy at intermediate wavelengths, the propagating velocity falls between the two extremes, i.e. first-layer and basement material shear wave velocity.

Reflections, refractions, and wave conversions

15. Another effect of horizontal layering in a medium is that elastic waves originating at the surface and traveling into the half-space may be partially reflected at a boundary to return to the surface. If more than one interface exists, waves may be reflected to the surface from each layer. When any reflected wave returns to the surface of the layered half-space, it encounters the interface between solid and void where it will be totally reflected. These conditions lead to a horizontally polarized shear wave trapped in a superficial layer and propagated by multiple total reflections (i.e. a Love wave, see fig. 2). For these polarized shear waves to propagate, the superficial layer must have a lower shear wave velocity than the next deeper layer. Macrogeometry features occurring in the propagation path cause wave losses due to energy refraction, reflection, and wave conversion (e.g. a Rayleigh wave encountering a discontinuity can become a source of new Rayleigh waves and body waves). The effects of these macrogeometry features can be accounted for with a frequency-dependent amplitude transmission coefficient. (Some existing solutions for the effects of macrogeometry found in the literature are presented and discussed in Appendix A.)

Derivation of Equations

16. Closed-form equations for computing the seismic signal (given the signal from a specific target) were derived within the framework of theoretical mechanics. The derivation makes use of the classical equations of motion to define the stress-strain relations in the propagating medium when the stress is acting on an infinitesimal rectangular parallelepiped.

Assumptions to simplify calculations

17. To develop an economical and practical mathematical

simulation of the phenomena shown in fig. 1, certain assumptions were made. These simplifying assumptions restricted the use of the model to a class of problems that met the assumptions. However, the model can be applied to other problems in which the assumptions are not met precisely, if a corresponding decrease in accuracy of computed results can be accepted.

18. In general, the assumptions can be divided into two classes: (a) those that describe the geometry and composition of the system, and (b) those that describe wave motion.

19. System assumptions. The medium through which the seismic waves propagate is assumed to be composed of horizontal layers. Properties within each layer are uniform in all directions (homogeneous and isotropic) and can be described by a consistent set of properties (e.g. shear wave velocity β , compression wave velocity α , and mass density ρ). The material is further assumed to be viscoelastic and thus allows the properties to take on complex values.

20. All layer boundaries are smooth (including the top surface) and abrupt. This implies that minor vertical discontinuities are small compared with seismic signal wavelengths, and the boundaries of adjacent layers are in close contact such that motion is transferred from one to another without loss (i.e. there is no shear between boundaries).

21. Major discontinuities (macrogeometry features) at the surface are large compared with seismic signal wavelengths. The effects of such discontinuities can be reduced to amplitude transmission coefficients (see paragraphs 59-60).

22. Wave motion assumptions. Predictions for particle or wave motion are made for a point source (force input) at some distance r from the source. To compare field-measured signals with predicted signals, the field-measured signal range must be great enough for the signal source to appear to originate from a point source. This would imply that the source dimensions (contact dimensions) are small compared with the seismic signal wavelength.

23. All motions associated with either the input signal or the output predictions are at a level low enough for the material to retain

its elastic properties; the material does not suffer permanent deformation or fracture under the applied stresses.

24. The predicted signals radiate from the source in circles of constant amplitude (axial symmetry). This requires that the input stresses be applied vertically or perpendicularly to the top surface, or that the observer be far enough away from the source for the contours of constant amplitude of particle motion to approximate circles.

25. Predictions of seismic signals are made for essentially surface motion only, i.e. at a depth much less than the seismic signal wavelength. To obtain predictions for depths that are a significant fraction of a wavelength, relations similar to those from which fig. 4 was calculated should be utilized.[2]

Equations of motion

26. The following paragraphs present the derivation of the equations (equations 34a and 34b) for computing the radial and vertical components of particle displacement as a function of range and time (given the signal source input and site properties). Part III of this report presents the equations transformed for efficient computer solution and discusses the computer solution. Part IV shows examples of the application of the computer solution at two field sites where measured data were available for comparison.

27. The stress applied to the surface element in a solid body does not generally act normal to that surface, but has components both normal to the plane and tangential to it. Within the body, any point P with space-fixed rectangular coordinates (x, y, and z) is then displaced to a new position (x + u, y + v, z + w; see equations 3a-3c). The components of stress can be resolved into nine elements as shown in fig. 5. They are denoted as p_{xx}, p_{yy}, p_{zz}, p_{xy}, p_{xz}, etc., the first letter in the subscript denoting the direction of the stress and the second letter defining the plane in which it is acting. Under the condition of an isotropic elastic body in equilibrium, the stress-strain relations can be written for small strains associated with elastic waves using Lamé's constants λ and μ:[3]

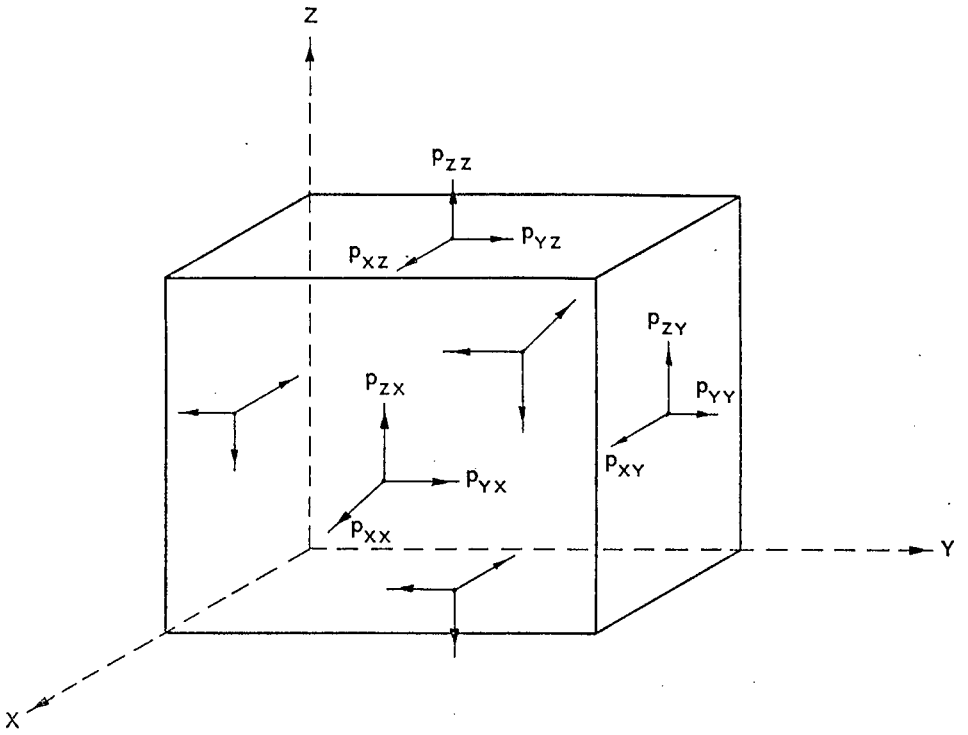

Fig. 5. Stress components acting on an infinitesimal rectangular parallelepiped

$$p_{xx} = \lambda\theta + 2\mu\left(\frac{\partial u}{\partial x}\right) \tag{1a}$$

$$p_{yy} = \lambda\theta + 2\mu\left(\frac{\partial v}{\partial y}\right) \tag{1b}$$

$$p_{zz} = \lambda\theta + 2\mu\left(\frac{\partial w}{\partial z}\right) \tag{1c}$$

$$p_{xy} = \mu\left(\frac{\partial u}{\partial y} + \frac{\partial v}{\partial x}\right) \tag{1d}$$

$$p_{yz} = \mu\left(\frac{\partial v}{\partial z} + \frac{\partial w}{\partial y}\right) \tag{1e}$$

$$p_{zx} = \mu\left(\frac{\partial w}{\partial x} + \frac{\partial u}{\partial z}\right) \tag{1f}$$

$$p_{xy} = p_{yx}\ ,\quad p_{xz} = p_{zx}\ ,\ \text{and}\quad p_{yz} = p_{zy} \tag{1g}$$

where the cubical dilatation θ is defined as

$$\theta = \frac{\partial u}{\partial x} + \frac{\partial v}{\partial y} + \frac{\partial w}{\partial z}$$

28. The equations of motion can be written as a sum of forces for each component:

$$\rho\left(\frac{d^2u}{dt^2}\right) = \rho X + \frac{\partial p_{xx}}{\partial x} + \frac{\partial p_{yx}}{\partial y} + \frac{\partial p_{zx}}{\partial z} \tag{2a}$$

$$\rho\left(\frac{d^2v}{dt^2}\right) = \rho Y + \frac{\partial p_{xy}}{\partial x} + \frac{\partial p_{yy}}{\partial y} + \frac{\partial p_{zy}}{\partial z} \tag{2b}$$

$$\rho\left(\frac{d^2w}{dt^2}\right) = \rho Z + \frac{\partial p_{xz}}{\partial x} + \frac{\partial p_{yz}}{\partial y} + \frac{\partial p_{zz}}{\partial z} \tag{2c}$$

where

ρ = mass density of the medium

t = time

X,Y,Z = body forces that are porportional to the mass in the volume element

29. It is convenient to define a scalar potential ϕ and a vector potential $\vec{\psi}\ (\psi_1,\psi_2,\psi_3)$, where

$$u = \frac{\partial \phi}{\partial x} + \frac{\partial \psi_3}{\partial y} - \frac{\partial \psi_2}{\partial z} \tag{3a}$$

$$v = \frac{\partial \phi}{\partial y} + \frac{\partial \psi_1}{\partial z} - \frac{\partial \psi_3}{\partial x} \tag{3b}$$

$$w = \frac{\partial \phi}{\partial z} + \frac{\partial \psi_2}{\partial x} - \frac{\partial \psi_1}{\partial y} \tag{3c}$$

or in vector form:

$$\begin{aligned} \vec{S}(u,v,w) &= \text{grad } \phi + \text{curl } \vec{\psi}(\psi_1,\psi_2,\psi_3) \\ &= \vec{\nabla}\,\phi + \vec{\nabla} \times \vec{\psi} \end{aligned} \tag{3d}$$

where $\vec{\nabla}$ is the nabla operator.

30. In general, the equations of motion (equation 2) represent

the propagation of a disturbance that involves both equivoluminal ($\theta = 0$) and irrotational ($\vec{\Omega} = 0$) motion, where $\theta = \text{div } \vec{S}(u,v,w)$ and $\vec{\Omega} = 1/2 \text{ curl } \vec{S}(u,v,w)$. However, by introduction of the potentials ϕ and ψ_γ , separate wave equations are obtained for these two types of motion. Assuming that the body forces can be neglected, the following equations can be formed:

a. For an irrotational disturbance ($\vec{\Omega} = 0$)

$$\vec{\nabla}^2 \phi - \left(\frac{1}{\alpha^2}\right)\left(\frac{\partial^2 \phi}{\partial t^2}\right) = 0 \tag{4a}$$

where

$$\alpha = \left(\frac{\lambda + 2\mu}{\rho}\right)^{1/2}$$

b. For an equivoluminal disturbance ($\theta = 0$)

$$\vec{\nabla}^2 \psi_\gamma - \left(\frac{1}{\beta^2}\right)\left(\frac{\partial^2 \psi_\gamma}{\partial t^2}\right) = 0 \tag{4b}$$

with

$$\gamma = 1, 2, 3$$

and

$$\beta = (\mu/\rho)^{1/2}$$

These equations indicate that two types of disturbances with velocities α and β can be propagated through an elastic solid. These disturbances are, respectively, compressional waves and distortional (or shear) waves.

31. Any realistic time-dependent function can be studied in the frequency domain in which the time dependency is separated as $e^{i\omega t}$ Equations 4a and 4b then become

$$\vec{\nabla}^2 \phi + \kappa_\alpha^2 \phi = 0 \tag{5a}$$

$$\vec{\nabla}^2 \psi_\gamma + \kappa_\beta^2 \psi_\gamma = 0 \tag{5b}$$

where

κ_α = wave number for the compressional wave ($= \omega/\alpha$)

κ_β = wave number for the shear wave (= ω/β)

ω = circular frequency (= $2\pi f$)

f = frequency

For the case of axial symmetry (paragraph 24), there is only one function ψ satisfying equation 5b.

Solution of the wave equations

32. Solutions of the wave equations (5a and 5b) can be obtained for cylindrical coordinates, r , χ , z so that axial symmetry conditions can be applied. The operator ∇^2 is then defined as:

$$\nabla^2 = \frac{\partial^2}{\partial r^2} + \left(\frac{1}{r}\right)\left(\frac{\partial}{\partial r}\right) + \frac{\partial^2}{\partial z^2}$$

The arbitrary solution of an equation of the form (i.e. the form of equation 5)

$$\nabla^2 A + \eta^2 A = 0 \qquad (6)$$

is

$$A = \exp\left[\pm\,(\delta z + im\chi)\right] J_m\left[r\left(\delta^2 + \eta^2\right)^{1/2}\right]$$

where

A = dependent variable of equation 6

δ,m = variable parameters

z = vertical distance from origin

i = $\sqrt{-1}$

χ = angular displacement

J_m = Bessel function of order m

r = range from origin

η = independent variable of equation 6

Because of axial symmetry, $\partial A/\partial\chi = 0$ (no azimuthal dependency), m is restricted to a value of zero, and

$$A = \exp(\pm\delta z) J_o\left[r\left(\delta^2 + \eta^2\right)^{1/2}\right]$$

If τ is defined as $\tau = \left(\delta^2 + \eta^2\right)^{1/2}$, then

$$A = \exp(\pm\delta z) J_o(r\tau)$$

The general solution of equation 6 can then be written:

$$A(r,z) = \int_o^\infty \left[A'(\tau)e^{-\delta z} + A''(\tau)e^{\delta z}\right] J_o(r\tau)d\tau \qquad (7)$$

where A' and A'' are constants associated with the minus and plus exponential functions of A.

33. The solution is unique only if the functions $A'(\tau)$ and $A''(\tau)$ can be determined from boundary conditions. By substituting ϕ_i or ψ_i for A, ν_i or ν_i' for δ, and κ for τ, and renaming the constants, the general solutions for the ith layer become

$$\phi_i(r,z) = \int_o^\infty \left[Q_i'(\kappa)J_o(\kappa r)e^{-\nu_i z} + Q_i''(\kappa)J_o(\kappa r)e^{\nu_i z}\right] d\kappa \qquad (8a)$$

$$\psi_i(r,z) = \int_o^\infty \left[S_i'(\kappa)J_o(\kappa r)e^{-\nu_i' z} + S_i''(\kappa)J_o(\kappa r)e^{\nu_i' z}\right] d\kappa \qquad (8b)$$

where

$$\nu_i = \left(\kappa^2 - \kappa_{\alpha i}^2\right)^{1/2}$$

$$\nu_i' = \left(\kappa^2 - \kappa_{\beta i}^2\right)^{1/2}$$

for $i = 1, 2, \ldots, n$, where n is the number of layers.

34. With equations 3a-3d and 1a-1g, the corresponding displacement and stress components can be expressed as:

$$q_i = \int_o^\infty \kappa J_o'(\kappa r)\left(Q_i'e^{-\nu_i z} + Q_i''e^{\nu_i z} - \nu_i' S_i' e^{-\nu_i' z} + \nu_i' S_i'' e^{\nu_i' z}\right)d\kappa \qquad (9a)$$

$$w_i = \int_o^\infty J_o(\kappa r)\left(-\nu_i Q_i' e^{-\nu_i z} + \nu_i Q_i'' e^{\nu_i z} + \kappa^2 S_i' e^{-\nu_i' z} + \kappa^2 S_i'' e^{\nu_i' z}\right) d\kappa \qquad (9b)$$

where q_i and w_i equal the radial and vertical components of the

displacement, respectively, and the stress p expressions are

$$(p_{zr})_i = \int_0^\infty \kappa J_o'(\kappa r) \left[- 2\mu_i \nu_i Q_i' e^{-\nu_i z} + 2\mu_i \nu_i Q_i'' e^{\nu_i z} + \mu_i \left(\nu_i'^2 + \kappa^2\right) S_i' e^{-\nu_i' z} + \mu_i \left(\nu_i'^2 + \kappa^2\right) S_i'' e^{\nu_i z} \right] d\kappa \qquad (9c)$$

$$(p_{zz})_i = \int_0^\infty J_o(\kappa r) \left(a_i Q_i' e^{-\nu_i z} + a_i Q_i'' e^{\nu_i z} - 2\mu_i \nu_i' \kappa^2 S_i' e^{-\nu_i' z} + 2\mu_i \nu_i' \kappa^2 S_i'' e^{\nu_i' z} \right) d\kappa \qquad (9d)$$

with $i = 1, 2, \ldots, n$,

$$J_o'(\eta) = \frac{dJ_o(\eta)}{d\eta}$$

$$a_i = 2\mu_i \nu_i^2 - \lambda_i \kappa_{\alpha i}^2$$

Boundary-condition equations
and solution for a point source

35. The ground is assumed to consist of several layers, with the interfaces between the layers normal to the z-direction. It is also assumed that the nth layer from the surface is welded at the nth interface to a rigid-material half-space. The rigid material by definition does not deform. From this and the assumption of welded contact, it follows that the material of the nth layer at the depth H_n from the ground surface does not deform, and there its strain approaches zero:

$$\left.\begin{aligned} q_n(r_1 z) &= 0 \\ w_n(r_1 z) &= 0 \end{aligned}\right\} \quad \text{at} \quad z = H_n \qquad (10)$$

There is no restriction on the stress components. At the other interfaces, the two layers in contact are again assumed to be welded together and the displacement and stress components must be equal across the boundary:

$$\left.\begin{aligned} q_i(r_1 z) &= q_{i+1}(r_1 z) \\ w_i(r_1 z) &= w_{i+1}(r_1 z) \\ \left[p_{rz}(r_1 z)\right]_i &= \left[p_{rz}(r_1 z)\right]_{i+1} \\ \left[p_{zz}(r_1 z)\right]_i &= \left[p_{zz}(r_1 z)\right]_{i+1} \end{aligned}\right\} \quad \text{for} \quad z = H_i \ , \quad i = 1, 2, \ldots n-1 \qquad (11)$$

36. At the free upper surface of the top (first) layer there is no restriction on the displacements. The stress is determined by the nature of the source of the disturbance. If there is no disturbance, the stress components at the free surface are zero. For a point source at the surface at the axis of symmetry of the coordinate system ($z = 0$, $r = 0$), which has only a vertical component, the stress components at that point become:

$$\left.\begin{aligned} \left[p_{rz}(r_1 z)\right]_1 &= 0 \\ \left[p_{zz}(r_1 z)\right]_1 &= -\frac{L}{2\pi}\int_0^\infty J_0(\kappa r)\kappa \, d\kappa \end{aligned}\right\} \quad \text{for} \quad z = 0 \qquad (12)$$

For n layers there are $4n$ unknown functions of equation 9, Q_i', Q_i'', S_i', and S_i'', which can be determined from the $4n$ boundary conditions.

37. An integral containing a Bessel function, as in equations 9a-9d and 12,

$$I(r) = \int_0^\infty f(\kappa) J_\ell(\kappa r)\kappa \, d\kappa$$

where $\ell = 0$ or $\ell = 1$, when multiplied by $J_\ell(\kappa' r) r \, dr$ and integrated over r gives

$$\int_0^\infty I(r) J_\ell(\kappa' r) r \, dr = \int_0^\infty J_\ell(\kappa' r) r \int_0^\infty f(\kappa) J_\ell(\kappa r)\kappa \, d\kappa \, dr$$

The right side of the equation is the Bessel-Fourier integral, which can be solved:

$$\int_0^\infty I(r)J_\ell(\kappa' r)r\,dr = f(\kappa')$$

By applying this procedure to equations 9a-9d and 12, and using $J_o'(\kappa r) = -J_1(\kappa r)$, equations containing functions can be derived from the equations containing integrals.

38. Then the boundary equations become, for surface $z = 0$ (equation 12):

$$p_{zr}: \quad -2\mu_1\nu_1 Q_1' + 2\mu_1\nu_1 Q_1'' + \mu_1\left(\nu_1'^2 + \kappa^2\right)S_1' + \mu_1\left(\nu_1'^2 + \kappa^2\right)S_1'' = 0 \tag{13a}$$

$$p_{zz}: \quad a_1 Q_1' + a_1 Q_1'' - 2\mu_1\nu_1'\kappa^2 S_1' + 2\mu_1\nu_1'\kappa^2 S_1'' = -\frac{L\kappa}{2\pi} \tag{13b}$$

For $z = H_i$ with $i = 1, 2, \ldots, n-1$ (equation 11):

$$q: \quad Q_i' e^{-\nu_i H_i} + Q_i'' e^{\nu_i H_i} - \nu_i' S_i' e^{-\nu_i' H_i} + \nu_i' S_i'' e^{\nu_i' H_i} = Q_{i+1}' e^{-\nu_{i+1} H_i}$$

$$+ Q_{i+1}'' e^{\nu_{i+1} H_i} - \nu_{i+1}' S_{i+1}' e^{-\nu_{i+1}' H_i} + \nu_{i+1}' S_{i+1}'' e^{\nu_{i+1}' H_i} \tag{14a}$$

$$w: \quad -\nu_i Q_i' e^{-\nu_i H_i} + \nu_i Q_i'' e^{\nu_i H_i}$$

$$+ \kappa^2 S_i' e^{-\nu_i' H_i} + \kappa^2 S_i'' e^{\nu_i' H_i} = -\nu_{i+1} Q_{i+1}' e^{-\nu_{i+1} H_i} + \nu_{i+1} Q_{i+1}'' e^{\nu_{i+1} H_i}$$

$$+ \kappa^2 S_{i+1}' e^{-\nu_{i+1}' H_i} + \kappa^2 S_{i+1}'' e^{\nu_{i+1}' H_i} \tag{14b}$$

$$p_{zr}: \quad -2\mu_i\nu_i Q_i' e^{-\nu_i H_i} + 2\mu_i\nu_i Q_i'' e^{\nu_i H_i} + \mu_i\left(\nu_i'^2 + \kappa^2\right)S_i' e^{-\nu_i' H_i}$$

$$+ \mu_i\left(\nu_i'^2 + \kappa^2\right)S_i'' e^{\nu_i' H_i} = -2\mu_{i+1}\nu_{i+1} Q_{i+1}' e^{-\nu_{i+1} H_i} + 2\mu_{i+1}\nu_{i+1} Q_{i+1}'' e^{\nu_{i+1} H_i}$$

$$+ \mu_{i+1}\left(\nu_{i+1}'^2 + \kappa^2\right)S_{i+1}' e^{-\nu_{i+1}' H_i} + \mu_{i+1}\left(\nu_{i+1}'^2 + \kappa^2\right)S_{i+1}'' e^{\nu_{i+1}' H_i} \tag{14c}$$

$$p_{zz}: \quad a_i Q_i' e^{-\nu_i H_i} + a_i Q_i'' e^{\nu_i H_i} - 2\mu_i \nu_i' \kappa^2 S_i' e^{-\nu_i' H_i}$$

$$+ 2\mu_i \nu_i' \kappa^2 S_i'' e^{\nu_i H_i} = a_{i+1} Q_{i+1}' e^{-\nu_{i+1} H_i} + a_{i+1} Q_{i+1}'' e^{\nu_{i+1} H_i}$$

$$- 2\mu_{i+1} \nu_{i+1}' \kappa^2 S_{i+1}' e^{-\nu_{i+1}' H_i} + 2\mu_{i+1} \nu_{i+1}' \kappa^2 S_{i+1}'' e^{\nu_{i+1} H_i} \qquad (14d)$$

And for $z = H_n$ (equation 10)

$$q: \quad Q_n' e^{-\nu_n H_n} + Q_n'' e^{\nu_n H_n} - \nu_n' S_n' e^{-\nu_n' H_n} + \nu_n' S_n'' e^{\nu_n' H_n} = 0 \qquad (15a)$$

$$w: \quad -\nu_n Q_n' e^{-\nu_n H_n} + \nu_n Q_n'' e^{\nu_n H_n} + \kappa^2 S_n' e^{-\nu_n' H_n} + \kappa^2 S_n'' e^{\nu_n' H_n} = 0 \qquad (15b)$$

39. The problem now is to obtain solutions for Q_1', Q_1'', S_1', and S_1''. These $4n$ equations can be expressed in a more compact form by introducing the following matrices:

$$\vec{X}_i = \begin{vmatrix} Q_i' e^{-\nu_i H_{i-1}} \\ Q_i'' e^{\nu_i H_{i-1}} \\ S_i' e^{-\nu_i' H_{i-1}} \\ S_i'' e^{\nu_i H_{i-1}} \end{vmatrix}$$

$$A_i = \begin{vmatrix} 1 & 1 & -\nu_i' & \nu_i' \\ -\nu_i & \nu_i & \kappa^2 & \kappa^2 \\ -2\mu_i \nu_i & 2\mu_i \nu_i & \mu_i\left(\nu_i'^2 + \kappa^2\right) & \mu\left(\nu_i'^2 + \kappa^2\right) \\ a_i & a_i & -2\mu_i \kappa^2 \nu_i' & 2\mu_i \kappa^2 \nu_i' \end{vmatrix}$$

$$D_i = \begin{vmatrix} e^{-\nu_i d_i} & 0 & 0 & 0 \\ 0 & e^{\nu_i d_i} & 0 & 0 \\ 0 & 0 & e^{-\nu_i' d_i} & 0 \\ 0 & 0 & 0 & e^{\nu_i' d_i} \end{vmatrix}$$

with $d_i = H_{i+1} - H_i$ (d_i = thickness of ith layer), and $H_o = 0$;

$$\vec{\phi} = \begin{vmatrix} 0 \\ 0 \\ 0 \\ 0 \end{vmatrix}$$

$$E = \begin{vmatrix} 1 & 0 & 0 & 0 \\ 0 & 1 & 0 & 0 \\ 0 & 0 & 1 & 0 \\ 0 & 0 & 0 & 1 \end{vmatrix}$$

$$C = \begin{vmatrix} 0 & 0 & 0 & 0 \\ 0 & 0 & 0 & 0 \\ 0 & 0 & 1 & 0 \\ 0 & 0 & 0 & 1 \end{vmatrix}$$

A_i^{-1} is the inverse of A_i : $A_i^{-1} A_i = E$

A_i^{-1} exists for $\mathrm{Det}(A_i) \neq 0$, or

$$-8\nu_i \nu_i' \mu_i^2 \kappa_{\alpha i}^2 \kappa_{\beta i}^2 \left(1 + \frac{\lambda_i}{2\mu_i}\right) \neq 0$$

$$\vec{b} = \begin{vmatrix} 0 \\ 0 \\ 0 \\ \\ \frac{-L\kappa}{2\pi} \end{vmatrix}$$

The equations expressing the boundary conditions (13a and b, 14a and b, and 15a and b) appear then as

$$CA_1\vec{X}_1 = \vec{b} \qquad (2 \text{ equations}) \tag{16}$$

$$A_iD_i\vec{X}_i = A_{i+1}\vec{X}_{i+1} \qquad (4 \text{ equations}) \tag{17}$$

$$(E - C)A_nD_n\vec{X}_n = \vec{\emptyset} \qquad (2 \text{ equations}) \tag{18}$$

After multiplication from the left with A_{i+1}^{-1}, equation 17 gives

$$A_{i+1}^{-1}A_iD_i\vec{X}_i = \vec{X}_{i+1}$$

or with

$$T_i \equiv A_{i+1}^{-1}A_iD_i$$

$$T_i\vec{X}_i = \vec{X}_{i+1} \qquad (4 \text{ equations}) \tag{19}$$

and applied to equation 18 gives, with $i = n - 1$,

$$(E - C)A_nD_nT_{n-1}\vec{X}_{n-1} = \vec{\emptyset} \tag{20}$$

After repeated application of equation 19

$$(E - C)A_nD_nT_{n-1}T_{n-2} \cdots T_2T_1\vec{X}_1 = \vec{\emptyset} \qquad (2 \text{ equations})$$

or with

$$G \equiv T_{n-1}T_{n-2} \cdots T_2T_1$$

$$(E - C)A_n D_n G\vec{X}_1 = \vec{\emptyset} \tag{21}$$

Equations 16 and 21 can be combined to:

$$[(E - C)A_n D_n G + CA_1]\vec{X}_1 = \vec{b} \qquad (4 \text{ equations})$$

or with

$$F \equiv (E - C)A_n D_n G + CA_1$$

$$F\vec{X}_1 = \vec{b} \tag{22}$$

There are four equations in only four variables that are the components of $\vec{X}_1$. These equations can be solved for $\mathrm{Det}(F) \neq 0$:

by using $\vec{y} = \vec{X}_1$ for $z = 0$ or $\vec{y} = \begin{vmatrix} Q_1' \\ Q_1'' \\ S_1' \\ S_1'' \end{vmatrix}$ (23a)

$$\Delta(\kappa) \doteq \mathrm{Det}(F) \tag{23b}$$

$$\Delta_{\ell s} = \ell - s \text{ subdeterminant of } \Delta$$

as

$$y_s = -\frac{L\kappa\Delta_{4s}(-1)^s}{2\pi\Delta} \tag{24}$$

where y_s is the sth component of the vector $\vec{y}$. The solution for the particle displacement at the surface $z = 0$, can now be expressed as

$$q_1(r) = -L\int_0^\infty J_1(\kappa r)Q(\kappa)\kappa^2 \, d\kappa \tag{25a}$$

$$w_1(r) = L\int_0^\infty J_0(\kappa r)W(\kappa)\kappa \, d\kappa \tag{25b}$$

with

$$\kappa Q(\kappa)L = (Q_1' + Q_1'') - \nu_1'(S_1' - S_1'') \tag{26a}$$

$$\kappa W(\kappa)L = -\nu_1(Q_1' - Q_1'') + \kappa^2(S_1' + S_1'') \tag{26b}$$

Since ν_i , ν_i' , and A_i are even functions of κ , the components of $\vec{y}$ and finally $Q(\kappa)$ and $W(\kappa)$ are even functions of κ .

40. The integrals (equations 25a and 25b) are then converted into integrals over the entire real axis by using

$$J_\ell(\kappa r) = \frac{1}{2}\left[H_\ell^{(1)}(\kappa r) + H_\ell^{(2)}(\kappa r)\right]$$

with $\ell = 0,1$

$$H_0^{(2)}(\kappa r) = -H_0^{(1)}(-\kappa r)$$

and

$$H_1^{(2)}(\kappa r) = H_1^{(1)}(-\kappa r)$$

where $H_\ell^{(1)}(\kappa r)$ and $H_\ell^{(2)}(\kappa r)$ are Hankel functions of the first and second kind, respectively:

$$q_1(r) = -L\int_0^\infty J_1(\kappa r)Q(\kappa)\kappa^2\,d\kappa$$

$$= -\frac{L}{2}\int_0^\infty \left[H_1^{(1)}(\kappa r) + H_1^{(1)}(-\kappa r)\right]Q(\kappa)\kappa^2\,d\kappa$$

$$= -\frac{L}{2}\int_0^\infty H_1^{(1)}(\kappa r)Q(\kappa)\kappa^2\,d\kappa - \frac{L}{2}\int_{-\infty}^0 H_1^{(1)}(\kappa r)Q(\kappa)\kappa^2\,d\kappa$$

$$= -\frac{L}{2}\int_{-\infty}^\infty H_1^{(1)}(\kappa r)Q(\kappa)\kappa^2\,d\kappa \tag{27a}$$

75128

$$w_1(r) = L \int_0^\infty J_o(\kappa r) W(\kappa) \kappa \, d\kappa$$

$$= \frac{L}{2} \int_0^\infty \left[H_o^{(1)}(\kappa r) - H_o^{(1)}(-\kappa r) \right] W(\kappa) \kappa \, d\kappa$$

$$= \frac{L}{2} \int_0^\infty H_o^{(1)}(\kappa r) W(\kappa) \kappa \, d\kappa + \frac{L}{2} \int_{-\infty}^0 H_o^{(1)}(\kappa r) W(\kappa) \kappa \, d\kappa$$

$$= \frac{L}{2} \int_{-\infty}^\infty H_o^{(1)}(\kappa r) W(\kappa) \kappa \, d\kappa \qquad (27b)$$

The integrals hold for $r > 0$. For $r = 0$: $J_1(0) = 0$ and $J_o(0) = 1$ lead to $q_1(0) = 0$

$$w_1(0) = L \int_0^\infty W(\kappa) \kappa \, d\kappa$$

$$= \frac{L}{2} \int_{-\infty}^\infty W(\kappa) |\kappa| \, d\kappa$$

The two integrals (27a and 27b) can be solved by contour integration in the complex κ-plane. The integrals have the following singularities:

a. Poles at $\kappa = \kappa_m$ for $\Delta(\kappa_m) = 0$, $m = 1, 2, 3, \ldots$

b. Branch points at $\kappa = \pm\kappa_{\alpha i}$ for $\nu_i = 0$

and at $\kappa = \pm\kappa_{\beta i}$ for $\nu_i' = 0$ with $i = 1, 2, \ldots, n$. Because of the existing branch points, the integrals are multivalued functions of κ . They are single-valued functions on a 4n-sheet Riemann (Re) surface. They can be made single-valued functions of κ by selecting a single sheet with certain cuts. Here the cuts are made for $\mathrm{Re}(\nu_i) = 0$ and $\mathrm{Re}(\nu_1') = 0$, and the selected sheet is defined by $\mathrm{Re}(\nu_i) > 0$ and $\mathrm{Re}(\nu_i') > 0$, $i = 1, 2, \ldots n$. The cuts are hyperbolas that can be verified as follows:

$$\nu_i = \left(\kappa^2 - \kappa_{\alpha i}^2 \right)^{1/2}$$

with $\mathrm{Re}(\nu_i) = 0$ gives

$$\mathrm{Im}\left(\kappa^2 - \kappa_{\alpha i}^2\right) = 0$$

and

$$\mathrm{Re}\left(\kappa^2 - \kappa_{\alpha i}^2\right) \leq 0$$

and leads to

$$\mathrm{Re}(\kappa)\mathrm{Im}(\kappa) = \frac{1}{2}\,\mathrm{Im}\left(\kappa_\alpha^2\right) \tag{28}$$

and

$$\mathrm{Re}^2(\kappa) - \mathrm{Im}^2(\kappa) \leq \mathrm{Re}\left(\kappa_\alpha^2\right) \tag{29}$$

Equation 28 is the equation of a hyperbola on the $[\mathrm{Re}(\kappa)\ ,\ \mathrm{Im}(\kappa)]$ or the complex κ plane, and equation 29 specifies which portion of it represents the cut. For large values of κ, with $\kappa >> 1/r$ and $r > 0$, the functions $H_o^{(1)}$ and $H_1^{(1)}$ can be approximated by

$$H_o^{(1)}(\kappa r) \simeq \left(\frac{2}{\pi\kappa r}\right)^{1/2} \exp\left[i\left(\kappa r - \frac{\pi}{4}\right)\right]$$

$$H_1^{(1)}(\kappa r) \simeq \left(\frac{2}{\pi\kappa r}\right)^{1/2} \exp\left[i\left(\kappa r - \frac{3\pi}{4}\right)\right]$$

Sommerfield's radiation condition for waves radiated away from the source,

$$\exp[i(\omega t + \kappa r)]$$

is satisfied for $\omega > 0$ and $\mathrm{Re}(\kappa) < 0$. This means that for positive values of ω, the real part of κ should be negative for radiated waves.

41. It can be seen that the behavior of the components of $\vec{y}$ when κ approaches infinity is, at the most, that of a polynominal in κ, since the largest term of Δ_{4m} increases, at the most, with the same exponential power as that of Δ. The result is that the amplitudes of the integrals of equations 27a and 27b have exponential character as κ approaches infinity and decay as

$$\exp[-\mathrm{Im}(\kappa)r] \tag{30}$$

for

$$\mathrm{Im}(\kappa) > 0$$

The integrals can be solved for the plane specified by

$$\mathrm{Re}(\nu_i) > 0$$

$$\mathrm{Re}(\nu_i') > 0$$

for $i = 1, 2, \ldots, n$

By application of Cauchy's theorem: the integral over a closed curve in the complex plane becomes $2\pi i$ times the sum of residues at the poles of the integrand, provided the integrand is analytic inside and on the closed curve except at a finite number of poles.

42. It can be shown that the integrals over an arc for κ at infinity over the positive imaginary half-plane and the loop along the cuts do not contribute to the integral. Therefore the integrals from minus to plus infinity on the real axis are equal to $2\pi i$ times the sum over the residues in the half-plane for $\mathrm{Im}(\kappa) \geq 0$.

43. The integral over the semiarc at infinity provides no contribution because the integrals approach zero exponentially as κ approaches infinity (see expression 30). The integrals along loops from infinity along the cut, around a branch point, and back to infinity do not contribute anything because it can be shown that the integrals have the same values on both sides of the cut: Going from one side of the cut around the corresponding branch point ν_i (or ν_i'), ν_i changes to $-\nu_i$ (or ν_i' to $-\nu_i'$). The value of the integrand will be the same value on both sides of the cut if it can be shown that it is an even function of ν_i and ν_i' . The symmetry of Δ in ν_i and ν_i' will be studied. Let the elements of F , A_m , A_m^{-1}, and D_m be denoted by f_{ab} , $a_{m\,ab}$, $a^{-1}_{m\,ab}$, and $d_{m\,ab}$, respectively. The matrix elements of F then become

$$f_{aj} = \begin{cases} \sum_{b=1}^{4} \sum_{c=1}^{4} \cdots \sum_{i=1}^{4} a_{n}^{ab} d_{n}^{bb} a_{n}^{-1\,bc} \cdots a_{m}^{de} d_{m}^{ee} a_{m}^{-1\,ef} \cdots a_{2}^{gh} d_{2}^{hh} a_{2}^{-1\,hi} a_{1}^{ij} d_{1}^{jj} & \text{for } a = 1, 2 \\ a_{1}^{aj} & \text{for } a = 3, 4 \end{cases} \tag{31}$$

For branch points and the corresponding cuts that originate from any layer, $m = 2, 3, \ldots n$, the variables ν_m and ν'_m appear only in

$$\sum_{e=1}^{4} a_{m}^{de} d_{m}^{ee} a_{m}^{-1\,ef} \tag{32}$$

If ν_m is replaced by $-\nu_m$, columns 1 and 2 of a_m interchange; and if ν'_m is replaced by $-\nu'_m$, columns 3 and 4 interchange:

$$a_{m}^{d1}(-\nu_m) = a_{m}^{d2}(\nu_m)$$

$$a_{m}^{d3}(-\nu'_m) = a_{m}^{d4}(\nu'_m)$$

$$a_{m}^{de}(-\nu_m) = a_{m}^{de}(\nu_m) \quad \text{for} \quad e = 3, 4$$

$$a_{m}^{de}(-\nu'_m) = a_{m}^{de}(\nu'_m) \quad \text{for} \quad e = 1, 2$$

Accordingly

$$d_{m}^{11}(-\nu_m) = d_{m}^{22}(\nu_m)$$

$$d_{m}^{33}(-\nu'_m) = d_{m}^{44}(\nu'_m)$$

$$d_{m}^{ee}(-\nu_m) = d_{m}^{ee}(\nu_m) \quad \text{for} \quad e = 3, 4$$

$$d_{m}^{ee}(-\nu'_m) = d_{m}^{ee}(\nu'_m) \quad \text{for} \quad e = 1, 2$$

and

$$a^{-1}_{m1f}(-\nu_m) = a^{-1}_{m2f}(\nu_m)$$

$$a^{-1}_{m3f}(-\nu'_m) = a^{-1}_{m4f}(\nu'_m)$$

$$a^{-1}_{mef}(-\nu_m) = a^{-1}_{mef}(\nu_m) \quad \text{for} \quad e = 3, 4$$

$$a^{-1}_{mef}(-\nu'_m) = a^{-1}_{mef}(\nu'_m) \quad \text{for} \quad e = 1, 2$$

44. Applying these results to expression 32, it can be seen that the substitution ν_m for $-\nu_m$ changes only the sequence in the summation $e = 1 \leftrightarrow e = 2$ (similarly, substituting ν'_m for $-\nu'_m$ changes the sequence in the summation $e = 3 \leftrightarrow e = 4$) and leaves the value of the sum in expression 32 unchanged. Therefore, Δ is an even function in ν_m and ν'_m for $m = 2, 3, \ldots n$. For the cut resulting from the first layer, the corresponding symmetrics are:

$$a_{1i1}(-\nu_1)d_{111}(-\nu_1) = a_{1i2}(\nu_1)d_{122}(\nu_1)$$

$$a_{1i3}(-\nu'_1)d_{133}(-\nu'_1) = a_{1i4}(\nu'_1)d_{144}(\nu'_1)$$

$$a_{1ij}(-\nu_1)d_{1jj}(-\nu_1) = a_{1ij}(\nu_1)d_{1jj}(\nu_1) \quad \text{for} \quad j = 3, 4$$

$$a_{1ij}(-\nu'_1)d_{1jj}(-\nu'_1) = a_{1ij}(\nu'_1)d_{1jj}(\nu'_1) \quad \text{for} \quad j = 1, 2$$

indicating that $\nu_1 \to -\nu_1$ interchanges columns 1 and 2 of the determinant $\Delta = \mathrm{Det}(F) = \mathrm{Det}(f_{aj})$ and $\nu'_1 \to -\nu'_1$ interchanges columns 3 and 4. Therefore, Δ is an odd function in ν_1 and ν'_1. In the same way the symmetrics of the subdeterminants Δ_{4s}, with $s = 1, 2, 3, 4$, can be determined:

Δ_{4s} is even in ν_m and ν'_m for $m = 2, 3, \ldots n$

and for $m = 1$:

Δ_{4s} is odd in ν_1' for $s = 1, 2$

Δ_{4s} is odd in ν_1 for $s = 3, 4$

$$\Delta_{41}(-\nu_1) = \Delta_{42}(\nu_1)$$

$$\Delta_{42}(-\nu_1) = \Delta_{41}(\nu_1)$$

$$\Delta_{43}(-\nu_1') = \Delta_{44}(\nu_1')$$

$$\Delta_{44}(-\nu_1') = \Delta_{43}(\nu_1')$$

The integrals (equations 27a and 27b) contain the functions κQ and κW . It will be shown that both functions are even in ν_m and ν_m' for $m = 1, 2, 3, \ldots , n$, which proves that the integrals along the loops around the branch points do not contribute to the contour integral. Equations 26a and 26b were:

$$\kappa Q(\kappa)L = (Q_1' + Q_1'') - \nu_1'(S_1' - S_1'')$$

$$\kappa W(\kappa)L = -\nu_1(Q_1' - Q_1'') + \kappa^2(S_1' + S_1'')$$

Using equations 23a and 24, it follows that:

$$-2\pi Q(\kappa) = \frac{(-\Delta_{41} + \Delta_{42}) - \nu_1'(-\Delta_{43} - \Delta_{44})}{\Delta}$$

$$-2\pi W(\kappa) = \frac{-\nu(-\Delta_{41} - \Delta_{42}) + \kappa^2(-\Delta_{43} + \Delta_{44})}{\Delta}$$

are subject to the substitutions $\nu_m \to -\nu_m$ and $\nu_m' \to -\nu_m'$. For $m = 2, 3, \ldots , n$ all functions are even in ν_m and ν_m' resulting in

$$Q(-\nu_m) = Q(\nu_m)$$

$$Q(-\nu'_m) = Q(\nu'_m)$$

$$W(-\nu_m) = W(\nu_m)$$

$$W(-\nu'_m) = W(\nu'_m)$$

Q and W are even functions in ν_m and ν'_m for $m = 2, 3, \ldots n$. For $m = 1$ and $\nu_1 \to -\nu_1$:

$$\Delta \to -\Delta$$

$$(-\Delta_{41} + \Delta_{42}) \to -(-\Delta_{41} + \Delta_{42})$$

$$-\nu_1(-\Delta_{41} - \Delta_{42}) \to \nu_1(-\Delta_{41} - \Delta_{42})$$

$$-\nu'_1(-\Delta_{43} - \Delta_{44}) \to \nu'_1(-\Delta_{43} - \Delta_{44})$$

$$\kappa^2(-\Delta_{43} + \Delta_{44}) \to -\kappa^2(-\Delta_{43} + \Delta_{44})$$

all being odd in ν_1 ; and for $m = 1$ and $\nu'_1 \to -\nu'_1$:

$$\Delta \to -\Delta$$

$$(-\Delta_{41} + \Delta_{42}) \to -(-\Delta_{41} + \Delta_{42})$$

$$-\nu_1(-\Delta_{41} - \Delta_{42}) \to \nu_1(-\Delta_{41} - \Delta_{42})$$

$$-\nu'_1(-\Delta_{43} - \Delta_{44}) \to \nu'_1(-\Delta_{43} - \Delta_{44})$$

$$\kappa^2(-\Delta_{43} + \Delta_{44}) \to -\kappa^2(-\Delta_{43} + \Delta_{44})$$

and being odd in ν'_1 .

45. Because both the denominators and the numerators of Q and W are odd functions, Q and W are even functions in ν_i and ν'_i . Combining the results shows that for all the layers, the loop integrals along the cuts and around the branch points cancel. The residues for poles on the positive imaginary half-plane of κ can be computed as

follows: The numerator, $f(\kappa)$, of the integral is analytic, except for the branch points, and therefore has no poles. The only poles occur for points where the denominator $\Delta(\kappa)$ approaches zero. The residue is then computed to be

$$\text{Res}_{\kappa=\kappa_m}\left[\frac{f(\kappa)}{\Delta(\kappa)}\right] = \left\{\frac{f(\kappa)}{\frac{d[\Delta(\kappa)]}{d\kappa}}\right\}_{\kappa=\kappa_m}$$

and the final solutions for equations 27a and 27b become:

$$q_1(r) = -i\pi L \sum_{m=1}^{\infty} H_1^{(1)}(\kappa_m r)\kappa_m^2 \,\text{Res}_{\kappa=\kappa_m}[Q(\kappa)] \tag{33a}$$

$$w_1(r) = i\pi L \sum_{m=1}^{\infty} H_o^{(1)}(\kappa_m r)\kappa_m \,\text{Res}_{\kappa=\kappa_m}[W(\kappa)] \tag{33b}$$

These results can then be converted to the time domain by multiplying by e^{iwt} as:

$$q_1(r,t) = -i\pi L e^{iwt} \sum_{m=1}^{m=b} H_1^{(1)}(\kappa_m r)\kappa_m^2 \,\text{Res}_{\kappa=\kappa_m}[Q(\kappa)] \tag{34a}$$

$$w_1(r,t) = i\pi L e^{iwt} \sum_{m=1}^{m=b} H_o^{(1)}(\kappa_m r)\kappa_m \,\text{Res}_{\kappa=\kappa_m}[W(\kappa)] \tag{34b}$$

An upper limit (m = b) was placed on the summation process, since at any one frequency, there is a finite number of poles or modes at which a signal can propagate (see paragraph 68).

46. For purely elastic media, there are several poles (or zeros of the determinant $\Delta(\kappa)$) along the real axis, symmetrical around $\kappa = 0$, and several poles that are apparently close to the imaginary axis. If the media are assumed to be slightly viscoelastic, the poles on the negative half of the real κ-axis move slightly into the positive imaginary half-plane. This removes any problem that would occur if the poles were on the real axis, i.e. the integration boundary. Accordingly, the poles from the positive real κ-axis move slightly away from the

real axis into the negative imaginary κ half-plane and, therefore, are clearly outside the closed curve of integration and are not used.

PART III: SIGNAL PREDICTIONS

47. Equations 34a and 34b were written for one frequency component. A more general expression for these equations is given below.

$$A_{\ell p}(r,t) = \sum_{n=-a}^{n=a} \left[\omega_n e^{i(\pi/2)}\right]^{p-1} D_n e^{i\omega_n t} \sum_{m=1}^{m=b} S_{m,n} B_{m,n,\ell} H^{(1)}_{(\ell-1)}(\kappa_{m,n} \cdot r) \qquad (35)$$

where

$A_{\ell,p}(r,t)$ = particle motion, in cm, as a function of range r and time t for ℓ^{th} component and p^{th} derivative

ℓ = 1, 2; 1 for vertical component and 2 for radial component

p = 0, 1, 2; 0 for particle displacement, 1 for particle velocity, and 2 for particle acceleration

r = range from source, m

t = time, sec

n = -a, -a+1, ... -1, 0, +1, +2, ... a-1, a; frequency numbers

ω_n = circular frequency, radians/sec

$i = \sqrt{-1}$

D_n = Fourier coefficient for source signal:

$$D_n = \frac{1}{T}\int_0^T f(t)e^{i\omega t}\, dt$$

T = period of source signal, sec

f(t) = source signal, dynes

m = 1, 2, ... b; mode numbers

$S_{m,n}$ = surface macrogeometry coefficients

$B_{m,n,\ell}$ = source coupling coefficients $= \omega\pi\kappa^2_{m,n} \operatorname{Res}_{\kappa=\kappa_{m,n}} [Q(\kappa)]$

for $\ell = 2$

$= -\omega\pi_{m,n} \operatorname{Res}_{\kappa=\kappa_{m,n}} [W(\kappa)]$

for $\ell = 1$

$H^{(1)}_{(\ell-1)}(\kappa_{m,n} \cdot r)$ = Hankel function (Bessel function of third kind) of first type and order $(\ell-1)$ for argument $(\kappa_{m,n} \cdot r)$

$\kappa_{m,n}$ = wave number for m^{th} mode and n^{th} frequency

48. It should be noted that the more general form of equation 35 makes use of Fourier transforms to widen the scope of problems that can be evaluated. The Fourier transform applied to the single-frequency analysis (equations 34a and 34b) allows the prediction of the seismic wave form resulting from a periodic complex stress function such as would be representative of a man or vehicle target. Further, the single multiplication factor $(i\omega)$ applied to the frequency domain signal allows the prediction of derivatives of time domain functions, and thus particle velocity and acceleration can be made available from equations 34a and 34b in addition to particle displacement. These equations have also been modified to include surface macrogeometry coefficients to allow predictions over macrogeometry features. Preliminary values for the surface macrogeometry coefficients can be estimated from the information presented in paragraph 59 and Appendix A.

49. A computer program has been written to implement the microseismic propagation equation (equation 35). This program, written in FORTRAN IV for the Honeywell-GE (General Electric) 440 computer at WES, can operate in a batch mode or remotely by teletype. Appendix B describes the program.

50. The conceptual steps for prediction of seismic signals are shown in the block diagram in fig. 6. This diagram is a generalization of the actual computational sequence used in the computer program (shown in table B3, Appendix B). The essential steps shown in fig. 6 are used to explain the computational procedures. The procedure is basically composed of two parts: (a) computation of the site coefficients and (b) transformation of the input signal to a predicted signal.

Computation of Site Coefficients

51. The site coefficients that must be determined to predict a signal include (a) wave numbers, (b) source coupling coefficients,

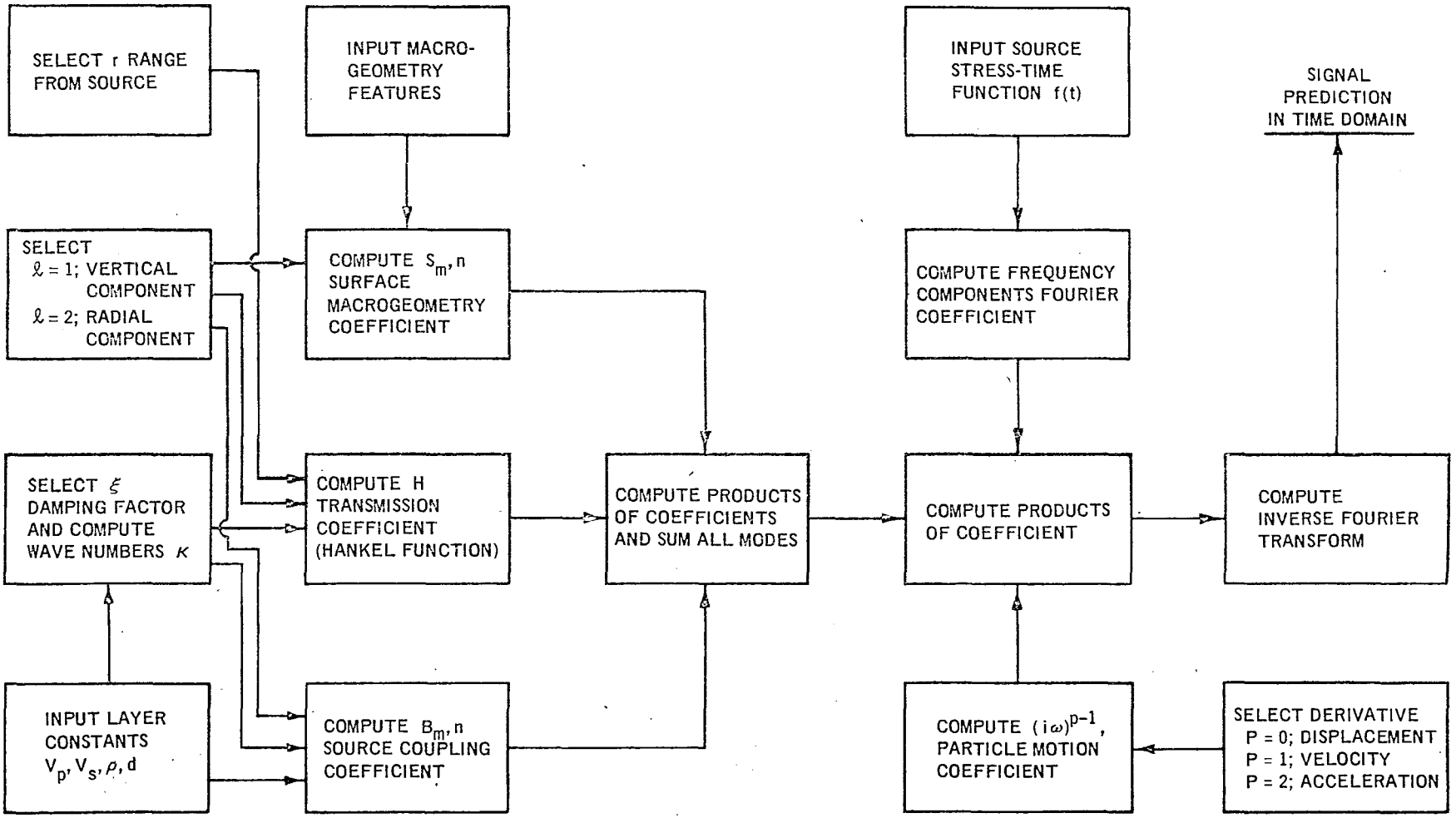

Fig. 6. Block diagram for prediction of seismic signals

(c) Hankel function, i.e. the transmission coefficients, and (d) surface macrogeometry coefficients. After the source coupling, transmission, and surface macrogeometry coefficients are computed, they are combined for each wave number of interest. This is accomplished by taking products of the three coefficients for each frequency and mode and summing the modal results, one sum for each frequency. The following paragraphs discuss the calculation of the site coefficients.

Wave numbers

52. The wave numbers (κ_R) for the frequencies of interest for the Rayleigh modes of propagation are determined by inserting the input layer constants (compression wave velocity α, shear wave velocity β, mass density ρ, and layer depth d) for each site layer into the expression $\Delta(\kappa)$ (see equation 23b) and noting the values of wave numbers for which $\Delta(\kappa)$ approaches zero. If the input layer constants are real (i.e. not complex), then many of the wave numbers for the various Rayleigh wave modes can be real. There can also be complex wave numbers, which indicate that waves propagating under this condition are attenuated with range; their effect on particle motion is normally small except at very near ranges. For complex wave numbers, both the real and the imaginary parts of the determinant $\Delta(\kappa)$ must approach zero. One method for observing the value of $\Delta(\kappa)$ is on a complex map of wave number κ, where the amplitude of z-axis is the value of $\Delta(\kappa)$. If the grid for κ is fine enough, lines for $\mathrm{Re}[\Delta(\kappa)] = 0$ and $\mathrm{Im}[\Delta(\kappa)] = 0$ can be drawn. The zeros are found as points where the two families of lines intersect, and always occur when the lines are at right angles. The cuts between branch points are predictable and can easily be found on the map as lines where the determinant changes sign.

53. The mapping process is too time-consuming for processing large amounts of data. A more practical approach is to use the κ_R values obtained from calculations by elastic theory and account for the viscous damping effects with an associated imaginary part proportional to the real part (i.e. of the form $\kappa_R(1 - i\xi)$, where ξ is the damping factor). To exploit this approach in the solution of practical problems, a computer program to determine the Rayleigh wave dispersion,

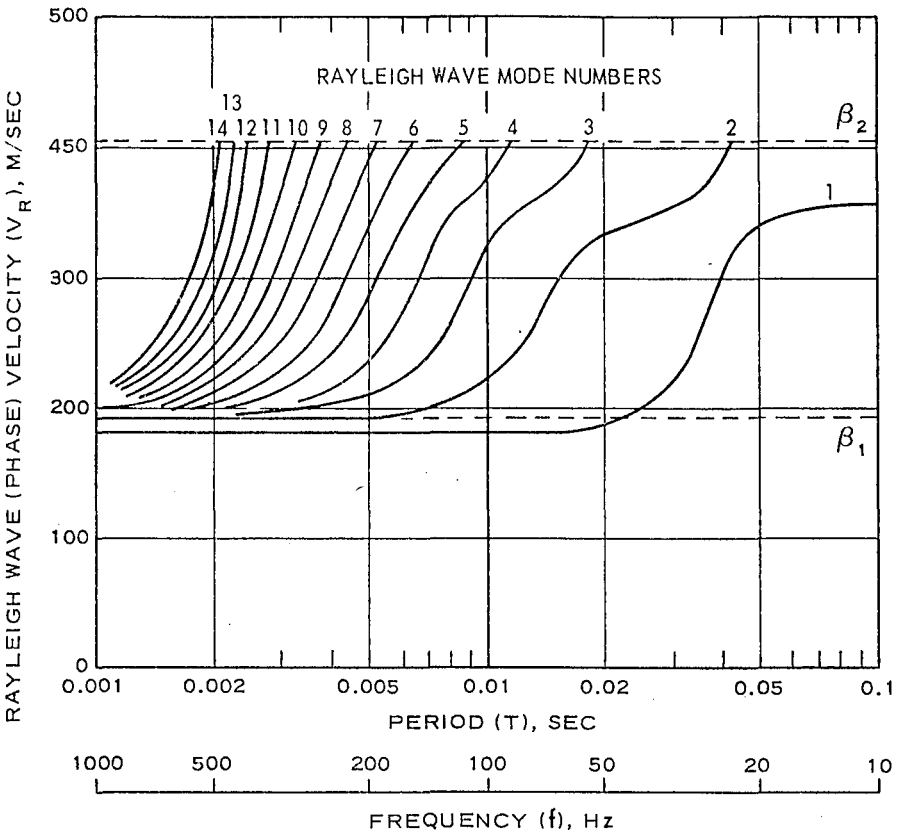

Fig. 7. Rayleigh wave velocity site 319, Panama Canal Zone[11]

i.e. Rayleigh wave velocity as a function of frequency, was used. (See Appendix C for a description of the program.) An example of the results of these calculations is shown in fig. 7. The terrain data used to derive the curves in the figure are as follows:

a. P-wave velocity of the first layer, $\alpha_1 = 488$ m/sec
b. S-wave velocity of the first layer, $\beta_1 = 195$ m/sec
c. Mass density of the first layer, $\rho_1 = 1.433$ g/cm^3
d. Thickness of the first layer, $d = 3.05$ m
e. P-wave velocity of the foundation, $\alpha_2 = 1021$ m/sec
f. S-wave velocity of the foundation, $\beta_2 = 408$ m/sec
g. Mass density of the foundation, $\rho_2 = 1.623$ g/cm^3

54. From the relations shown in fig. 7 the value of κ_R can be determined for each frequency of interest by the relation

$$\kappa_R = \frac{2\pi f}{V_R}$$

where

κ_R = wave number for the Rayleigh wave

f = frequency, Hz

V_R = Rayleigh wave velocity, m/sec

55. It is shown in fig. 7 that as the period increases, the first-mode Rayleigh wave (phase) velocity approaches the Rayleigh wave velocity of a homogeneous half-space made up of the second-layer material. This Rayleigh wave velocity is somewhat less than the shear wave velocity of of the second layer (see fig. 3). As the mode number becomes increasingly larger, the Rayleigh wave velocity increases more rapidly as a function of period. For the higher order modes, a cutoff frequency (that increases with mode number) is reached below which extremely rapid attenuation occurs.[3] As the period decreases, the Rayleigh wave phase velocity for the first mode becomes slightly less than the shear wave velocity in the first layer. For all other modes shown, the Rayleigh wave velocity approaches that of shear waves in the first layer. In this example the wave numbers were calculated from real input layer constants. To use κ_R values in equation 35 such that the effects of viscous damping can be approximated, κ_R must be multiplied by $(1 - i\xi)$, i.e. $\kappa_R(1 - i\xi)$ must be substituted for κ in equation 35, where ξ is the viscous damping factor discussed in paragraph 13. The viscous damping factors typically range from 0.01 to 0.1, and a value of 0.03 has been found to be a good compromise for a wide range of conditions.

Source coupling coefficients

56. The source coupling coefficients are computed by subroutine NDATA (see Appendix B), which essentially solves the following equations:

$$B_{m,n,\ell} = -\omega\pi\kappa_{m,n} \operatorname{Res}_{\kappa=\kappa_{m,n}} [W(\kappa)] \quad \text{for} \quad \ell = 1$$

$$B_{m,n,\ell} = \omega\pi\kappa^2_{m,n} \operatorname{Res}_{\kappa=\kappa_{m,n}} [Q(\kappa)] \quad \text{for} \quad \ell = 2$$

where

$B_{m,n}$ = coupling coefficient for the mth mode and n^{th} frequency

$W(\kappa)$ = amplitude coefficient, vertical component

$Q(\kappa)$ = amplitude coefficient, radial component

The subroutine requires as inputs (a) the layer constants for each layer (α, β, ρ, and d), (b) the wave number for each mode to be used in the calculation, and (c) a value for ℓ to designate the Rayleigh wave motion component (i.e. $\ell = 1$ for vertical component and $\ell = 2$ for radial component).

Transmission coefficients

57. The subroutine HAN2 (Appendix B) is used to compute the transmission (Hankel function) coefficients. The subroutine solves the equation

$$H^{(1)}_{(\ell-1)}(\kappa_{m,n} \cdot r) = J_{(\ell-1)}(\kappa_{m,n} \cdot r) + iN_{(\ell-1)}(\kappa_{m,n} \cdot r)$$

where

$H^{(1)}_{(\ell-1)}(\kappa_{m,n} \cdot r)$ = Hankel function of the first type and order $(\ell-1)$ for argument $(\kappa_{m,n} \cdot r)$

J = Bessel function of the first kind

N = Bessel function of the second kind

ℓ = component of Rayleigh wave motion; $(\ell-1)$ designates the vertical component and $(\ell-2)$ designates the radial component

The argument of the Hankel function is formed from the product of wave number $\kappa_{m,n}$ and range r from the source. It is through the Hankel function that phase shifting and attenuation of the input signal take place, since it is the only coefficient in which the range r is used.

58. For negative values of κ, the Hankel function (Bessel functions of the third kind) can be written as follows:

a. For the vertical component

$$H^{(1)}_{o}(\kappa \cdot r) = J_{o}(|\kappa \cdot r|) + iN_{o}(|\kappa \cdot r|)$$

b. For the radial component

$$H_1^{(1)}(\kappa \cdot r) = J_1(|\kappa \cdot r|) - iN_1(|\kappa \cdot r|)$$

The Bessel functions are shown in fig. 8; fig. 8a shows the J and N functions for real arguments and fig. 8b shows the Hankel function $H_o^{(1)}(\kappa \cdot r) = Me^{iX_o}$ for a complex argument ($\kappa \cdot r = X + iY$). Note that when $Y = 0$, figs. 8a and 8b show identical information.

Surface macrogeometry coefficients

59. Signal predictions made to date have been based on the assumption that the Rayleigh waves are traveling through a medium with a

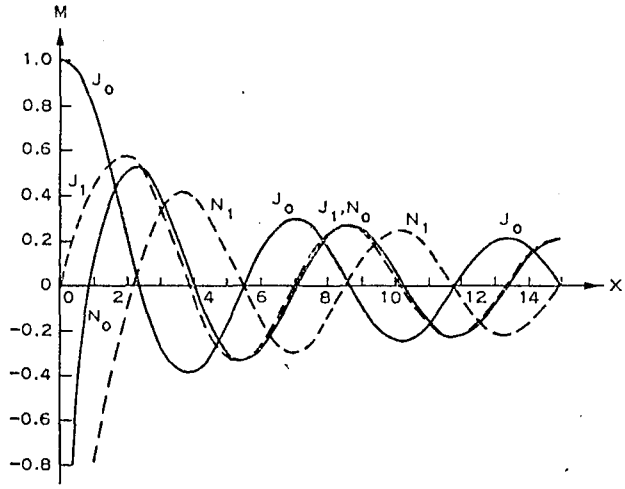

a. $J_o(x)$, $N_o(x)$, $J_1(x)$, $N_1(x)$

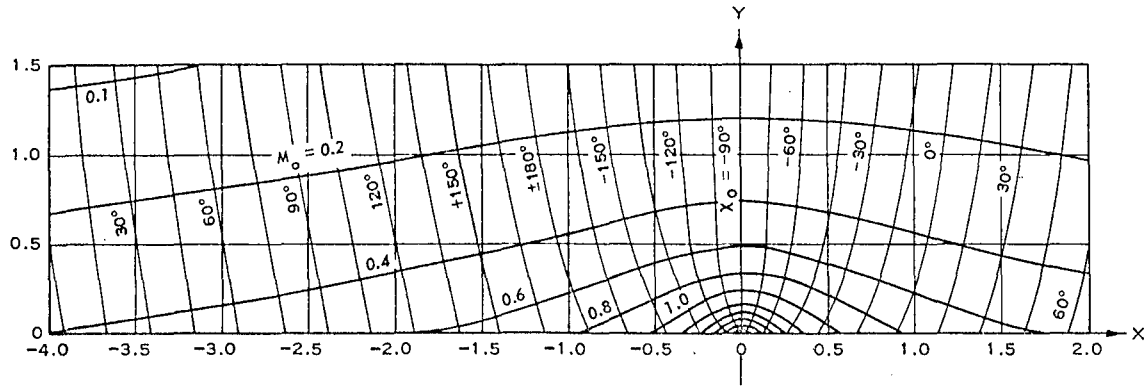

b. CONTOUR LINES OF THE MODULUS AND PHASE OF THE HANKEL FUNCTION $H_o^{(1)}(X + iY) = Me^{iX_o}$

Fig. 8. Bessel functions

smooth surface boundary. For this case the surface macrogeometry coefficients are defined as being equal to 1. If the surface boundary has features with geometric dimensions comparable to that of a propagating wavelength, the signal will experience a change in amplitude. During the development of the model, no attempt was made to derive experimental or theoretical solutions for the effects of surface geometry on Rayleigh waves; however, some solutions were found in the literature. One of the solutions shows how a wedge reduces the amplitude of a surface wave. Part of the wave is reflected at the break in slope, and a part is transmitted. The square of the macrogeometry transmission coefficient is shown plotted in fig. 9, where χ is the angle of the change in slope and σ is Poisson's ratio. The corresponding phase change of the wave is shown in fig. 10. Fig. 11 shows theoretical and experimental results for the macrogeometry transmission coefficients when the surface wave negotiates a step in surface elevation; the macrogeometry coefficients are plotted versus $\omega H/\beta$, where ω is a circular frequency, H the step height, and β the shear wave velocity of the homogeneous medium.

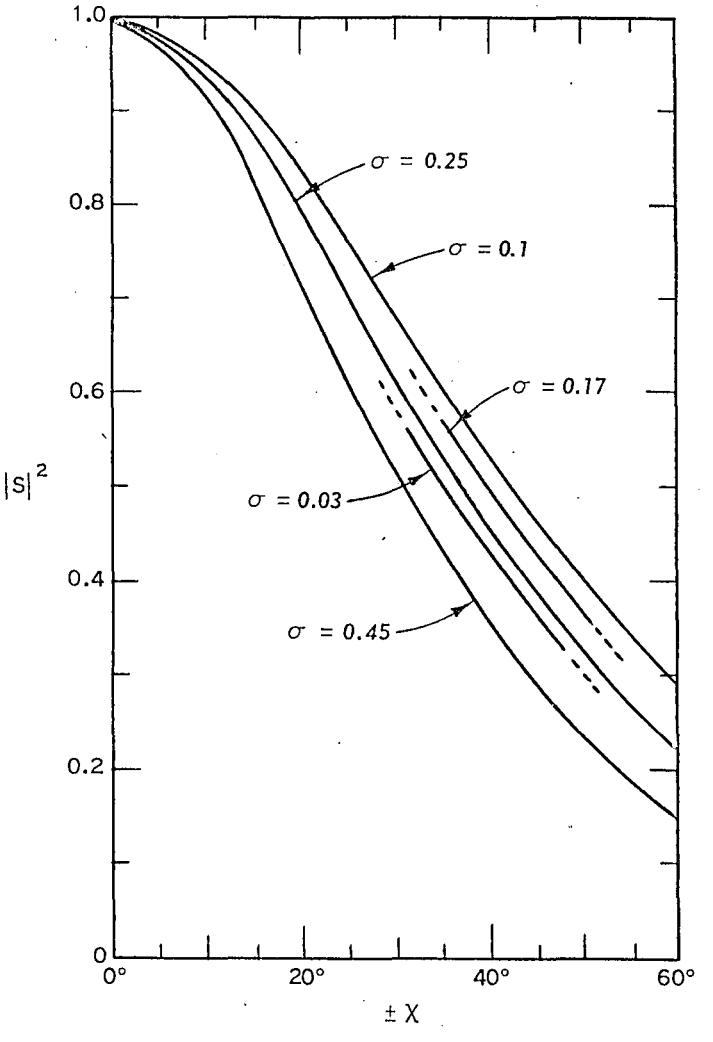

Fig. 9. Absolute square of macrogeometry transmission coefficient S, an even function of wedge angle χ (from reference 12)

60. These solutions and others found in the literature can be used for

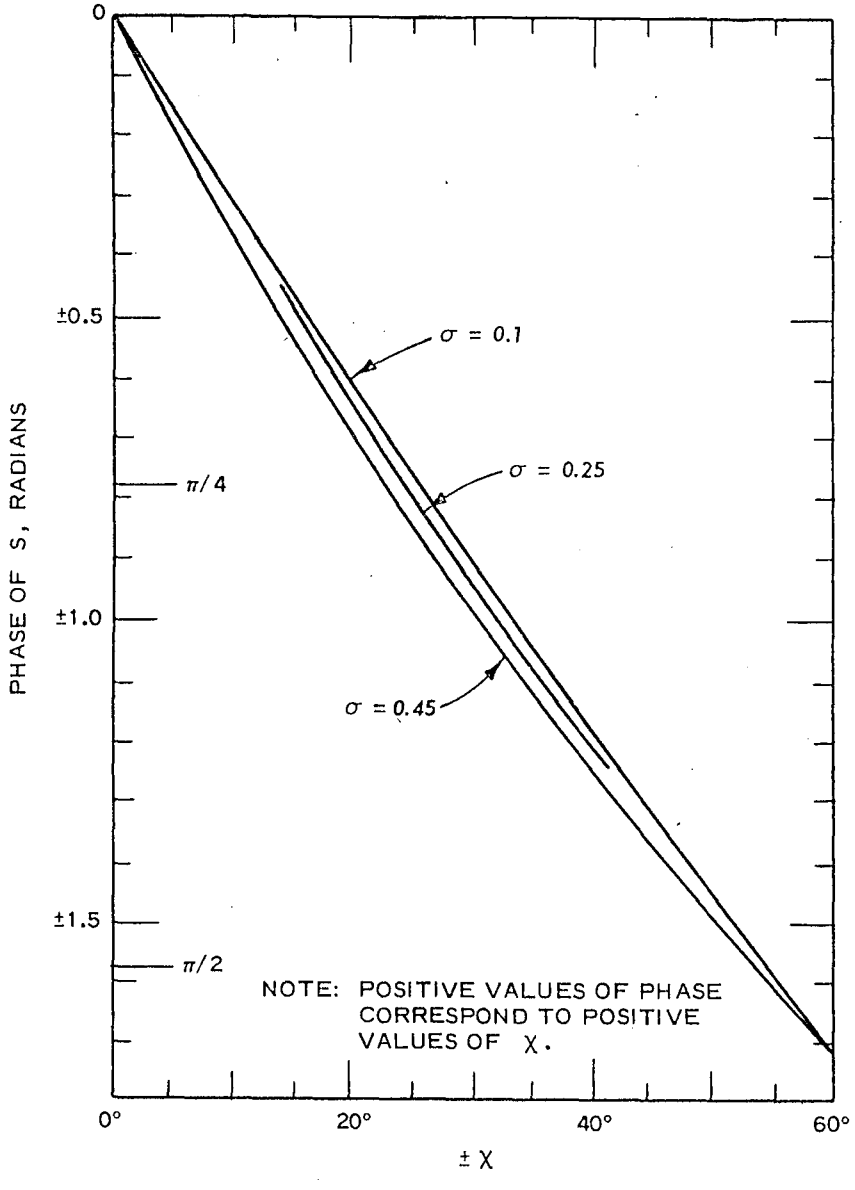

Fig. 10. Phase of $S(\chi,\sigma)$, an odd function of wedge angle χ (from reference 12)

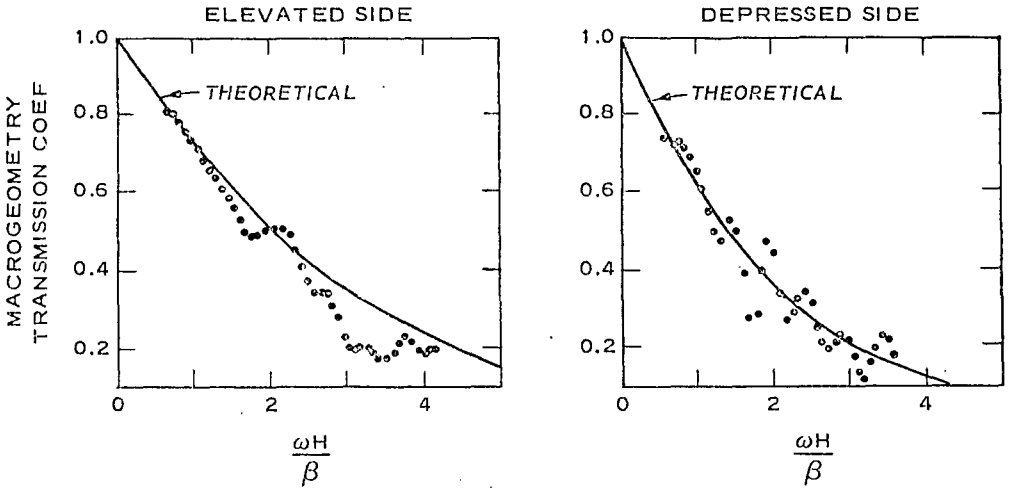

Fig. 11. Theoretical and experimental macrogeometry transmission coefficients for waves incident from elevated and depressed sides of step (from reference 13)

prelimimary values of the factor $S_{m,n}$ in equation 35. It should not be expected that sufficient information is available to estimate values of S_m for all the terrain features found in nature. A considerable amount of effort was devoted to searching out the relevant information in the literature. The results of this work are described in more detail in Appendix A. Study of Appendix A reveals that solutions exist for only a very few geometric shapes, i.e. wedges, steps, and ditches. For this reason additional research is needed to assess the effects of surface macrogeometry on the propagation of Rayleigh waves.

Signal Transformation

61. The site coefficients described above are used with a stress-time function and particle motion coefficients to arrive at a prediction of particle velocity, particle displacement, or particle acceleration (see fig. 6). The method or sequence in which this is accomplished is discussed below.

Stress-time function

62. The input signal consists of a stress-time function and describes the force applied at a point by some stimulus. The stimulus can

be an uncontrolled source, such as footsteps applied to the surface of the ground or a vehicle traveling over the terrain, or it can be a controlled source, such as a precision hammer drop in which a mass drops a predetermined distance to impact the ground.

63. Once the stress-time history is defined, the frequency components are computed by the Fourier transform method (computer subroutines FTT and RFFT, Appendix B). If the stress-time function is periodic, the Fourier transform can be reduced from calculations on the entire stress-time history to calculations on data during one period. In general, the signal to be analyzed will be a numerical description of the stress-time history (not a mathematical function), so a solution of the Fourier integral can be approximated by numerical integration. There are several techniques for doing this. They all require that the signal be digitized at a rate such that there are at least two sample points for the highest frequency component of interest in the stress-time function. The frequencies chosen in the Fourier transform must, of course, be compatible with the frequencies of the combined site coefficients. Methods for determining the stress-time history for targets of military interest are being developed. A general solution will require that separate subroutines or computer programs be developed to provide the stress-time signal as a function of source and surface and substrata conditions. In the examples to follow in Part IV, the specific stress-time histories used will be described.

Particle motion coefficients

64. The stress-time function and the site coefficients are combined to arrive at a prediction of a signal of particle motion versus time at some range r. If the particle displacement or acceleration is desired, a simple particle motion coefficient can be generated, which, when applied in the frequency domain, gives the proper signal in the time domain. The coefficient is the value of $\left(\omega e^{i\pi/2}\right)^{P-1}$. When $P = 0$, the time domain signal is particle displacement; when $P = 1$, the time domain signal is particle velocity; and when $P = 2$, the time domain signal is particle acceleration. This ability to take derivatives and

integrals in the time domain by simply multiplying and dividing by the factor ($i\omega$) is one of the basic properties of Fourier transforms.

Signal formation

65. To arrive at a predicted signal in the time domain, the inverse Fourier transform must be taken (computer subroutines INFTT and INRFFT, Appendix B) of the product of the combined site coefficients, the stress-time Fourier coefficients, and the particle motion coefficients. This time domain signal is repetitive as a result of the periodic input source.

PART IV: EXAMPLE OUTPUTS OF THE MODEL

66. To illustrate some of the key outputs of the model, i.e. computation of the wave numbers, source coupling coefficients, transmission coefficients, and seismic signal predictions, and to show the effects of changing the values of some of the inputs to the model on the predicted signal, data from WES study site 319 were selected as inputs. Also data from WES study site 341 were used to illustrate the capability of matching predicted signals with field-measured ones. The two sites were in diverse geographical locations: Site 319 was in the Alpha Grid in the Panama Canal Zone[11] and site 341[14] was in the East Range at Fort Huachuca, Arizona.

Coefficients for WES Study Site 319

67. The following paragraphs discuss the results using the data from site 319, which are tabulated below.

a. P-wave velocity of first layer, $\alpha_1 = 488$ m/sec

b. S-wave velocity of first layer, $\beta_1 = 195$ m/sec

c. Mass density of first layer, $\rho_1 = 1.433$ g/cm^3

d. Thickness of first layer, $d = 3.05$ m

e. P-wave velocity of foundation, $\alpha_2 = 1021$ m/sec

f. S-wave velocity of foundation, $\beta_2 = 408$ m/sec

g. Mass density of foundation, $\rho_2 = 1.623$ g/cm^3

h. Viscous damping coefficient, $\xi = 0.03$ or 0

Wave numbers

68. Using the information above, the wave numbers for Rayleigh modes 1, 2, and 3 were calculated as discussed in paragraphs 52-55, and are shown in fig. 12. The first mode is the primary mode of propagation and a value for Rayleigh wave phase velocity can be found at all frequencies. Waves at the higher order modes do not propagate efficiently at the lower frequencies, and thus the Rayleigh wave phase velocities are specified for the upper frequency range. There are, of course, many more high-order modes (including complex modes) that could be used

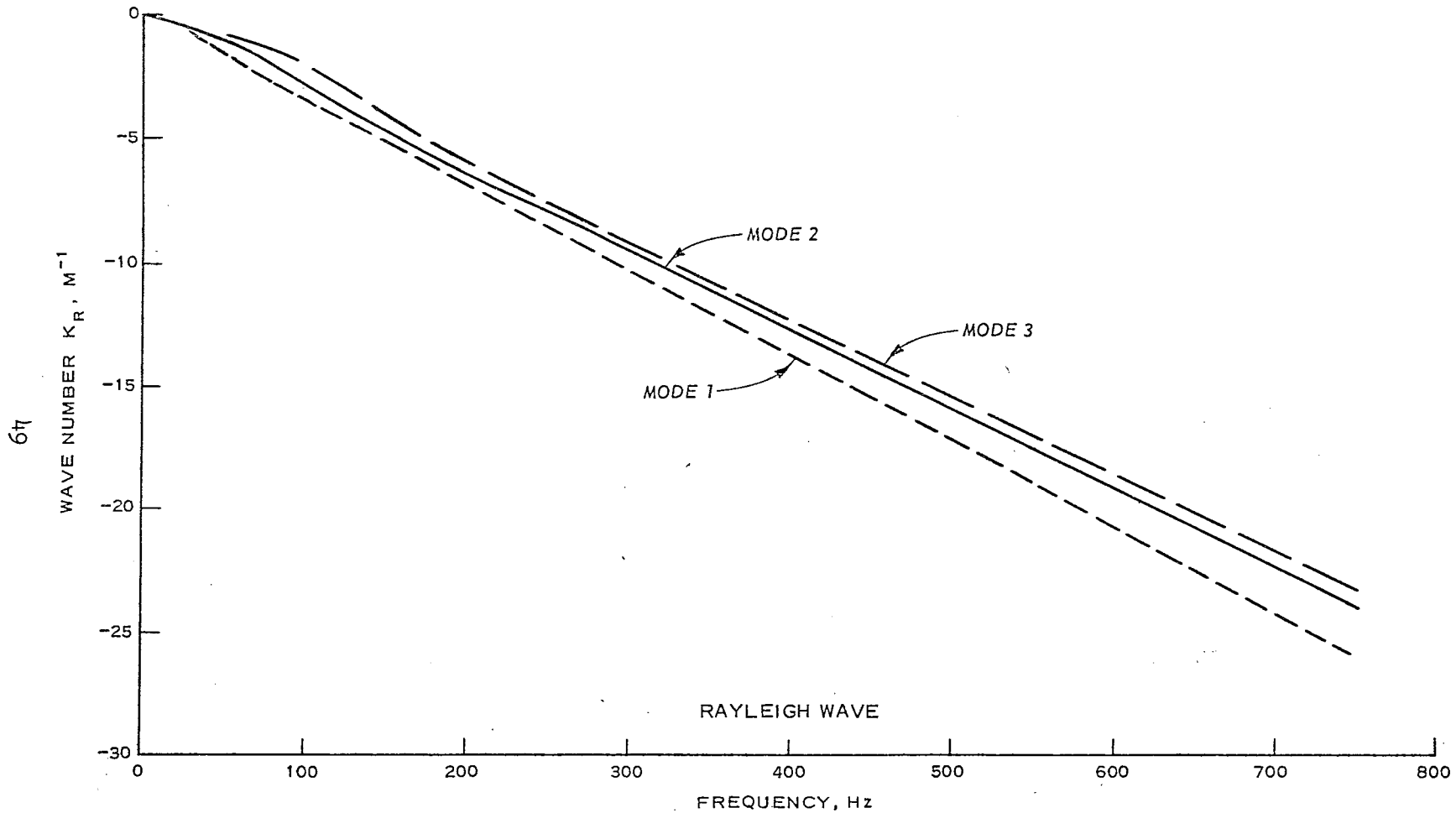

Fig. 12. Wave number versus frequency for site 319, Alpha Grid, Panama Canal Zone

in the prediction, but since the cutoff frequency (paragraph 55) increases correspondingly, their contribution to predicted signals becomes very small. This is especially true when attenuation is considered, and the amplitudes at high frequencies are found to be reduced at a greater rate with range than those at low frequencies. Note that since only real site properties are used for this example, the calculated wave number is not complex. The κ_R factor must be modified with a damping coefficient if viscous damping effects are to be accounted for in ε prediction (see paragraph 53). For the prediction for site 319 a damping coefficient ξ of zero (i.e. elastic condition), or 0.03, was used.

Coupling coefficients

69. Using the site properties and the wave number information, the coupling coefficients were calculated for the vertical and radial components for modes 1, 2, and 3 (paragraph 56), and are shown in fig. 13. These coefficients were calculated with complex values (the damping factor $\xi = 0.03$) and are, therefore, the values one would expect for a viscoelastic system. For comparison, the effects of coupling coefficients computed for elastic values (i.e. $\xi = 0$) are demonstrated on predicted signals using the fundamental mode only (see paragraph 71).

70. Vertical component. Fig. 13 shows the mode 1 curve of coupling coefficient versus frequency (0-200 Hz) for the viscoelastic system for both real and imaginary components. For this example, the real part is a nonsmooth function that increases in the negative direction with increasing frequency. The imaginary part of the curve has absolute values much less than the real part and is positive for all frequencies except at about 43 Hz. For mode 2, amplitudes are shown for the 23.26- to 200-Hz frequency band for both the real and imaginary parts. The absolute values of the coupling coefficient are much less for mode 2 than for mode 1. From 23.26 to about 100 Hz the real part of the function increases in the negative direction. The imaginary part is nearly zero through most of the frequency range, but assumes relatively large values from about 60 to 110 Hz. For mode 3 the coupling coefficients are shown for the 52.63- to 200-Hz frequency band. The real part of

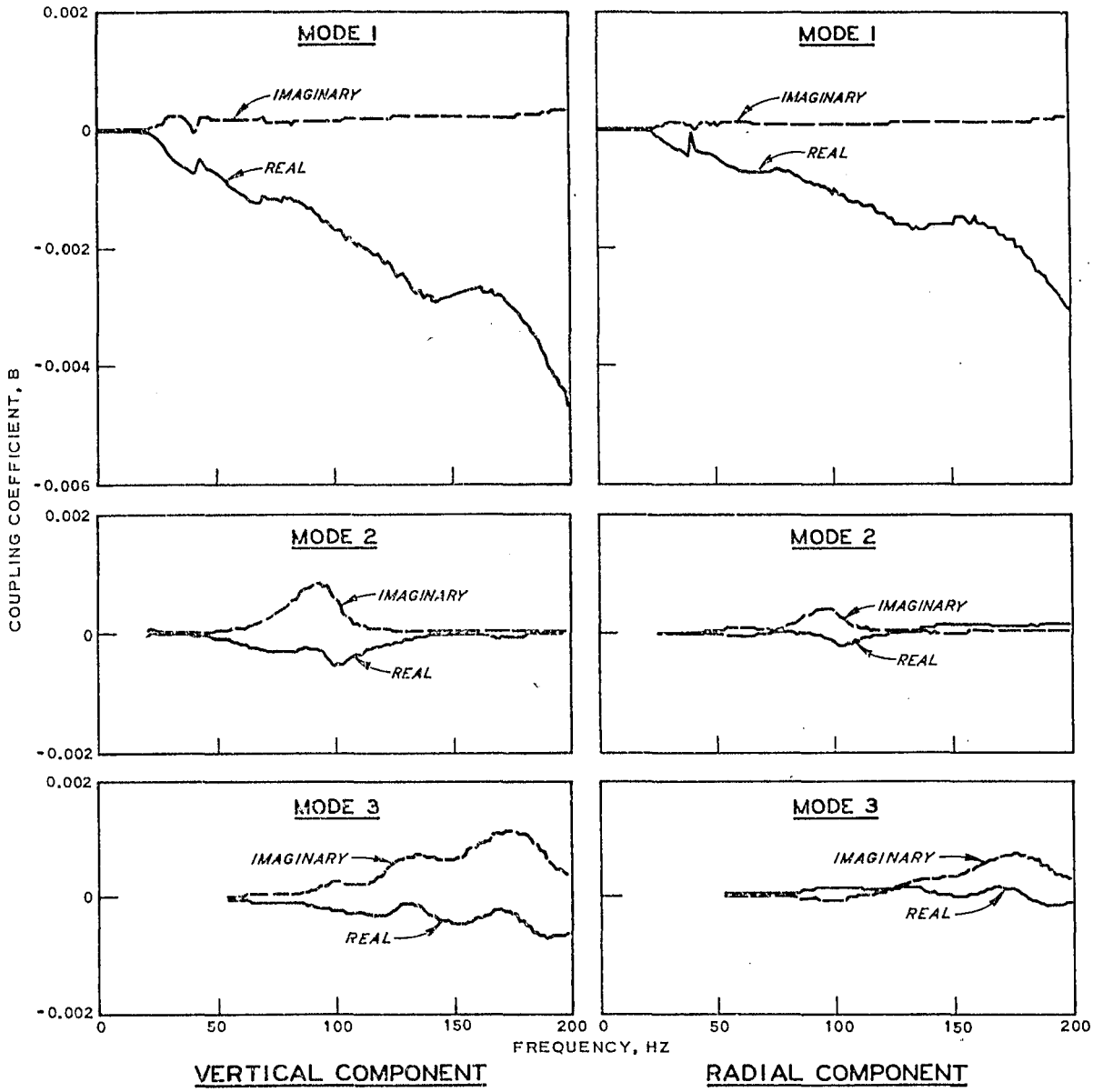

Fig. 13. Source coupling coefficients (viscoelastic) for site 319

the curve is negative, whereas the imaginary part is positive and has absolute values that are higher than the real values.

71. Radial component. In general, for this example the radial component of the coupling coefficient follows approximately the same trends as the vertical component (fig. 13). However, the absolute magnitude is consistently less. In both the vertical and radial components, the largest absolute values of the coupling coefficient were computed for mode 1. Also, mode 1 had values throughout the total frequency range shown (0-200 Hz), whereas modes 2 and 3 had values from 23.26 and 52.62 Hz, respectively, to 200 Hz. The fundamental mode (mode 1) is the mode that couples the majority of the energy to the propagating medium. This, in addition to the fact that many soils propagate only relatively low-frequency seismic energy efficiently, suggests that for many practical problems only the fundamental propagation mode need be considered.

Transmission coefficients (Hankel function)

72. The transmission coefficients were computed as discussed in paragraphs 57-58. The real and imaginary transmission coefficients for this example (site 319 data and a range r of 10 m computed using the subroutine HAN2, Appendix B) are shown in fig. 14.

Signal Predictions for WES Study Site 319

73. With the site coefficients obtained for site 319, as discussed in the preceding paragraphs, the radial and vertical components of particle velocity were computed for a viscoelastic medium using four different force-time histories. The input signals, their Fourier transforms, and the predicted seismic signals are shown in fig. 15 and are discussed in the following paragraphs.

Input stress signals, time domain and frequency domain

74. Four different stress-time curves were used as input signals for this site. The time domain signals are shown in fig. 15 and are

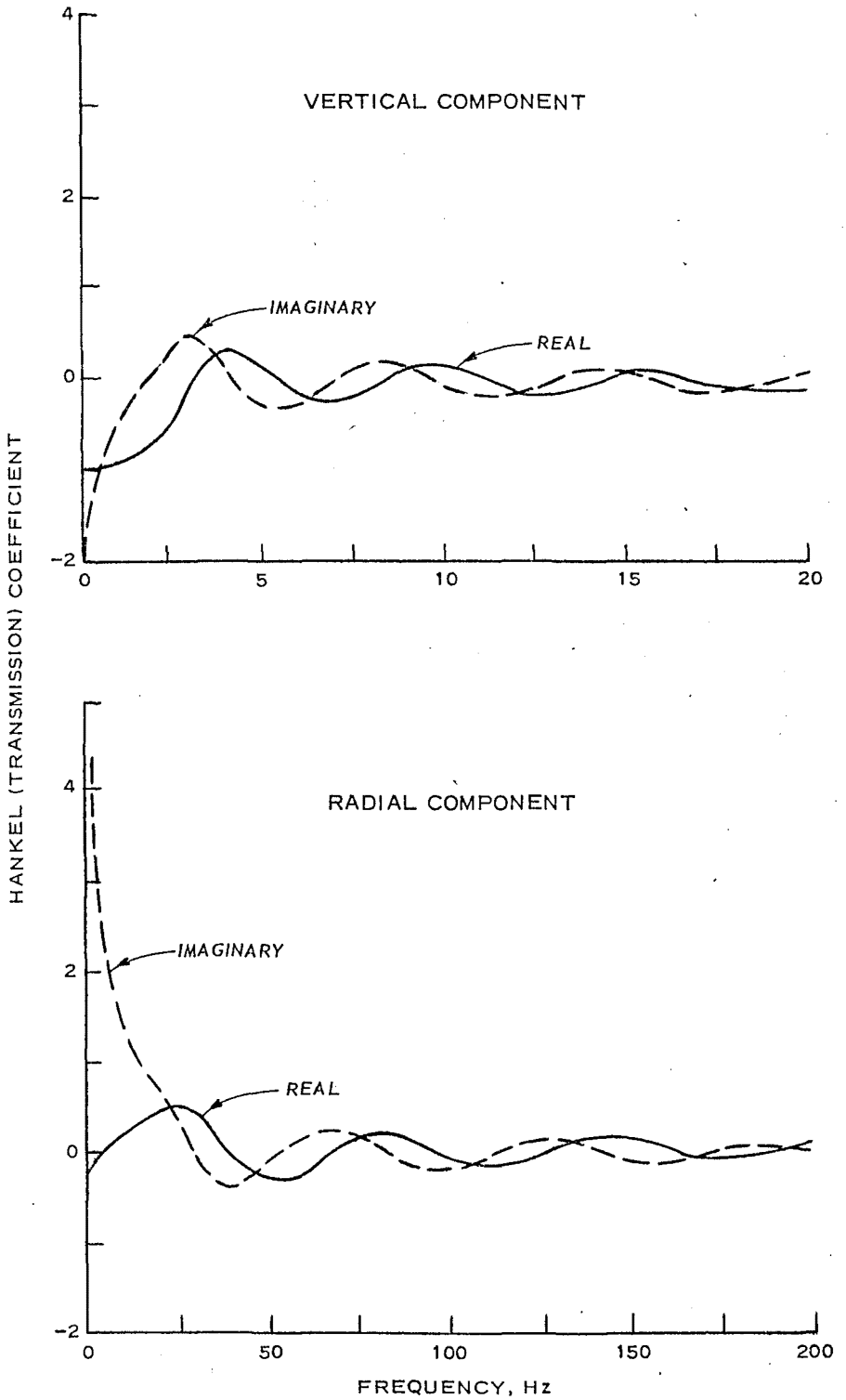

Fig. 14. Hankel (transmission) coefficients for site 319 at r = 10

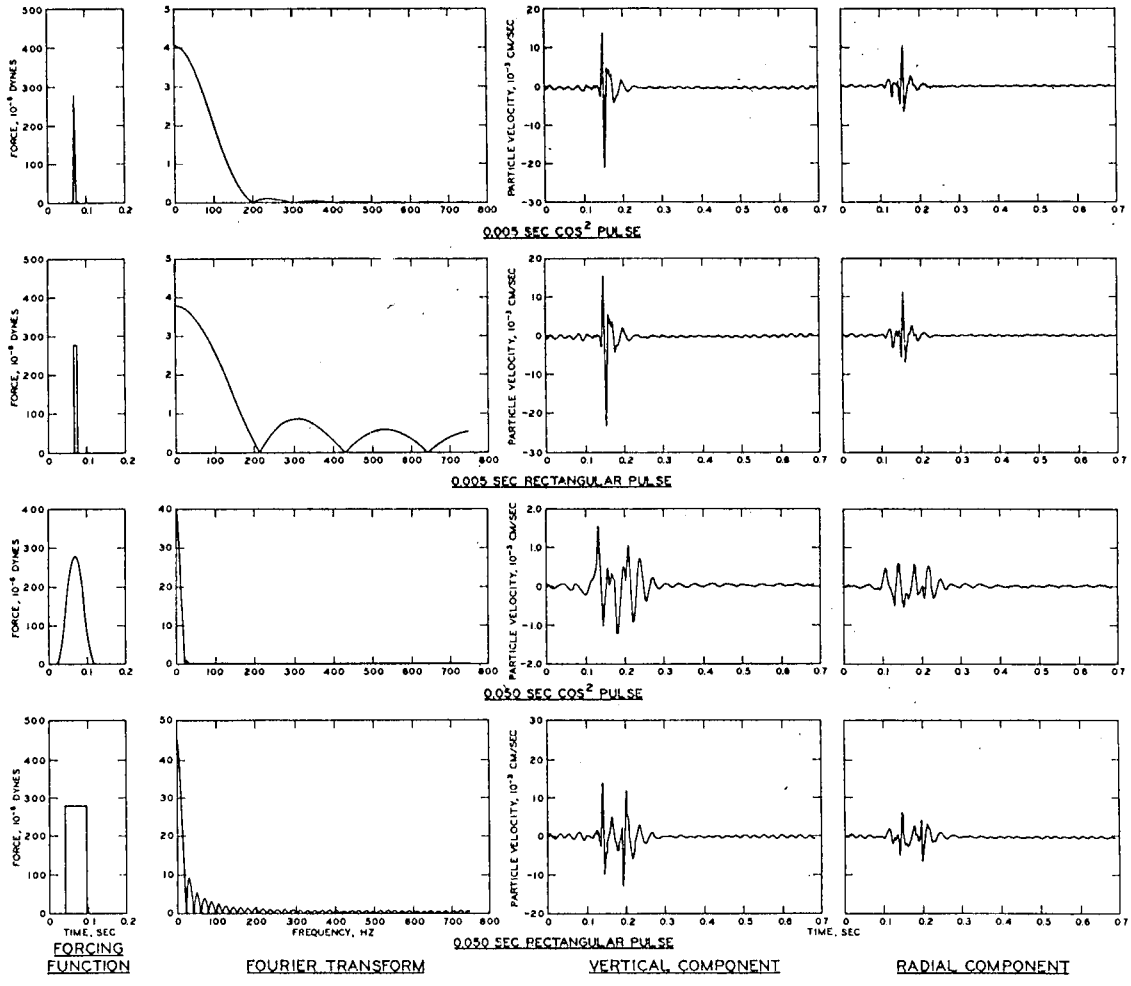

Fig. 15. Stress signals (time domain and frequency domain) and corresponding predicted particle velocity signals (vertical and radial components) for site 319 viscoelastic coupling coefficients, $\xi = 0.03$, $r = 10$ m

(from top to bottom): (a) a cosine-squared pulse 0.005 sec wide, (b) a rectangular pulse 0.005 sec wide, (c) a cosine-squared pulse 0.050 sec wide, and (d) a rectangular pulse 0.050 sec wide. All the pulses had peak amplitudes of 277×10^6 dynes. The variations were chosen to show the extremes of functions that might represent a footstep signal. The pulse-width variation of 0.005-0.050 sec will, under most circumstances, bracket the duration of a footstep. The variation from a cosine-squared pulse to a rectangular pulse should cover the extremes of shapes caused by the differences in loading rates.

Fourier transforms

75. The Fourier spectrum (i.e. stress signal in the frequency domain) for each of the pulses is shown in fig. 15. The narrow pulses contain higher frequencies than the wider pulses. Also, the rectangular pulses have higher amplitudes at high frequencies than the cosine-squared pulses.

Output signals, multimode predictions

76. The vertical and radial components of particle velocity were predicted for site 319 at a range of 10 m using the first three Rayleigh propagation modes. The results are shown in fig. 15; the root mean square (rms) and peak amplitudes and spans are summarized below:

		Particle Velocity, 10^{-3} cm/sec	
		Vertical Component	Radial Component
Input:	cosine-squared T = 0.005 sec $F_{max} = 277 \times 10^6$ dynes		
Output:	rms amplitude	1.810	0.969
	peak amplitude	14.123	10.220
	span	34.815	16.760
Input:	rectangular pulse T = 0.005 sec $F_{max} = 277 \times 10^6$ dynes		
Output:	rms amplitude	1.992	1.062
	peak amplitude	15.939	11.368
	span	38.980	18.373

(Continued)

		Particle Velocity, 10^{-3} cm/sec	
		Vertical Component	Radial Component
Input:	cosine-squared pulse T = 0.050 sec F_{max} = 277 × 10^6 dynes		
Output:	rms amplitude	0.280	0.144
	peak amplitude	1.544	0.596
	span	2.759	1.155
Input:	rectangular pulse T = 0.050 sec F_{max} = 277 × 10^6 dynes		
Output:	rms amplitude	1.951	1.027
	peak amplitude	13.995	6.284
	span	26.788	12.577

The following definitions apply:

a. T = source pulse width at an amplitude of one-half the peak of maximum value.

b. F_{max} = the maximum value of the force pulse.

c. Output rms amplitude = the square root of the sum of the squares of the Fourier coefficients for the particle motion curve.

d. Output peak amplitude = the highest positive value in the particle motion curve.

e. Output span = the range between the highest positive value and the lowest negative value in the particle motion curve.

77. The curves in fig. 15 show that both 0.050-sec force-time signals gave predicted signals of longer duration than the 0.005-sec force-time signals. Also, the radial component had less amplitude than the vertical component. Further, the 0.050-sec cosine-squared force-time signal generated a very low amplitude signal in comparison with the other three input signals. From the data tabulated in the preceding paragraph, it can be seen that the input signals of short duration generated vertical component signals whose spans were greater (i.e. 34.8 and 38.9 compared with 2.7 and 26.8 for the cosine-squared and rectangular signals, respectively) than those of the signals of longer duration. Also the 0.050-sec rectangular pulse generated vertical component rms and peak amplitude values that were about the same as the corresponding

values generated for both of the 0.005-sec input signals. The vertical component of the seismic signal predicted for the 0.050-sec cosine-squared pulse is very low in amplitude, as would be expected. For example, this force-time trace represents a slow, smoothly applied load similar to that resulting from a man creeping. Field test results have shown that a man creeping generates very little seismic energy.

Single-mode predictions

78. The multimode predictions are more correct than single-mode predictions; however, the computations required to consider more than one mode are much more complex. Since the amplitudes of the source coupling coefficients were generally small for the higher order modes compared with those for the fundamental mode, it was believed that the predicted signals might be sufficiently defined using the fundamental mode responses alone to study many classes of problems. For example, the relative effect of the damping and coupling coefficients on the attenuation and dispersion of the Rayleigh wave could be studied using the simplified computations if the predictions were sufficiently accurate.

79. The fundamental and multimode predictions for site 319 at 10 m are compared in fig. 16. These results, which are typical of many analyzed, show that the fundamental mode retains the basic wave form obtained using the multimode calculations; however, the amplitude is commonly reduced.

80. Although the single-mode and multimode predictions do not yield identical results, it was believed that they were sufficiently similar to allow the use of the fundamental mode prediction for studying the trends emerging in the predicted signal resulting from changes in the damping and coupling coefficients and the input stress-time function. To illustrate these changes the four input signals shown in fig. 15 were used. For each input signal the following combination of damping and coupling coefficients were input into the model to study the effect of the predicted particle motion signal.

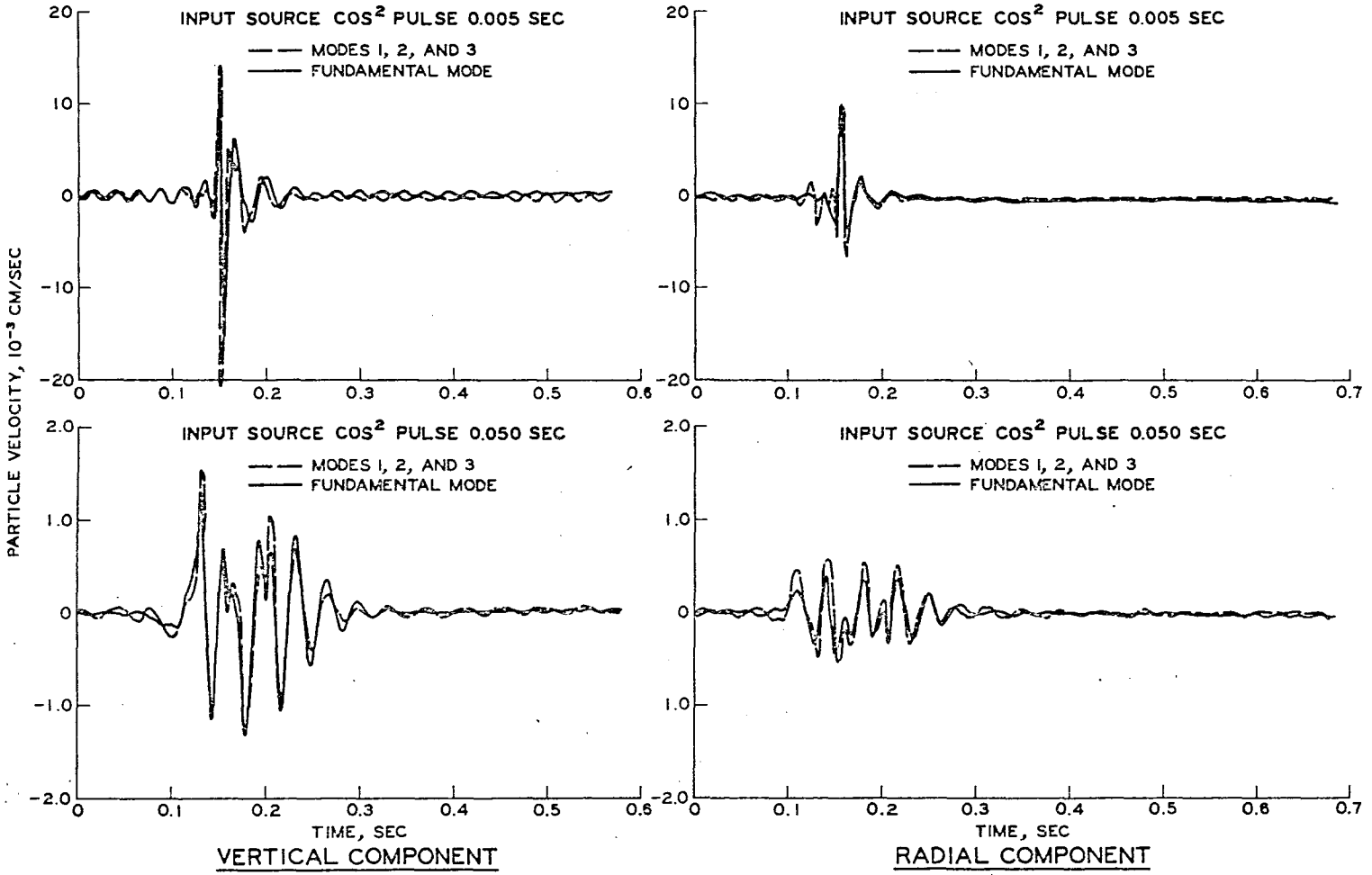

Fig. 16. Comparison of fundamental and multimode predictions, site 319 viscoelastic coupling coefficients, $\xi = 0.03$, $r = 10$ m

Force-Time Function	Damping Coefficient, ξ	Coupling Coefficient, B	Fig. No.
Cosine-squared pulse, 0.005 sec	Elastic	Elastic	17
	0.03	Viscoelastic	
	0.03	Elastic	
Cosine-squared pulse, 0.050 sec	0.03	Viscoelastic	
	0.03	Elastic	18
Rectangular pulse, 0.005 sec	Elastic	Elastic	
	0.03	Elastic	
Rectangular pulse, 0.050 sec	0.03	Elastic	19

Table 1 gives a summary of peak and rms amplitudes and spans of the fundamental mode predictions.

81. The predicted waves have characteristics that are somewhat similar throughout the prediction ranges of 5, 10, 20, 30, and 40 m. As the range increases, the travel time of the wave from the source increases. Since each set of curves has a common time reference, the group velocity of the waves can be calculated by observing the delay time as the range increases (see figs. 17-19).

82. The effects of dispersion as the range increases can be seen in figs. 17-19 by the increase in pulse width with increasing range. Dispersion is caused by the differences in velocities of the frequency components in the propagating waves. The approximate pulse length of the input signal can be identified by noting the pulse length of the predicted signal even in the presence of dispersion (compare data in fig. 17 with those in fig. 18; also see fig. 19). In general, a long input signal gives a long output signal, and a short input gives a correspondingly shorter output. The output shapes will vary, however, at different ranges and with differing input pulse shapes.

83. There are obvious differences between the curves of radial and vertical particle motion and between the curves of particle displacement and particle velocity (and in particle acceleration if these curves are computed). In all the curves calculated in this study, the vertical component was larger than (up to twice as large as) the radial component (see figs. 15, 16, and 20). This would probably not be true

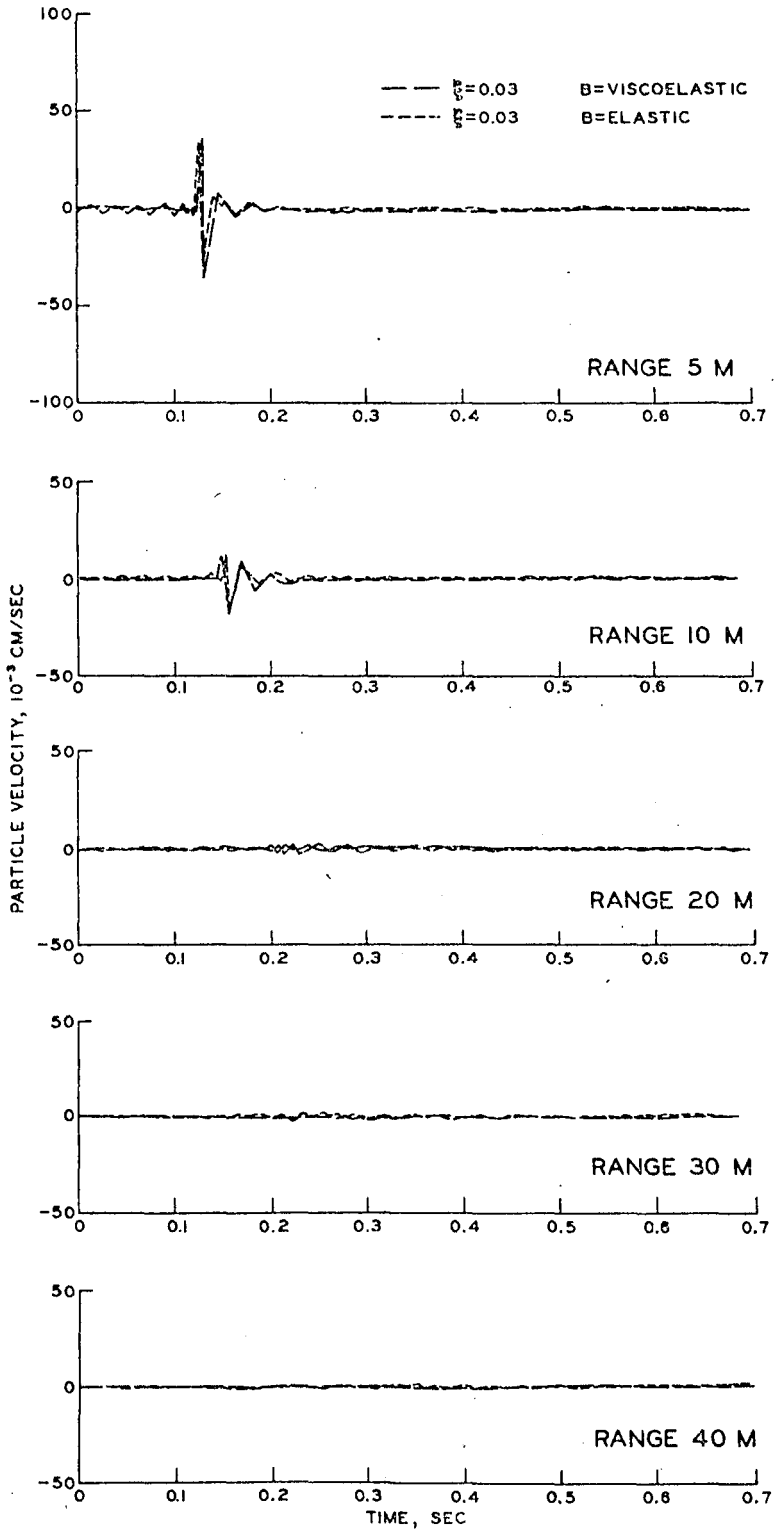

Fig. 17. Effects of damping and coupling coefficients on fundamental mode predictions, vertical component. Site 319, input source cosine-squared pulse 0.005 sec (sheet 1 of 2)

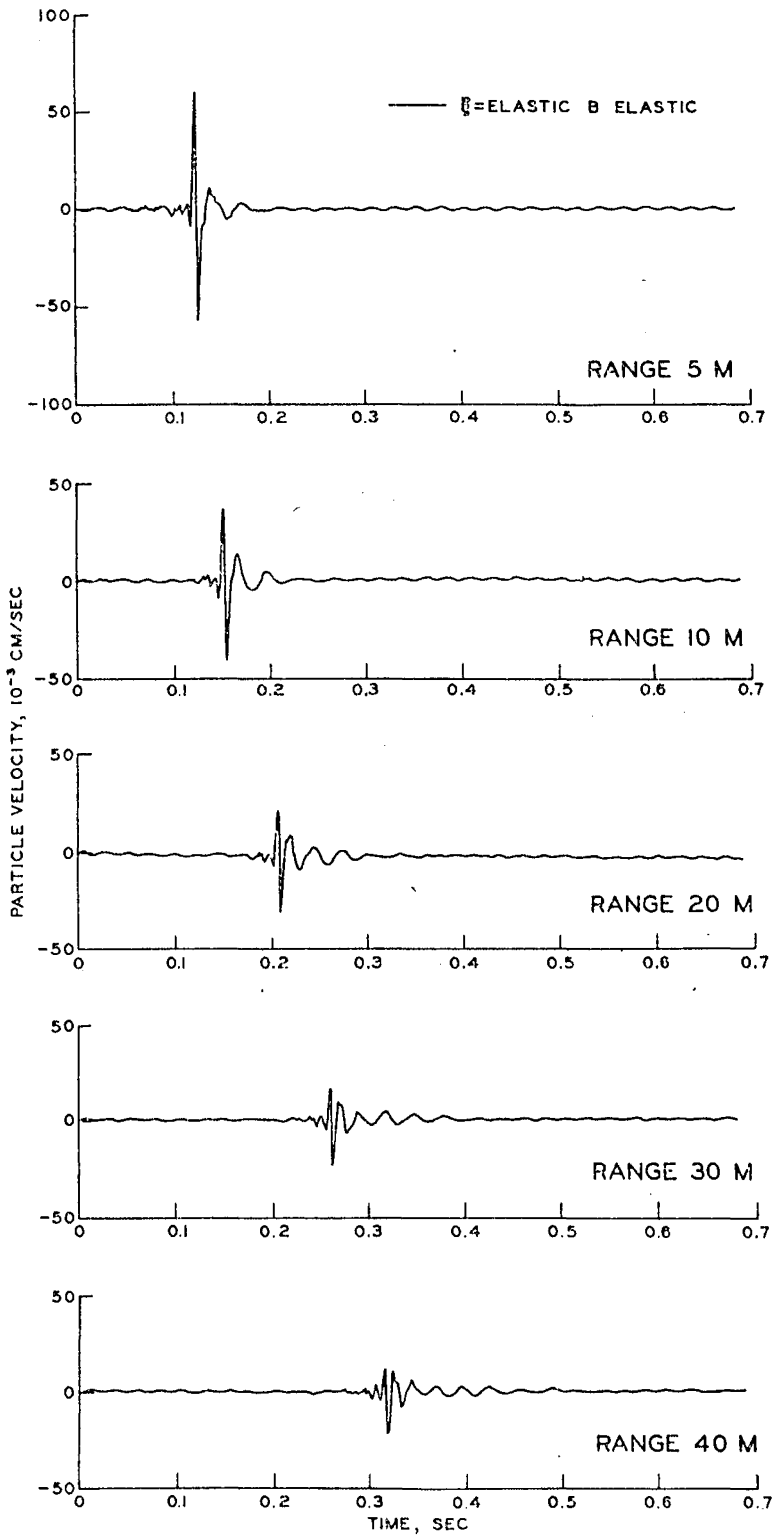

Fig. 17 (sheet 2 of 2)

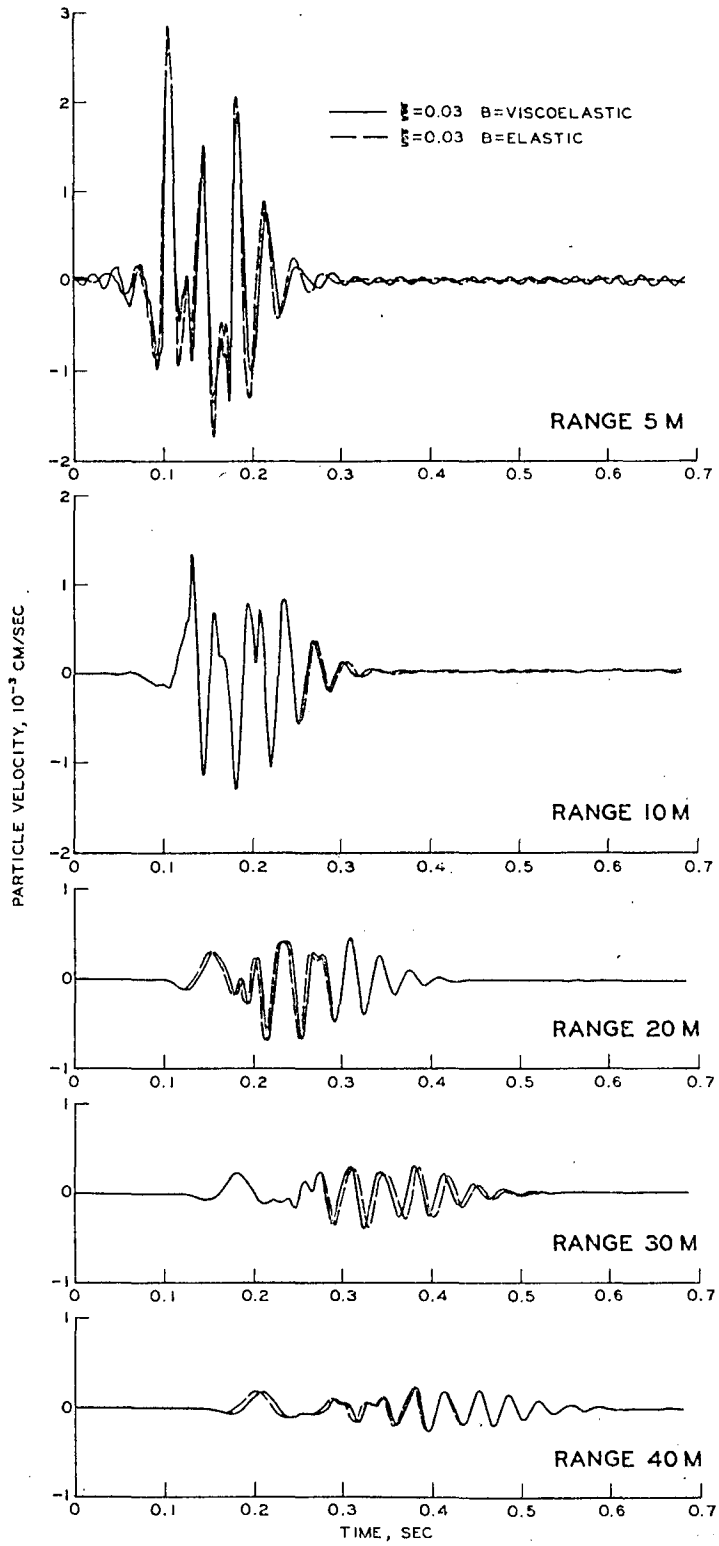

Fig. 18. Effects of damping and coupling coefficients on fundamental mode predictions, vertical component. Site 319, input source cosine-squared pulse 0.050 sec

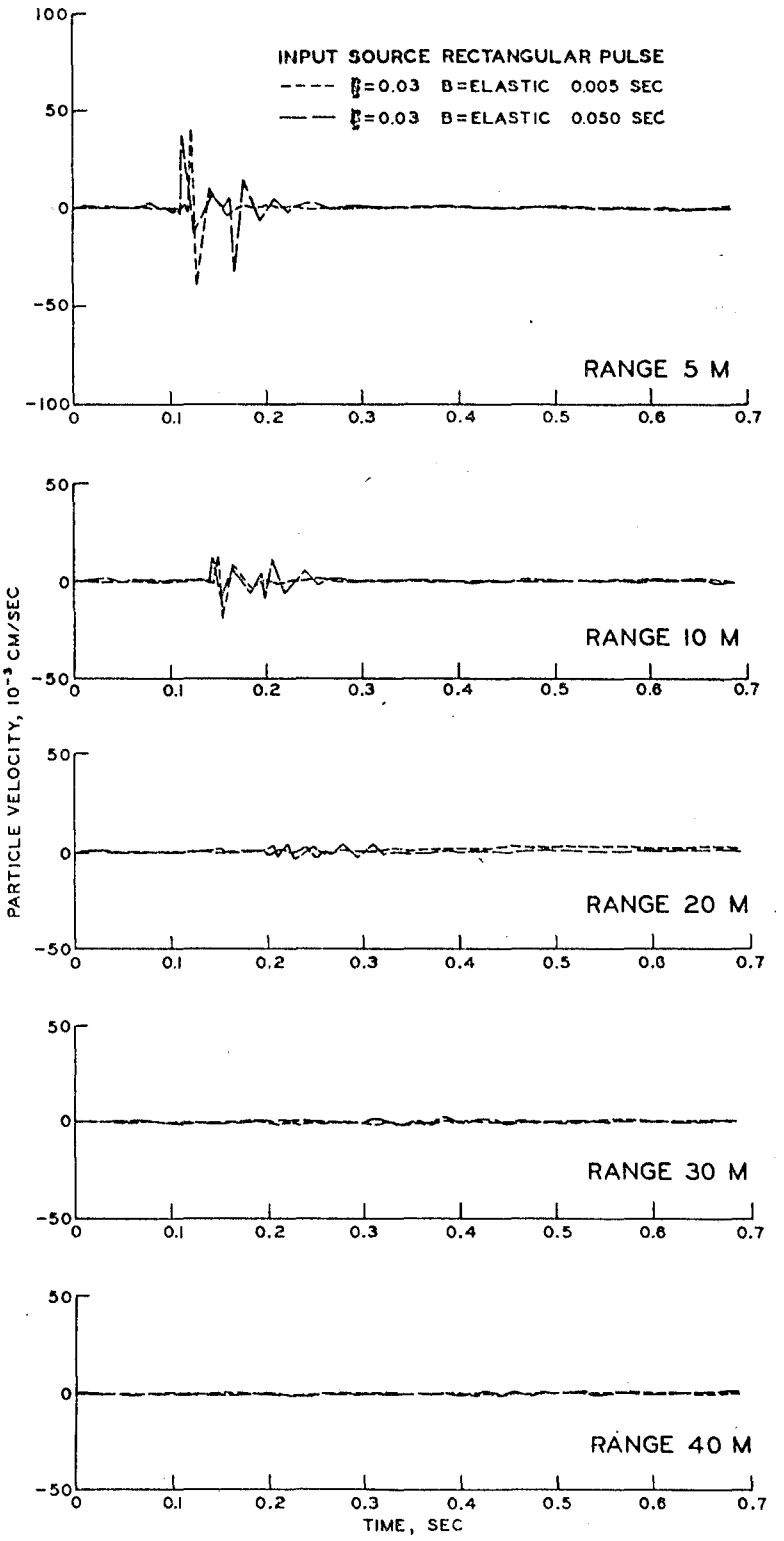

Fig. 19. Effects of damping and coupling coefficients on fundamental mode predictions, vertical component. Site 319, input sources 0.050 and 0.005 sec (sheet 1 of 2)

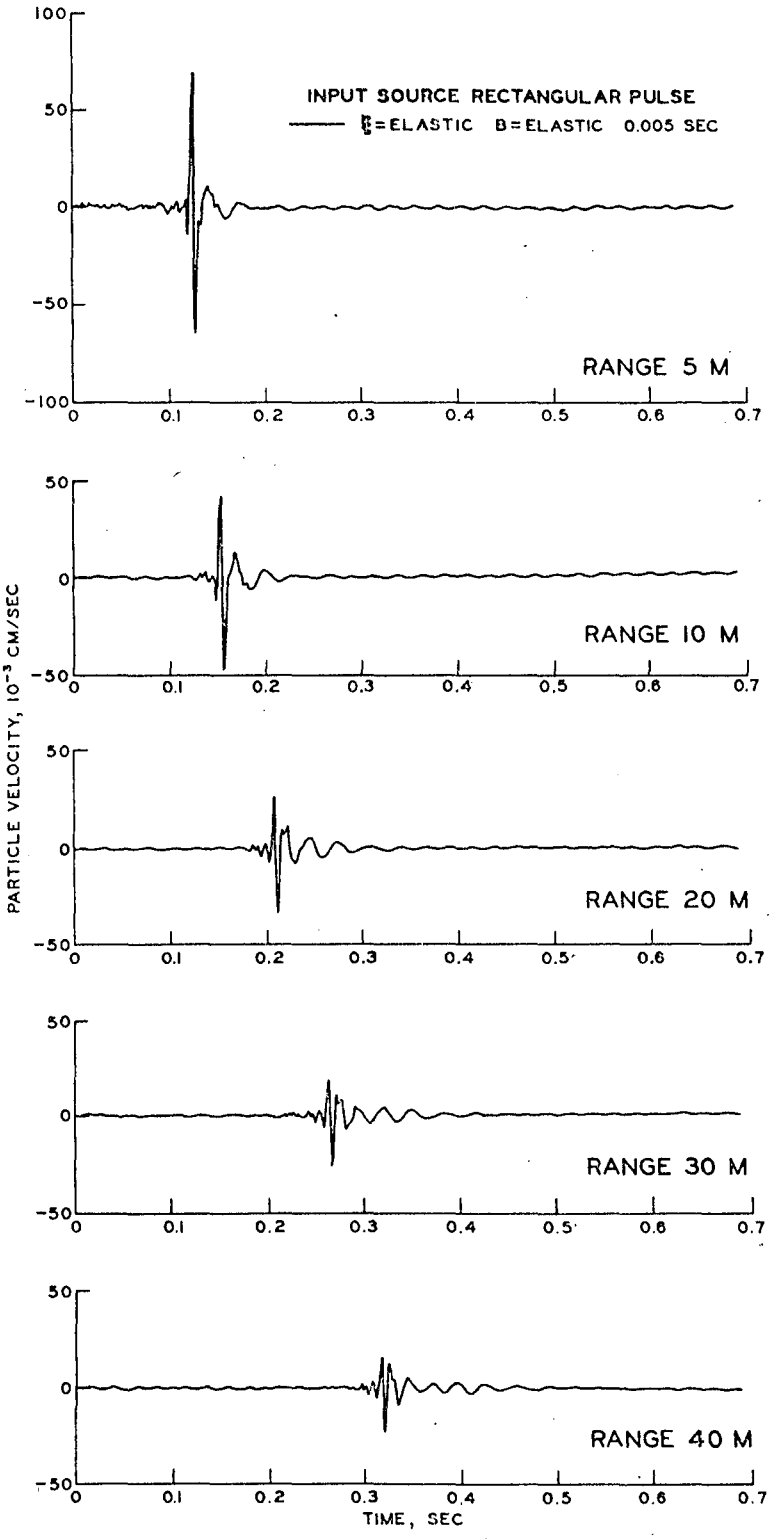

Fig. 19 (sheet 2 of 2)

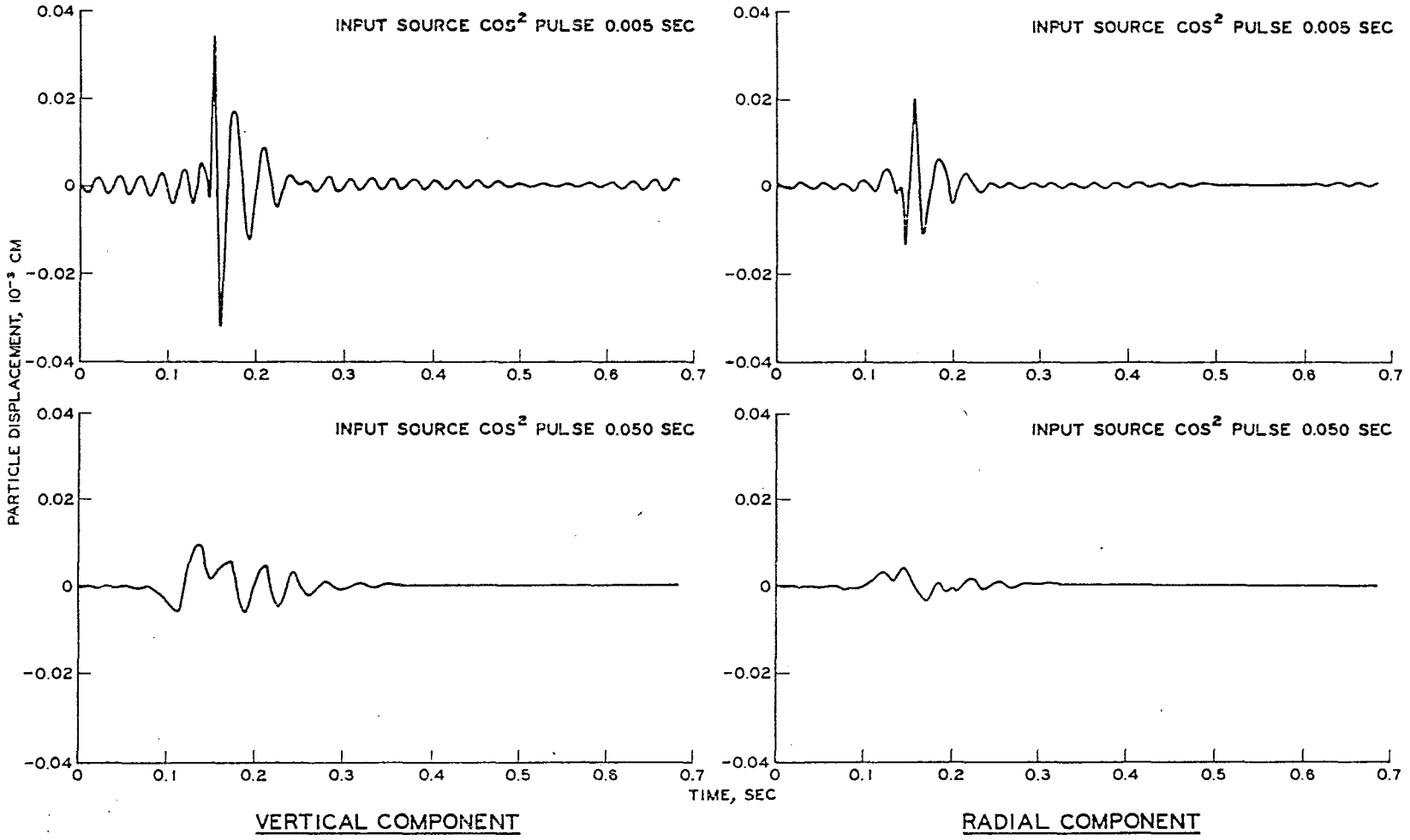

Fig. 20. Particle displacement signals, fundamental mode, site 319 viscoelastic coupling coefficients, $\xi = 0.03$, $r = 10$ m

if the input signal were other than a vertical pulse; an input signal with a horizontal component will cause a maximum increase in the radial component of the predicted signal for positions in the plane of the input signal, and proportionately less increase for other angles. The curves of particle displacement and velocity differ in shape because the velocity curve is the first derivative of displacement (compare figs. 20 and 16). In other words, the velocity curve gives the instantaneous slope of the displacement curve.

84. Also shown for comparison are curves computed with the damping factor equal to zero (elastic media) or equal to 0.03 (see figs. 17 and 19). Both show a decrease in amplitude with range, though the curves with a damping factor ξ of 0.03 decrease much faster due to the added attenuation from the damping factor. Note that for the elastic system (with geometric attenuation alone), the predicted signals still are abrupt and crisp; all the high-frequency components are still present in the predicted signals at far ranges, though modified by dispersion. When damping is added, the high-frequency components are attenuated at a higher rate than low-frequency components, and at far ranges, lose their distinction from one another. This would make it difficult to identify the source of seismic signals on the basis of a single signal if the range were large or if the damping coefficient were large (except for extremely low frequency signals, damping is apparent to some degree for all terrain materials).

85. Predictions were made for input signals coupled to the ground composed of elastic media and of viscoelastic media. For the source coupling coefficients in viscoelastic media, soil constants were assumed to be compatible with the previously calculated wave number and a damping factor of 0.03. The use of the viscoelastic coupling coefficient reduced the amplitude of the predicted signals by 10-20 percent (see table 1) without disturbing the wave shape very much (see figs. 17 and 18). Thus, for this site, the source coupling coefficients were not greatly influenced when a viscoelastic system was substituted for an elastic one. An approximation of this type (i.e. using elastic instead of viscoelastic source coupling coefficients) may prove useful if the

value for the damping factor is to be varied at each prediction site, since only one table of elastic source coupling coefficients would be needed.

86. There is very little difference in the shape of predicted curves when the input signal is changed from a 0.005-sec cosine-squared pulse to a 0.005-sec rectangular pulse (compare figs. 17 and 19). The amplitude is slightly less for the cosine-squared pulse than for the rectangular pulse. The shapes of the predicted curves might have varied more if higher frequencies had been considered in the elastic media situations. (Due to limitations in number size, the computer could compute coupling coefficients only up to approximately 200 Hz.) For viscoelastic media situations, the high frequencies would be subject to attenuation and would contribute less and less to the predicted signal as the range increased.

87. The predicted signals for particle motion differed greatly in shape and amplitude when the input signal was changed from a 0.050-sec cosine-squared pulse to a 0.050-sec rectangular pulse (compare figs. 18 and 19; also see fig. 15). The cosine-squared pulse produced relatively low-amplitude particle motion curves with approximately constant amplitude peaks during the duration of the signal. The rectangular pulse produced particle motion curves whose maximum amplitudes were very large at near ranges, but decayed rapidly at far ranges (though not as rapidly as for the 0.005-sec pulses). The predicted signals from the rectangular pulse appear to be generated from the two edges of the pulse, and result in a positive-going portion of the particle velocity curves from the leading edge and a negative-going portion of the particle velocity curve from the trailing edge.

Measured and Predicted Signals for WES Study Site 341

88. Although it is beyond the scope of this report to present a validation of the model, it is of interest to compare measured and predicted signals for site 341, which is at Fort Huachuca, Arizona. The site properties are as follows:

a. P-wave velocity of first layer, α_1 = 365 m/sec

b. S-wave velocity of first layer, β_1 = 204 m/sec

c. Mass density of first layer, γ_1 = 1.75 g/cm^3

d. Thickness of first layer, d = 1.15 m

e. P-wave velocity of foundation = 818 m/sec

f. S-wave velocity of foundation = 333 m/sec

g. Mass density of foundation = 1.9 g/cm^3

h. Viscous damping coefficient = 0.03

The Rayleigh wave numbers for the fundamental mode, calculated as discussed in paragraphs 52-55 for the data above, are shown in fig. 21. Fig. 22 shows the real and imaginary values, respectively, of the source coupling coefficients for the vertical component, which were calculated

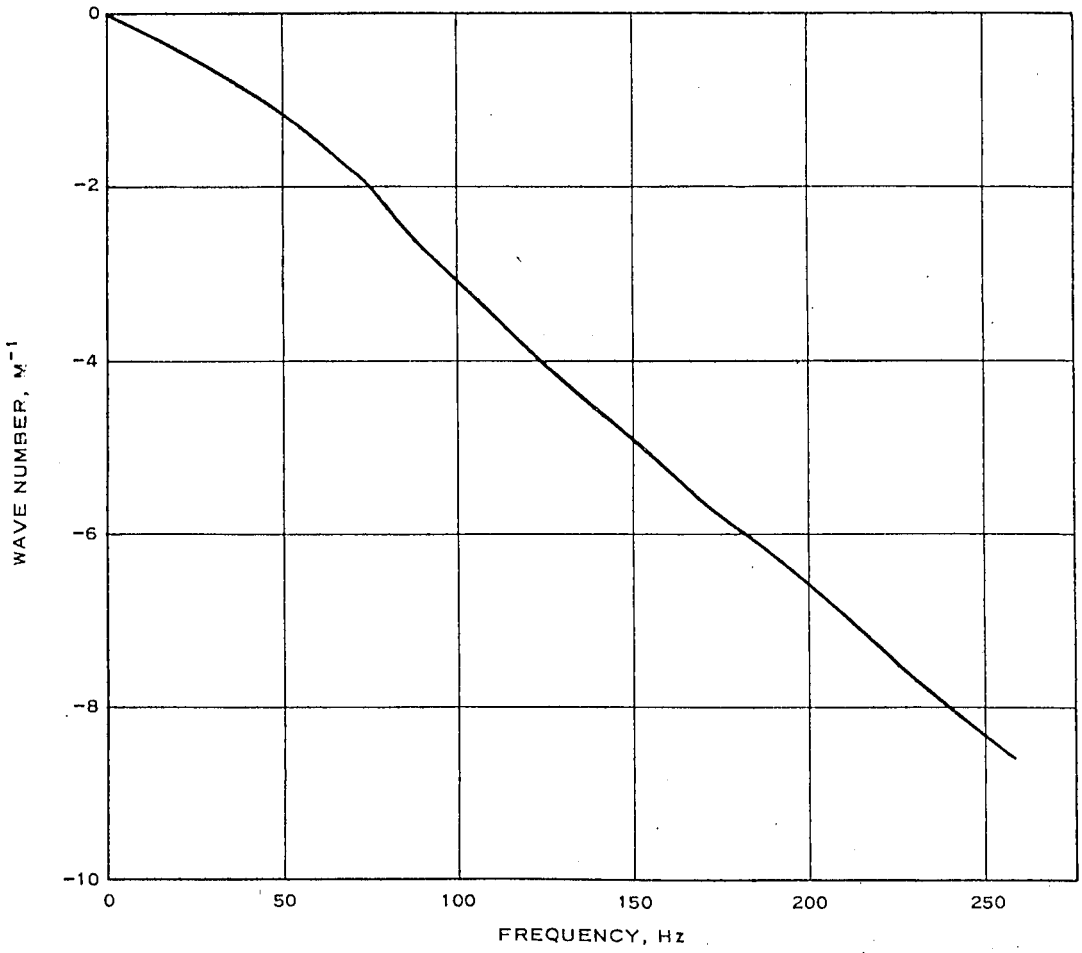

Fig. 21. Wave numbers for site 341, Fort Huachuca, Arizona

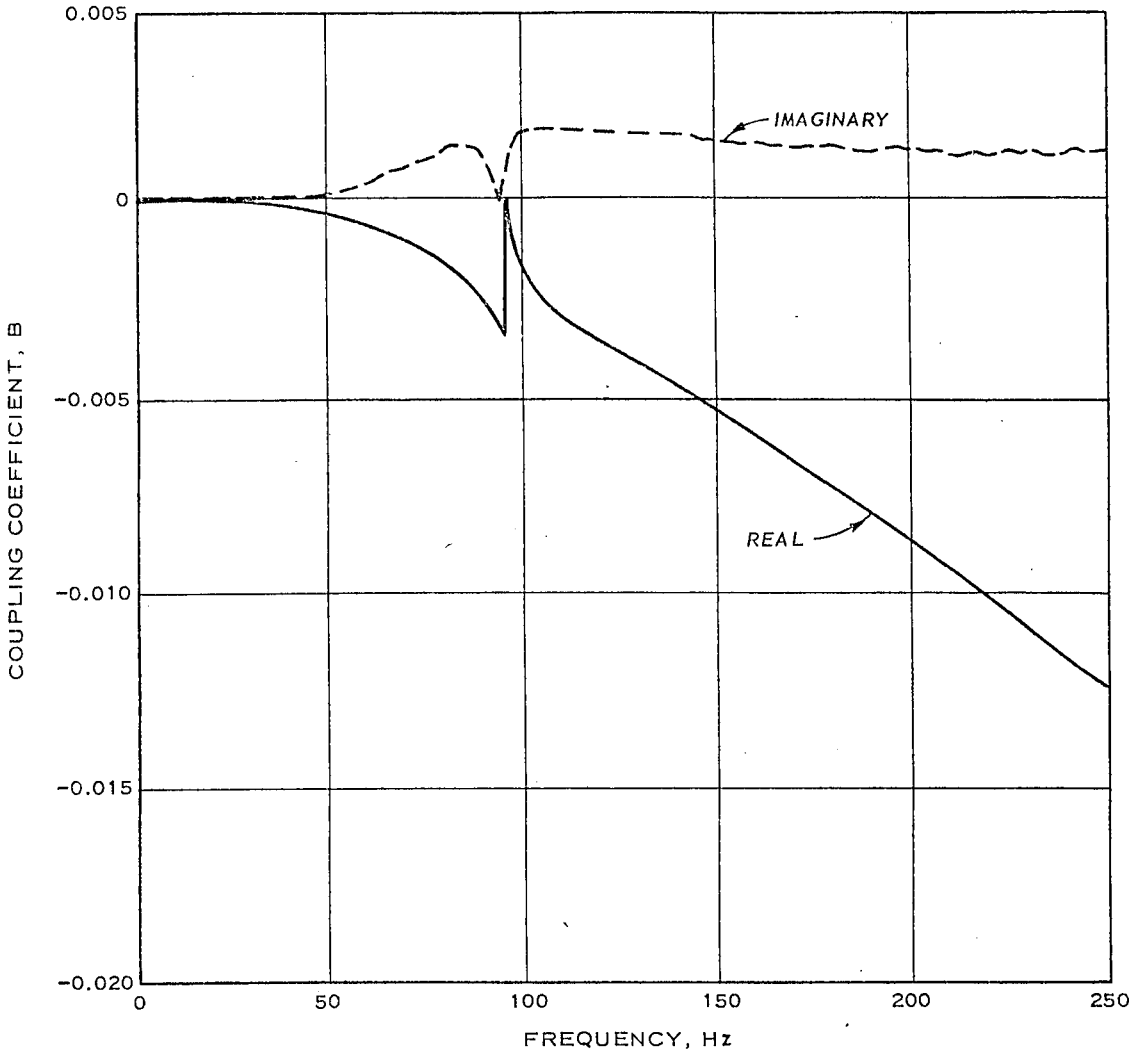

Fig. 22. Real and imaginary values of the source coupling coefficients for the vertical component, site 319

for a viscoelastic system (i.e. the damping coefficient was 0.03).

Measured signals

89. The energy source of the measured signals was a special drop-hammer apparatus (fig. 23), designed by WES. The drop hammer provided a controlled energy source whose seismic response could be compared in amplitude and frequency with that resulting from an average footstep. The hammer, which consists of a 9.9-kg annular weight with a Teflon sleeve, is connected by a metal guidepost to the footing, which is a plywood base topped by two layers of 0.2-cm-thick hard rubber and two layers of 1.9-cm-thick soft foam rubber. The vertical component of particle

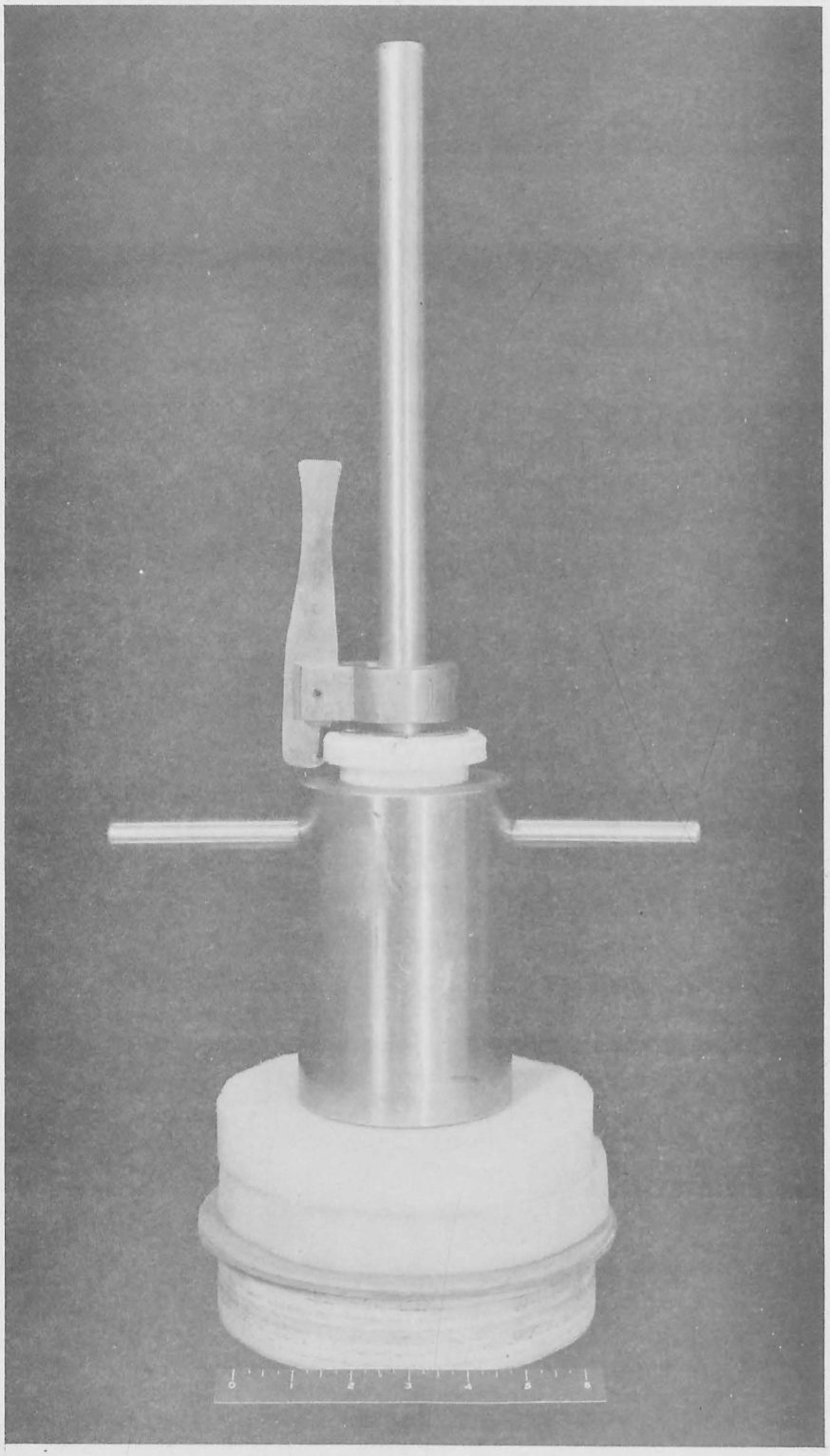

Fig. 23. Drop-hammer apparatus

motion resulting from the drop hammer was measured (see right side of fig. 24) at 5, 10, 15, 20, 25, 30, 40, 50, 60, 70, 80, 90, and 100 m using an HS-10 geophone. The geophone output was recorded on analog FM magnetic tape. A wide-band-frequency (from 2 to 300 Hz), battery-powered recording system was used to obtain continuous high-quality data and an adequate dynamic range. All instruments used in the seismic tests were calibrated in accordance with the National Bureau of Standards procedures, and no filtering of any type was used.

Predicted signals

90. To illustrate the capability of matching predicted signals with measured signals, a stress-time function had to be derived for the drop hammer. As stated in paragraph 89, the drop hammer was designed to produce a seismic signal that was very similar in amplitude and frequency to that produced by an "average" man.[11] The average man weighs 71.18×10^6 dynes and walks at a normal walk rate, i.e. 90 steps per min. Drop-hammer and footstep signatures have been measured at many sites in diverse environments, and good correlation has been observed in nearly every situation. This emphasizes that the drop hammer is stressing the ground in much the same manner as does a footstep. For this reason it is assumed that the maximum force applied to the ground by the drop hammer corresponds to the man's weight. Laboratory measurements have indicated that the restoring force associated with the drop-hammer-soil system is a nonlinear function of the displacement of the drop-hammer weight. The time-dependent forces exerted on the ground were calculated by using the Runge-Kutta method to numerically solve the differential equation of motion of the drop-hammer weight subject to a nonlinear restoring force. The calculations indicate that the forcing function can be approximated by a cosine-squared pulse.

91. In order to study the variation in the output signal caused by a change in the input cosine-squared pulse period, particle velocity signals were predicted for pulse periods varying from 0.005 to 0.050 sec over ranges of 5 to 80 m for the terrain conditions measured at site 341. The peak amplitude was held constant at a value of 277 megadynes and the record length was chosen to be compatible with a normal

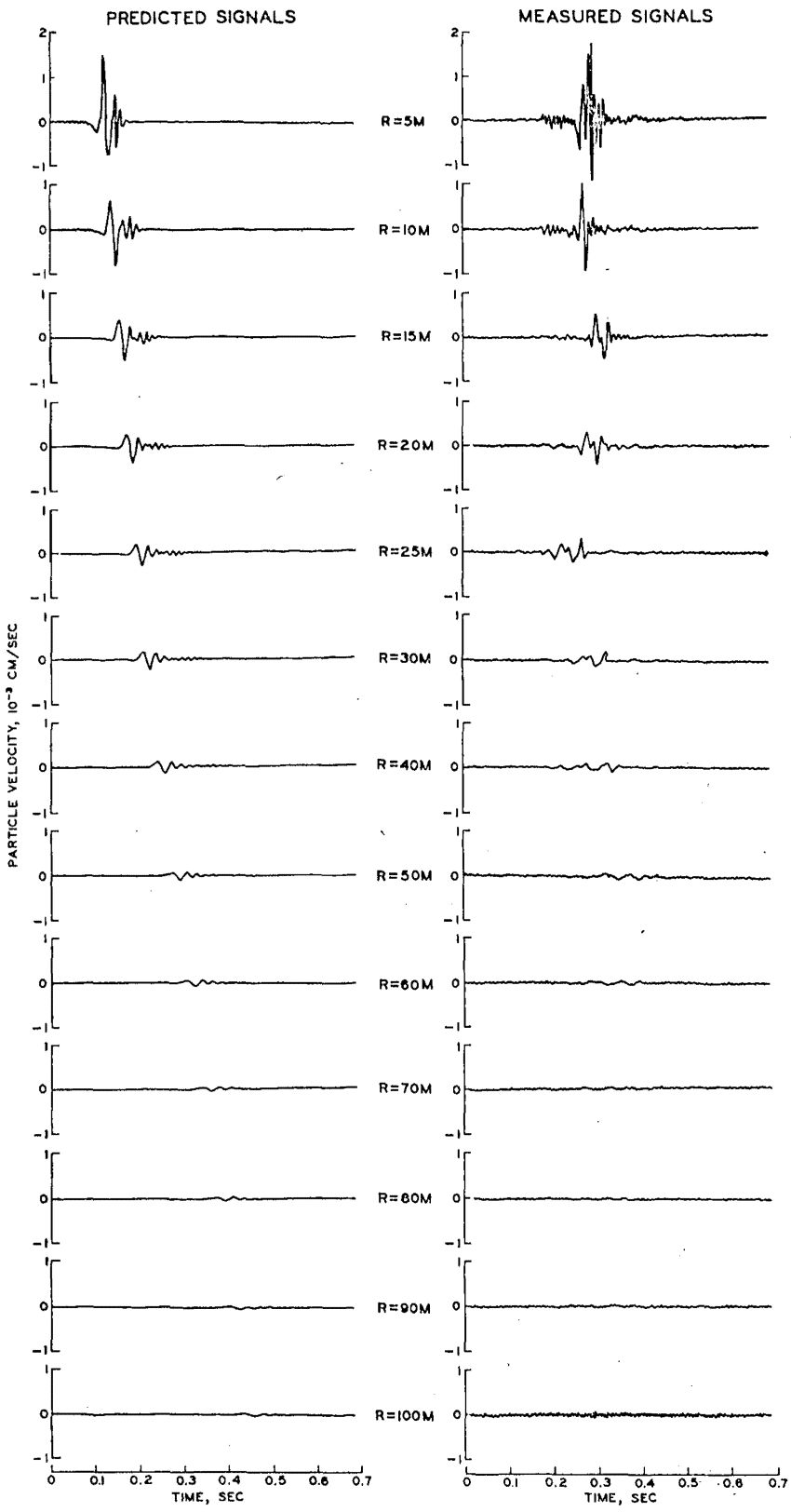

Fig. 24. Simulated footstep signatures

walk rate of approximately 90 steps per min (i.e. record length was 0.68 sec). Peak amplitudes for the vertical components of the wave were extracted from these predicted signals and the results are shown in fig. 25. There appears to be a large contrast in peak amplitudes for short periods or for near ranges, which decreases as the period or range increases. For example at a range of 5 m, the peak amplitude varies over nearly two orders of magnitude as the pulse width varies from 0.005 to 0.050 sec; at a range of 80 m, the amplitude varies by a factor of 2. In a similar manner, with a pulse width of 0.005 sec, the peak amplitude varies nearly 2-1/2 orders of magnitude for a range change of 5 to 80 m and slightly more than 1 order of magnitude for a pulse width of 0.050 sec. This would suggest that the source pulse width is just as important as attenuation with range in determining signal levels propagating in ground media.

92. Peak amplitudes were extracted from the measured signals (right side of fig. 24) and were compared, on a relative amplitude basis, with the computed peak amplitudes in fig. 25. These comparisons indicated that a cosine-squared pulse width of approximately 0.016 sec would generate peak amplitudes that would decrease with range in the same proportion as shown by the measured values. It was found that reducing the peak amplitude on the cosine-squared pulse from 277 megadynes to 71.18 megadynes (i.e. 71.18 megadynes is the equivalent force applied to the ground by the weight of the average man) would make the absolute peak amplitudes of the computed and measured signals match. This stress-time function, i.e. cosine-squared pulse with peak amplitude and pulse width 71.18 megadynes and 0.016 sec, respectively, was used to generate the predicted signals shown on the left side of fig. 24.

Comparison of measured and predicted signals

93. Fig. 24 shows that the measured and predicted signals have similar wave form appearance and they compare well in amplitude, frequency content, and duration. The similarity in amplitude can be seen more directly in the comparison of span and peak amplitudes shown in fig. 26. Also the frequency content of the cosine-squared pulse

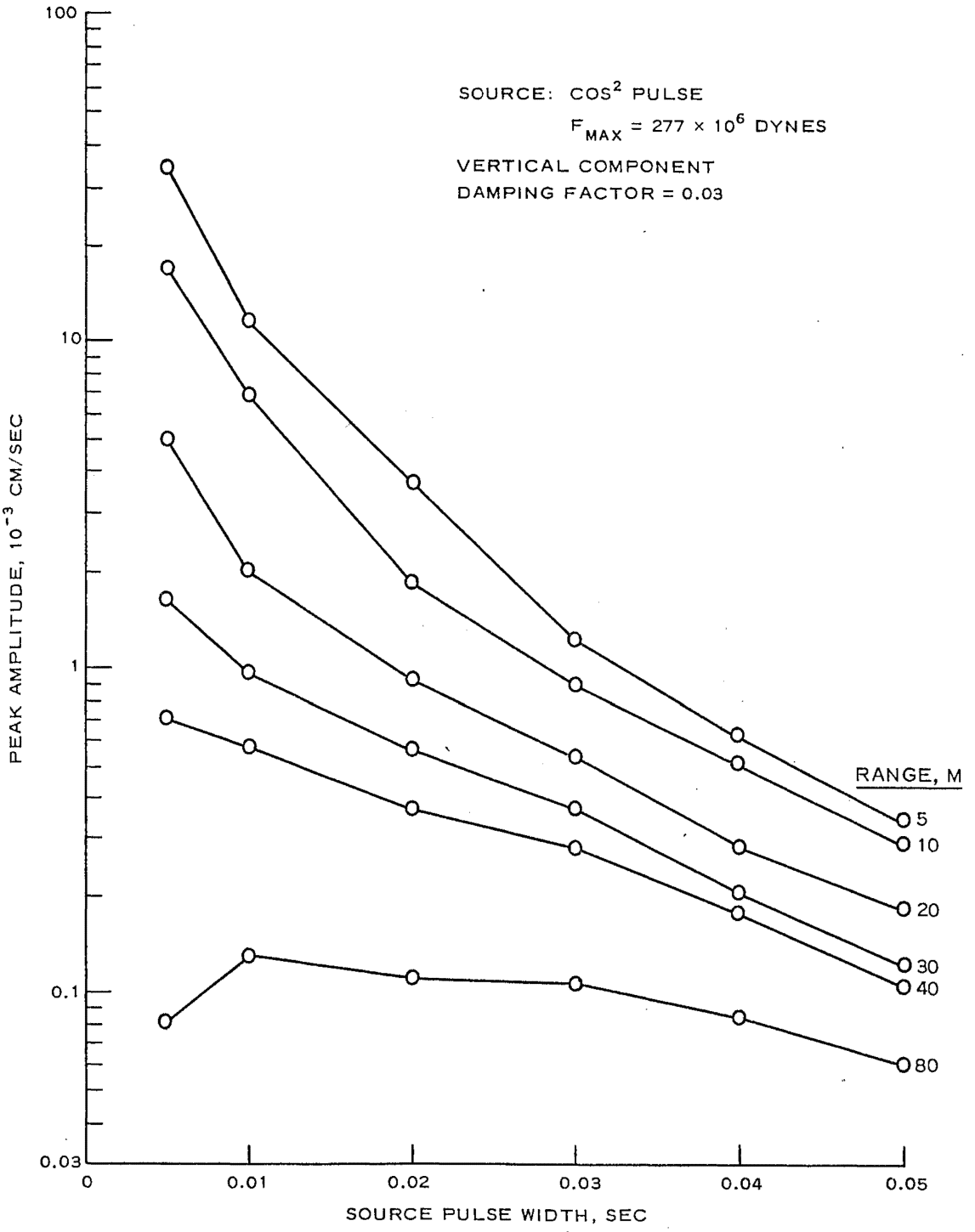

Fig. 25. Peak amplitude of predicted particle velocity signal at various ranges as a function of source pulse width

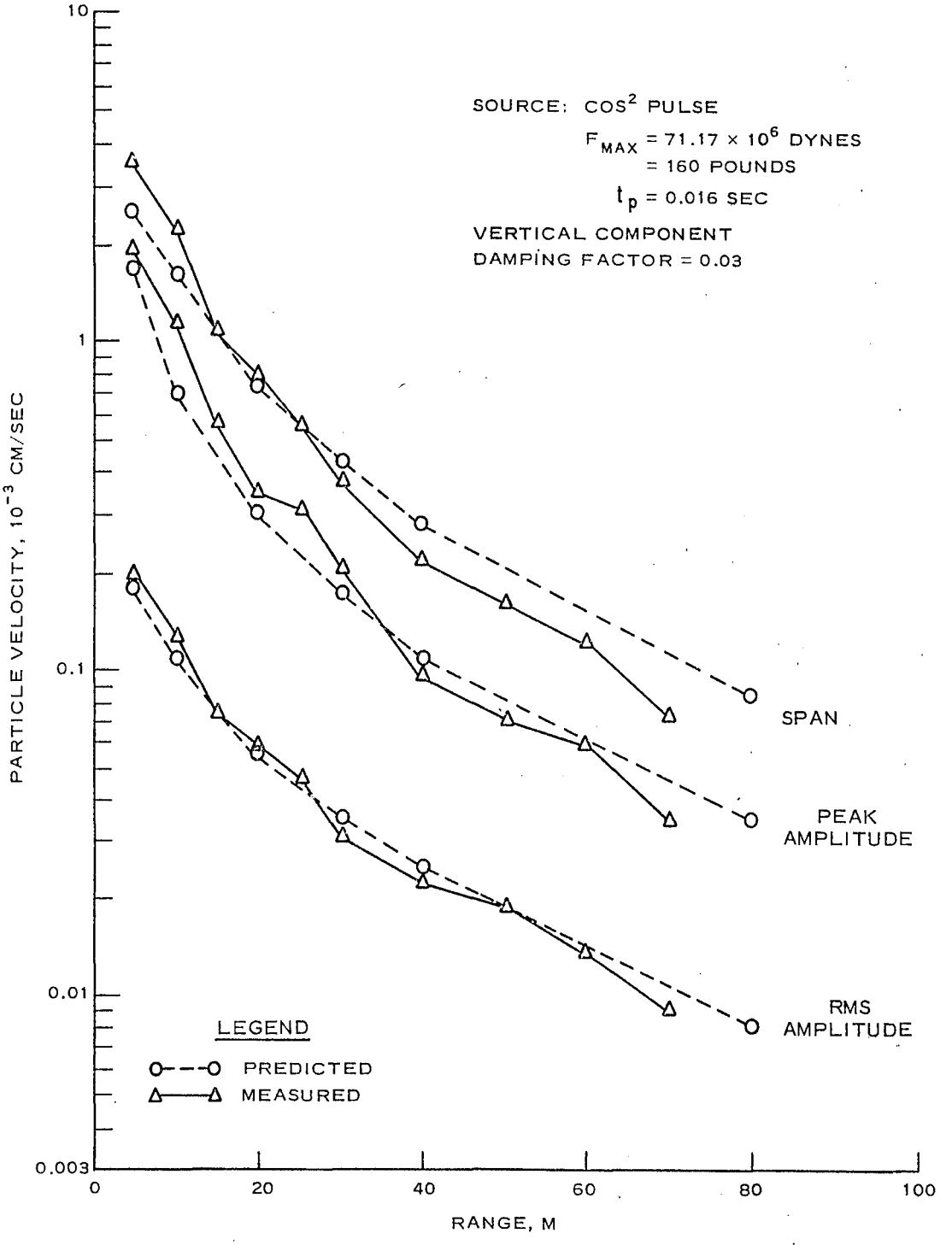

Fig. 26. Measured and predicted signal characteristics for a simulated footstep

appears to match that of the drop hammer, as indicated by the close agreement of the rms amplitude versus range curve in fig. 26 for the predicted and measured signals. The predicted and measured values do not compare exactly because the measured signals have noise-resulting friction between the drop hammer and its shaft as it slides down to impact the padded foot. This noise is readily apparent (fig. 24) on the leading edge of dominant signal, especially for distances out to 15 m. In addition, discrepancies exist because of the use of only the fundamental mode in the computation of the particle motion signal. Further, the site properties were computed from samples that were assumed to be representative of the entire site, and local variations existed that had some (even if small) effect on the measured signal. Also, the cosine-squared pulse approximates, but does not duplicate exactly, the true shape of the drop-hammer stress-time function, and this resulted in some differences between the predicted and measured signals.

94. The results presented in figs. 24 and 26 are for one site only and are not conclusive, but similar results have been derived for other sites using similarily derived forcing functions. In addition, some predictions using forcing functions derived for the M151 and M113 vehicles have been made and compared with measured values. From the results obtained to date at WES, it seems reasonable to assume that the model is functioning as intended.

PART V: CONCLUSIONS AND RECOMMENDATIONS

95. Inasmuch as the overall objective of the study reported herein was to develop a mathematical model for predicting microseismic waves as a function of (a) low energy sources representative of military targets, i.e. vehicles, men, etc., (b) substrate conditions, (c) surface macrogeometry, and (d) distance from source, it is concluded that the objective was reached. Very limited validation of the model was pursued, since its comprehensive development and validation were beyond the scope of this study. Therefore, it is recommended that:

a. The model be further validated using forcing functions and terrain inputs that will exercise it throughout a range that is representative of the military targets (forcing functions) of interest and worldwide terrain conditions.

b. Once the model is validated, the sensitivity of its output to the various terrain inputs that are used to make a prediction (e.g. α, β, ρ, d, and ξ for each layer) be studied so that the input requirements can be simplified. It is also of interest to determine under what conditions the high-order modes of Rayleigh wave can be eliminated and under what conditions the source coupling coefficients are similar for an elastic and a viscoelastic medium. It is expected that this information would permit significant economies in computation for a large number of problem classes.

c. A study be conducted to determine under what conditions the published coefficients for surface geometry can be used and to develop additional means for computing surface geometry coefficients when needed.

d. A study be conducted to determine the effect of surface properties (vegetation, variation in soil density, moisture content, plasticity, etc.) in modifying the magnitude of the applied forces that generate seismic waves.

e. The study in d above be expanded to study the effects of temperature and frozen materials on seismic wave propagation.

f. Efforts be made to determine the stress applied to the ground from other sources of military interest (e.g. high-energy explosives, aircraft, acoustics, energy, vehicles, etc.).

g. Efforts be made to improve the model operation and

predictive capability so it can be used more efficiently for a number of military problems. Examples of the problems of interest include the following:

(1) Preparation of military geographic intelligence products for existing and prototype seismic sensors.

(2) Establishing trade-offs between sensor design complexity and terrain data requirements for deployment.

(3) Development of sensor deployment criteria.

(4) Design of sensor fields against specific military threats.

(5) Evaluation of concepts for artillery ranging using seismic techniques.

LITERATURE CITED

1. Richart, F. E., Jr., "Foundation Vibrations," Transactions, American Society of Civil Engineers, Vol 127, Part 1, 1962, pp 863-898.

2. Richart, F. E., Jr., Hall, J. R., Jr., and Woods, R. D., Vibrations of Soils and Foundations, Prentice-Hall, Englewood Cliffs, 1970.

3. Ewing, W. M., Jardetzky, W. S., and Press, F., Elastic Waves in Layered Media, McGraw-Hill, New York, 1957.

4. Weissmann, G. F. and Hart, R. R., "Damping Capacity of Some Granular Soils," Special Technical Publication No. 305, 1961, American Society for Testing and Materials, Philadelphia, Pa.

5. Hall, J. R., Jr. and Richart, F. E., Jr., "Dissipation of Elastic Wave Energy in Granular Soils," Journal of the Soil Mechanics and Foundations Division, American Society of Civil Engineers, Vol 89, No. SM6, Nov 1963, pp 27-56.

6. Whitman, R. V., "Stress-Strain-Time Behavior of Soil in One Dimensional Compression," Report R63-25, 1963, Massachusetts Institute of Technology, Cambridge, Mass.

7. Barkan, D. D., Dynamics of Bases and Foundations, McGraw-Hill, New York, 1962.

8. Stevens, H. W., "Measurement of the Complex Moduli and Damping of Soils Under Dynamic Loads," Technical Report No. 173, 1966, U. S. Army Cold Regions Research and Engineering Laboratory, Hanover, N. H.

9. Hardin, B. O., "The Nature of Damping in Sands," Journal of the Soil Mechanics and Foundations Division, American Society of Civil Engineers, Vol 91, No. SM1, Jan 1965, pp 63-97.

10. Kolsky, H., Stress Waves in Solids, Dover, New York, 1963.

11. Marcuson, W. F. III and Leach, R. E., "Seismic and Environmental Characteristics of the Sensor Test Areas in the Panama Canal Zone; Wet-Season Conditions," Technical Report M-72-2, Report 2, May 1973, U. S. Army Engineer Waterways Experiment Station, CE, Vicksburg, Miss.

12. Kane, J. and Spence, J., "Rayleigh Wave Transmission on Elastic Wedges," Geophysics, Vol 28, No. 5, Oct 1963, pp 715-723.

13. Woods, R. D., "Screening of Surface Waves in Soils," Journal of the Soil Mechanics and Foundations Division, American Society of Civil Engineers, Vol 94, No. SM4, Jul 1968, pp 951-979.

14. West, H. W. and Rohani, B., "Effects of Terrain on the Propagation of Microseismic Waves and Implantation Characteristics of Air-Delivered Sensors at Fort Huachuca, Arizona, Wet- and Dry-Season Conditions," Technical Report M-73-3, Jun 1973, U. S. Army Engineer Waterways Experiment Station, CE, Vicksburg, Miss.

15. Lapwood, E. R., "The Transmission of a Rayleigh Pulse Round a Corner," Geophysical Journal, Vol 4, 1961, pp 174-196.

16. Kraut, E. A., "Diffraction of Elastic Waves by a Rigid 90° Wedge," Bulletin of the Seismological Society of America, Vol 58, No. 3, Jun 1968, pp 1083-1096.

17. Alterman, Z. S. and Rotenberg, A., "Seismic Waves in a Quarter Plane," Bulletin of the Seismological Society of America, Vol 59, No. 1, Feb 1969, pp 347-368.

18. Kane, J., "The Superposition Principle and Diffraction in Sectors," Journal of Mathematical Mechanics, Vol 28, 1966, pp 207-219.

19. Hudson, I. A. and Knopoff, L., "Transmission and Reflection of Surface Waves at a Corner, Rayleigh Waves (Theoretical)," Journal of Geophysical Research, Vol 69, No. 2, Jan 1964, pp 281-289.

20. Mal, A. K. and Knopoff, L., "Transmission of Rayleigh Waves at a Corner," Bulletin of the Seismological Society of America, Vol 56, No. 2, Apr 1966, pp 455-466.

21. de Bremaecker, J. C., "Transmission and Reflection of Rayleigh Waves at Corners," Geophysics, Vol 23, No. 2, Apr 1958, pp 253-266.

22. Knopoff, L. and Gangi, A. F., "Transmission and Reflection of Rayleigh Waves by Wedges," Geophysics, Vol 25, No. 6, Dec 1960, pp 1203-1214.

23. Pilant, W. L., Knopoff, L., and Schwab, F., "Transmission and Reflection of Surface Waves at a Corner, Rayleigh Waves (Experimental)," Journal of Geophysical Research, Vol 69, No. 2, Jan 1964, pp 291-297.

24. Gangi, A. F., "Experimental Determination of P Wave/Rayleigh Wave Conversion Coefficients at a Stress-Free Wedge," Journal of Geophysical Research, Vol 72, No. 22, Nov 1967, pp 5685-5692.

25. Lewis, D. and Dally, J. W., "Photoelastic Analysis of Rayleigh Wave Propagation in Wedges," Journal of Geophysical Research, Vol 75, No. 17, Jun 1970, pp 3387-3398.

26. Mal, A. K. and Knopoff, L., "Transmission of Rayleigh Waves Past a Step Change in Elevation," Bulletin of the Seismological Society of America, Vol 55, No. 2, Apr 1965, pp 319-334.

27. Herrera, I., "On a Method to Obtain a Green's Function for a Multilayered Half Space," Bulletin of the Seismological Society of America, Vol 54, No. 4, Aug 1964, pp 1087-1096.

28. McGarr, A. and Alsop, L. E., "Transmission and Reflection of Rayleigh Waves at Vertical Boundaries," Journal of Geophysical Research, Vol 72, No. 8, Apr 1967, pp 2169-2180.

29. Viktorov, I. A., "The Effects of Surface Defects on the Propagation of Rayleigh Waves," Soviet Physics, Doklady, Vol 3, 1958, pp 304-306.

30. Kuo, J. T. and Thompson, G. A., "Model Studies on the Effect of a Sloping Interface on Rayleigh Waves," Journal of Geophysical Research, Vol 68, No. 22, Nov 1963, pp 6187-6197.

31. Drake, L. A., "The Propagation of Love and Rayleigh Waves in Non-Horizontally Layered Media," Transactions, American Geophysical Union, Vol 52, No. 11, Nov 1971, p 866.

32. Ottaviani, M., "Elastic-Wave Propagation in Two Evenly-Welded Quarter-Spaces," Bulletin of the Seismological Society of America, Vol 61, No. 5, Oct 1971, pp 1119-1152.

33. Woods, R. D. and Richart, F. E., Jr., "Screening of Elastic Surface Waves by Trenches," Proceedings, International Symposium on Wave Propagation and Dynamic Properties of Earth Materials, University of New Mexico Press, Albuquerque, N. Mex., 1968, pp 275-285.

34. Cheek, J. B., Radhakrishnan, N., and Tracy, F. T., "Application of Spline Interpolation Methods to Engineering Problems," Miscellaneous Paper 0-71-2, Jul 1971, U. S. Army Engineer Waterways Experiment Station, CE, Vicksburg, Miss.

Table 1

Particle Motion Amplitudes, Fundamental Mode Predictions

Source Signal	Range m	Damping Coefficient,* ξ	Coupling Coefficient, B	Component	Motion	Amplitude Peak	rms	Span	Units	Fig. No.
Source Pulse Width = 0.005 sec, Peak Amplitudes = 277 × 10^6 Dynes										
Cosine-squared pulse	5	Elastic	Elastic	Vertical	Velocity	60.380	5.151	117.490	10^{-3} cm/sec	16
	10					36.602	3.644	79.361		16
	20					23.384	2.577	52.165		16
	30					16.434	2.104	39.807		16
	40					13.006	1.822	32.251		16
Rectangular pulse	5					69.433	5.825	134.307		18
	10					42.531	4.120	91.159		18
	20					27.633	2.914	60.690		18
	30					19.622	2.379	46.580		18
	40					15.522	2.060	37.889		18
Cosine-squared pulse	5	0.03	Viscoelastic			35.15	3.028	64.51		16
	10					11.85	1.491	27.14		16
	20					2.96	0.599	6.68		16
	30					1.26	0.318	2.64		16
	40					0.68	0.193	1.40		16
	10			Radial	Velocity	9.603	0.815	13.787		15
	10			Vertical	Displacement	0.0341	0.00483	0.0665	10^{-3} cm	19
	10			Radial	Displacement	0.0206	0.00240	0.0340	10^{-3} cm	19
	5		Elastic	Vertical	Velocity	35.56	3.378	71.49	10^{-3} cm/sec	16
	10					11.44	1.690	29.06		16
	20					3.32	0.696	7.62		16
	30					1.62	0.374	3.11		16
	40					0.85	0.227	1.76		16
Rectangular pulse	5					40.534	3.738	80.927		18
	10					13.165	1.839	32.751		18
	20					3.544	0.744	8.320		18
	30					1.737	0.396	3.372		18
	40					0.892	0.240	1.852		18
Source Pulse Width = 0.050 sec, Peak Amplitude = 277 × 10^6 Dynes										
Cosine-squared pulse	5	0.03	Viscoelastic	Vertical	Velocity	2.374	0.438	3.738		17
	10					1.364	0.272	2.569		17
	20					0.432	0.153	1.034		17
	30					0.305	0.103	0.940		17
	40					0.217	0.075	0.429		17
	10			Radial		0.405	0.109	0.872		15
	10			Vertical	Displacement	0.00901	0.00195	0.0153	10^{-3} cm	19
	10			Radial	Displacement	0.00398	0.00083	0.00630	10^{-3} cm	19
	5		Elastic	Vertical	Velocity	2.86	0.481	4.61	10^{-3} cm/sec	17
	10					1.33	0.299	2.66		17
	20					0.48	0.168	1.16		17
	30					0.31	0.112	0.71		17
	40					0.23	0.081	0.48		17
Rectangular pulse	5					35.157	3.808	69.371		18
	10					11.583	2.047	20.986		18
	20					3.693	0.972	8.096		18
	30					2.696	0.582	4.869		18
	40					1.414	0.385	2.839		18

* From reference 1.

APPENDIX A: EFFECTS OF SURFACE MACROGEOMETRY ON PROPAGATION OF RAYLEIGH WAVES

Literature Survey

1. Rayleigh waves are true surface waves, since they travel along the free surface of the half-space near which the wave motion is confined. If any disturbance occurs in an infinite medium, there will be no Rayleigh waves; only body or compressional and shear waves will occur. The attenuation of the amplitude of Rayleigh waves is usually inversely proportional to $r^{-1/2}$ (where r is the distance from the source). When a Rayleigh wave is traveling on the free surface of a wedge, its direction changes along the corner (see fig. A1a). After it reaches the edge of the corner, it becomes a diffracted Rayleigh wave. It is of interest to note that the rate at which the diffraction amplitude falls off at the corner is much greater than that of simple inverse spreading. A rapid reduction of Rayleigh wave amplitude in excess of that experienced in propagation over flat surfaces indicates a deflection of the topography; therefore, the change in amplitude of Rayleigh waves indicates the irregularities of the earth's surface.

Effects of a wedge on Rayleigh waves

2. The geometric shape of a 90-deg-angle wedge is a basic significant representation of the terrain. In a large scale, the continental shelf, the ocean-continental boundary, a canyon, or a valley, and in a smaller scale, a trench, a dike, or a step increase in elevation can all be defined as wedges. The problem of Rayleigh wave propagation on a wedge-shaped medium is an important one in geophysics. An analytical solution to this problem is very difficult because both scalar and vector potential functions must be considered, and because the governing motion equations are not separable. In addition, the phenomena in wave diffraction at a corner are also very complex.

3. Theoretical studies. In recent years, several investigators using different techniques attempted to obtain an approximate solution for Rayleigh waves traveling along the free surface of a homogeneous

elastic wedge toward the apex. The first analysis of transmission of Rayleigh waves at a corner of a 90-deg wedge was given by Lapwood.[15*] He considered the case of an impulsive source on one face of the boundary and found an iterative solution by transform methods, from which he was able to isolate the parts that describe both the Rayleigh pulse incident on the corner and the pulse transmitted around the corner. Kraut[16] considered the same problem, but reduced it to a Weiner-Hopf problem with two complex variables. It was solved by analogy with a half-plane problem under the assumption that an appropriate matrix factorization of Green's elastic functions could be made. Alterman and Rotenberg[17] solved for the case of an elastic quarter-plane by a finite difference scheme. A point source emitting a compressional pulse was located along the diagonal inside the quarter-plane. Complete theoretical seismograms for the horizontal and vertical components of displacement were obtained.

4. For the problem of wedges having arbitrary angles, Kane and Spence[12,18] introduced analytical continuation and superposition methods to iterate between the faces of a wedge. Their first iteration yielded the macrogeometry transmission coefficients $S_{m,n}$ desired by seismologists. The procedure is very simple. Hudson and Knopoff[19] used a representation theorem for elastic wave propagation and Green's theorem to obtain approximate values for the complex macrogeometry reflection and transmission coefficients for Rayleigh waves incident upon a corner. They obtained macrogeometry transmission coefficients $S_{m,n}$ of Rayleigh waves similar to those reported in references 12 and 18. Mal and Knopoff[20] investigated the transmission of Rayleigh waves around a corner and obtained a second-order approximation. Their theoretical results represent a considerable improvement in reducing the discrepancy between theory and experiment (see next paragraph).

5. Experimental studies. For the phenomena involved when a Rayleigh wave is incident upon a corner whose angle is between 0 and 180 deg, de Bremaecker[21] found that the Rayleigh wave bends its path only for

---

* Numbers refer to similarly numbered references in Literature Cited, main text.

angles between 0 and 45 deg; for larger angles, wide and a priori unpredictable variations in both macrogeometry reflection and transmission coefficients occur. The Rayleigh wave travels to the extremity of the corner from which point it is transmitted and reflected. For a right-angle corner, about 50 percent of the energy incident as Rayleigh wave is converted into body waves, divided approximately equally between compression and shear waves. Knopoff and Gangi[22] found no significant differences in the structure of the transmission and reflection curves they observed as compared with those observed by de Bremaecker. Only significant shifts in the peaks, both in angle and in magnitude, were observed, since the Poisson's ratios for their experiments were different.

6. Pilant, et al.,[23] indicated that their experimental amplitude measurements agreed quite well with previous experimental evidence, but agreement with first-order theory was only fair for angles in the range of 0 to 70 deg. For angles greater than 90 deg, both the amplitude and phase underwent large variations that were not adequately explained by first-order theory. Gangi[24] obtained coefficients of conversion of compression waves to Rayleigh waves (and vice versa) at a wedge apex. He found that minimums in the conversion coefficients exist for a compression wave incident at grazing angles and maximums exist for compression waves at near-normal incidence to the wedge face. He also found that the conversion coefficients were larger for larger wedge angles. Lewis and Dally[25] used photoelastic analysis of Rayleigh wave propagation on wedges. Macrogeometry transmission and reflection coefficients based on both stress and displacement were established for wedges with included angles ranging from 0 to 140 deg. The results indicated that the macrogeometry transmission and reflection coefficients were rapidly changing functions of wedge angles. Comparisons of the experimental results of Lewis and Dally with the theoretical predictions of Mal and Knopoff[20] in most cases showed reasonable agreement.

Effect of a step discontinuity of
the free surface on Rayleigh waves

7. Rayleigh waves on media with laterally heterogeneous geometries propagate with a change in amplitude that should be related to structural

changes. Mal and Knopoff[26] considered the propagation of Rayleigh waves in a model with a homogeneous, isotropic, elastic half-space that was bounded by a horizontal surface and underwent a sudden change in elevation along a vertical plane. They used a Green's function method of approximation developed by Herrera[27] to obtain the elastic wave field due to a Rayleigh wave incident from either the elevated or the depressed side of the step. They considered two versions of approximations: (a) height of the step in the free surface smaller than the wavelength of the incident Rayleigh waves, and (b) height of the step larger than the wavelength; however, neither approximation agreed very well with experiments. McGarr and Alsop[28] also considered the Rayleigh wave-step discontinuity problem. They used an approximate variation method to compute macrogeometry reflection and transmission coefficients for a step discontinuity on the free surface of an otherwise homogeneous half-space and of two quarter-spaces with different densities and elastic constants welded together to form a half-space. Experimental data from these cases showed good agreement with computed results. The technique of McGarr and Alsop is limited, however, to situations in which most of the energy can be accounted for by the total Rayleigh field.

Effect of a
trench on Rayleigh waves

8. Various surface defects in the path of a Rayleigh wave are known to cause wave attenuation, produce a reflected Rayleigh wave, and also produce longitudinal and transverse waves scattered into the medium. Viktorov[29] reported an experimental study of single-surface defects, such as a slit (crack) cut into the surface along which a Rayleigh wave was propagated, or a semicylindrical groove (hollow) in the surface. Woods[13] conducted a broader investigation to determine the effectiveness of trench and sheet-wall barriers as vibration isolators and to develop guidelines for the design of these barriers.

Effect of sloping
interface on Rayleigh waves

9. The theoretical study of the problem of propagation of Rayleigh waves across a structure of various layer thicknesses, such as a

continental margin or a transitional region at the foot of a mountain range, involves considerable mathematical difficulties. The exact solution of the problem in general form has not been found. Since this problem is easily adaptable to model experiments, seismic modeling techniques have been used to study the effect of a surface layer whose thickness varies gradually as a linear function of horizontal distance on Rayleigh wave dispersion. From their experimental results, Kuo and Thompson[30] found that (a) the effect of a sloping interface on the phase velocity must be considered because the velocity changes nonlinearly with distance, and the phase velocities of Rayleigh waves in the region of a sloping interface are independent of the direction of wave propagation; and (b) the phase velocities of Rayleigh waves in a region of uniform thickness are found to be unaffected by the nearby sloping layer, and the velocities are the appropriate Rayleigh wave phase velocities for that thickness, regardless of the direction of wave propagation. Unfortunately, Kuo and Thompson did not study the amplitude of Rayleigh waves in this problem quantitatively.

Some Results from the Literature

Wedges having arbitrary angles

10. Theoretical approach. Kane and Spence[12] introduced the Kirchoff-Hyygen method, which is useful for estimating the macrogeometry transmission coefficients $S_{m,n}$ of seismic Rayleigh waves propagating past wedge-shaped obstacles (fig. A1). They considered an isolated wedge with free boundaries, and the following conditions:

a. Rayleigh wave incident from $X = -\infty$ along the left face of a free elastic wedge.

b. Angle χ is positive when measured counterclockwise from the horizontal axis X, or $X = 0$.

Thus, negative values of χ correspond to elastic wedges whose interior angles are less than π radians (fig. A1a), and positive values to wedges whose interior angles are greater than π radians (fig. A1b).

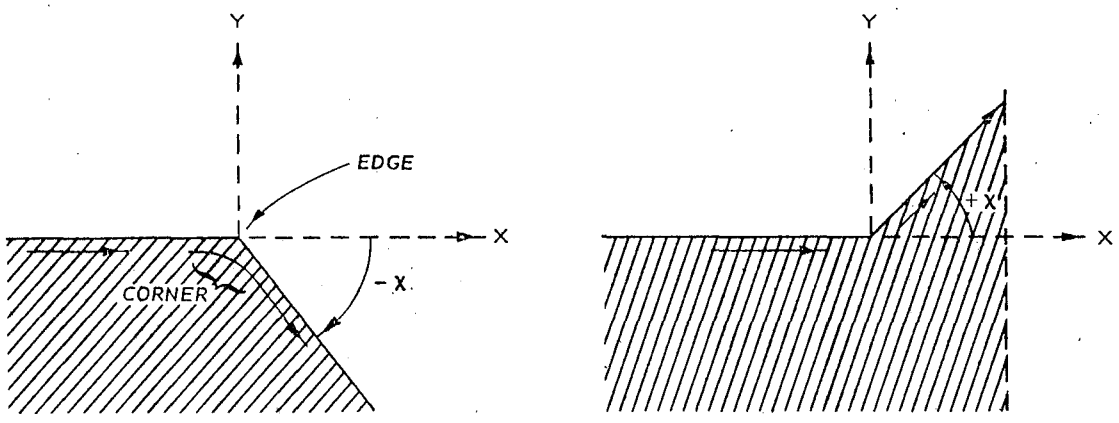

a. ELASTIC WEDGE WITH INTERIOR ANGLE LESS THAN π RADIANS

b. ELASTIC WEDGE WITH INTERIOR ANGLE GREATER THAN π RADIANS

Fig. A1. Seismic Rayleigh waves propagating past wedge-shaped obstacles

If $\chi = 0$, then the wedge degenerates into a half-space with no discontinuity at the origin.

11. An equation for the macrogeometry transmission coefficient $S_{m,n}$ of a Rayleigh wave on the second face (inclined surface) of the wedge was formulated as follows:

$$S_{m,n}(\chi,\sigma) = \frac{A(\kappa_R,\chi)\dot{S}(\kappa_R) - B(\kappa_R,\chi)Q(\kappa_R)}{\frac{d}{d\kappa}\,\mathrm{Det}\,(\kappa)\Big|_{\kappa=\kappa_R}} \qquad (A1)$$

which is a function of the wedge angle χ and Poisson's ratio σ. When there is no discontinuity,

$$\lim_{\chi\to 0} S_{m,n}(\chi,\sigma) = 1$$

The symbols used in equation A1 and in the equations below are defined as:

κ_R = wave number of Rayleigh waves

κ_α = wave number of compression waves = $\omega^2\rho/(\lambda + \mu)$

κ_β = wave number of shear waves = $\omega^2\rho/\mu$

(κ is defined over the complex wave number plane)

ω = circular frequency

ρ = mass density

λ, μ = Lamé constants

z = amplitude of incident Rayleigh wave

$$\text{Det } (\kappa) = \begin{vmatrix} P(\kappa) & Q(\kappa) \\ R(\kappa) & S(\kappa) \end{vmatrix}$$

$$P(\kappa) = 2\kappa\mu\sqrt{\kappa_\alpha^2 - \kappa^2}$$

$$Q(\kappa) = \mu\left(2\kappa^2 - \kappa_\beta^2\right)$$

$$R(\kappa) = -\lambda\kappa_c^2 - 2\mu\left(\kappa_\alpha^2 - \kappa^2\right)$$

$$S(\kappa) = -2\kappa\mu\sqrt{\kappa_\beta^2 - \kappa^2}$$

$$\text{Det } (\kappa) = 0 \text{ , at } \kappa = \kappa_R$$

$$A(\kappa,\chi) = \frac{P(\alpha)}{\kappa - \alpha(\chi)} + z\,\frac{Q(\beta)}{\kappa - \beta(\chi)}$$

$$B(\kappa,\chi) = \frac{R(\alpha)}{\kappa - \alpha(\chi)} + z\,\frac{S(\beta)}{\kappa - \beta(\chi)}$$

$$\alpha(\chi) = \kappa_R \cos\chi - i\sqrt{\kappa_R^2 - \kappa_\alpha^2}\sin\chi$$

$$\beta(\chi) = \kappa_R \cos\chi - i\sqrt{\kappa_R^2 - \kappa_\beta}\sin\chi$$

Where κ_R is a solution of

$$\left(2\kappa_R^2 - \kappa_\beta^2\right)^2 - 4\kappa_R^2\sqrt{\kappa_R^2 - \kappa_\alpha^2}\sqrt{\kappa_R^2 - \kappa_\beta^2} = 0$$

Note that for small values of χ , both $\alpha(\chi)$ and $\beta(\chi)$ are approximately equal to κ_R .

12. The numerical evaluation of equation A1 is straightforward. Fig. A2 shows the agreement between theory and experiment for the range $-60 \text{ deg} < \chi < +70 \text{ deg}$. In fig. A3, $S_{m,n}(\chi,\sigma)^2$ is an even function of χ , and a function of Poisson's ratio σ . For fixed χ , the magnitude

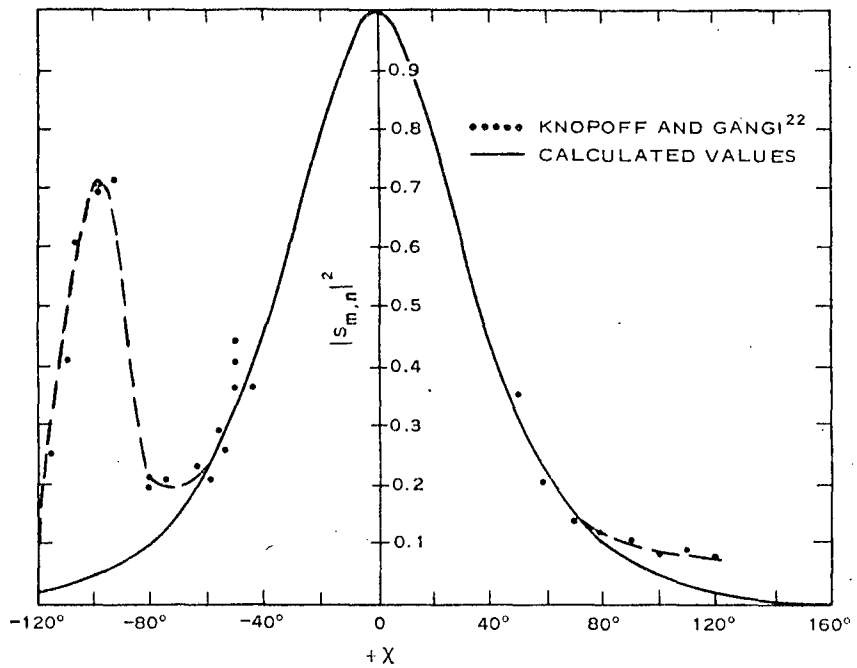

Fig. A2. A comparison of the leading term in an iteration of $|S_{m,n}|^2$ with the measured data of Knopoff and Gangi for Poisson's ratio $\sigma = 0.266$ (from reference 12)

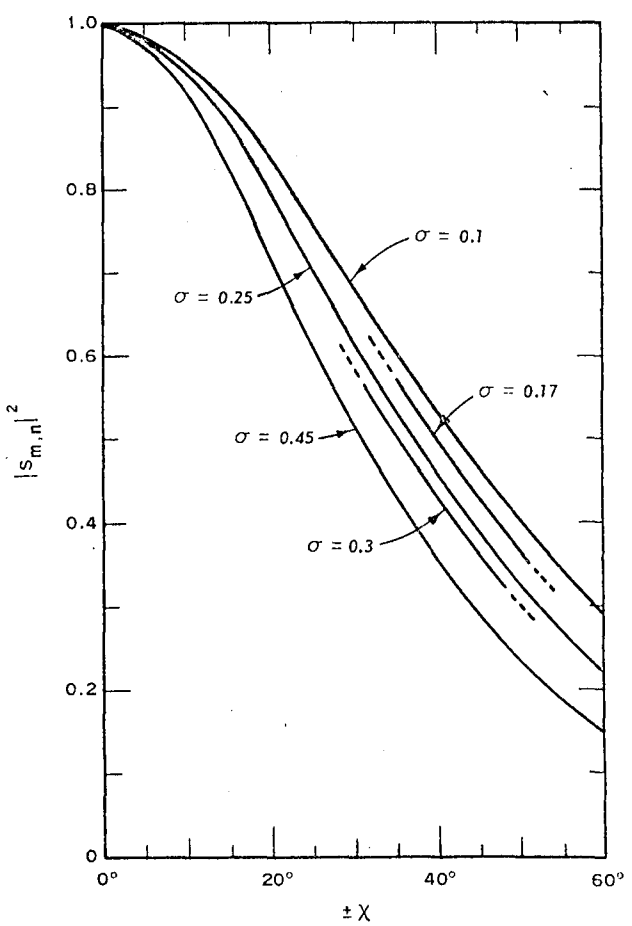

Fig. A3. The absolute square of the macrogeometry transmission coefficient $S_{m,n}$ which is an even function of the wedge angle X (from reference 12)

of transmission coefficients varies inversely as Poisson's ratio. In fig. A4, the phase of $S_{m,n}(\chi,\sigma)$ is an odd function of χ. This phase variation is almost linear and is insensitive to changes in Poisson's ratio.

13. Experimental results. The energy reflection and transmission coefficients of Rayleigh waves as functions of wedge angles are shown in

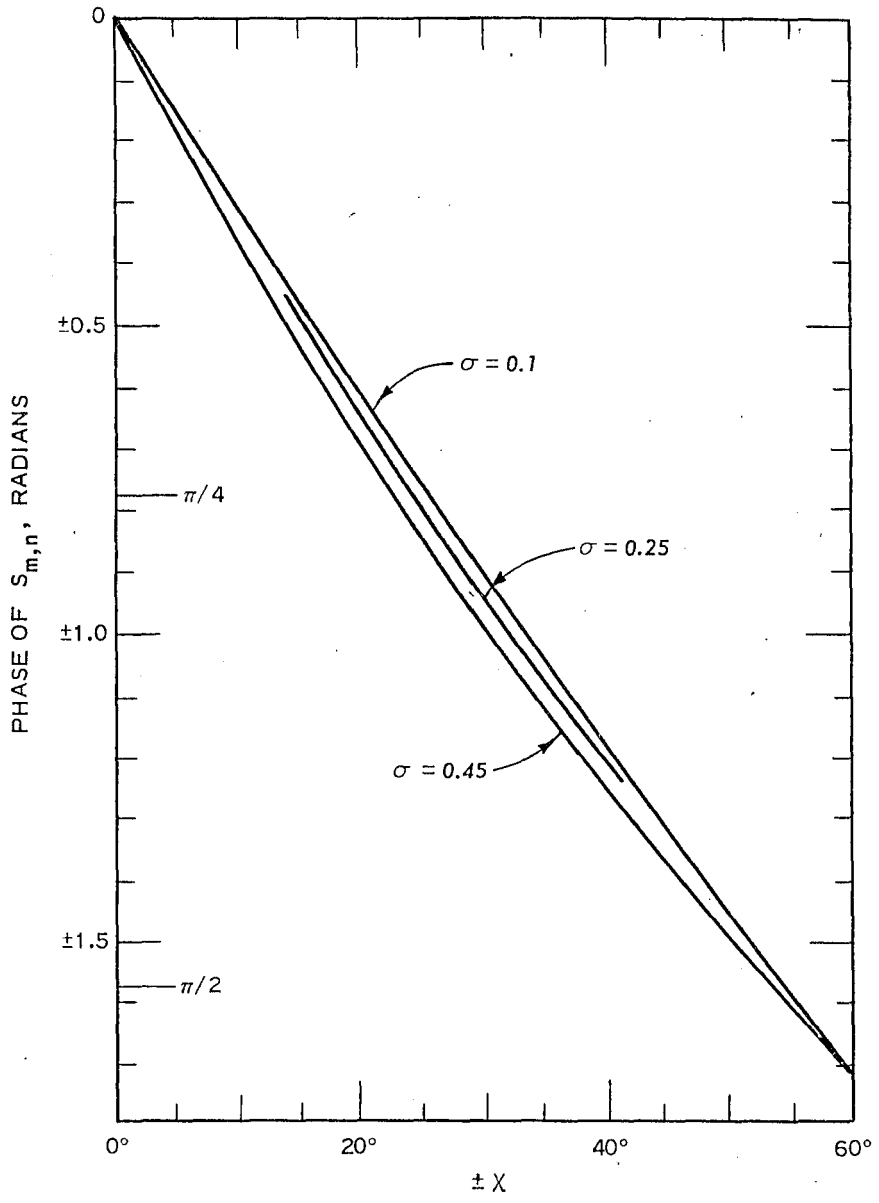

Fig. A4. The phase of $S_{m,n}$ which is an odd function of the wedge angle χ. Positive values of phase correspond to positive values of χ (from reference 12)

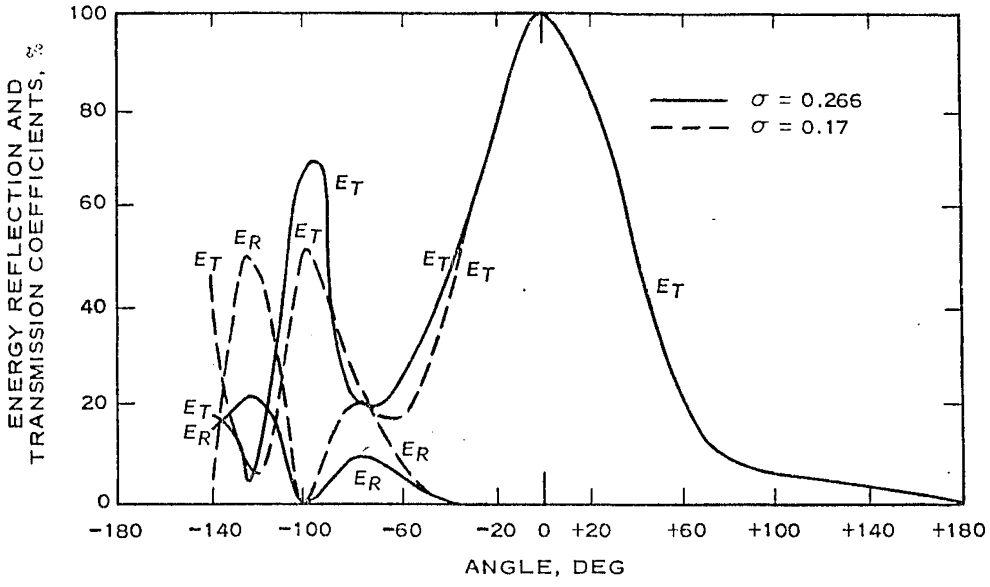

Fig. A5. Energy reflection and transmission coefficients. Results for aluminum (σ = 0.266) are compared with those obtained by de Bremaecker (σ = 0.17) (from references 21 and 22)

fig. A5. These data are the experimental results of de Bremaecker[21] and Knopoff and Gangi.[22] Significant shifts in the peaks, both in angle and in magnitude, are observed, since the Poisson's ratios used for the two experiments were different.

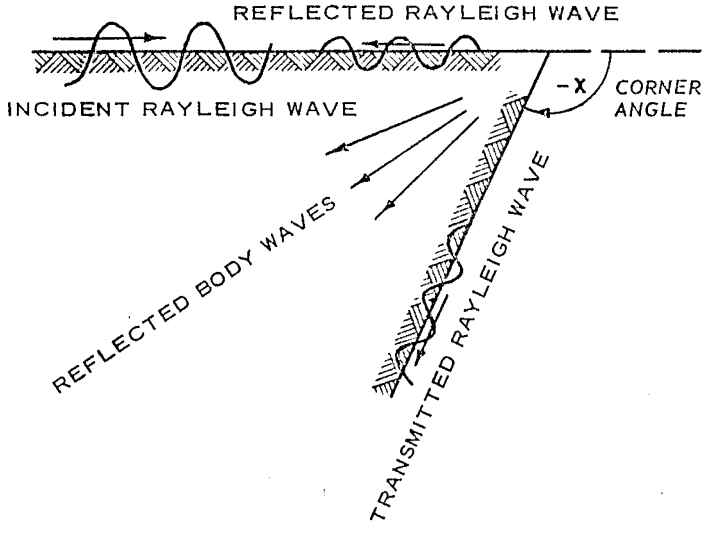

Fig. A6. Partition of Rayleigh wave energy at a corner (from reference 2)

14. As shown in fig. A6, an incident Rayleigh wave at a corner is partitioned among three types of waves: (a) a reflected Rayleigh wave, (b) a transmitted Rayleigh wave, and (c) reflected body waves. Fig. A7 shows the ratios of reflected Rayleigh wave energy to incident Rayleigh wave energy as functions of the corner angle, as determined in

model studies by Viktorov,[29] de Bremaecker,[21] and Pilant, et al.[23] It is interesting to note that the minimum Rayleigh wave energy is reflected at a corner angle of about -100 deg. The reflected Rayleigh wave energy is negligible over angles of 0 to -20 deg.

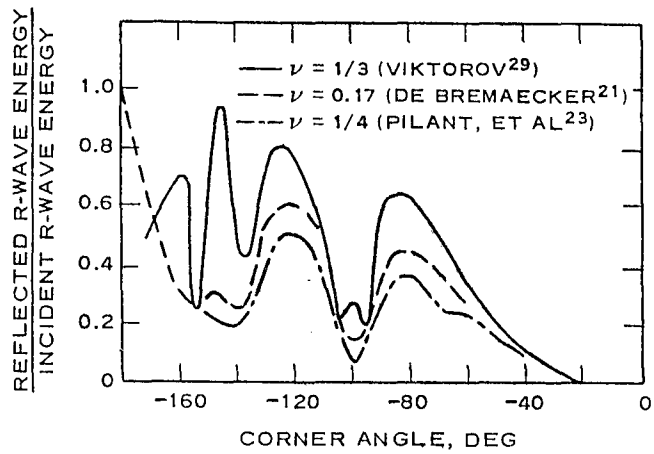

Fig. A7. Ratio of reflected R-wave energy to incident R-wave energy versus corner angle (from reference 2)

Step discontinuity of the free surface

15. The advent of long-period ocean bottom seismographs has made direct measurements of Rayleigh wave transmission across continental margins possible. Mal and Knopoff[26] and McGarr and Alsop[28] have attacked this problem of margin effects on Rayleigh waves with an integral representation theory and an approximate variational method, respectively. The latter shows reasonably accurate predictions of the transmission coefficients in comparison with model experiments. In this section, only the results of McGarr and Alsop are presented. The detailed mathematical derivations of the reflection and transmission coefficients can be found in reference 23. Fig. A8 is a

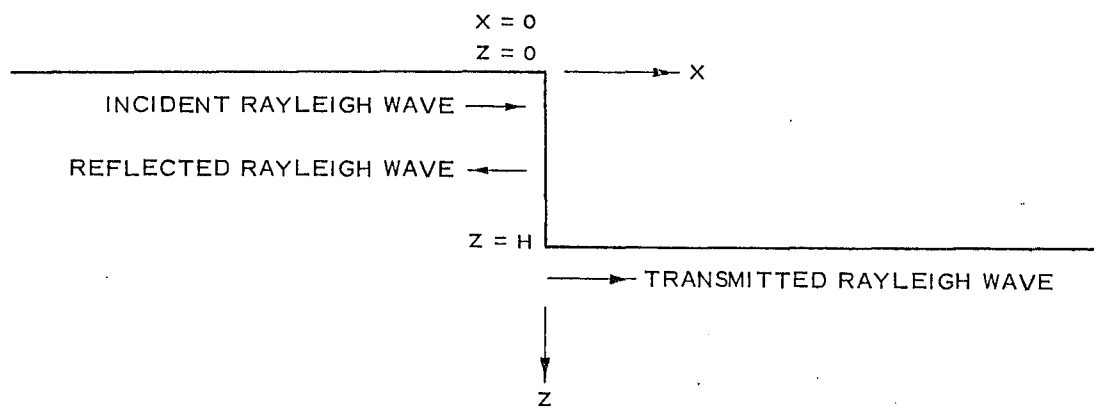

Fig. A8. Schematic diagram illustrating the case of a Rayleigh wave incident on the elevated side of a step in an otherwise homogeneous half-space (from reference 28)

schematic diagram for wave transmission from the elevated side to the depressed side of a step. It is reasonably assumed that the only Rayleigh modes that exist are the fundamental modes on either side of the step. Drake,[31] from his analysis of models of the Sierra Nevada and of a continental boundary for Rayleigh wave motion, shows that 95 percent of the incident energy is transmitted in the fundamental mode.

16. Theoretical calculations and experimental data are compared in figs. A9 and A10. The macrogeometry reflection and transmission coefficients were obtained by dividing each Fourier component of reflected or transmitted pulses by that of the direct pulse. The coefficients were then expressed as functions of the dimensionless variable $\omega H/\beta$, where ω is the angular frequency, H is the height of the step, and β is the shear wave velocity. The computed and observed reflection coefficients (fig. A9) are not in good agreement because the size of the model was limited and the signal-to-noise ratio of the reflected wave was much less than that of the transmitted wave. From the viewpoint of energy transport distribution, the reflection coefficient is unimportant compared with the transmission coefficient. Fig. A10 shows fair agreement between the theoretical and experimental transmission coefficients for waves incident on both sides of a step. In short, both the experimental and theoretical results show that the transmission and reflection coefficients are significantly less when waves are propagated from the depressed side to the elevated side of a step discontinuity than when propagated in the opposite direction. This probably means that more body waves are generated by this type of discontinuity.

Vertical discontinuity

17. An experiment was also performed by McGarr and Alsop[28] to ascertain the effect of vertical boundaries (discontinuity) on Rayleigh waves traveling from one type of material to another. Fig. A11 shows an experimental model in which two quarter-spaces with different densities and elastic constants were welded together to form a half-space. In general, the model experiments have shown that the theory developed by McGarr and Alsop[28] provides an accurate description of the effect of a

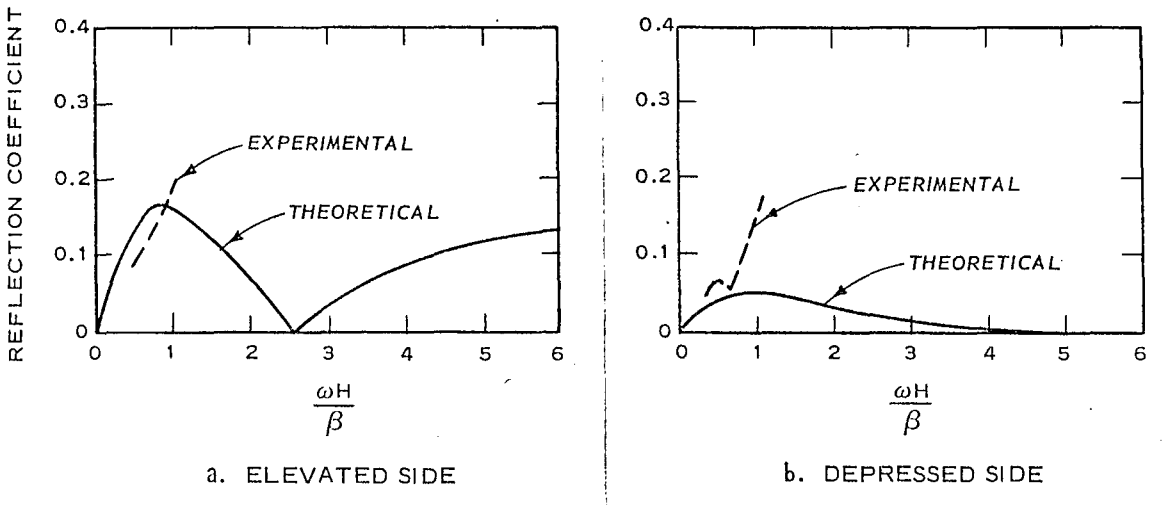

Fig. A9. Comparisons of theoretical and experimental reflection coefficients for waves incident on a step discontinuity (from reference 28)

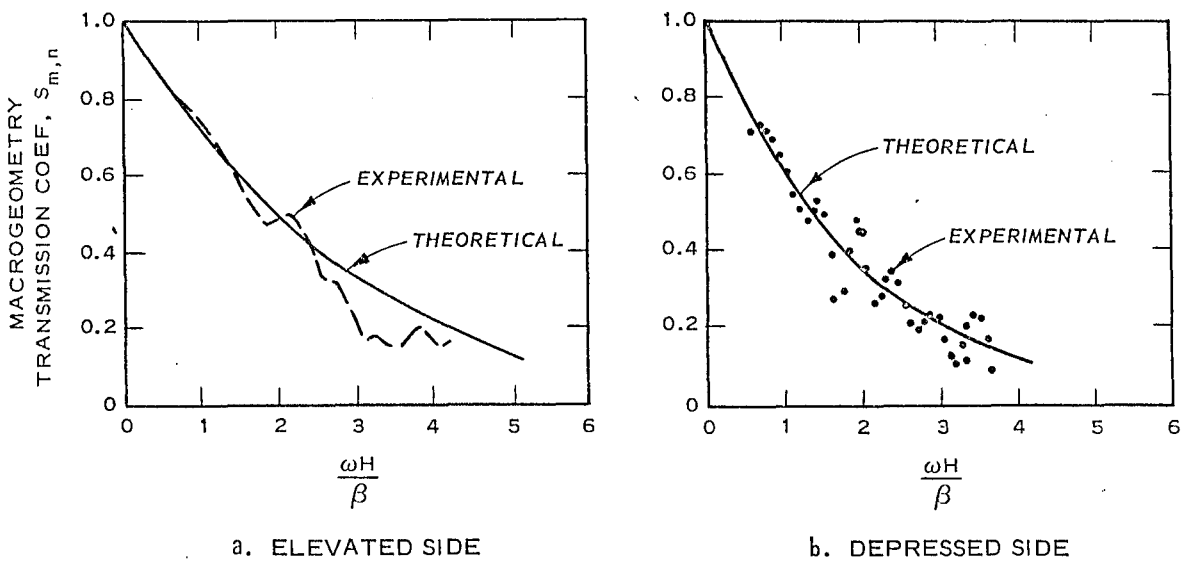

Fig. A10. Comparisons of theoretical and experimental macrogeometry transmission coefficients for waves incident on a step discontinuity (from reference 28)

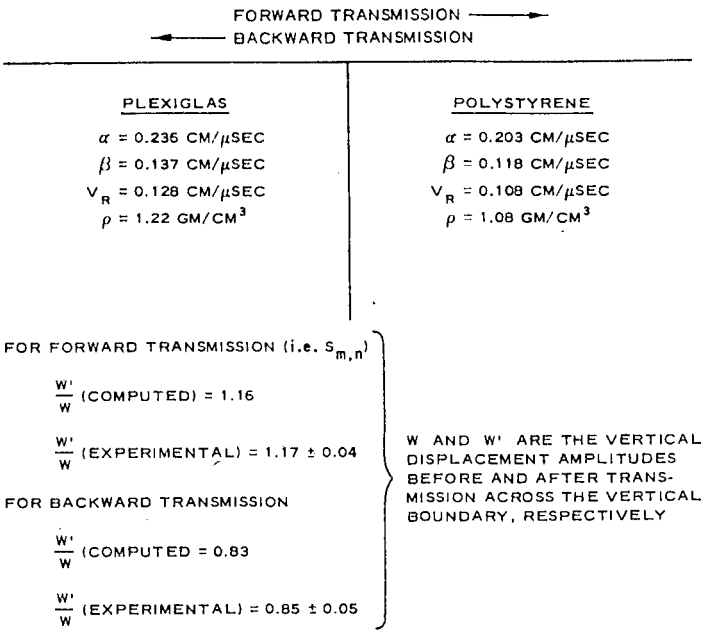

Fig. A11. Schematic diagram illustrating transmission from Plexiglas to polystyrene and vice versa (from reference 28)

vertical discontinuity on Rayleigh waves as long as the contrast between wave velocities is not great.

18. Ottaviani[32] studied both the elastic-wave propagation with a compressional line source in a quarter-space and in a two quarter-space by using the finite difference method. Reflected, converted, transmitted, and diffracted phases are identified and interpreted. Surface and interface waves, originated at the corner by diffraction of the source pulse, are investigated as a function of the rigidity contrast and the velocity contrast between the two media and of the position of the source. The coefficient of transmission for Rayleigh waves around the corner in a quarter-space is almost equal to that of the coefficient of reflection. The finding is in agreement with earlier experimental results obtained by de Bremaecker[21] and Knopoff and Gangi.[22] The amplitude of R becomes very large at the corner and the major axis of the ellipse of polarization at the corner point is inclined 45 deg toward the positive x-axis.

Trench discontinuity
(experimental study)

19. For a better understanding of Rayleigh wave screening patterns as functions of barrier size (depth H, length L, and width w), distance r from the source to the barrier, and length of the surface waves λ_R, Woods and Richart[13,33] conducted several model experiments to investigate the effectiveness of trenches as vibration isolators. Fig. A12 shows the soil properties of the field site and a schematic drawing of the instrumentation. The important screening effects can be seen in figs. A13 and A14. Fig. A13 shows the amplitudes of vertical displacements for three tests with trenches of constant depth, but variable length. Fig. A14 shows amplitude reduction factor* contours for the same three tests. From these contours, the extent of the influence of the increased length of the trench can be seen. Three changes in the contours due to increased trench length are evident: (a) increased width of the screened zone, (b) increased length of the screened zone, and (c) decreased amplitude reduction factors in the screened zone.

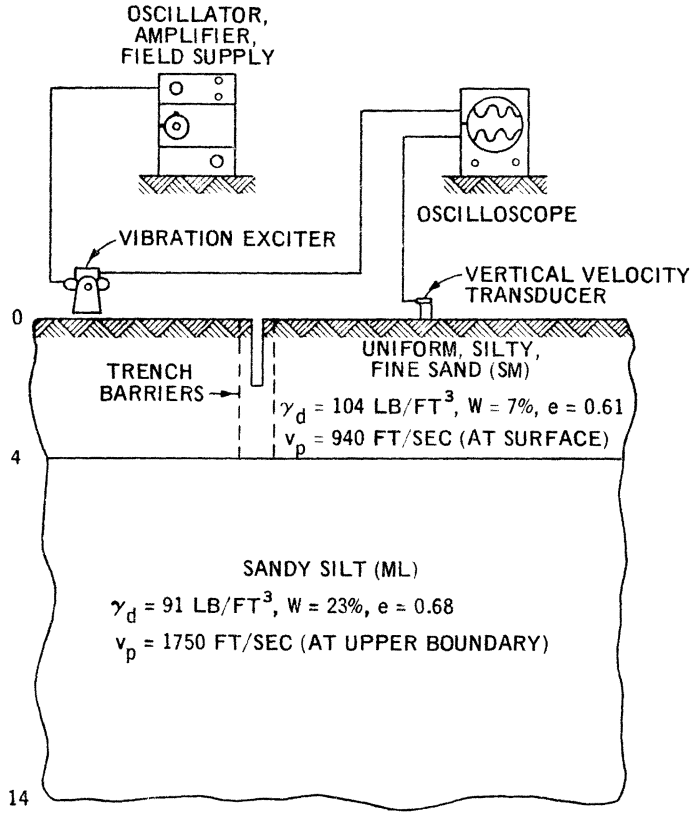

Fig. A12. Field site soil properties and schematic of instrumentation (from reference 13)

20. The specifying amplitude reduction factor and an effectively screened

* Amplitude reduction factor is defined as the ratio of the amplitude of a Rayleigh wave measured after a trench is dug to the amplitude measured before the trench is dug.

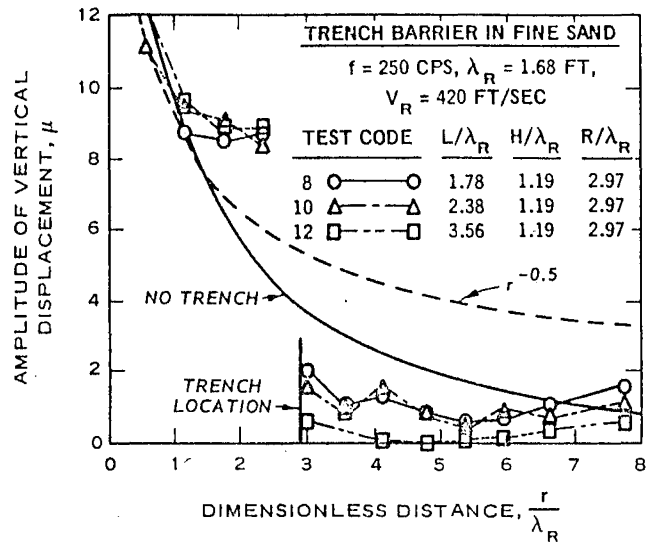

Fig. A13. Amplitude of vertical displacement versus distance from source for a trench in fine sand (from reference 13)

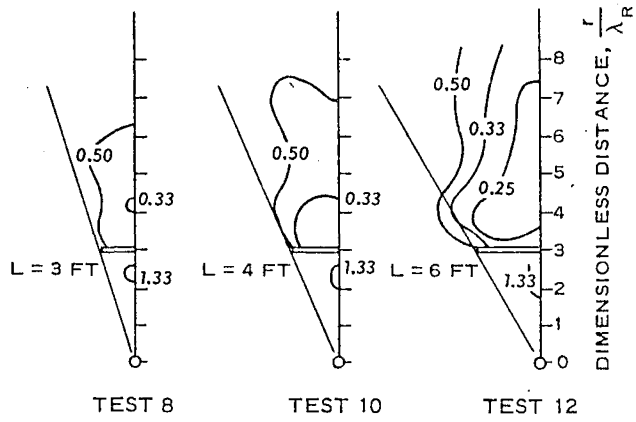

Fig. A14. Comparison of amplitude reduction factor contours for constant trench depth and variable trench length (from reference 13)

zone are two criteria required for design of isolation barriers. Woods[13] found the following important results.

a. A minimum depth of $H/\lambda_R = 0.6$ was required for a trench to satisfy the amplitude reduction factor of 0.25. The zone screened extended to a distance at least $10\lambda_R$ from the source of excitation.

b. To maintain the same degree of isolation, the scaled area of the trench $\left[(H/\lambda_R)(L/\lambda_R) = HL/(\lambda_R)^2\right]$ should be increased as the distance from the source r increases. The scaled area should be at least 2.5 at $r = 2\lambda_R$ and at least 6 at $r = T\lambda_R$.

c. Trench width had little influence on the effectiveness of open trenches for W/λ_R between 0.13 to 0.91.

d. Amplitude magnification of vertical motion occurred in front of (on the same side as the exciter) and near the ends of the trench caused by reflected and diffracted waves, respectively.

A sloping interface (seismic model studies)[31]

21. For a uniformly horizontal layer overlying a half-space, the phase velocity of Rayleigh waves for a given Fourier component is

$$V_R = \frac{\Delta x}{\Delta t} = \frac{\omega}{\kappa}$$

where V_R is constant, as illustrated in fig. A15a; Δx = distance between a pair of adjacent stations, x_2 and x_1 ; and Δt = difference of arrival times, t_2 and t_1 , for a particular phase.

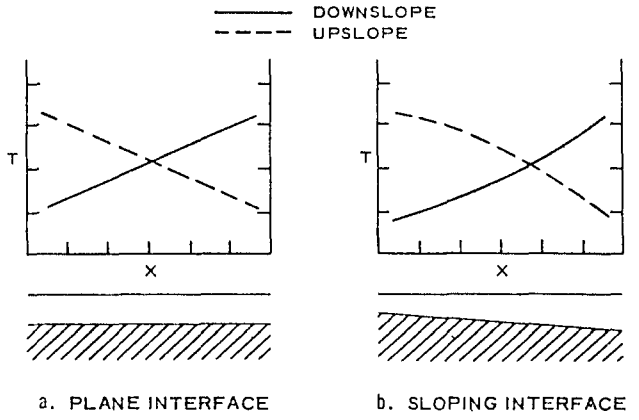

Fig. A15. Time-distance plots for determination of Rayleigh wave phase velocities (from reference 30)

22. For a sloping interface with a linear variation in layer thickness, the time-distance plot for a given Fourier component is no longer linear, i.e. the $t - x$ curves for upslope and downslope become convex downward and convex upward, respectively, if the velocities of surface layer are less than that of the underlying half-space (fig. A15b). The observed phase velocity becomes an effective phase velocity. Since the local phase velocity is a single-value function, the effective phase velocity is independent of the direction of wave propagation. The effective phase velocity C^*, as in the case of a flat layer, can be defined as

$$C^* = \frac{\Delta x}{\Delta t} = \frac{\omega(x_2 - x_1)}{\int_{x_1}^{x_2} \phi' \, dx} = \frac{(x_2 - x_1)}{\int_{x_1}^{x_2} \frac{dx}{C_x(x)}}$$

As the distance between a pair of adjacent stations approaches zero, the effective phase velocity approaches a limiting value, which is defined as local phase velocity C_x.

$$\frac{1}{C_x} = \lim_{\Delta x \to 0} \frac{\Delta t}{\Delta x} = \frac{\phi'}{\omega} = \frac{\kappa}{\omega}$$

23. The experimental model of Kuo and Thompson[30] (fig. A16) was two-dimensional and 1/6 in. thick, and consisted of a Plexiglas surface layer and a Panelyte half-space. The surface layer ranged from 1/4 to 3/4 in. in depth with a dip of approximately 2-1/2 deg.

24. Oscillograms of the inversely dispersed Rayleigh waves at various distances for the downslope and the upslope profiles are shown in fig. A17. For the downslope profile, the energy of the incident wave is almost totally transmitted. Because the slope of the interface is only 2-1/2 deg, the transmitted Rayleigh wave train is nearly free from any interference. For the upslope profile, the energy is not totally transmitted from the thick-layer region to the thin-layer region; a part

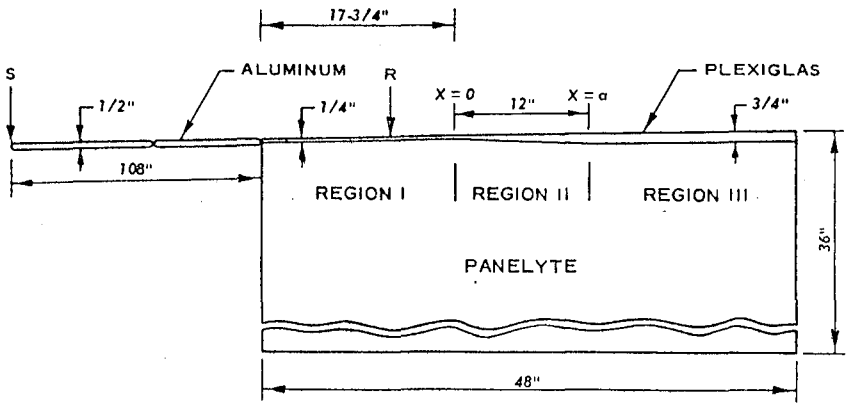

Fig. A16. Seismic model (from reference 30)

is converted into reflected waves. Such a conversion may result in the interference of the incident wave.

25. Fig. A18 shows the observed phase velocities of Rayleigh waves at various distances along the profiles for a given Fourier component. The phase velocity of Rayleigh waves gradually decreases in the downslope profile and gradually increases in the upslope profile. The velocities in the regions of uniformly thick layers are found to be unaffected by the sloping layer.

26. These experimental findings are very important for understanding and interpreting the propagation of Rayleigh waves on a sloping interface.

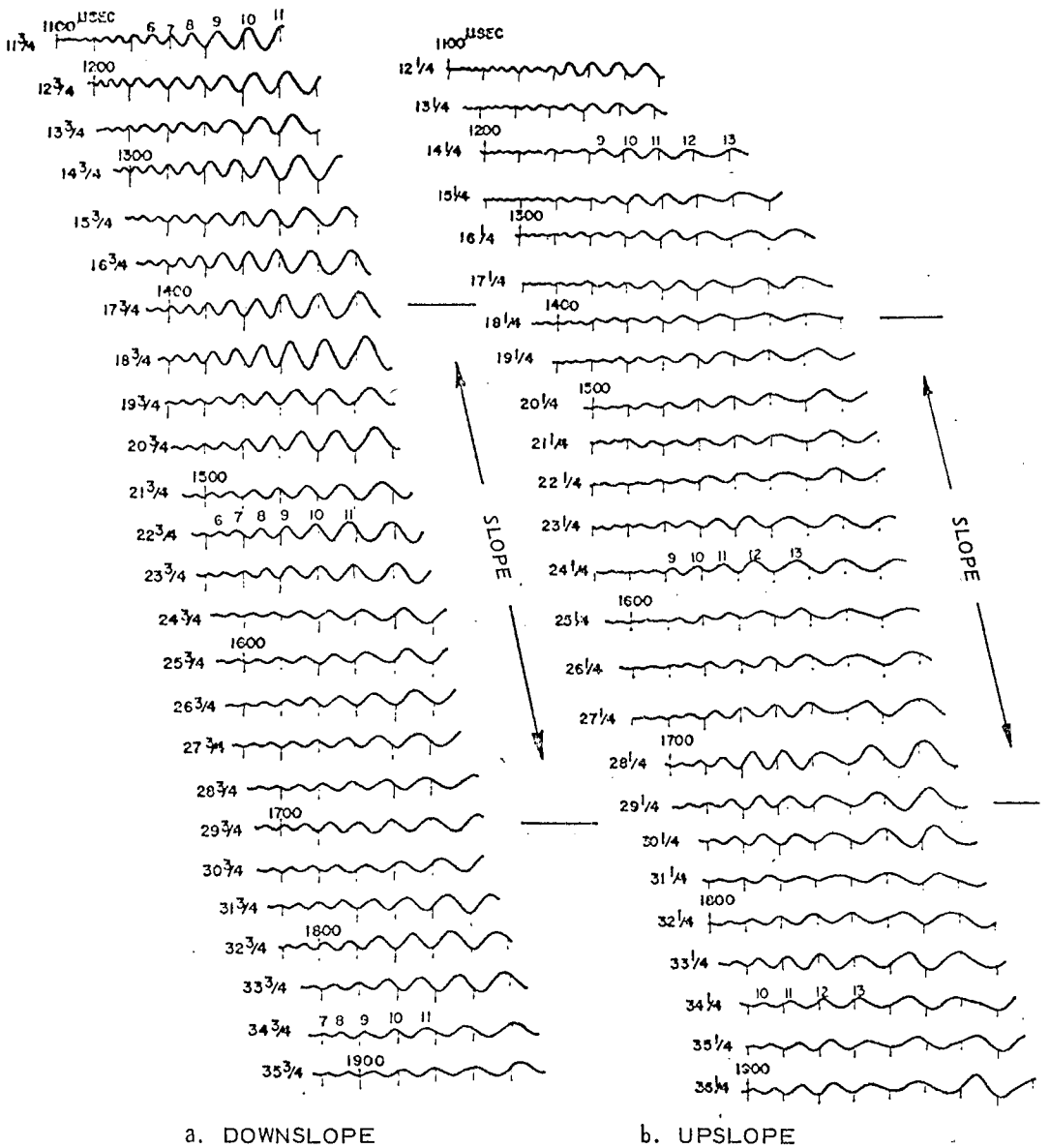

Fig. A17. Oscillograms showing dispersed wave train at various distances along (a) downslope and (b) upslope profiles (from reference 30)

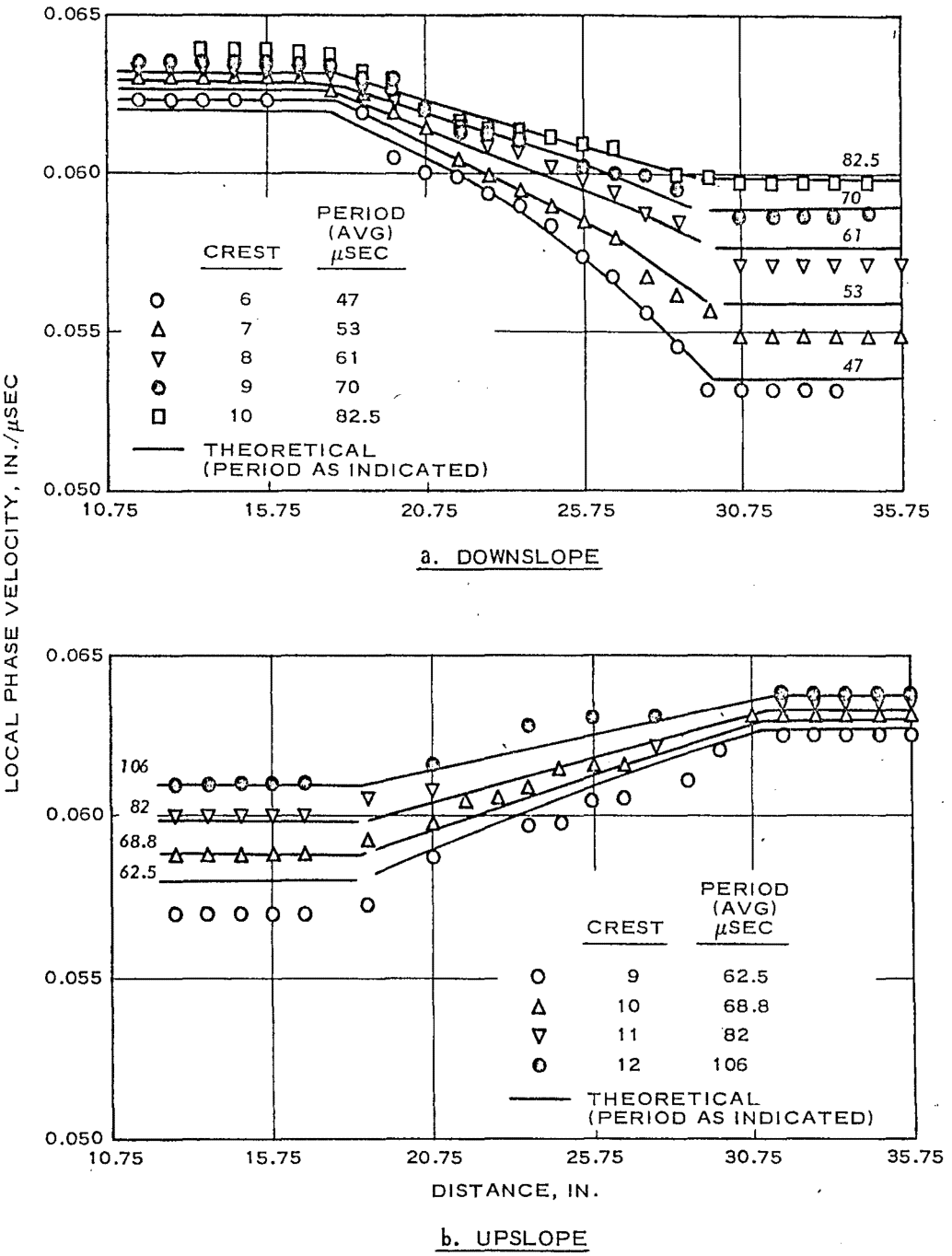

Fig. A18. Local phase velocity of Rayleigh waves as a function of distance, theoretically calculated (from reference 25)

APPENDIX B: COMPUTER PROGRAM TO PREDICT MICROSEISMIC SIGNALS IN TERRAIN MATERIALS

Function and Methods

1. A computer program was written to implement the microseismic propagation equation (see paragraph 47 in the main text). The ground was modeled as an isotropic, layered, viscoelastic structure with a viscous damping coefficient for each layer. Any type of periodic stress signal can be used as a source of excitation for the system. The program writes a data file for either the vertical or radial component of particle displacement, particle velocity, or particle acceleration at selected ranges. In addition, outputs from the predicted signal, the positive and negative peak amplitudes, the rms amplitude, and the average thresholds are produced as data files. These files can be saved from any problem for later use in other programs.

2. The program is written in FORTRAN IV language for the Honeywell G-437 digital computer with three output tapes and a high-speed printer. Typical running time for a two-layer, single-mode problem with 200 frequency components is 4 min. With 512 frequency components and 5 soil layers, the code requires about 28K storage.

Input

3. A description of the input variables is given in table B1, with a sample deck setup shown in fig. B1.

Output

4. A listing of output variables and their descriptions are shown (in order of appearance) in table B2, and printer output for a sample problem is presented in fig. B2. In addition, a magnetic tape is produced on which there are 1024 predicted peak particle velocity values for the given environmental conditions.

Program Listings

5. A listing of the entire computer program is shown in table B3.

Flow Charts

6. A schematic diagram for the entire program is shown in fig. B3. An index of the subroutines used and the function of each is shown in table B4; detailed flow charts of the main program and the subroutines are given in figs. B4-B29.

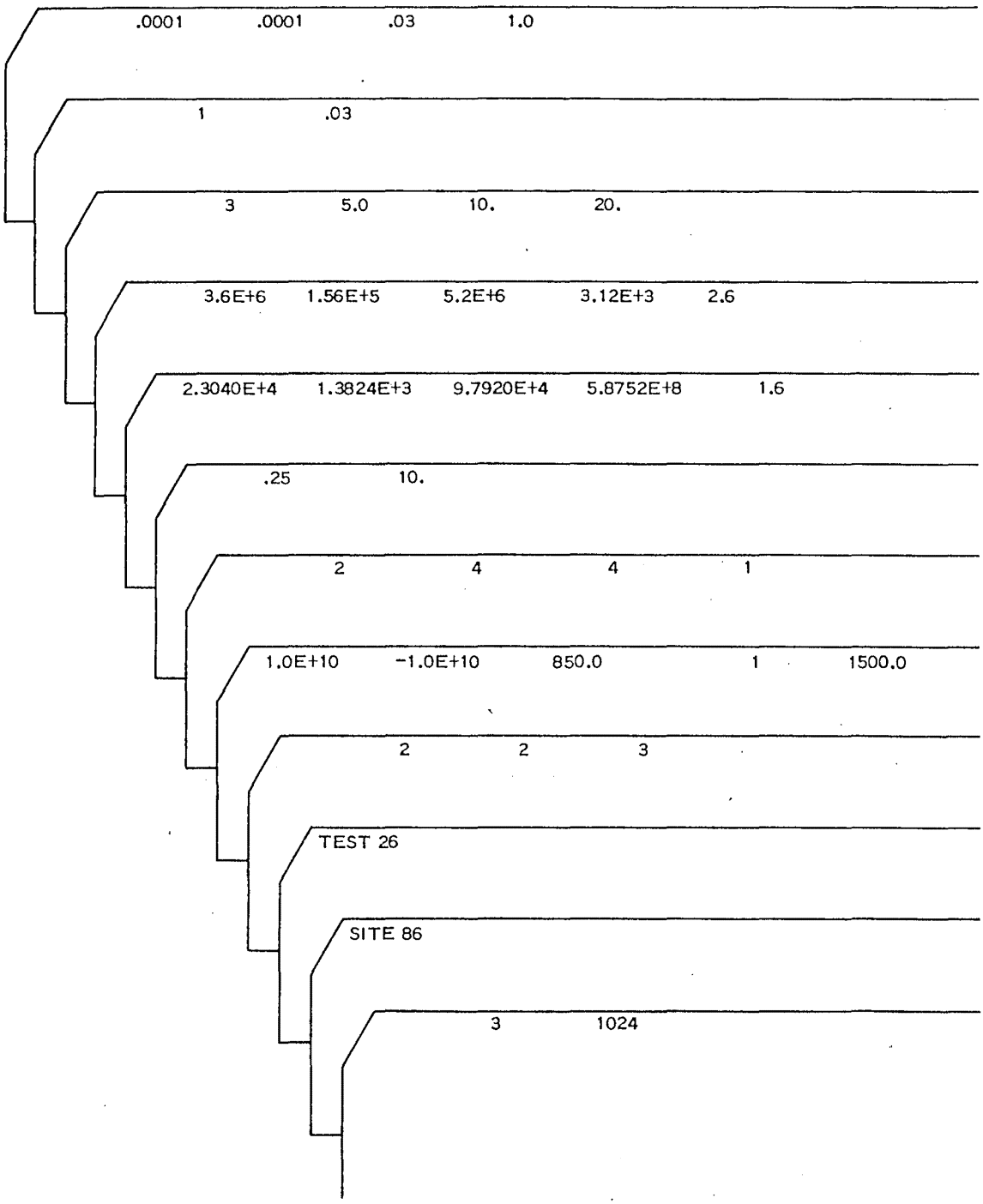

Fig. B1. Input card setup of a sample problem

```
    ORIGINAL SERIES
    66.400800    64.137000    61.873200
    FOURIER COEFFICIENTS
    71.512544     -.001316     0.302890     1.755280     -1.373347
     2.738365
     RECONSTRUCTION ORIGINAL SERIES
    66.400800    64.137000    61.873200
CMAX=      5.672CMIN=      0.000NO. HARMONIC=     512AZ=    71.51254
H(2)=     0.16497E=07 PHI(2)=     -.24387E+01
                                SEISMIC DATA
                    AVG POWER                    RMS
SEISMIC INPUT            2670.8 (MD)2          51.680 MD
TOTAL INPUT              2670.8 (MD)2          51.680 MD
SEISMIC OUTPUT      .33114E-04 (10-3 cm/sec)2   .57545E-02 10-3 cm/sec
TOTAL OUTPUT        .34399E-04 (10-3 cm/sec)2   .58651E-02 10-3 cm/sec
  YMAX1=          100.96  CMAX=           5.6725  YMAX=     0.16380E-01
PREDICTED YMIN=    -.432231E-01
  NO. OF POINTS= 1024      PEROID SEC.=          0.68267
  TRIGH =.38100E-01  NHIGH =     0
  TRIGM =.95250E-01  NMED =     0
  TRIGL =    0.23812  NLOW =     0
```

NOTE: See table B2 for output variable definition.

Fig. B2. Printer sample output

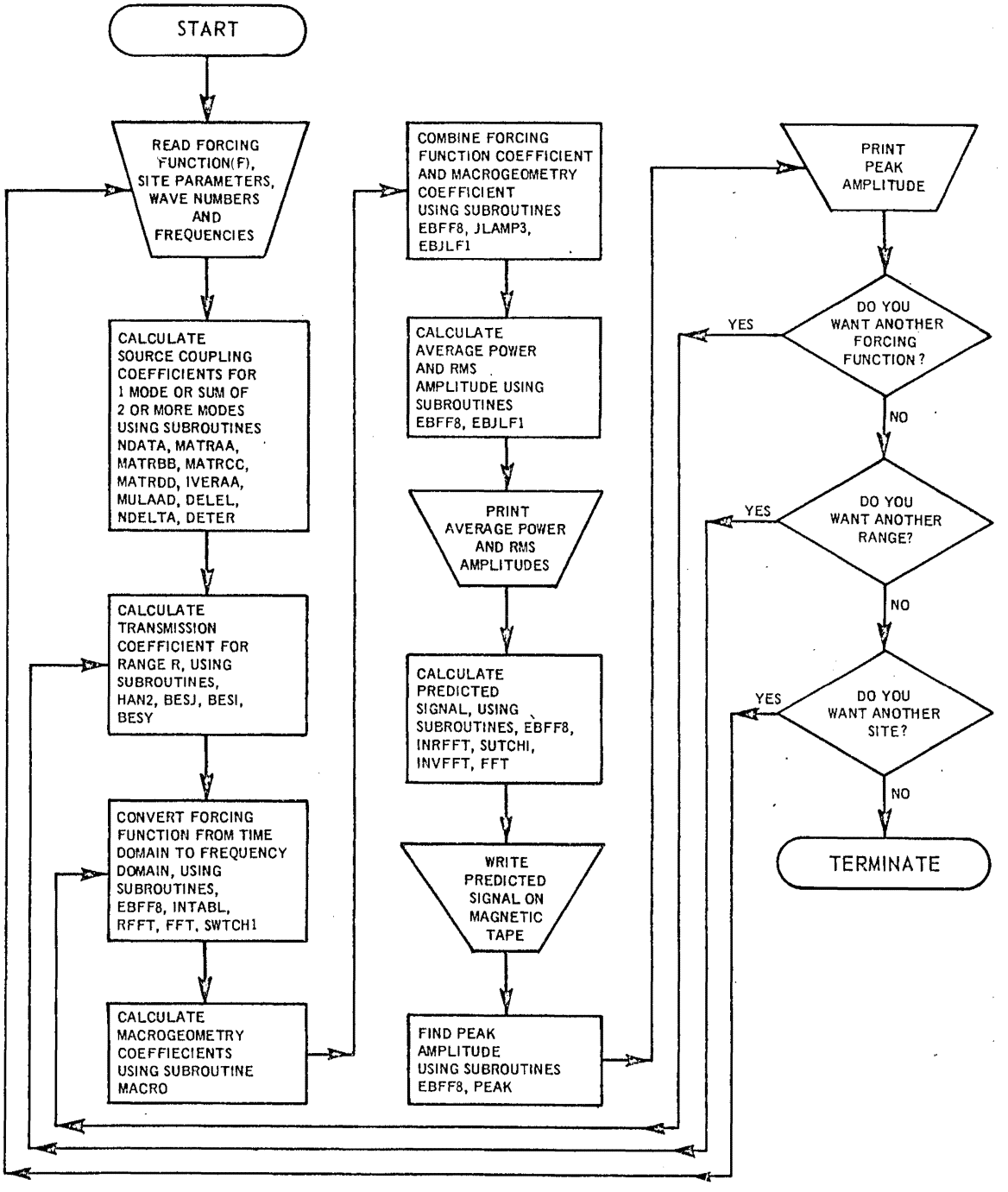

Fig. B3. General seismic model schematic diagram

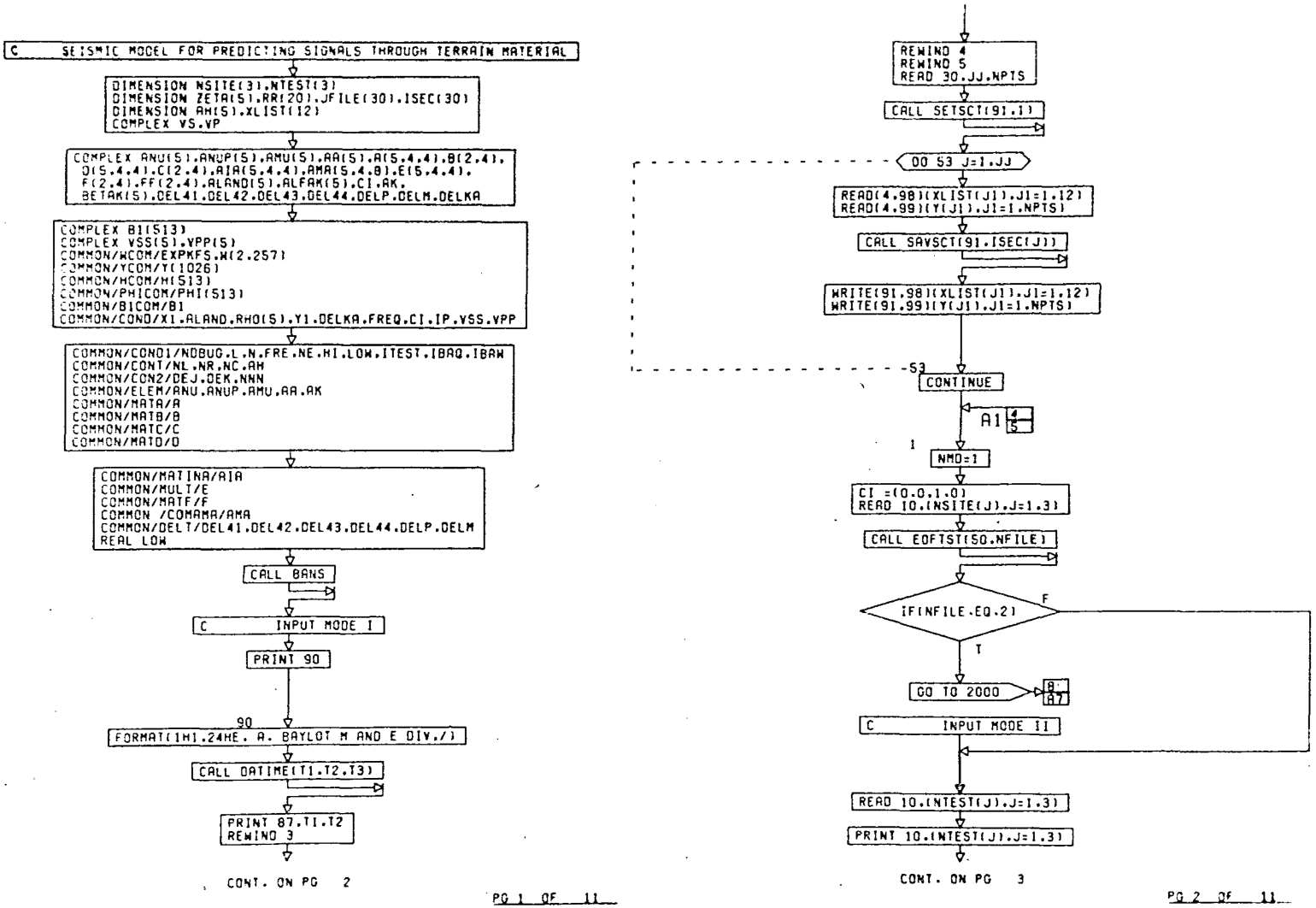

Fig. B4. Flow chart of main program (sheet 1 of 5)

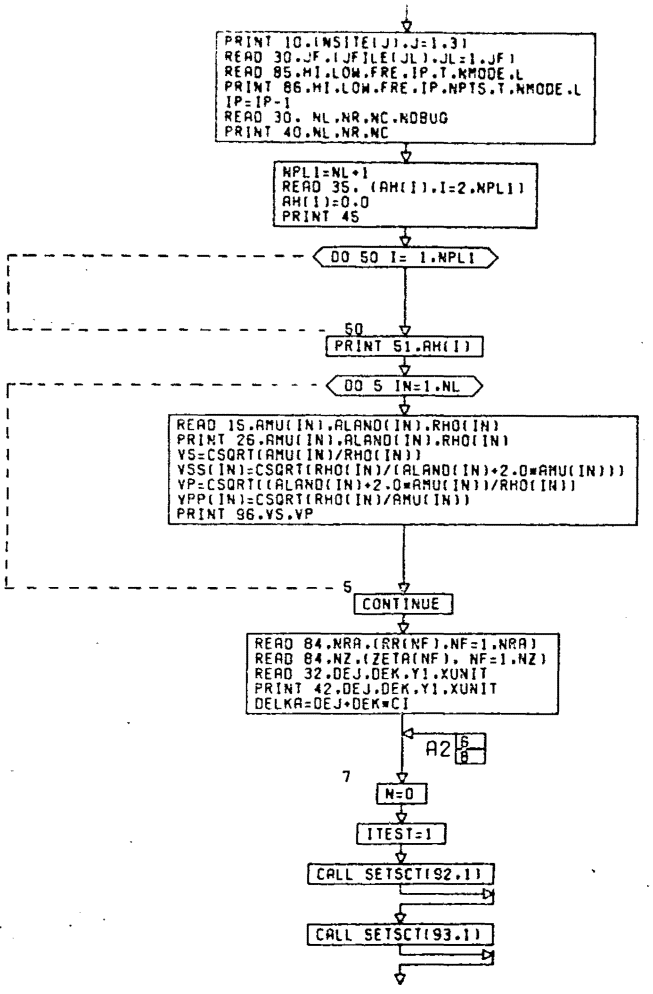

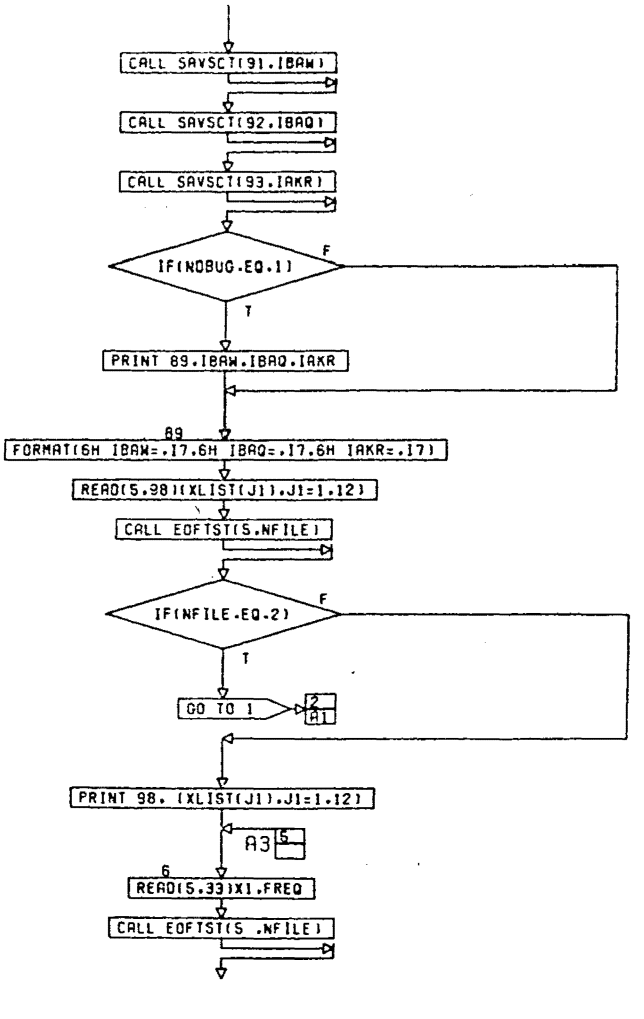

Fig. B4 (sheet 2 of 5)

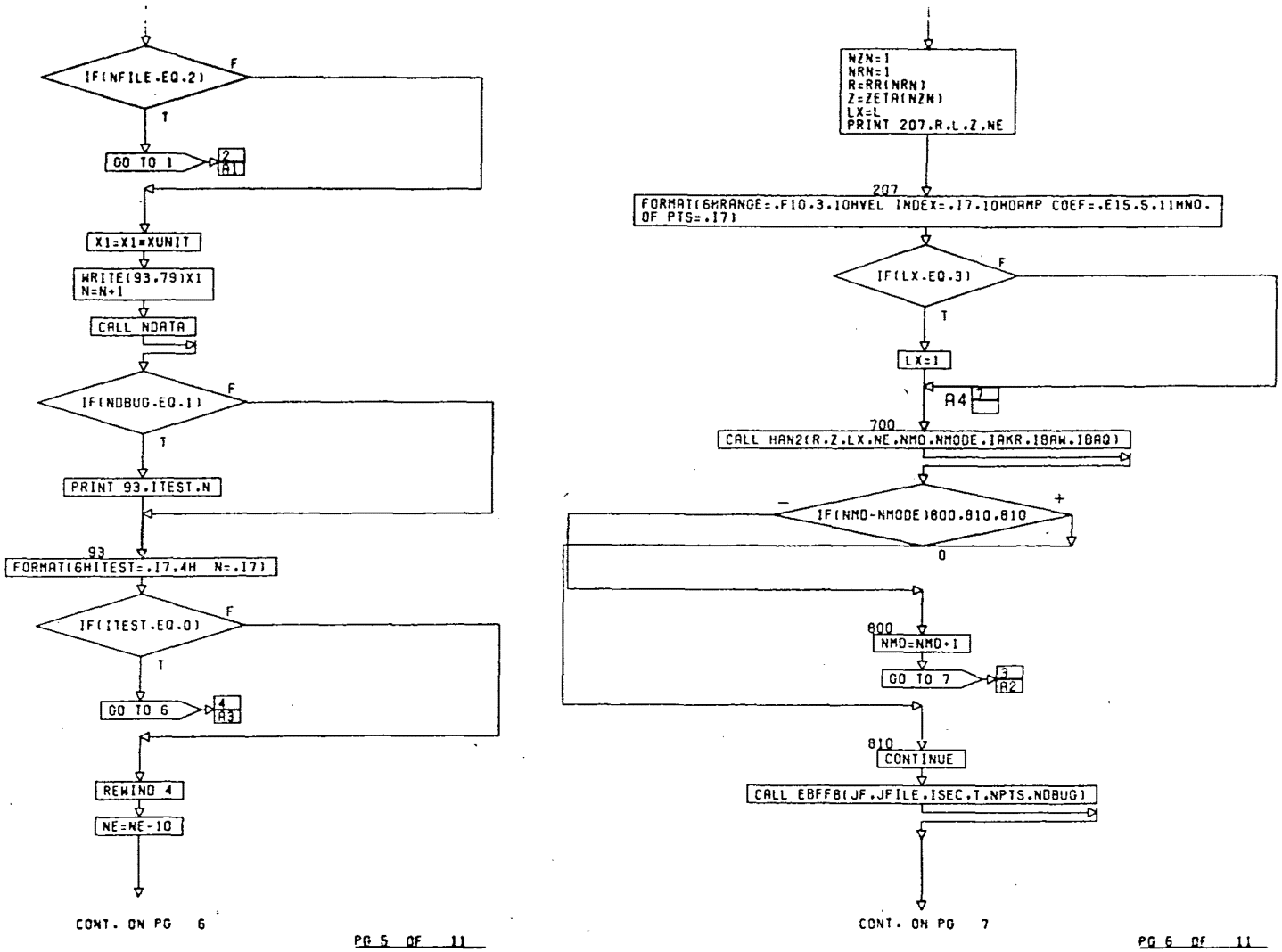

Fig. B4 (sheet 3 of 5)

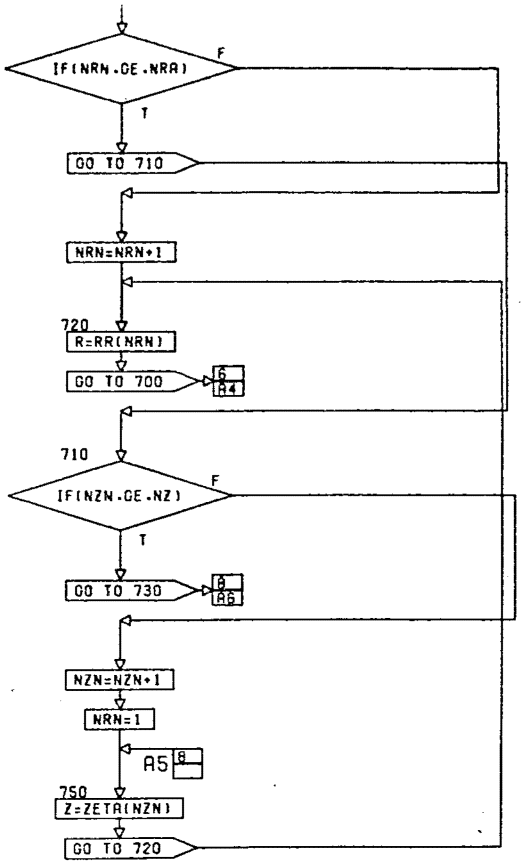

CONT. ON PG 8

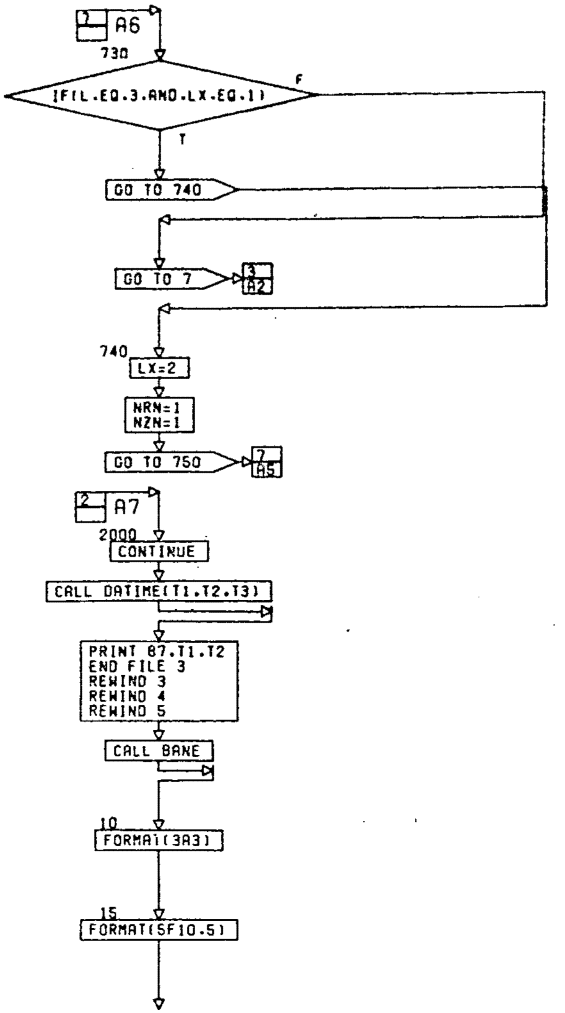

CONT. ON PG 9

Fig. B4 (sheet 4 of 5)

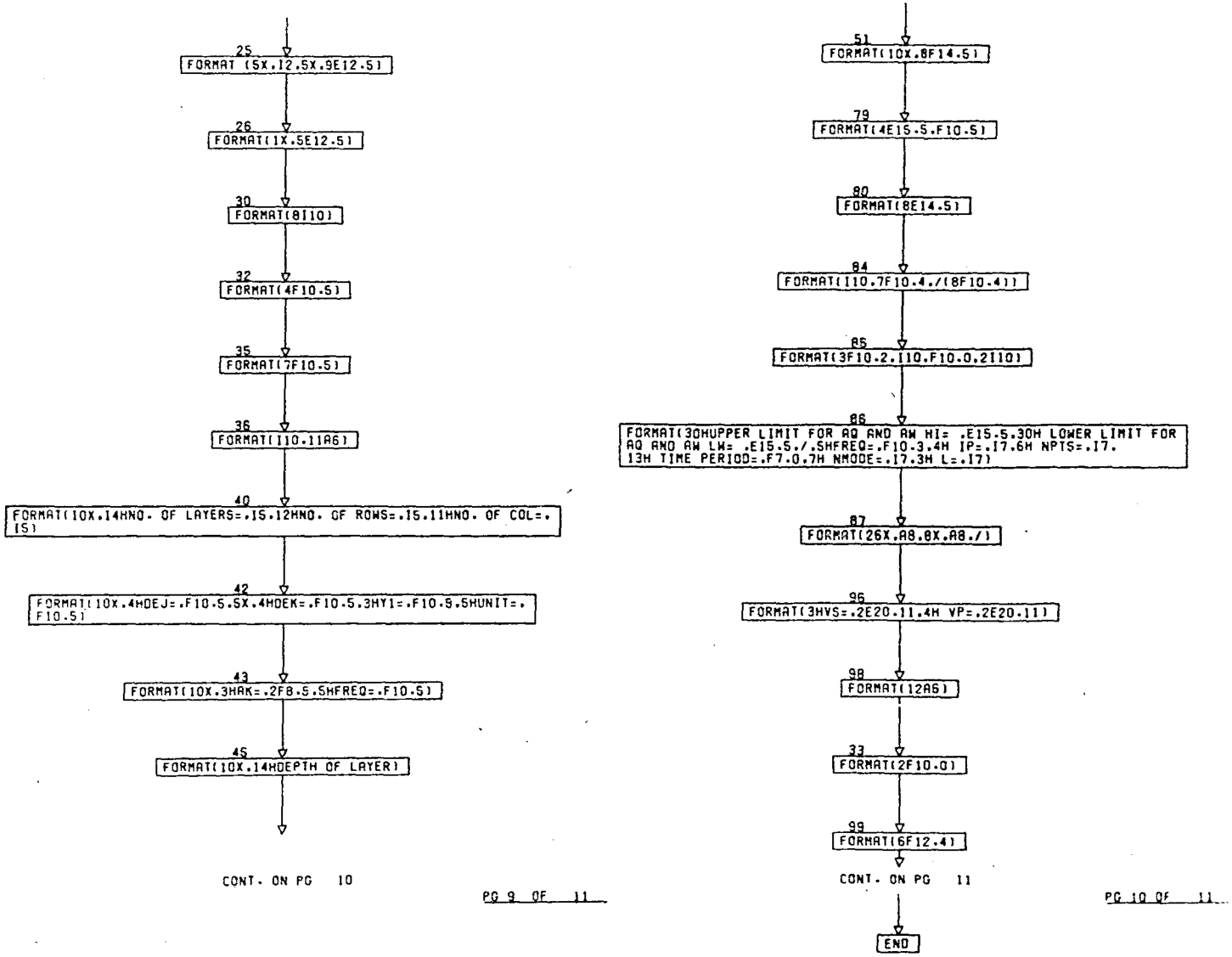

Fig. B4 (sheet 5 of 5)

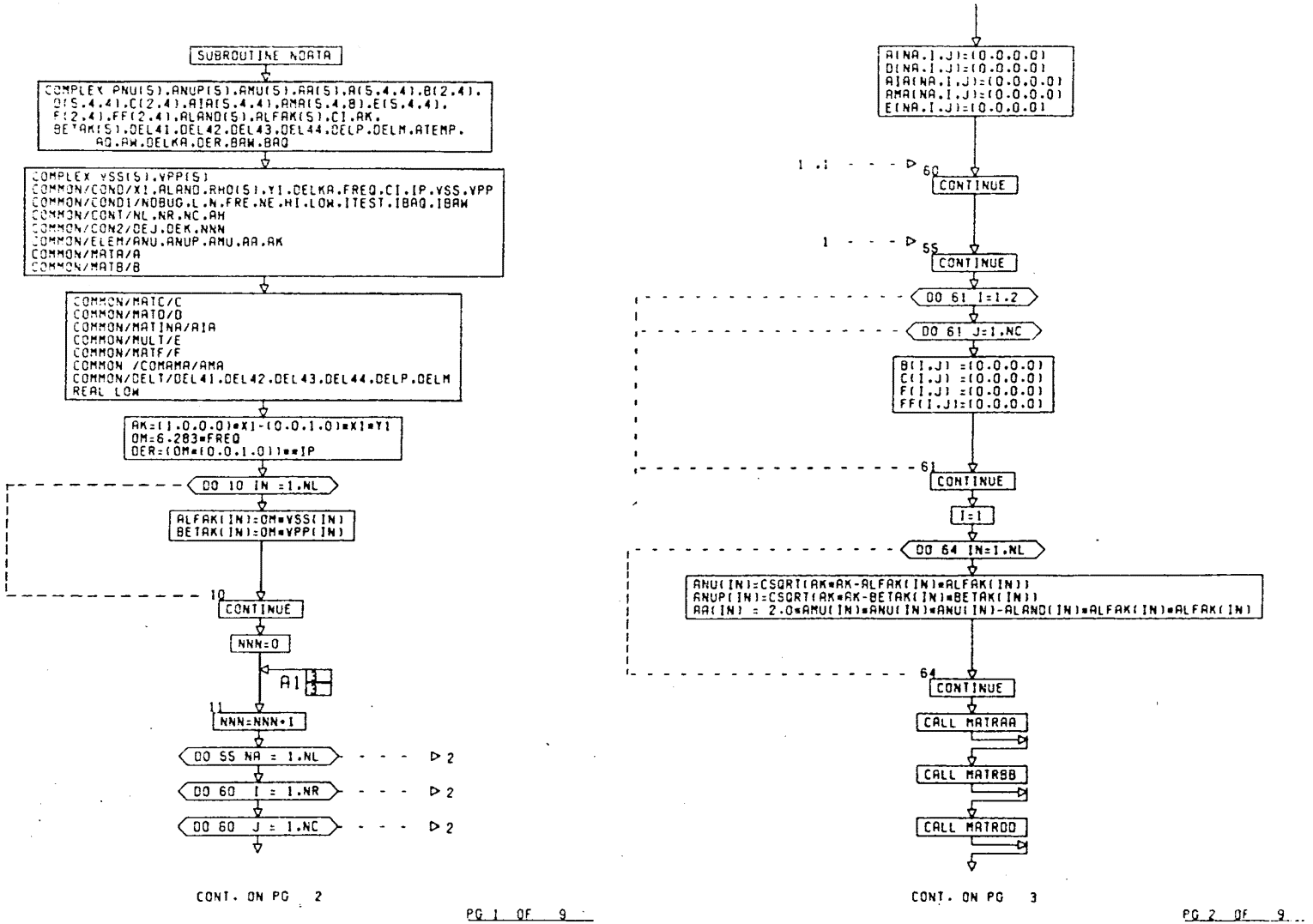

Fig. B5. Flow chart of subroutine NDATA (sheet 1 of 5)

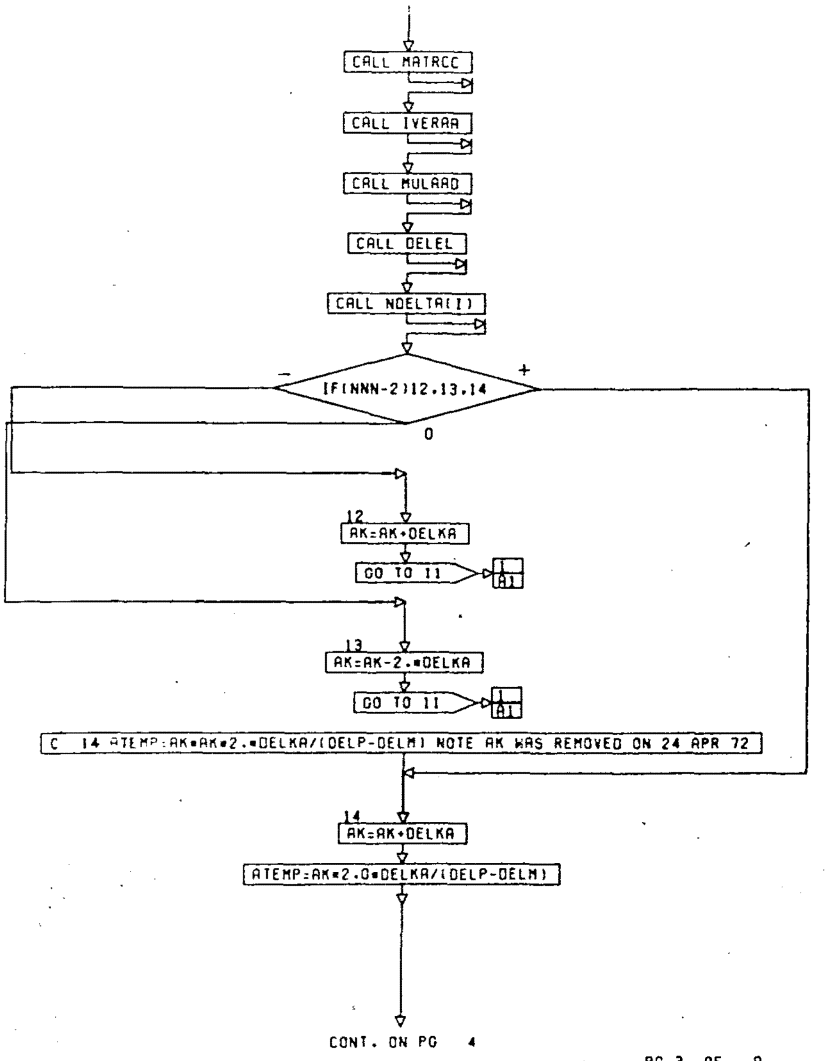

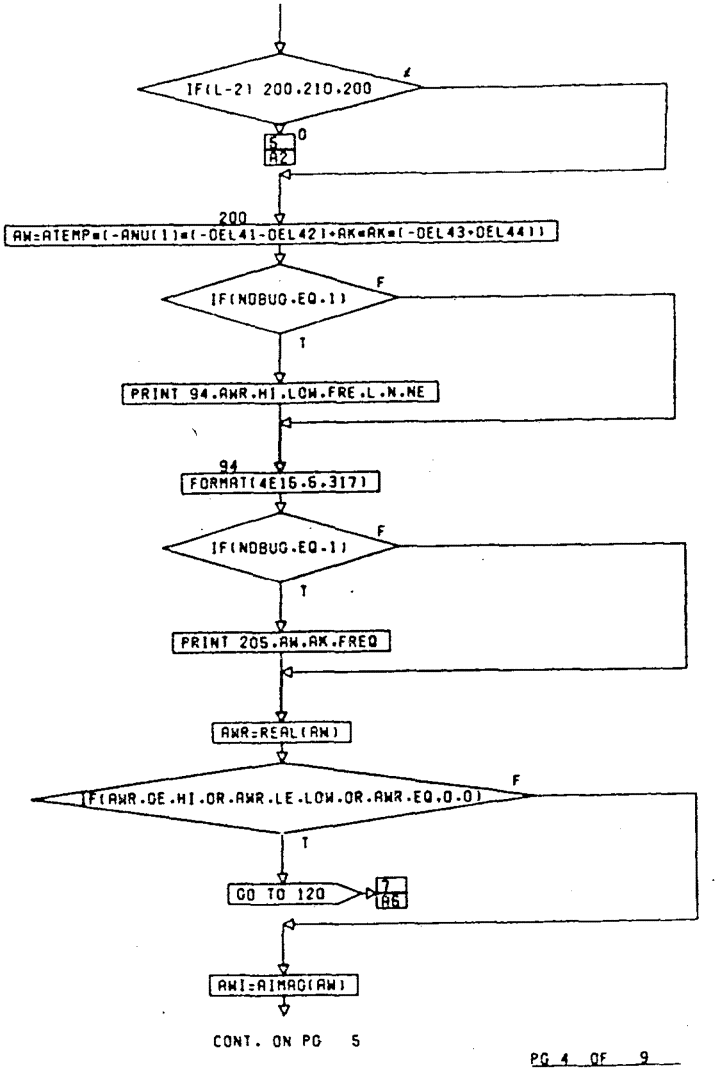

Fig. B5 (sheet 2 of 5)

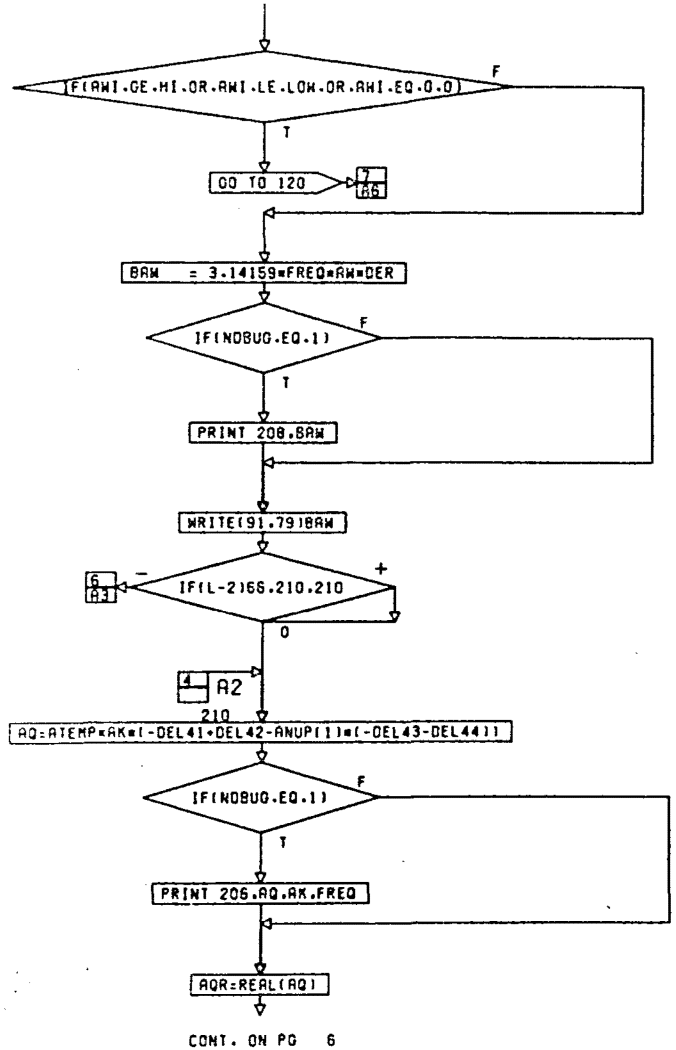

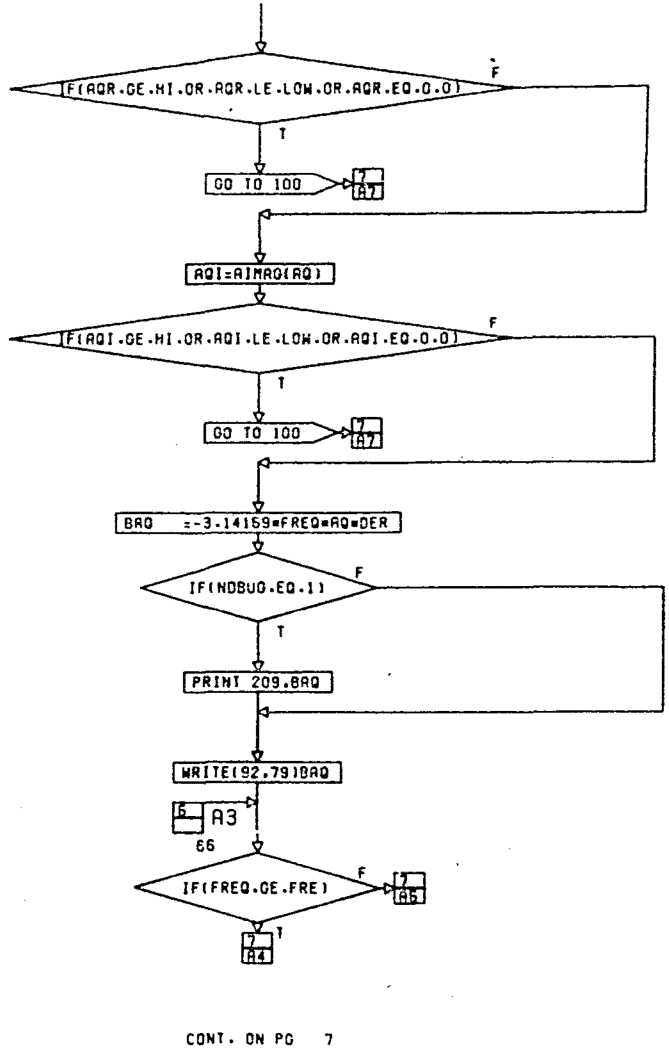

Fig. B5 (sheet 3 of 5)

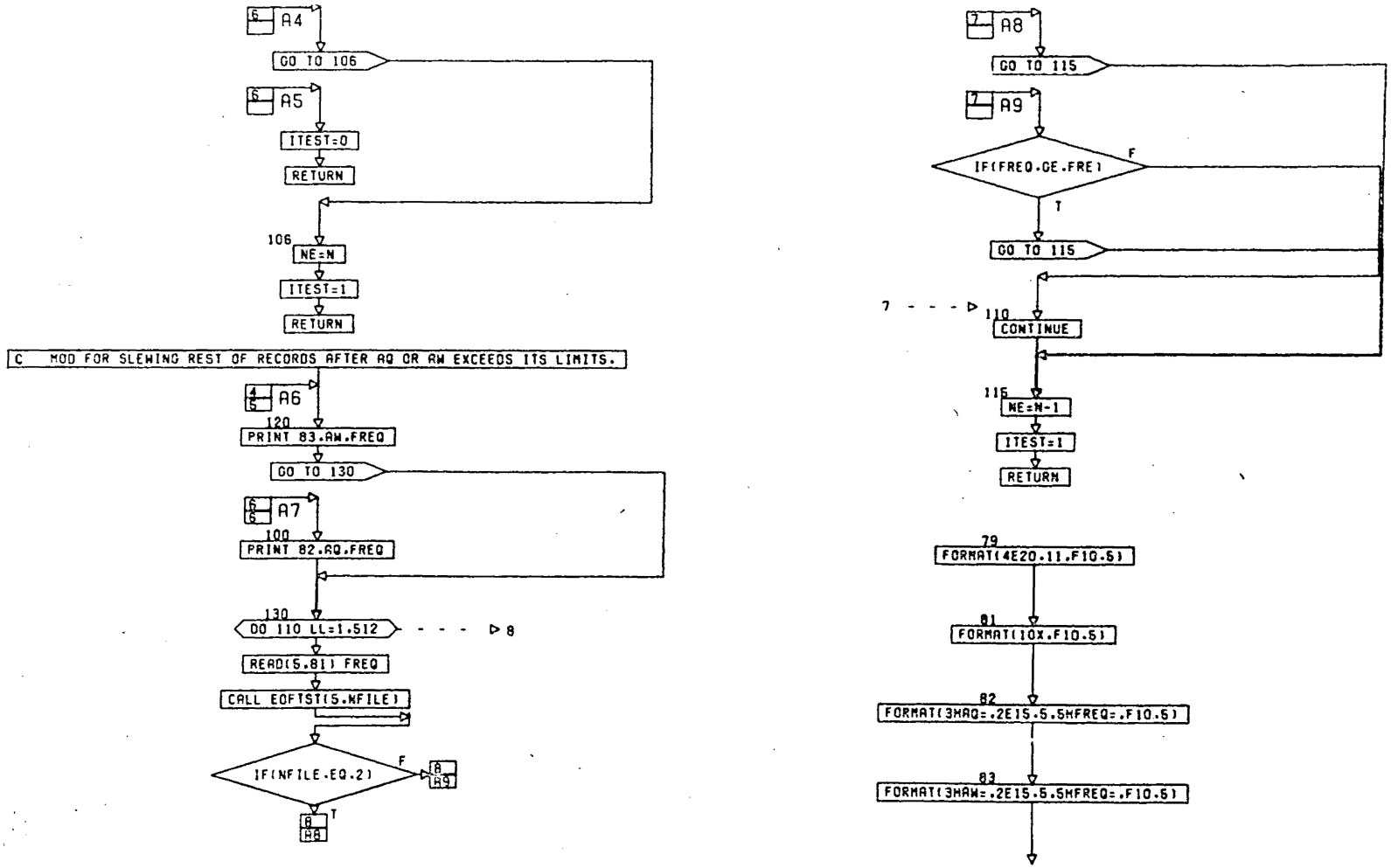

Fig. B5 (sheet 4 of 5)

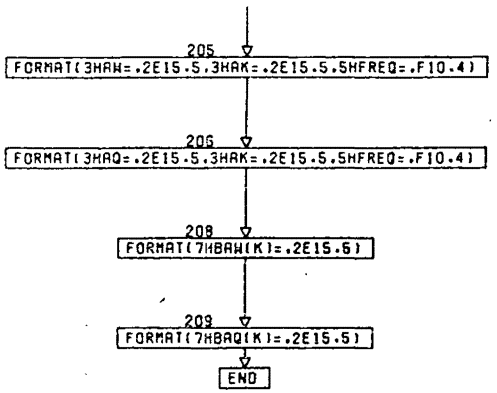

Fig. B5 (sheet 5 of 5)

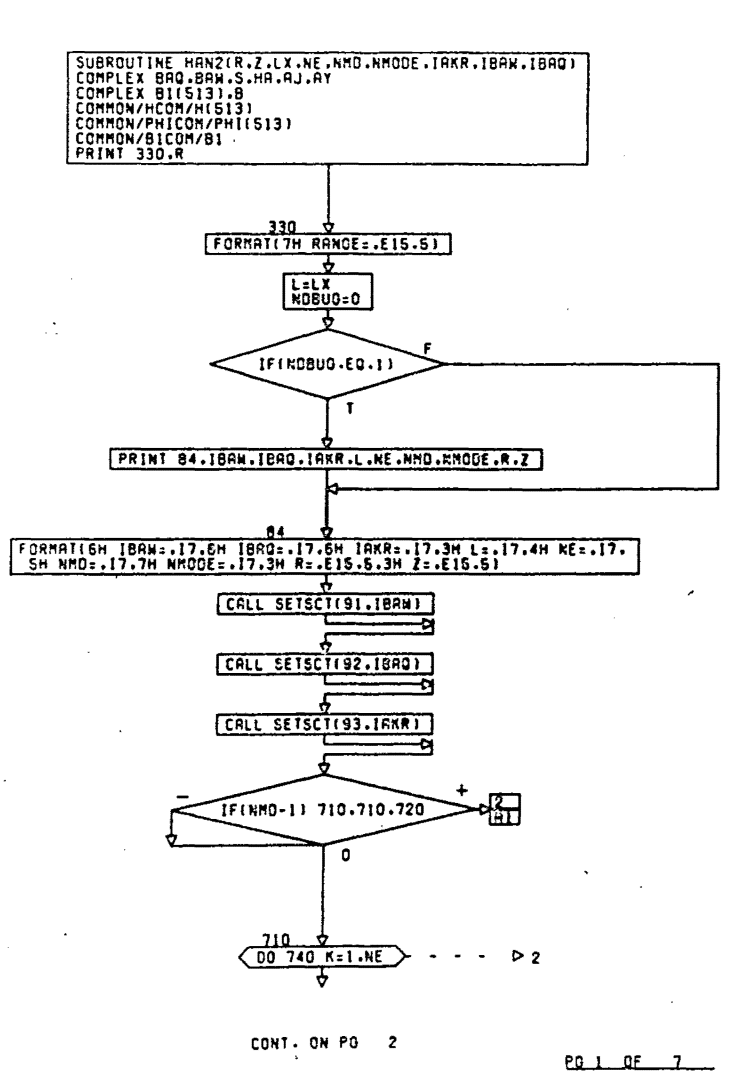

Fig. B6. Flow chart of subroutine HAN2 (sheet 1 of 4)

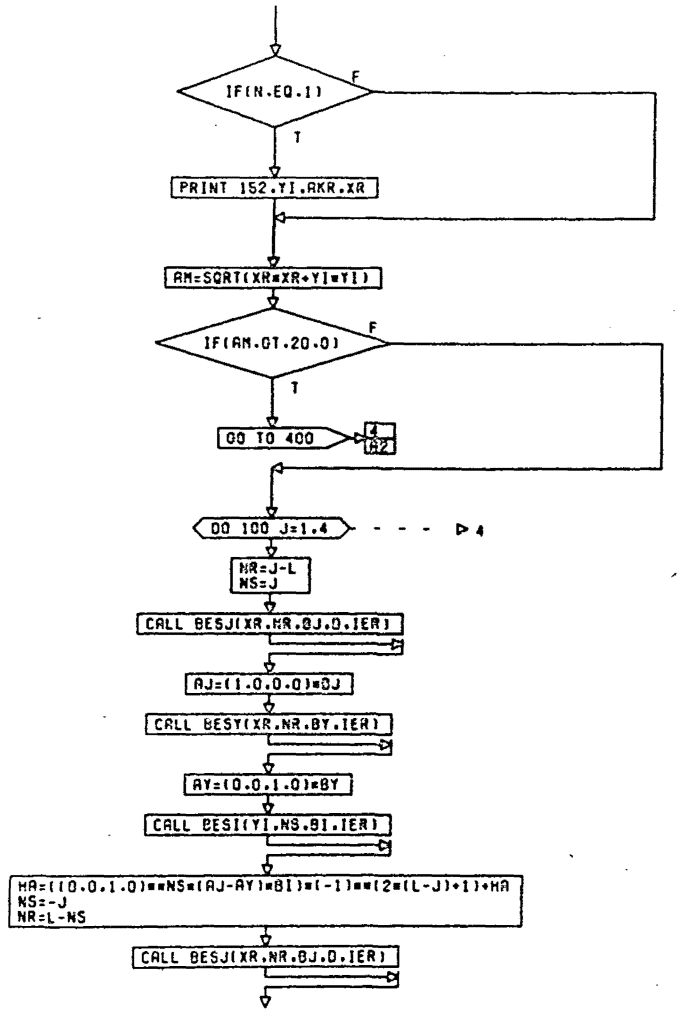

CONT. ON PG 4

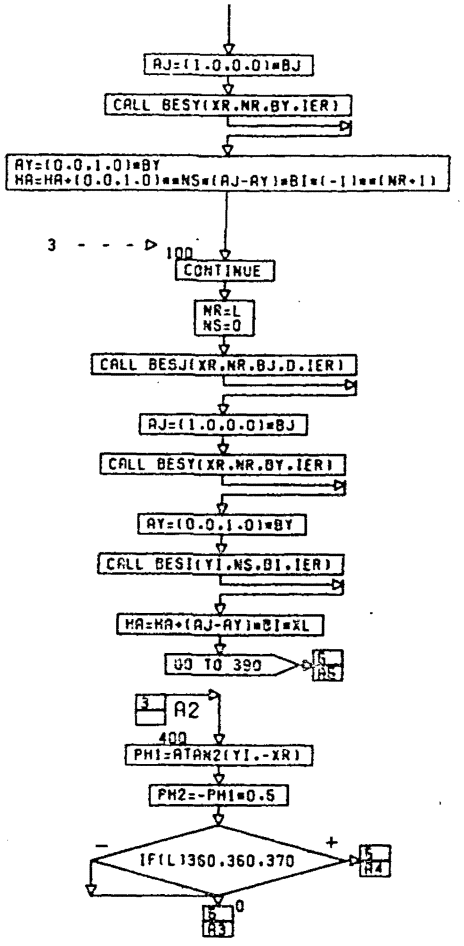

CONT. ON PG 5

Fig. B6 (sheet 2 of 4)

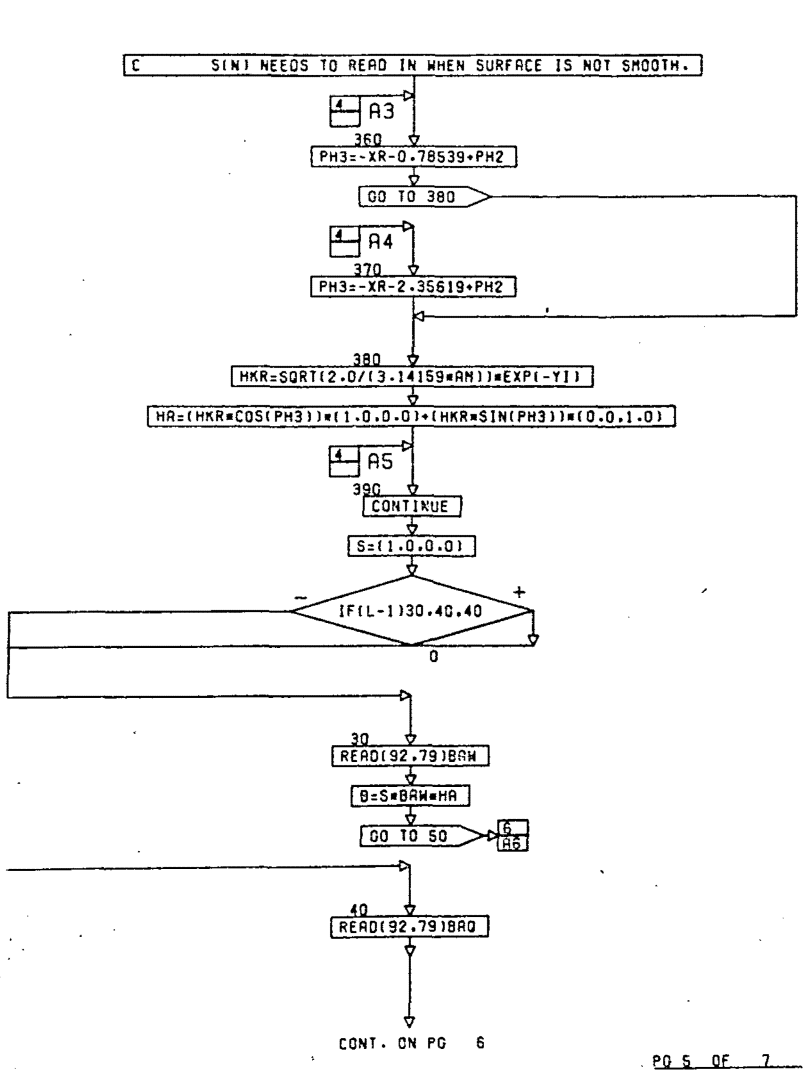

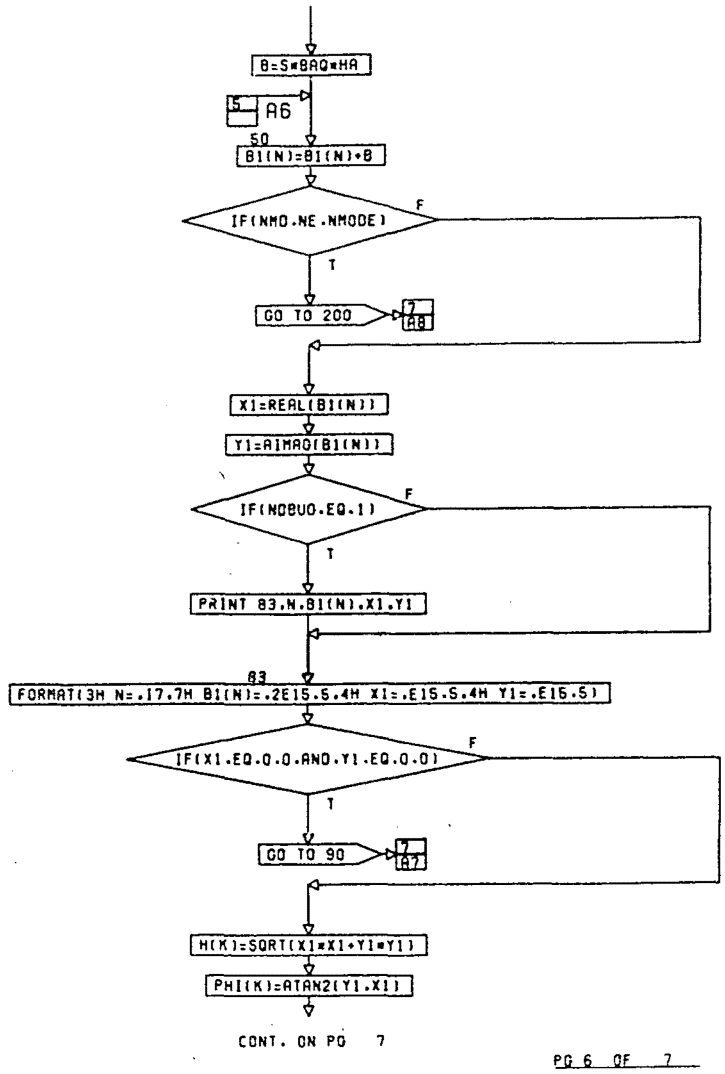

Fig. B6 (sheet 3 of 4)

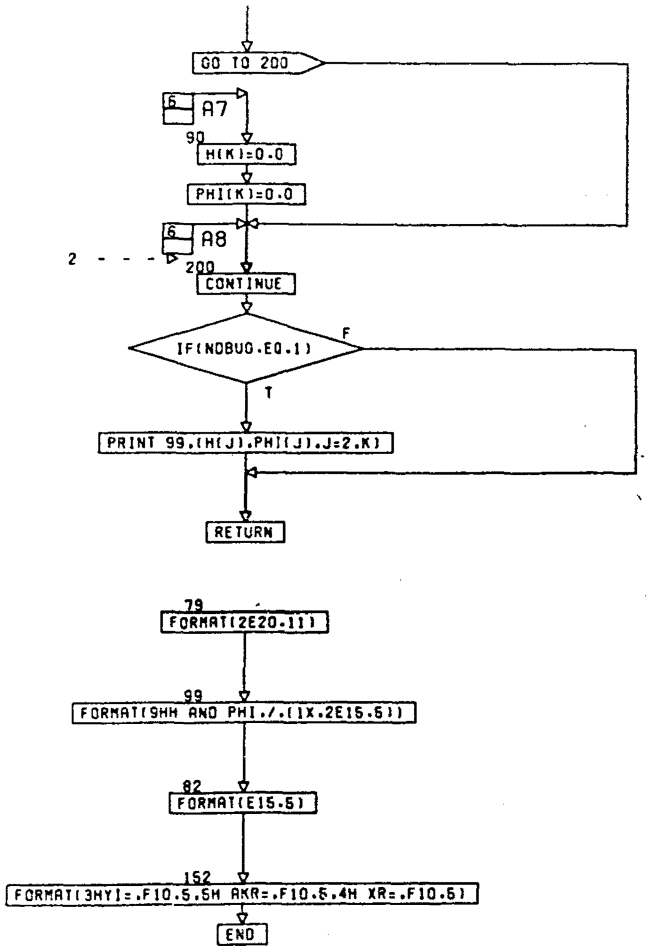

Fig. B6 (sheet 4 of 4)

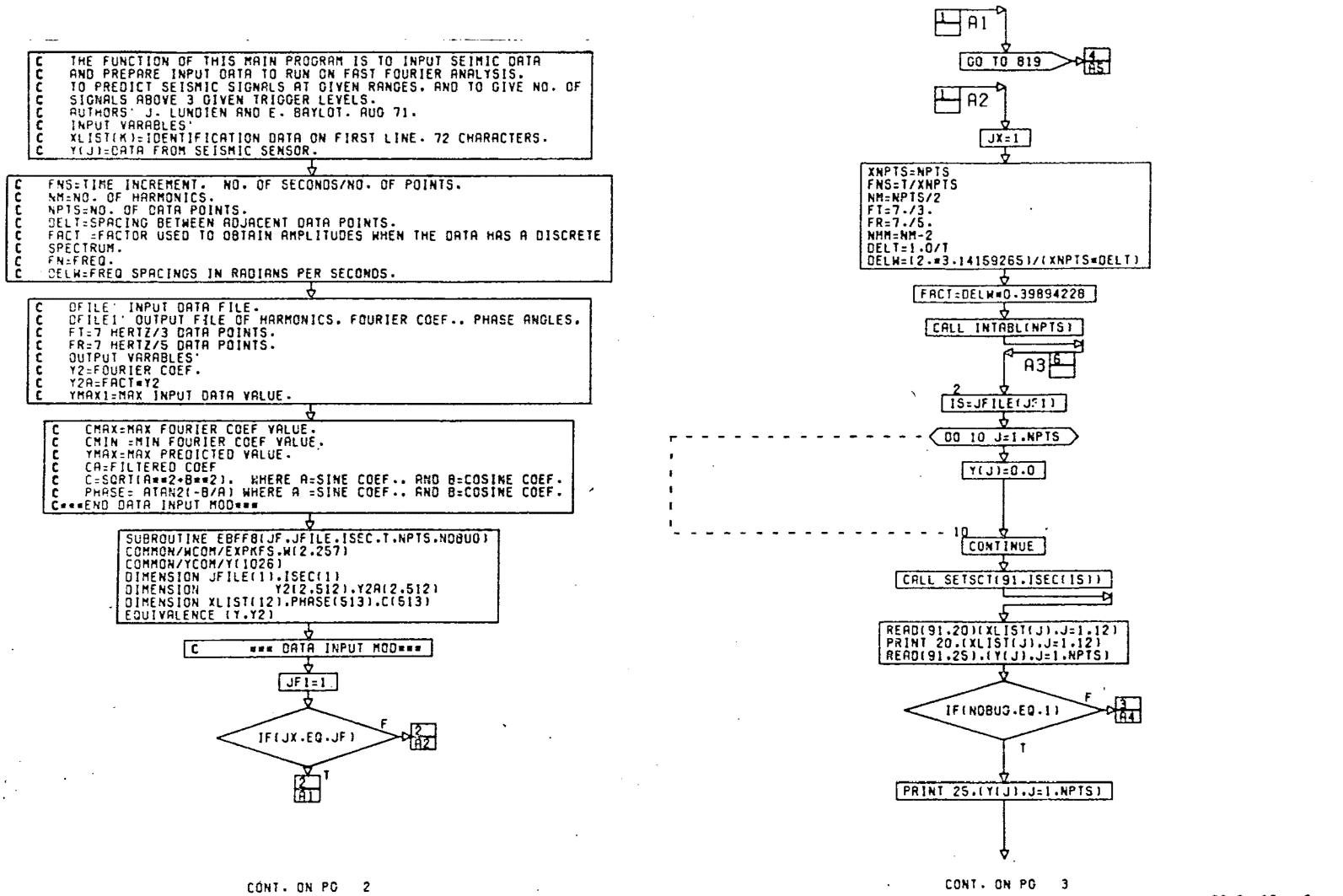

Fig. B7. Flow chart of subroutine EBFF8 (sheet 1 of 3)

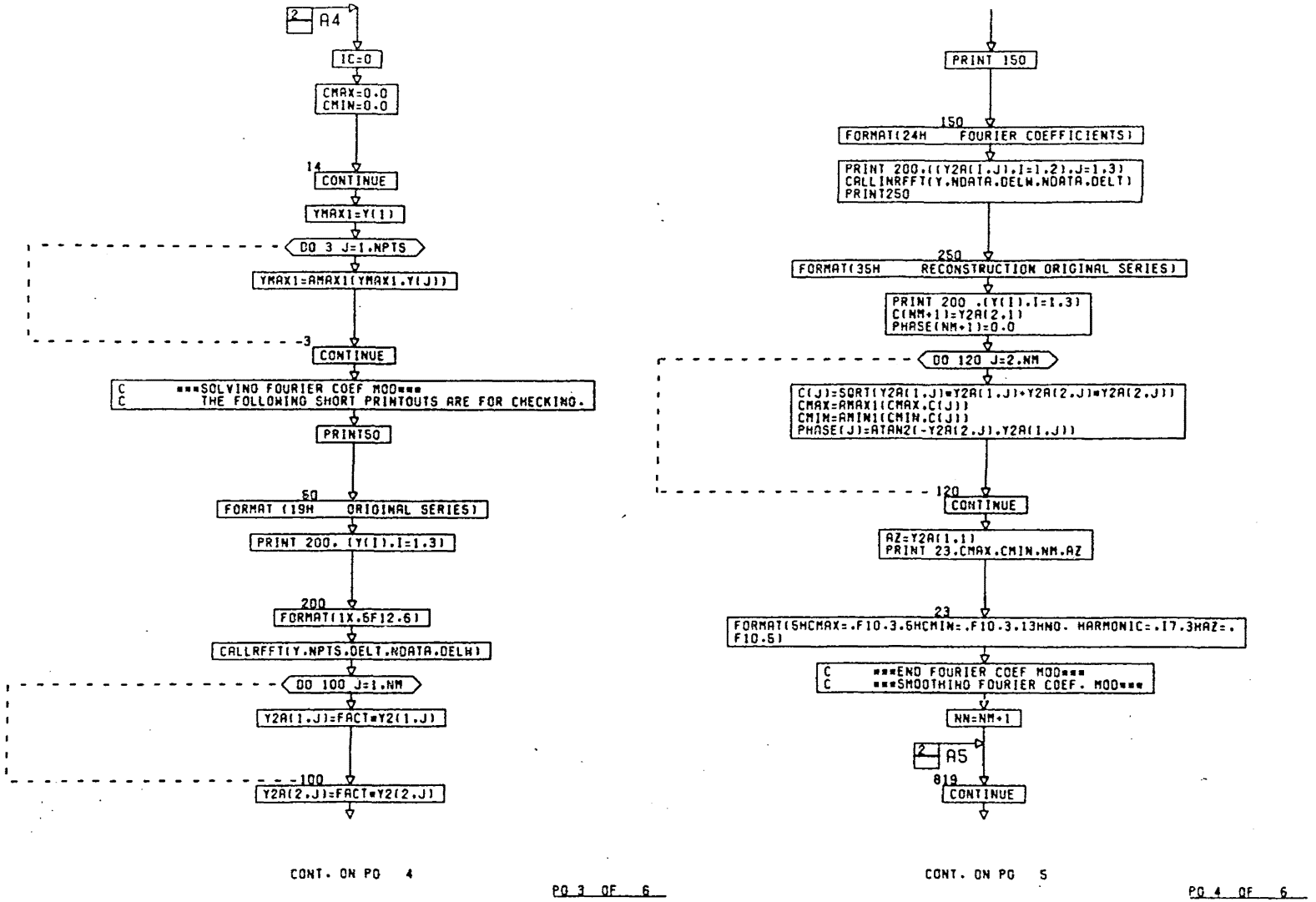

Fig. B7 (sheet 2 of 3)

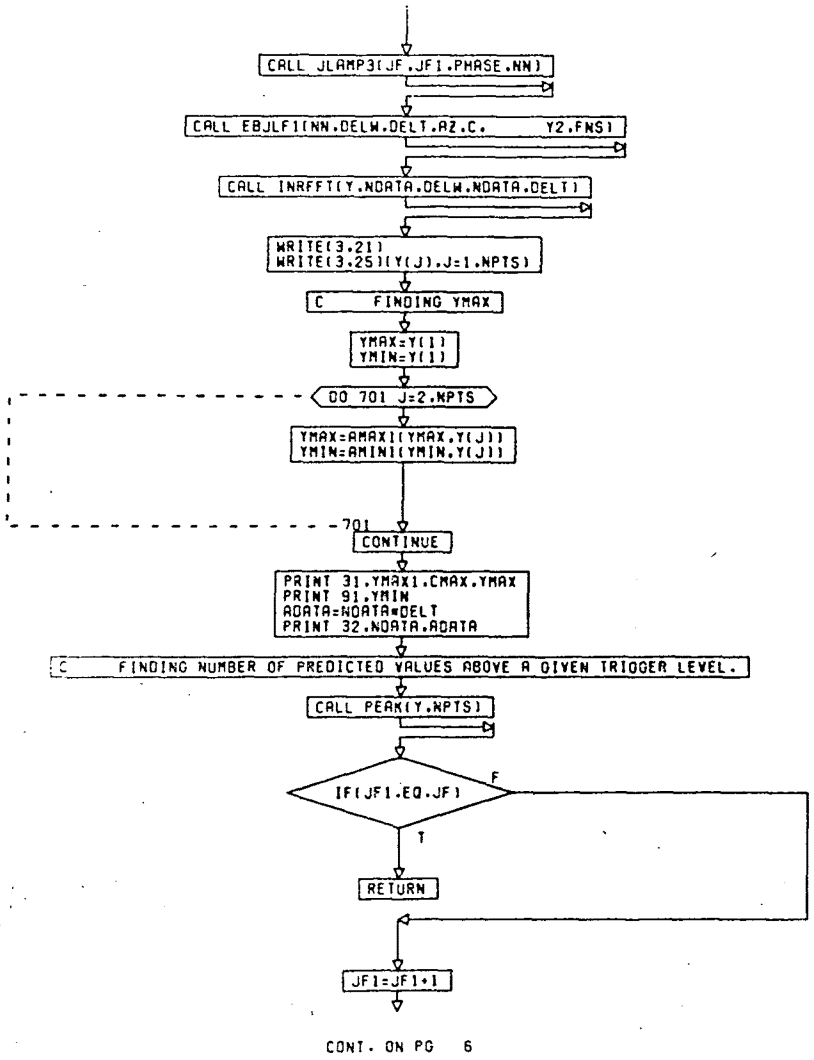

PG 5 OF 6

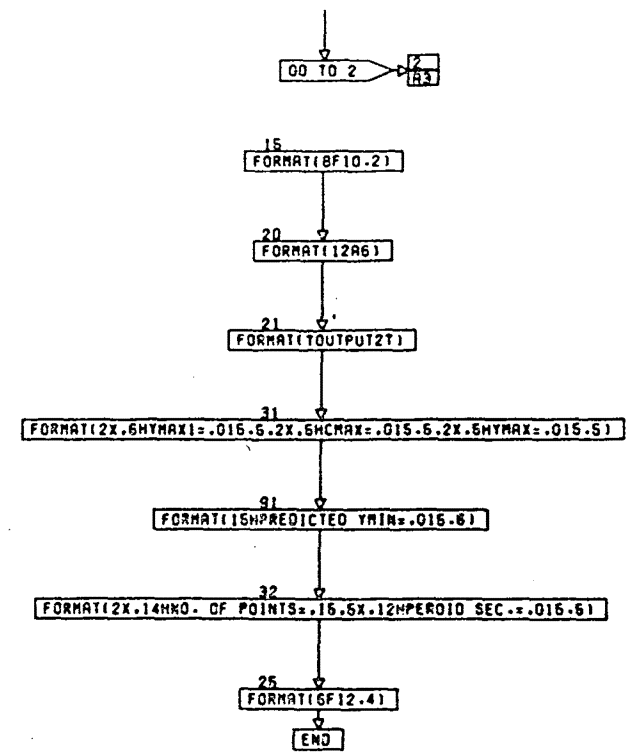

PG 6 FINAL

Fig. B7 (sheet 3 of 3)

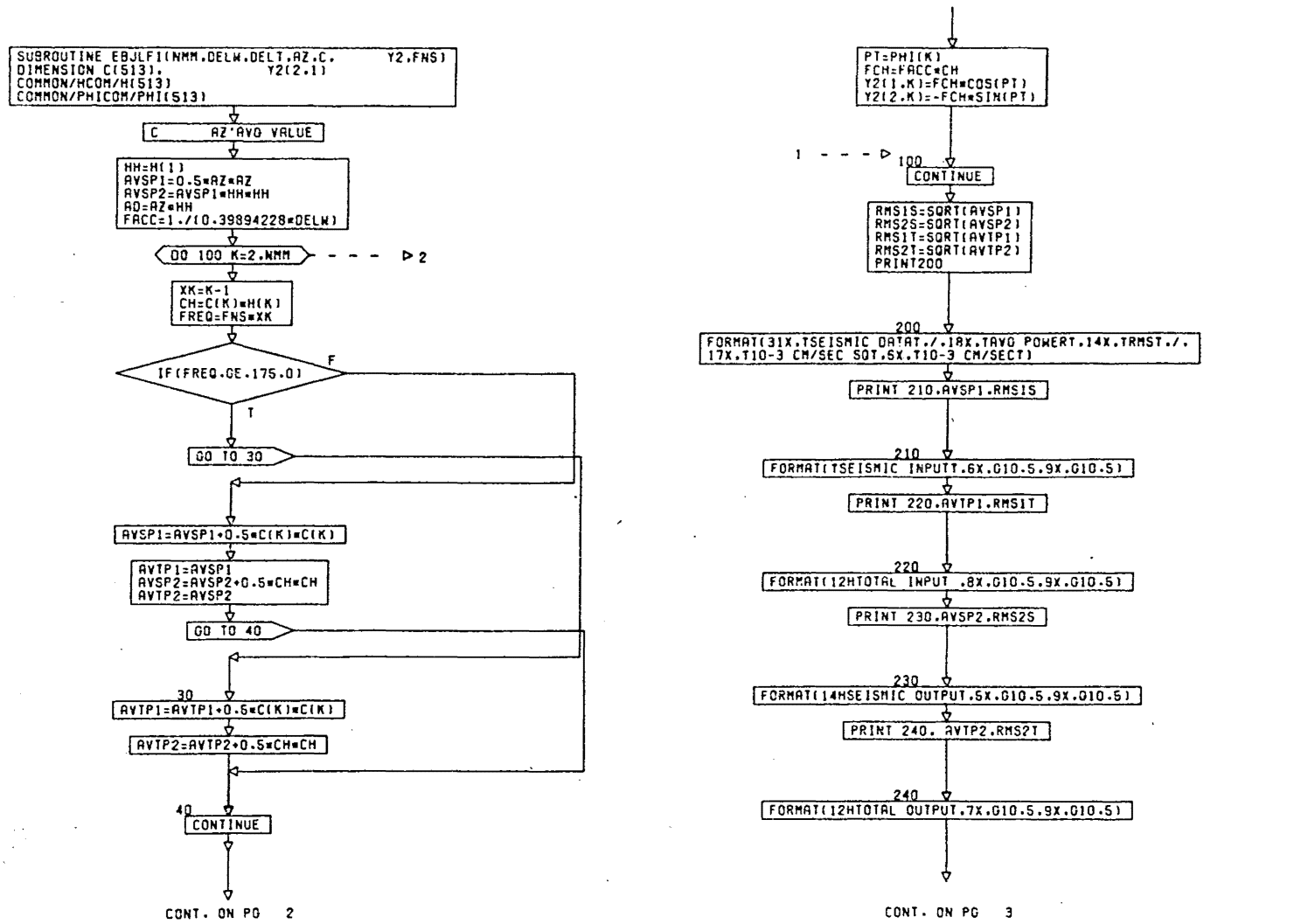

Fig. B8. Flow chart of subroutine EBJLF1 (sheet 1 of 2)

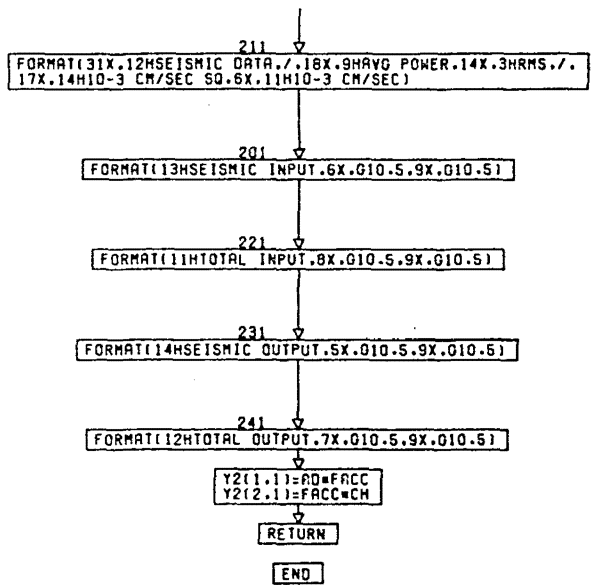

PQ 3 FINAL

Fig. B8 (sheet 2 of 2)

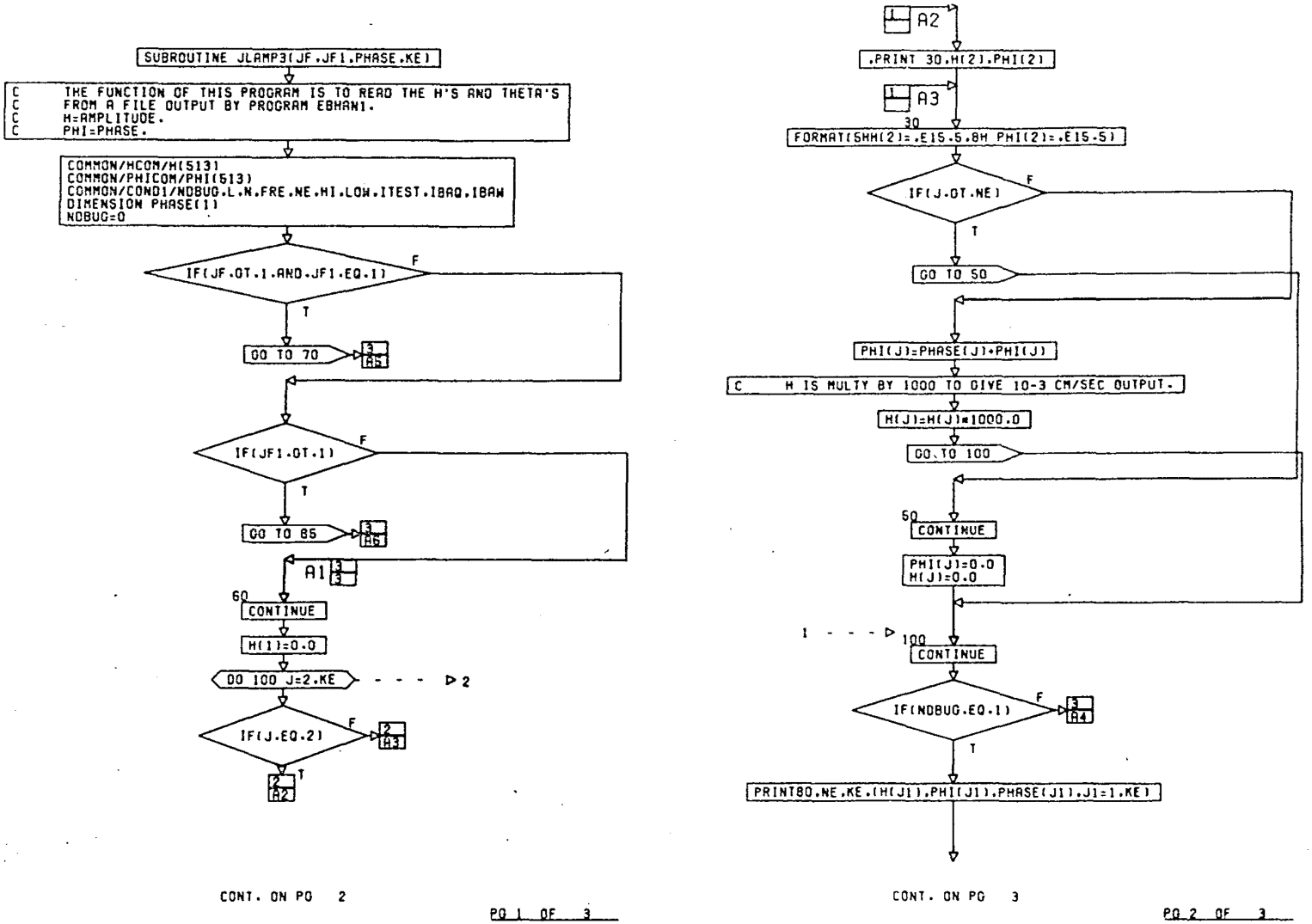

Fig. B9. Flow chart of subroutine JLAMP3 (sheet 1 of 2)

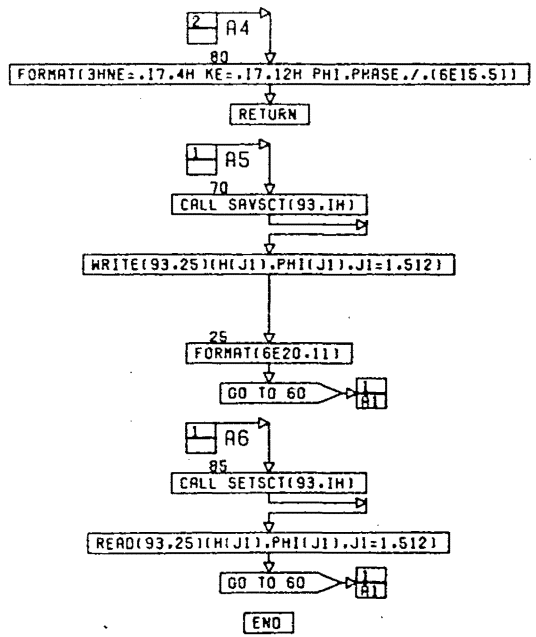

Fig. B9 (sheet 2 of 2)

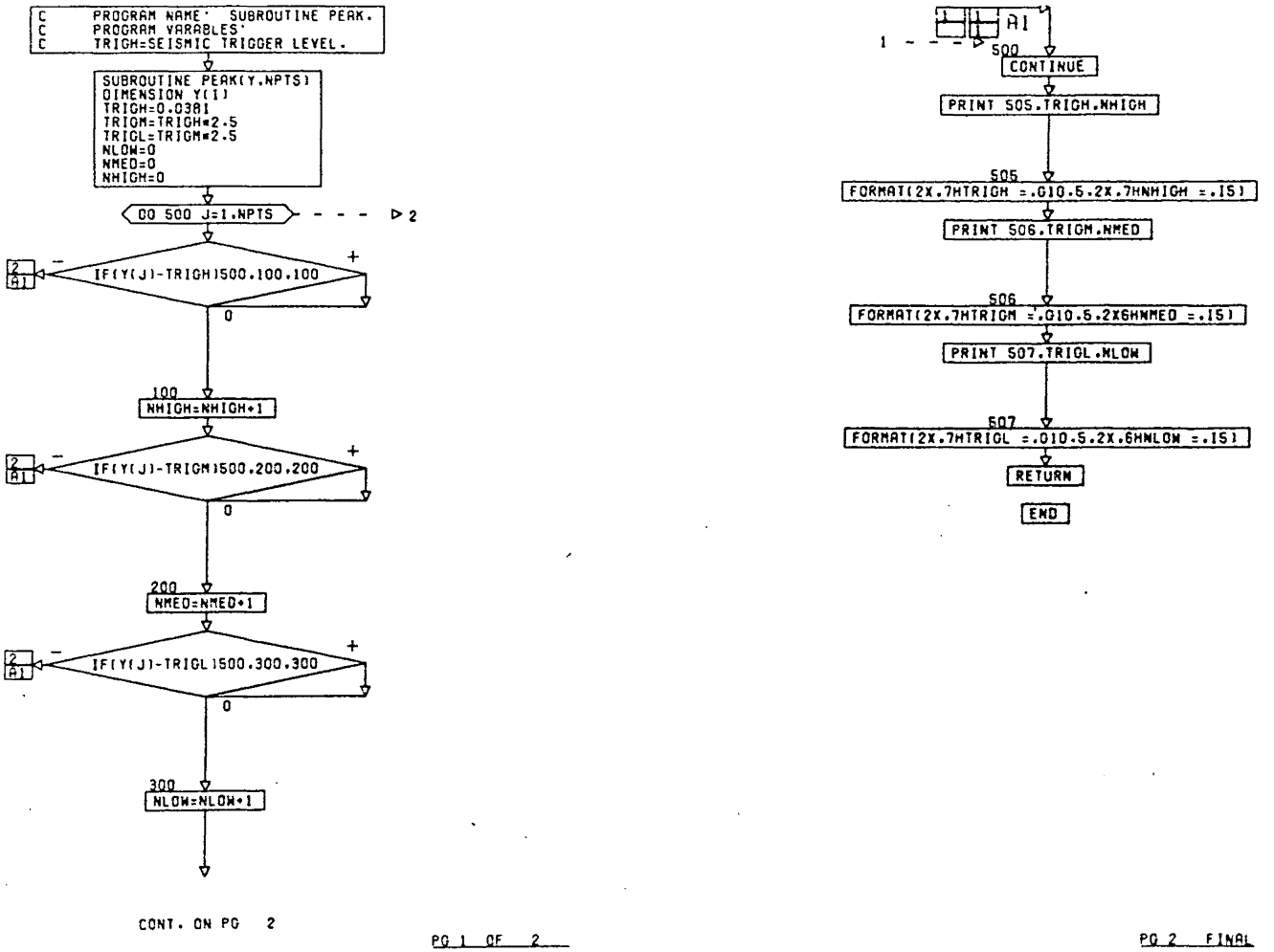

Fig. B10. Flow chart of subroutine PEAK

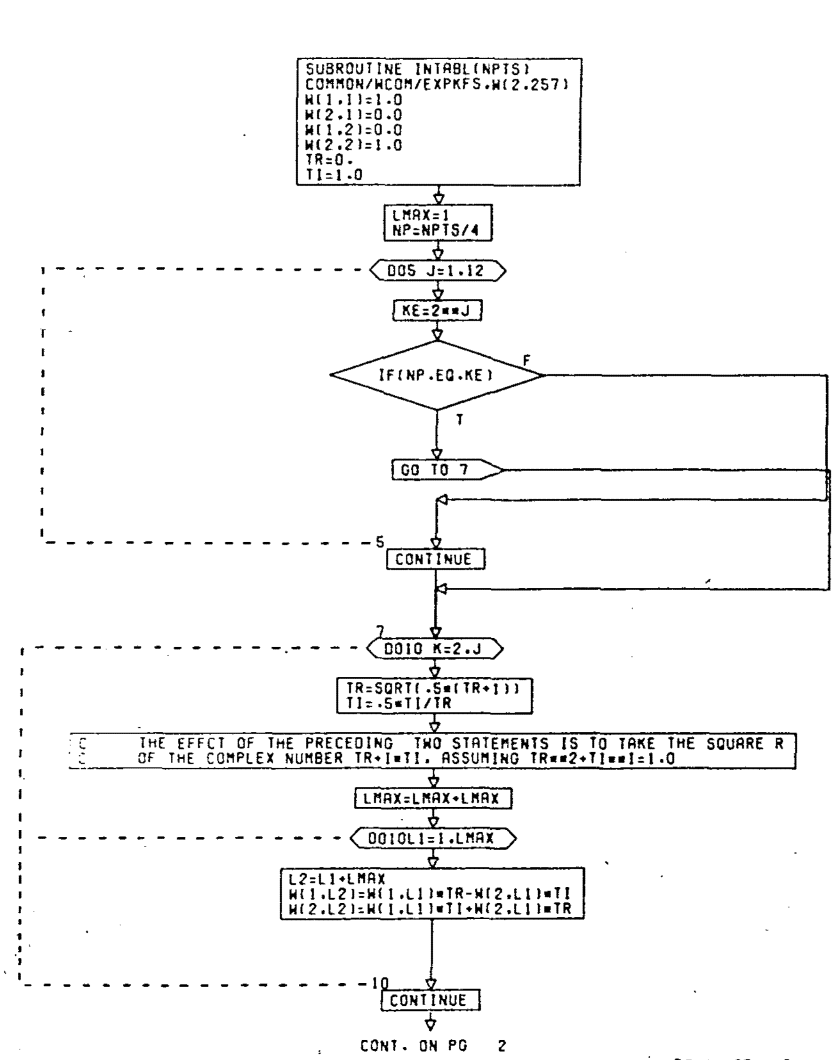

Fig. B11. Flow chart of subroutine INTABL

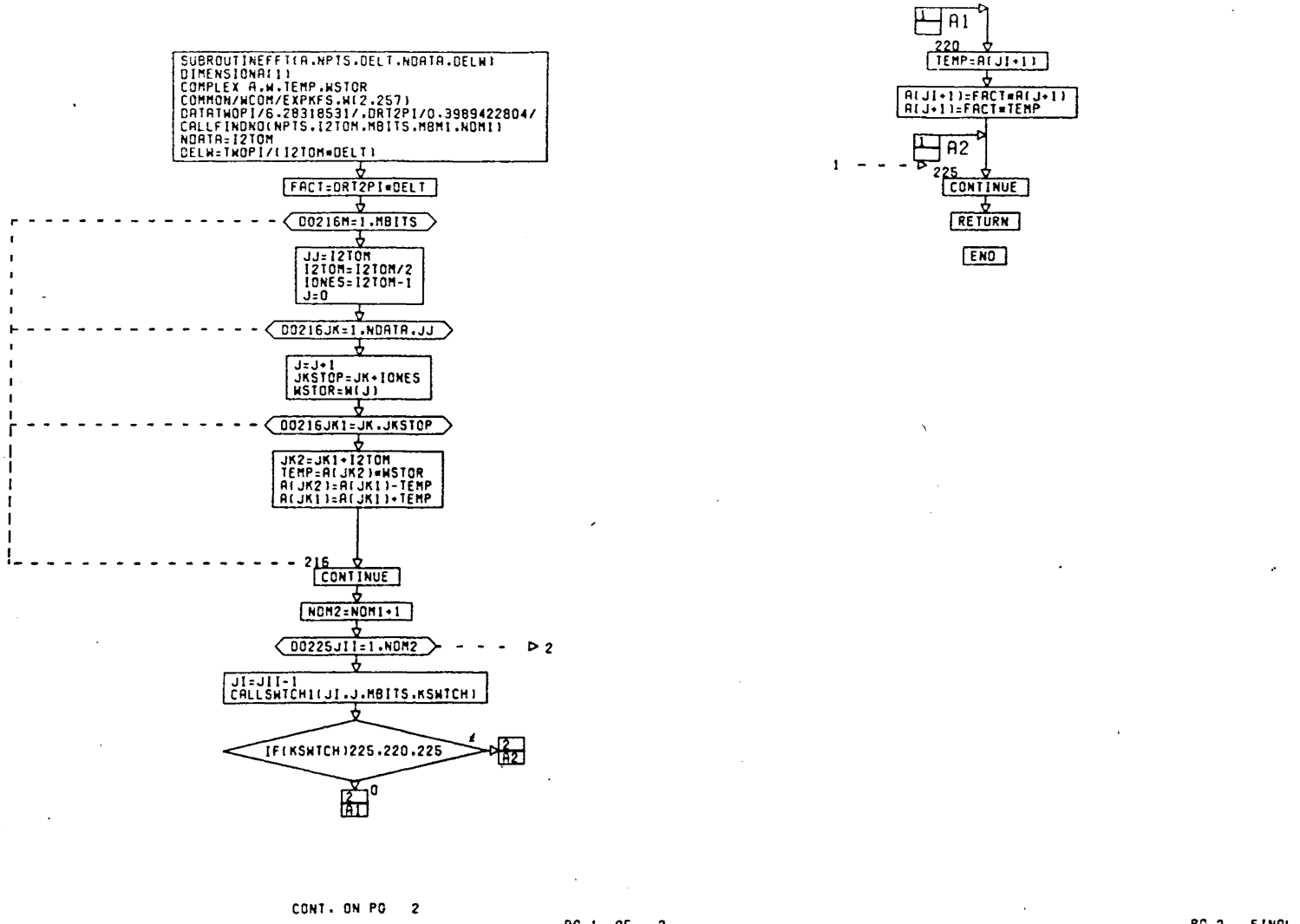

Fig. B12. Flow chart of subroutine FFT

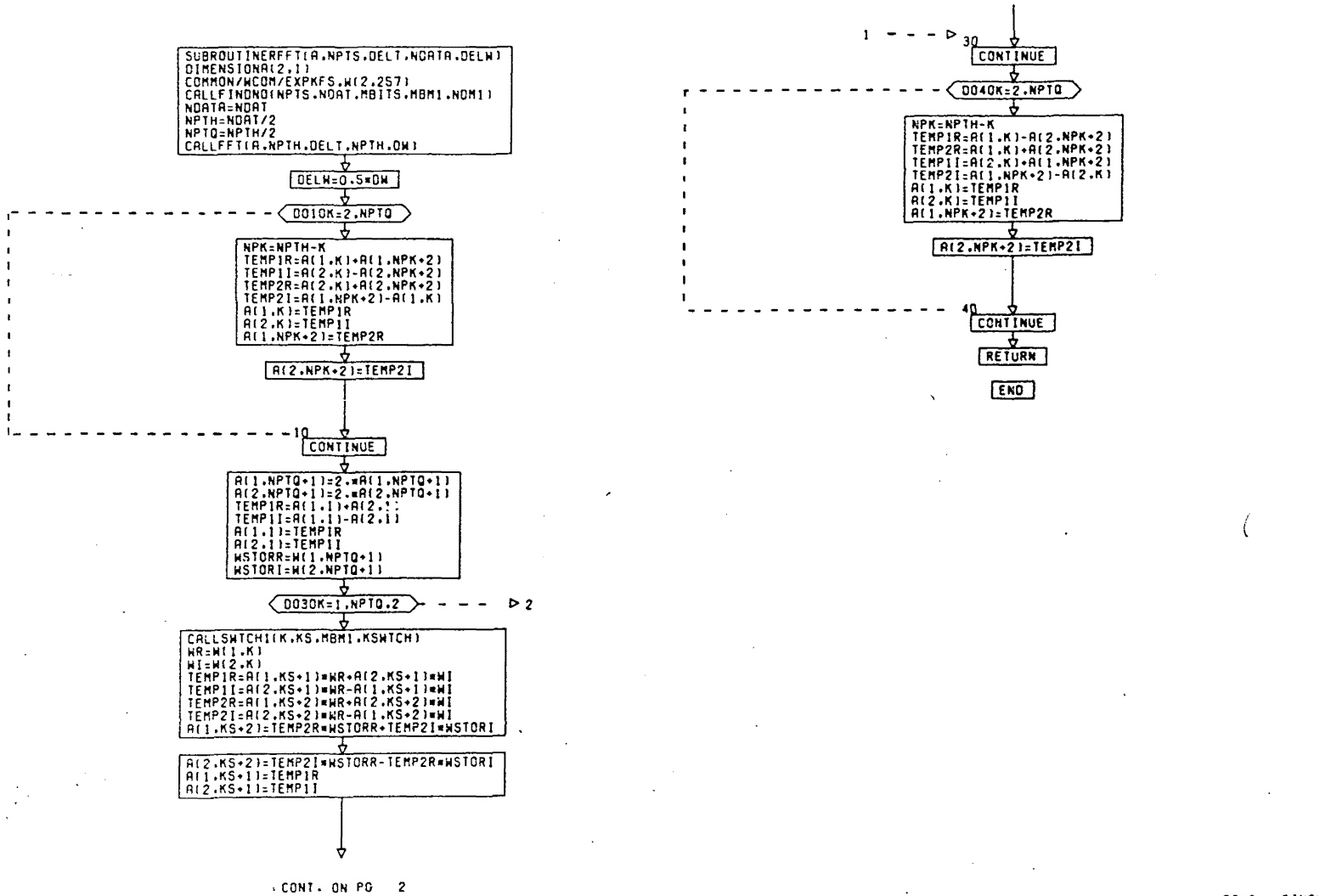

Fig. B13. Flow chart of subroutine RFFT

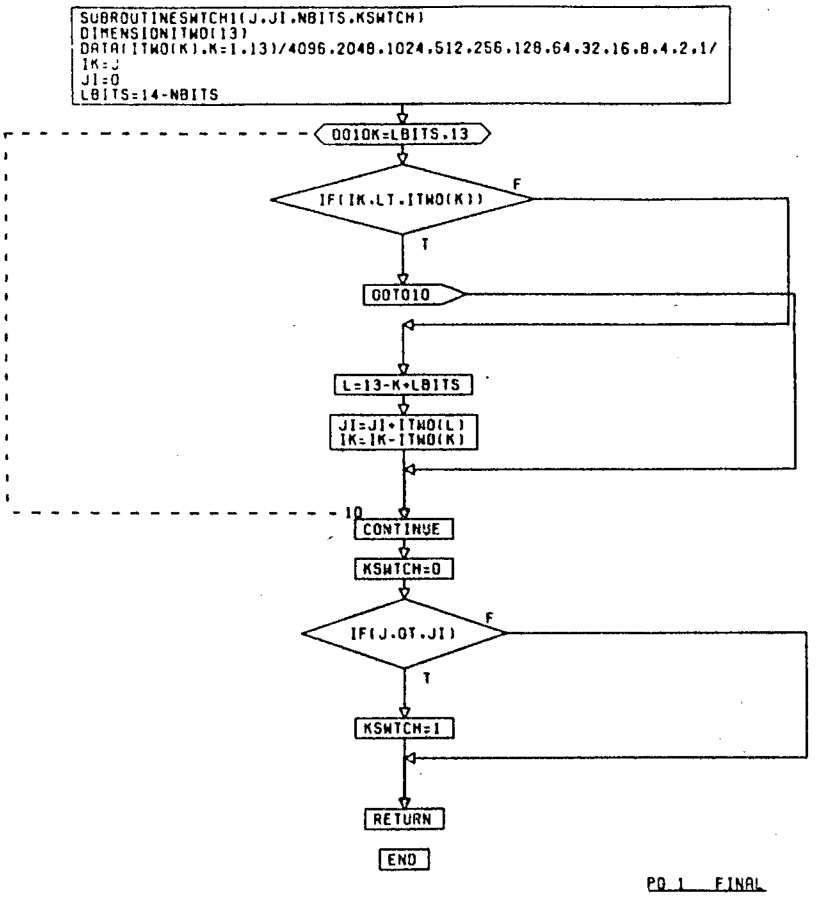

Fig. B14. Flow chart of subroutine SWTCH1

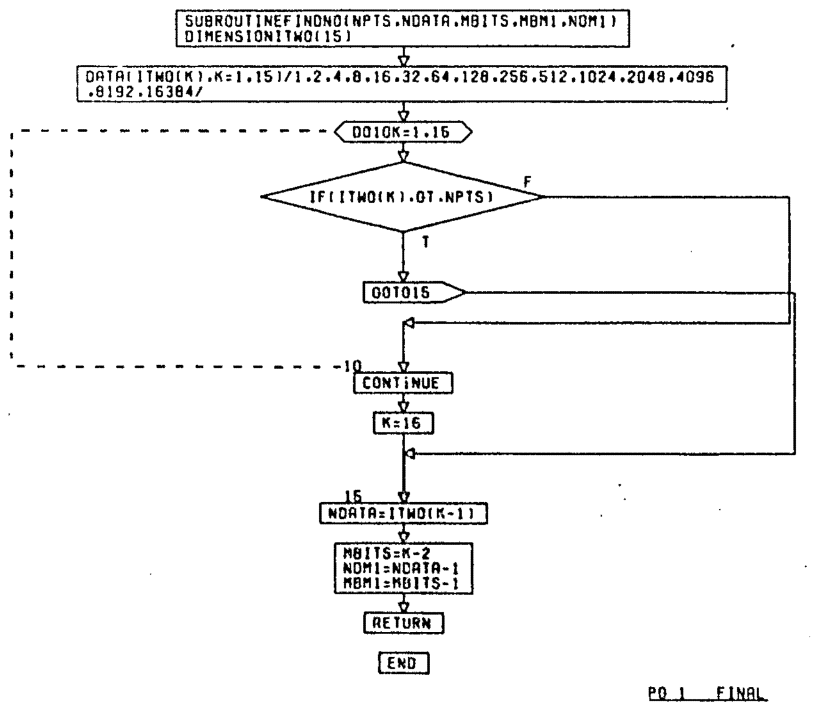

Fig. B15. Flow chart of subroutine FINDNO

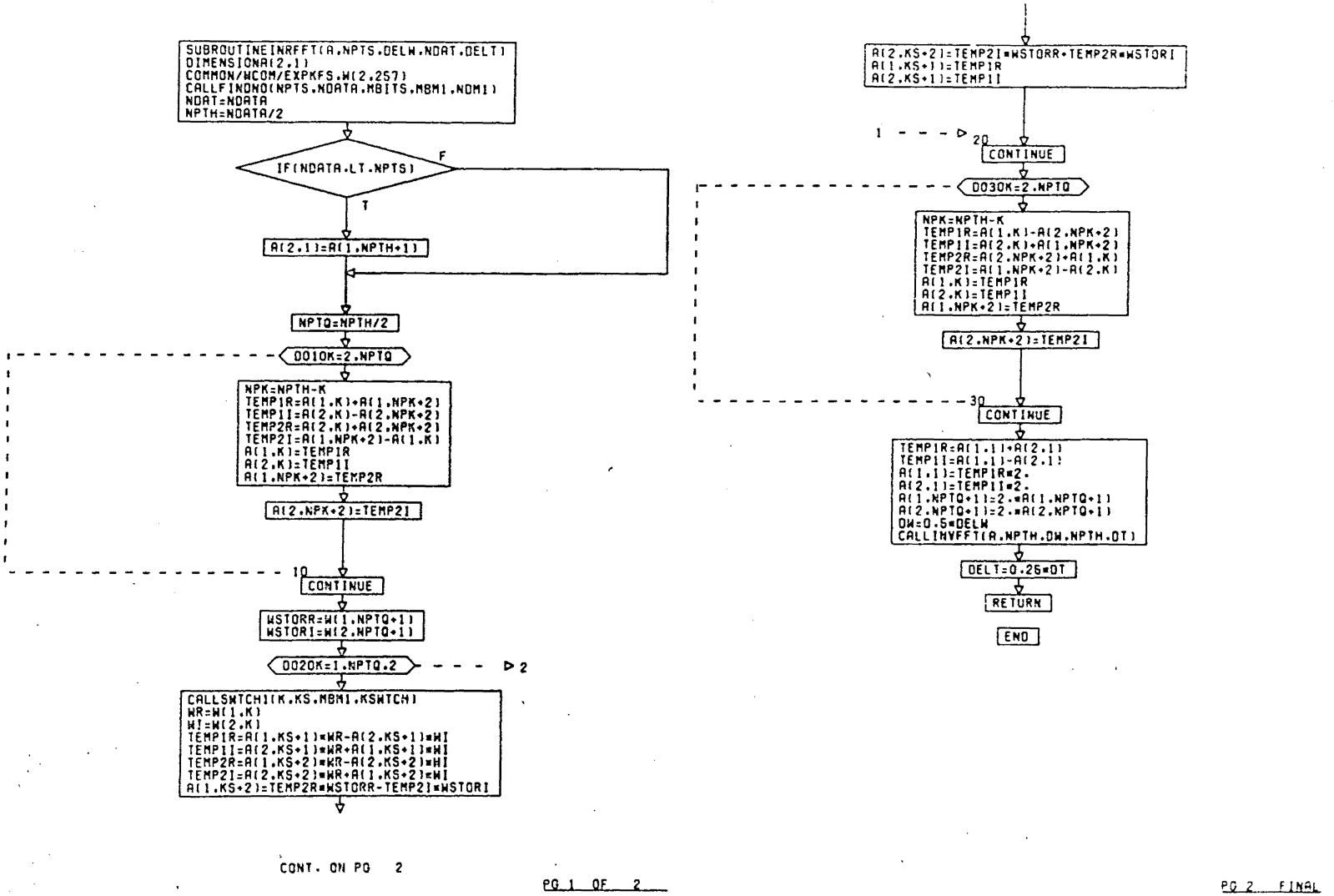

Fig. B16. Flow chart of subroutine INRFFT

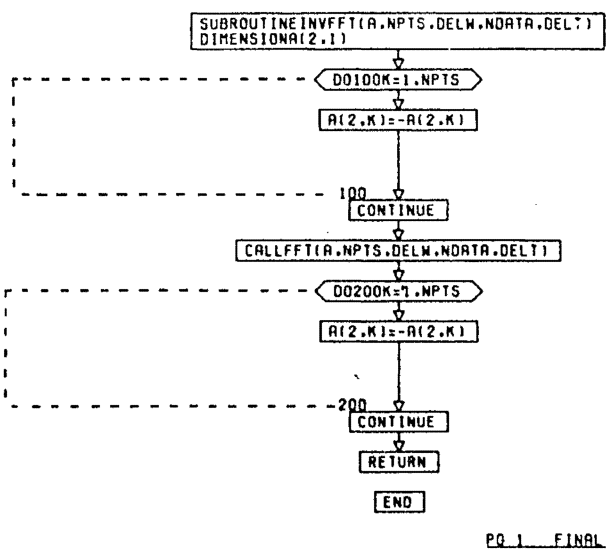

Fig. B17. Flow chart of subroutine INVFFT

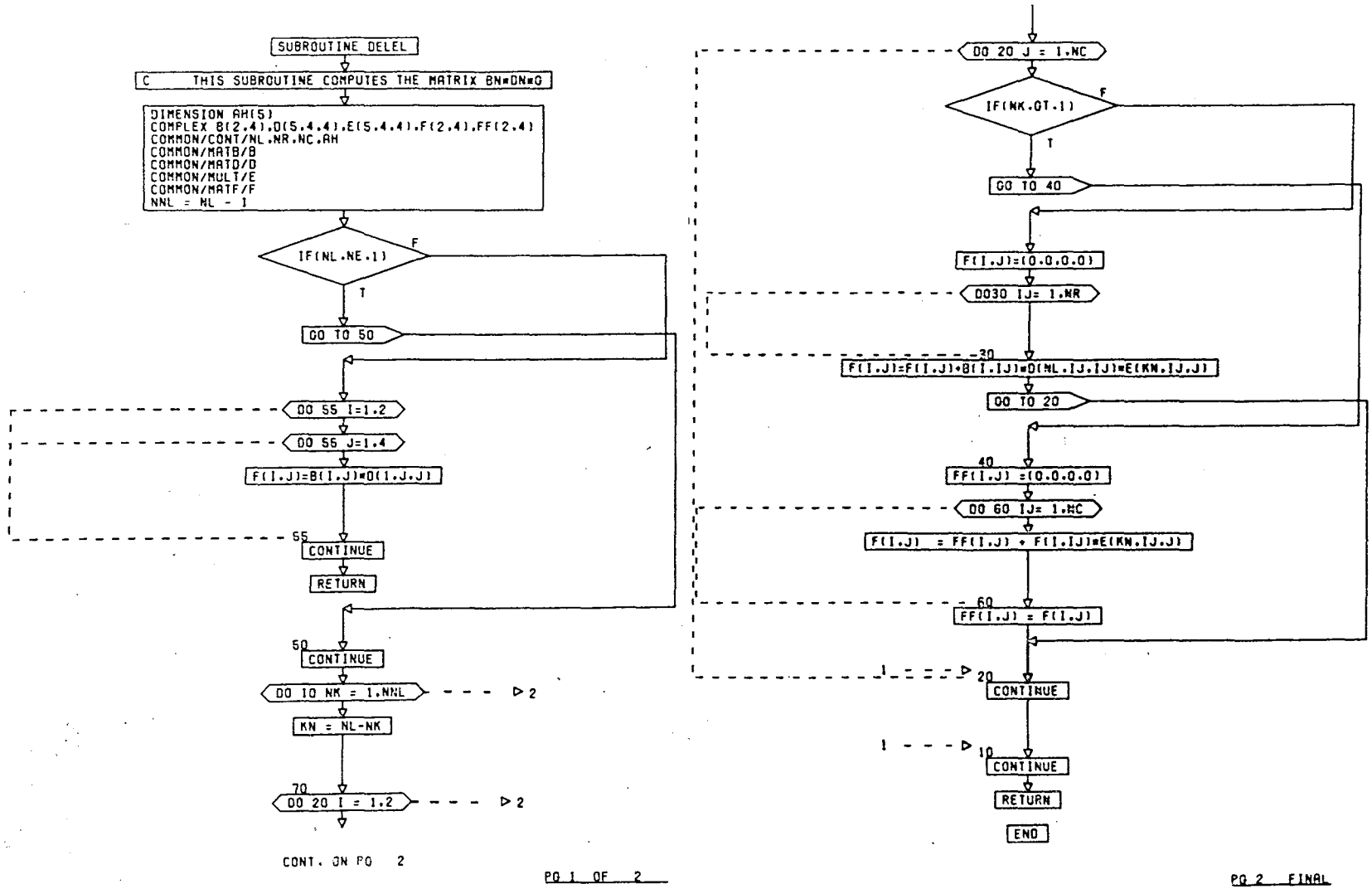

Fig. B18. Flow chart of subroutine DELEL

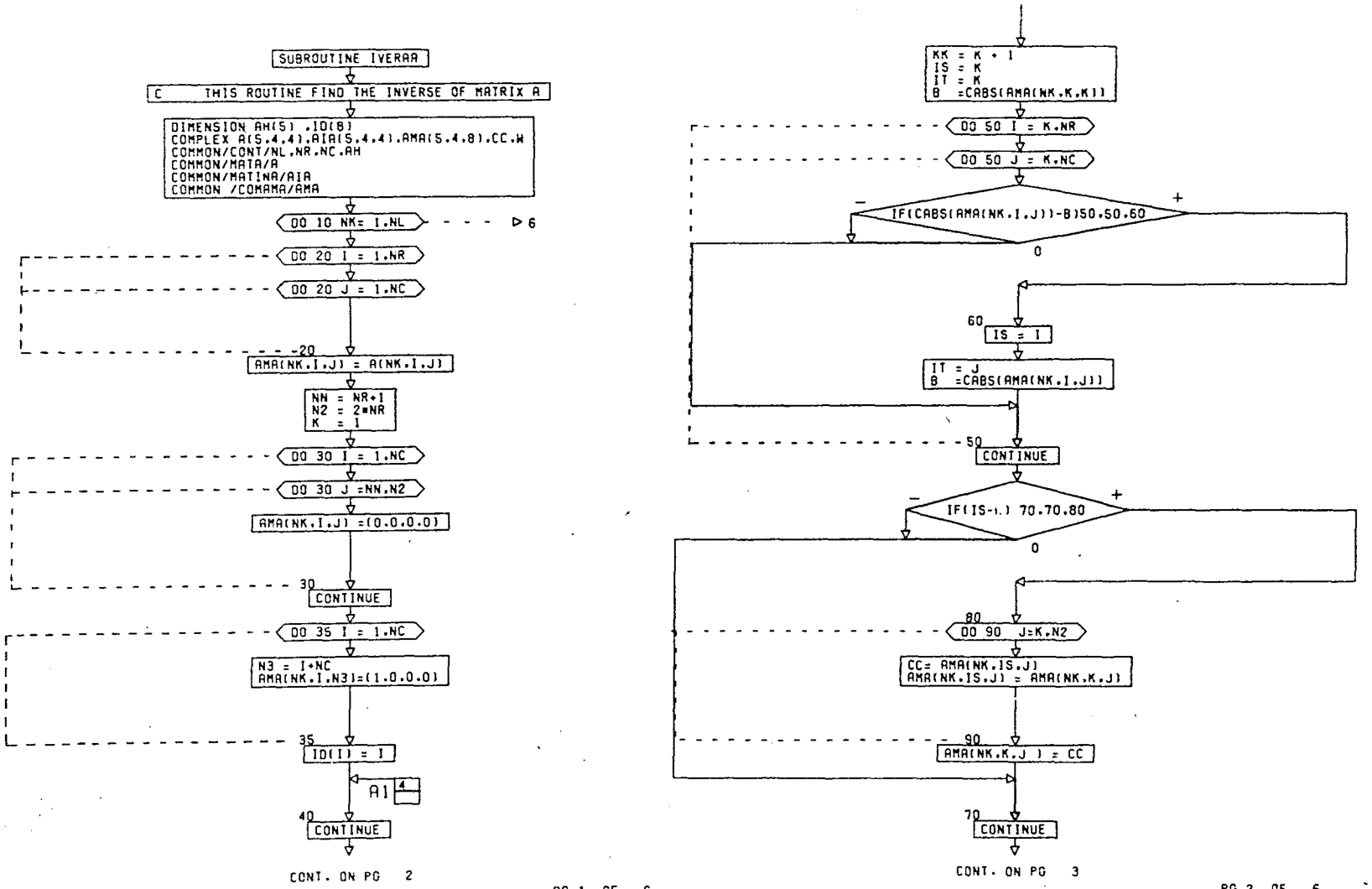

Fig. B19. Flow chart of subroutine IVERAA (sheet 1 of 3)

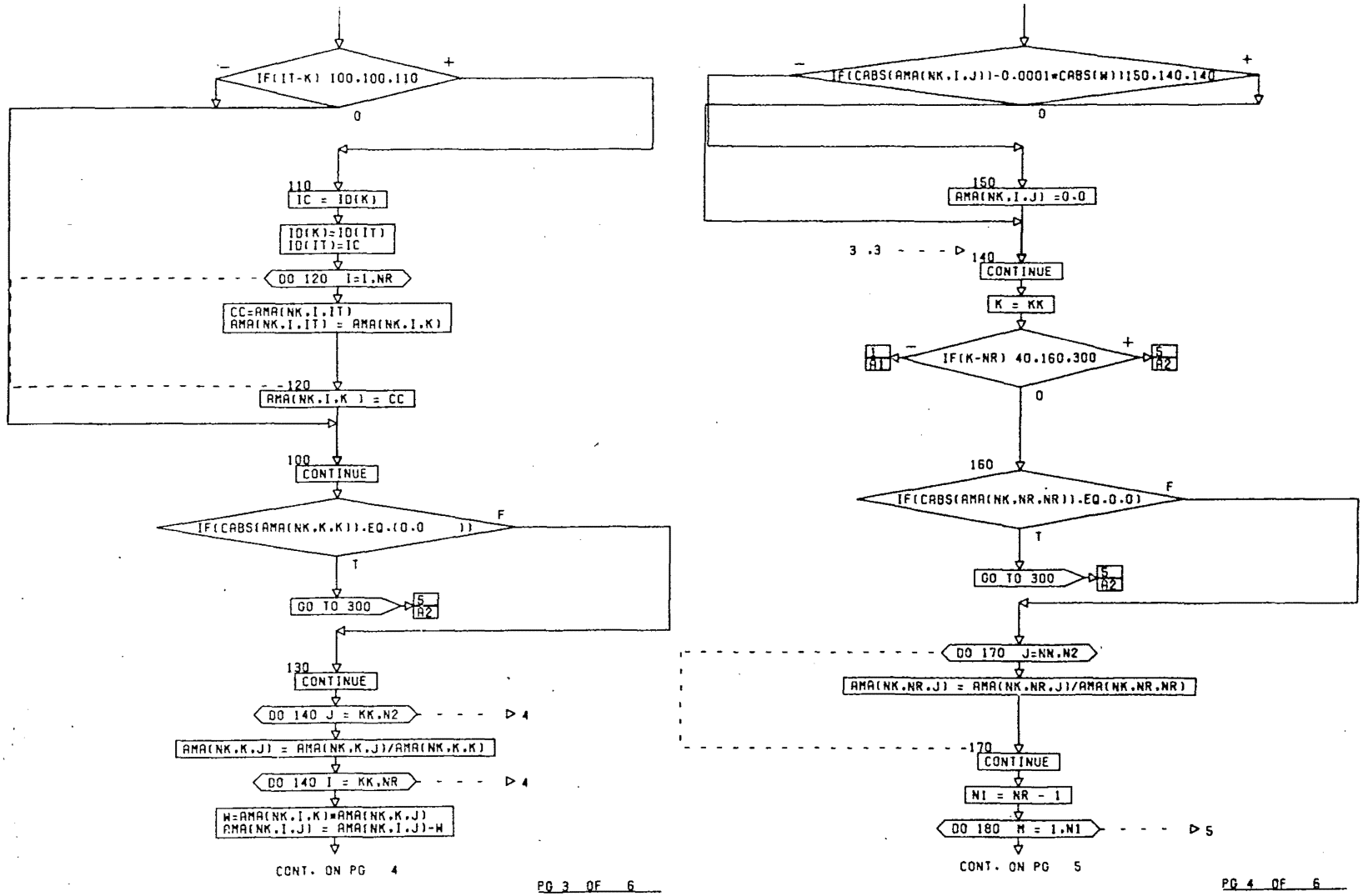

Fig. B19 (sheet 2 of 3)

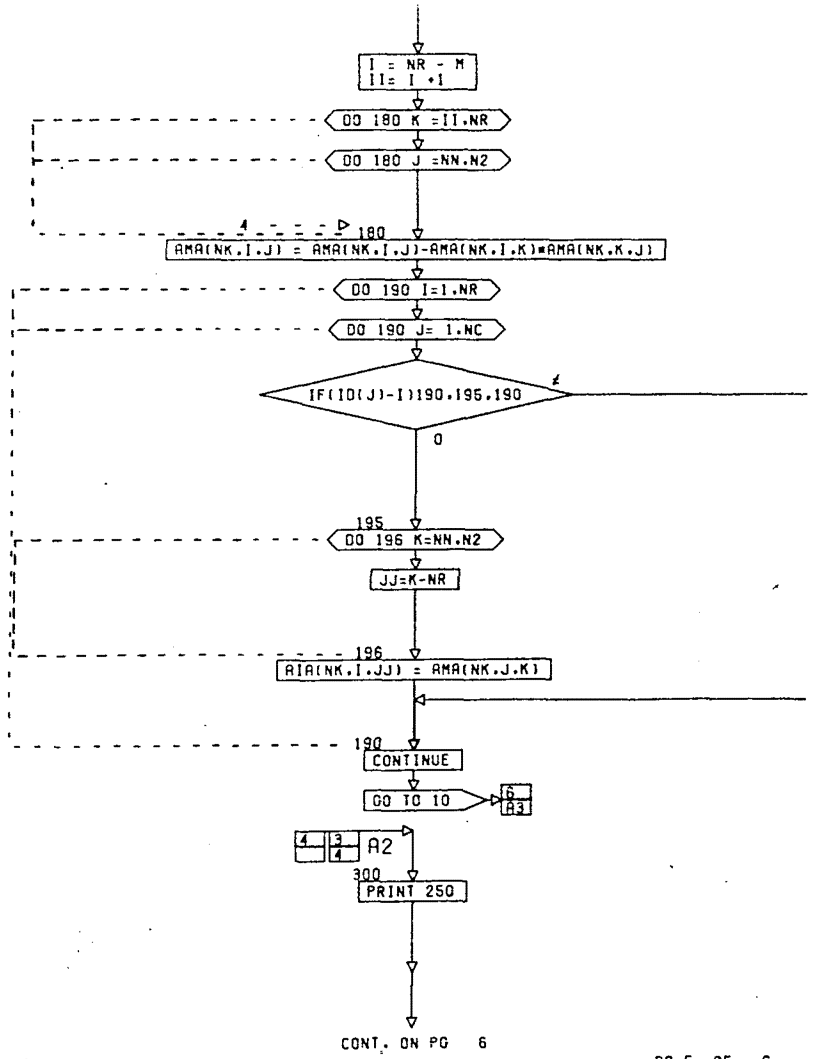

PG 5 OF 6

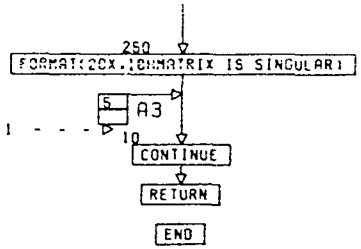

PG 6 FINAL

Fig. B19 (sheet 3 of 3)

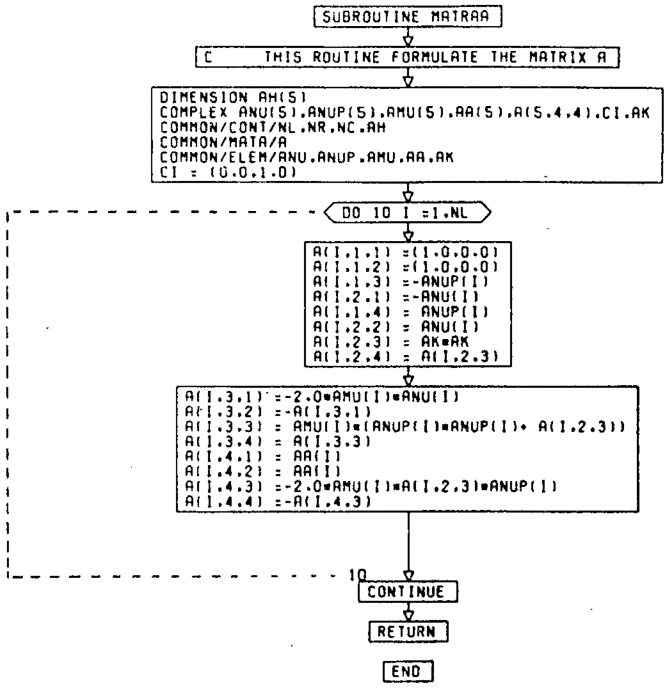

Fig. B20. Flow chart of subroutine MATRAA

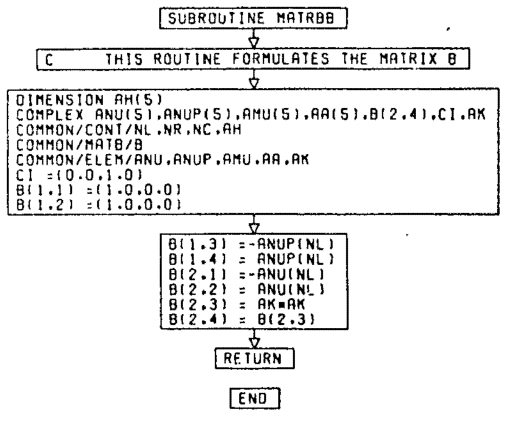

Fig. B21. Flow chart
of subroutine MATRBB

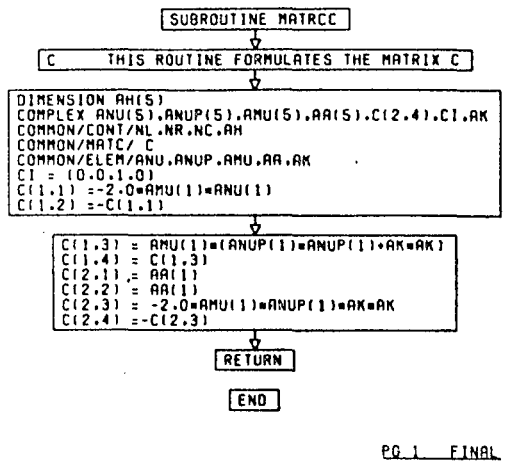

Fig. B22. Flow chart of subroutine MATRCC

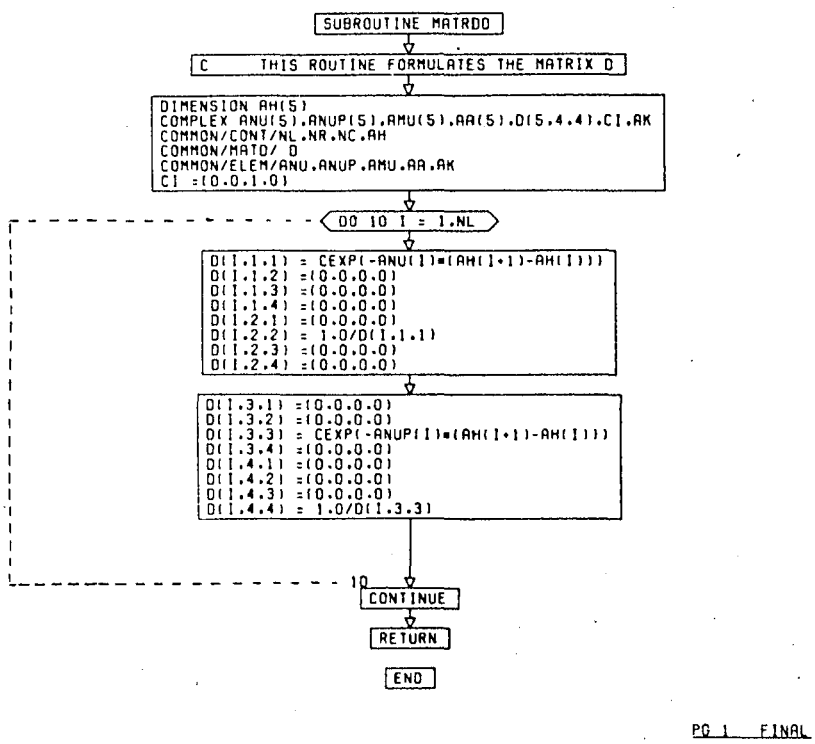

Fig. B23. Flow chart of subroutine MATRDD

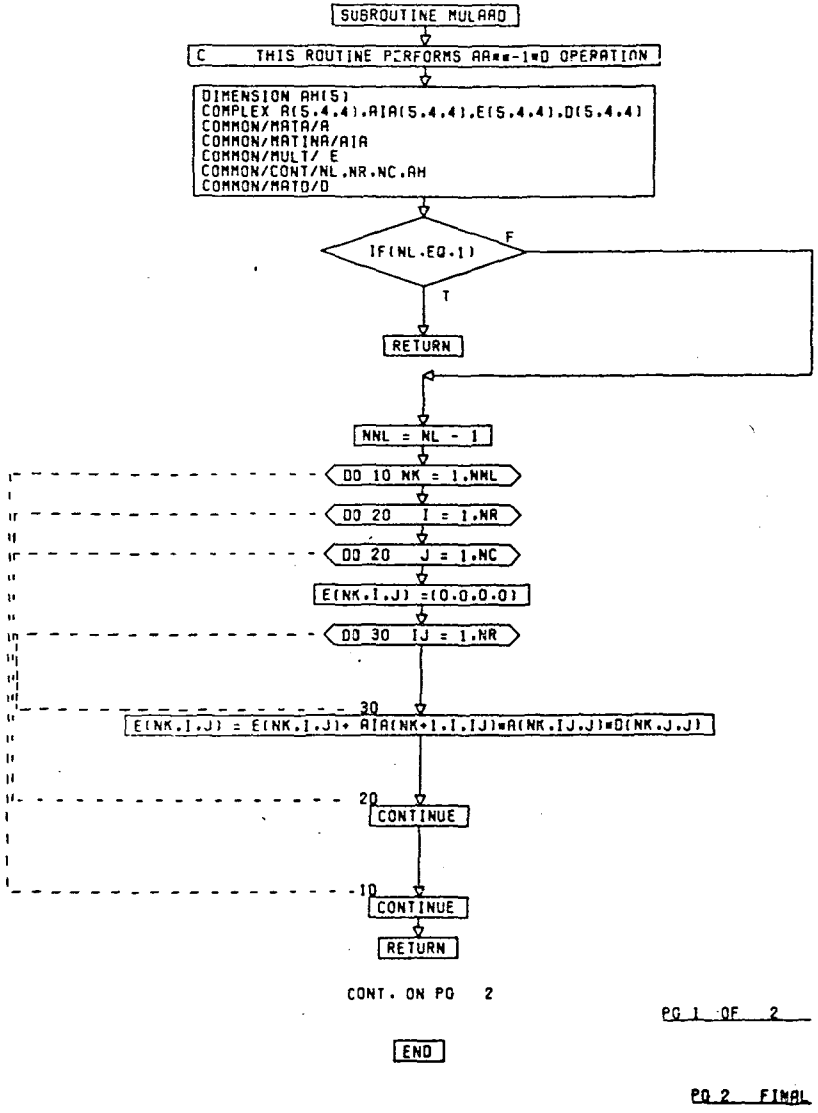

Fig. B24. Flow chart of subroutine MULAAD

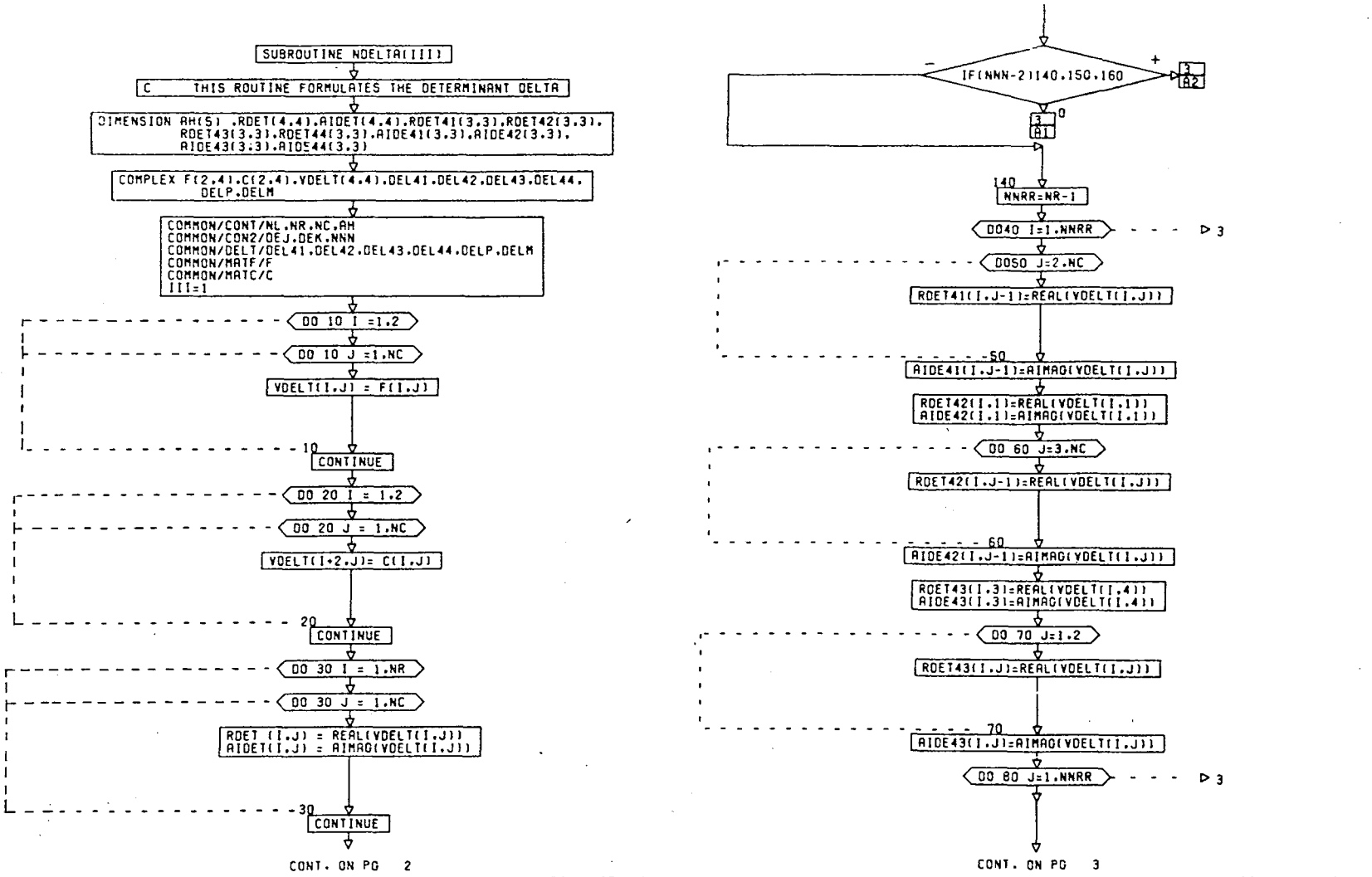

Fig. B25. Flow chart of subroutine NDELTA (sheet 1 of 2)

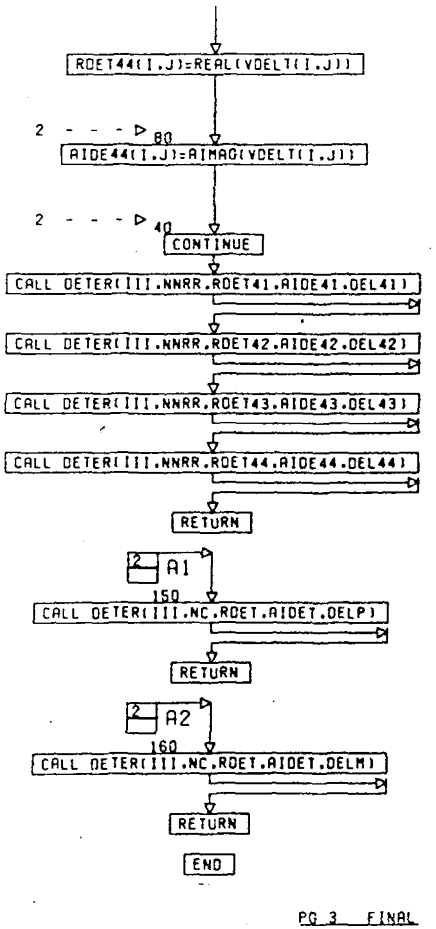

Fig. B25 (sheet 2 of 2)

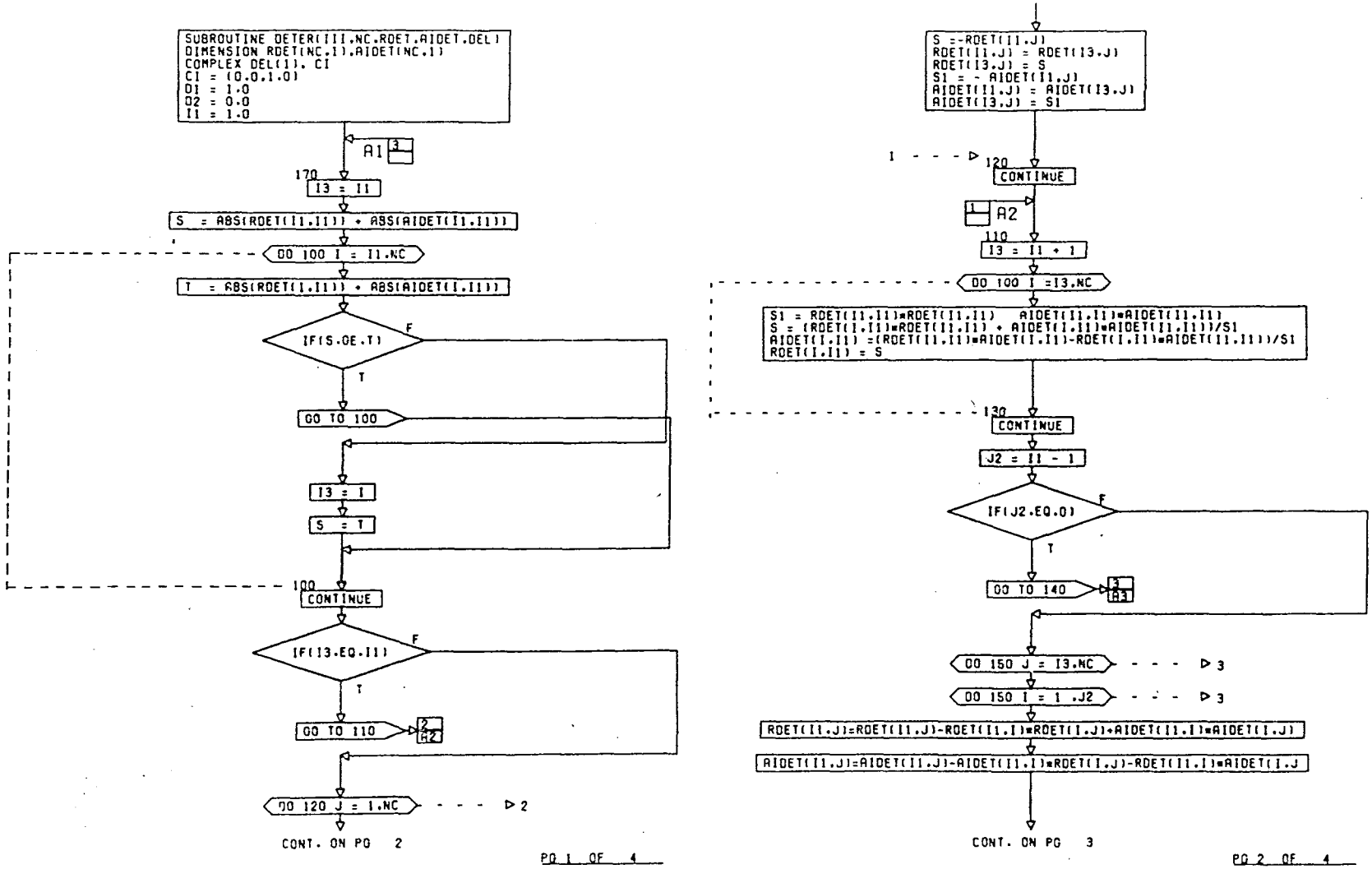

Fig. B26. Flow chart of subroutine DETER (sheet 1 of 2)

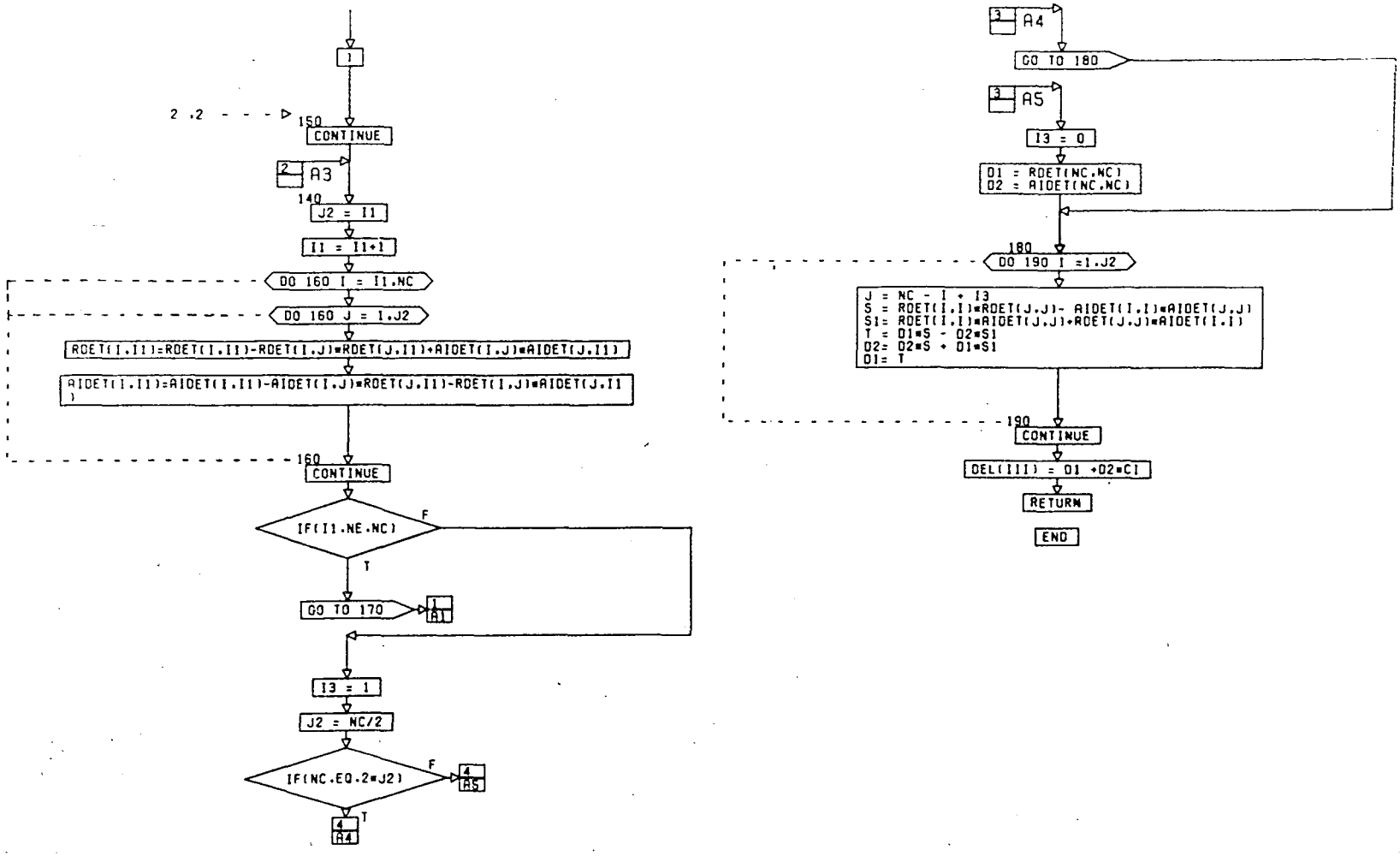

Fig. B26 (sheet 2 of 2)

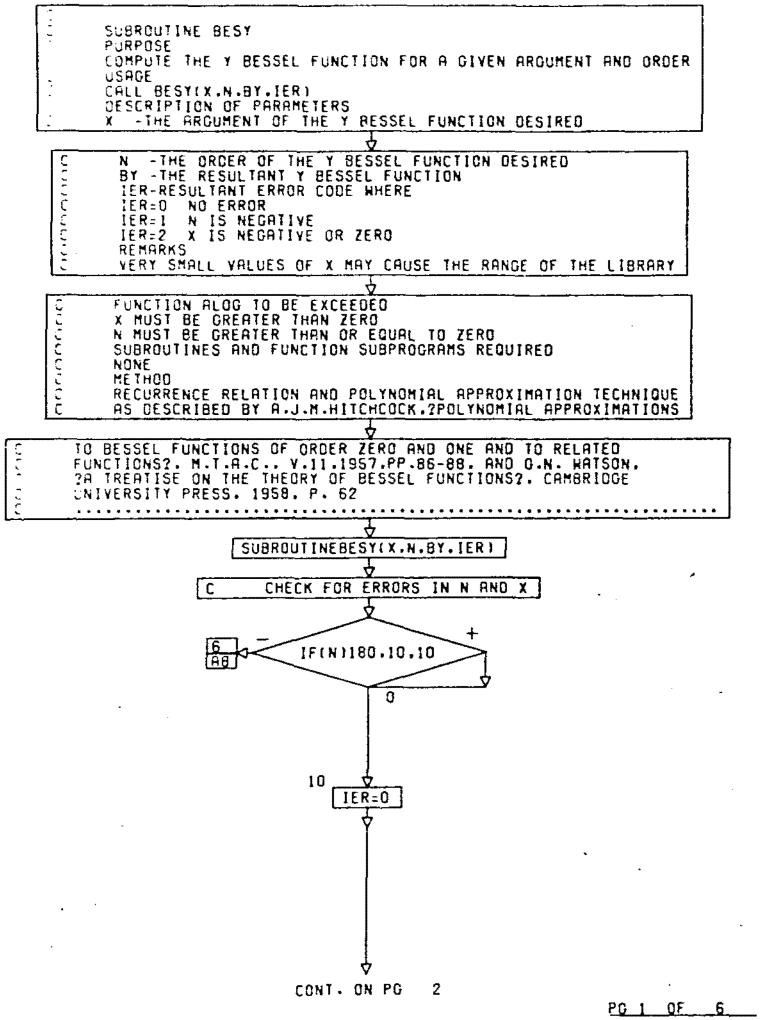

Fig. B27. Flow chart of subroutine BESY (sheet 1 of 3)

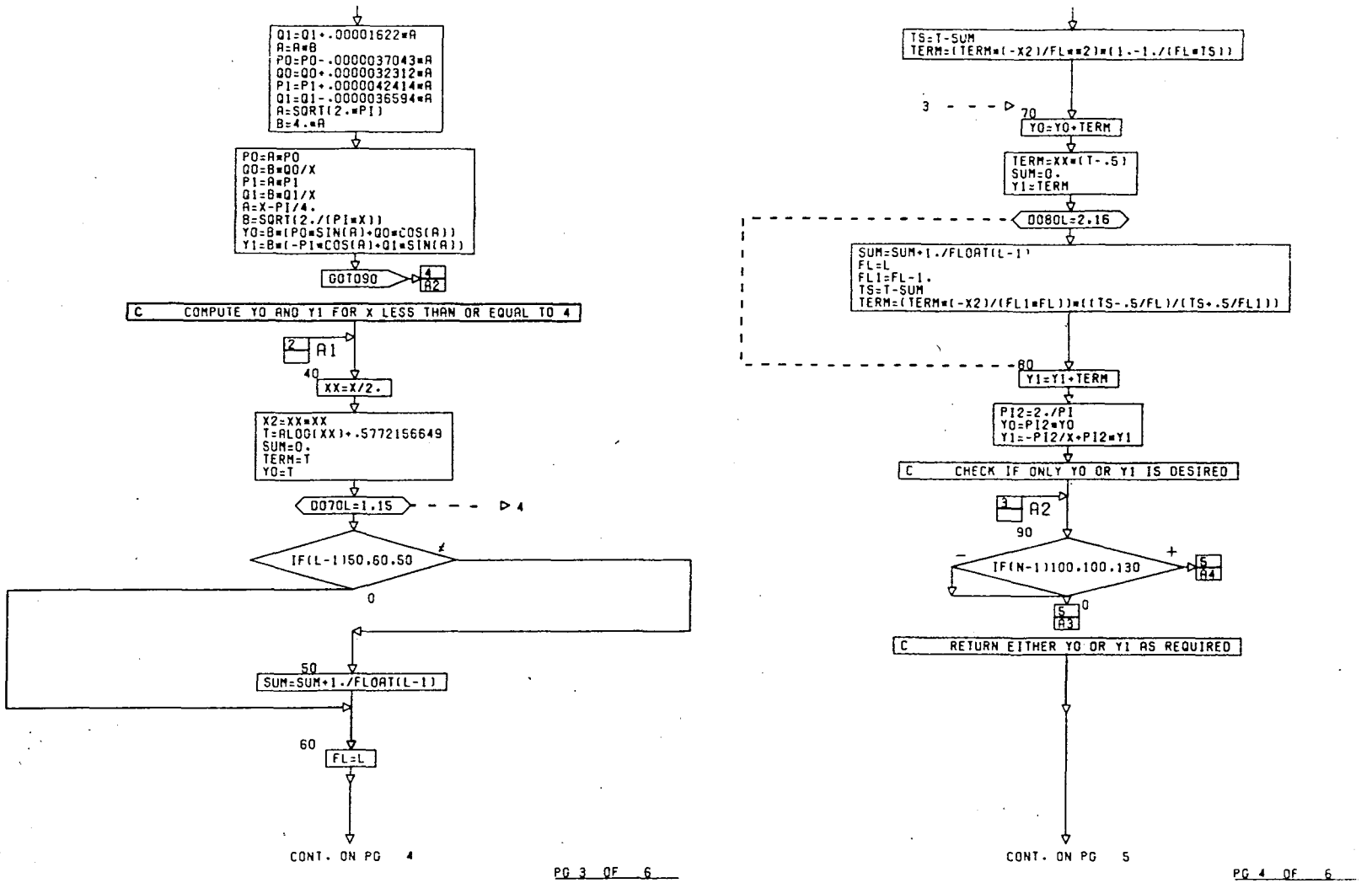

Fig. B27 (sheet 2 of 3)

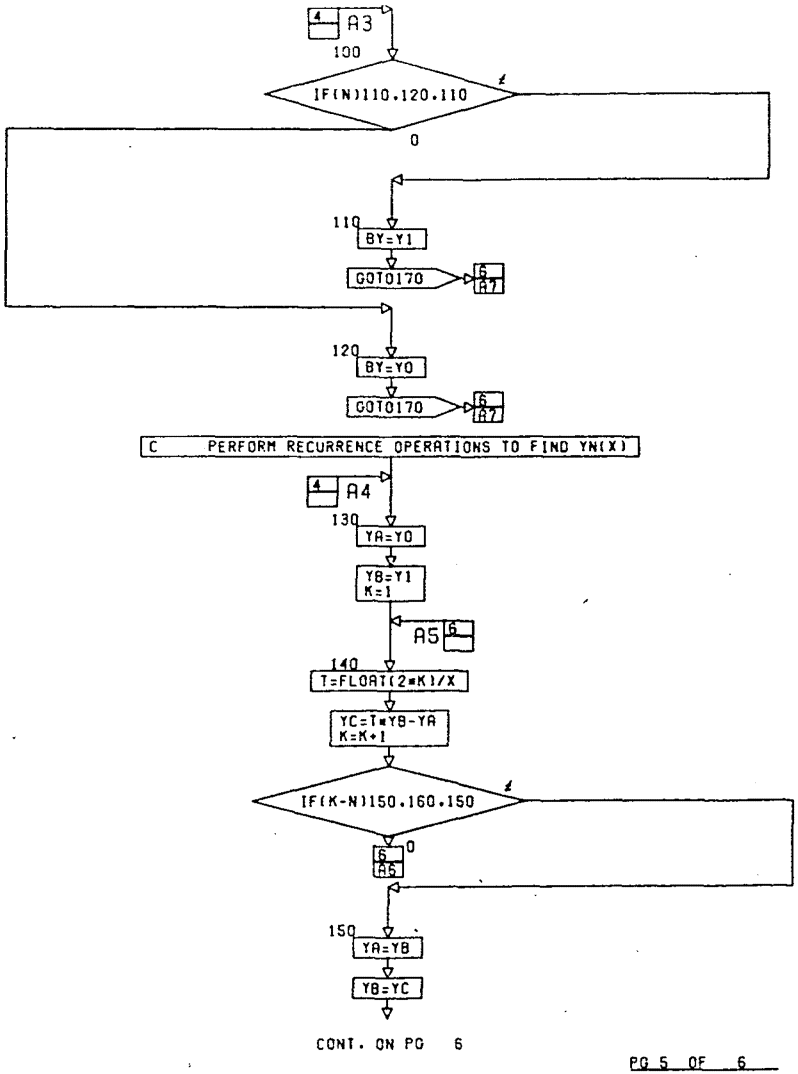

PG 5 OF 6

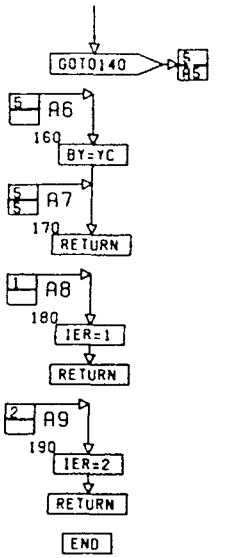

PG 6 FINAL

Fig. B27 (sheet 3 of 3)

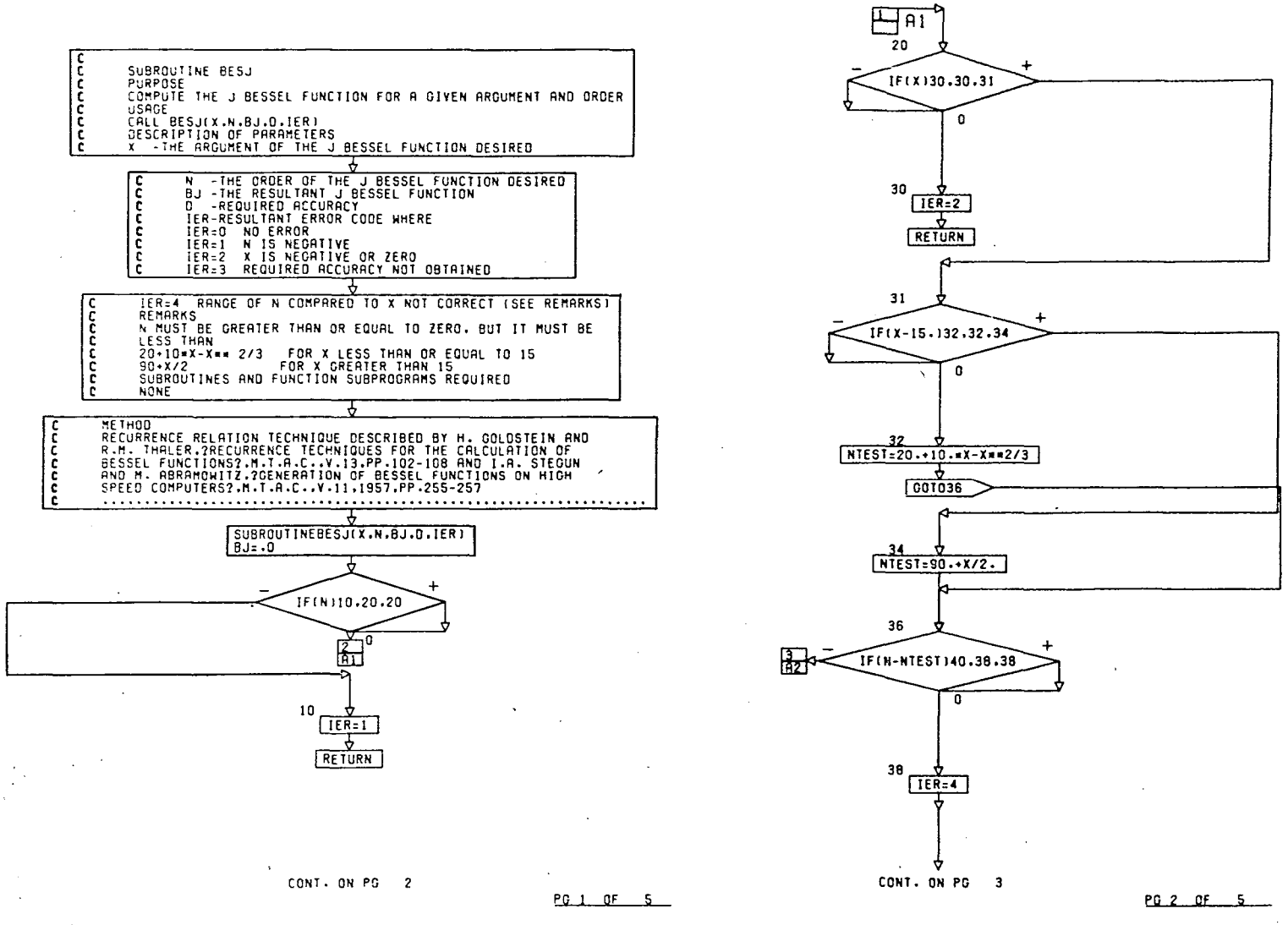

Fig. B28. Flow chart of subroutine BESJ (sheet 1 of 3)

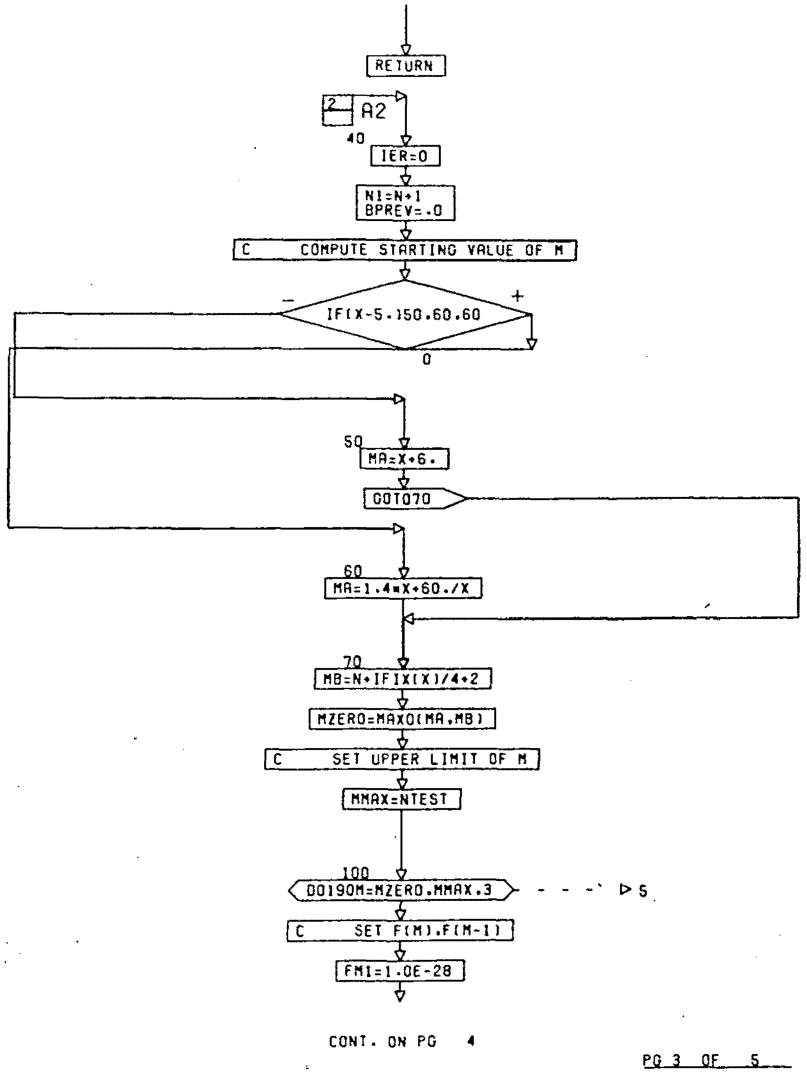

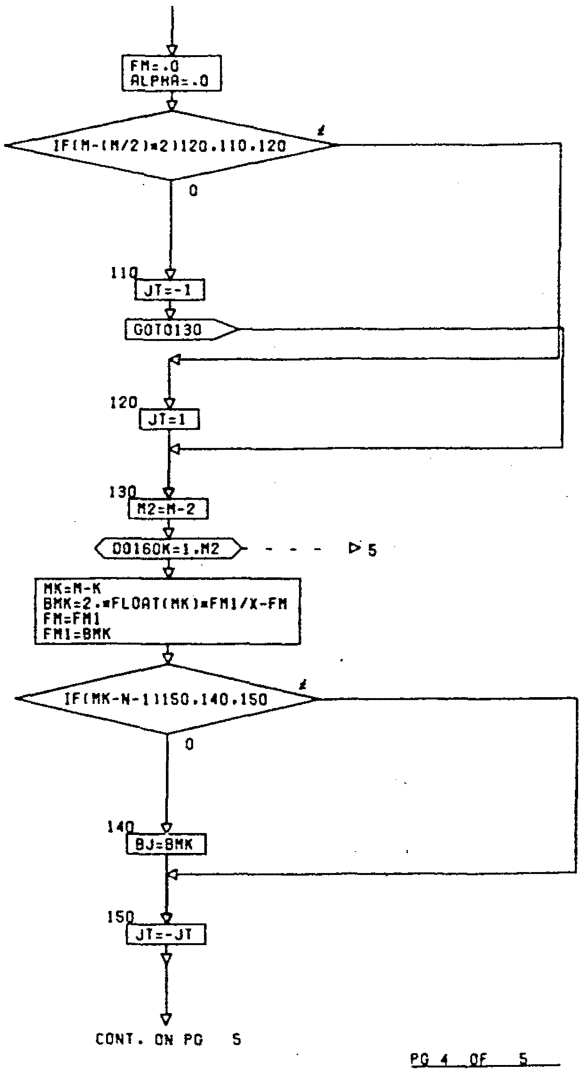

Fig. B28 (sheet 2 of 3)

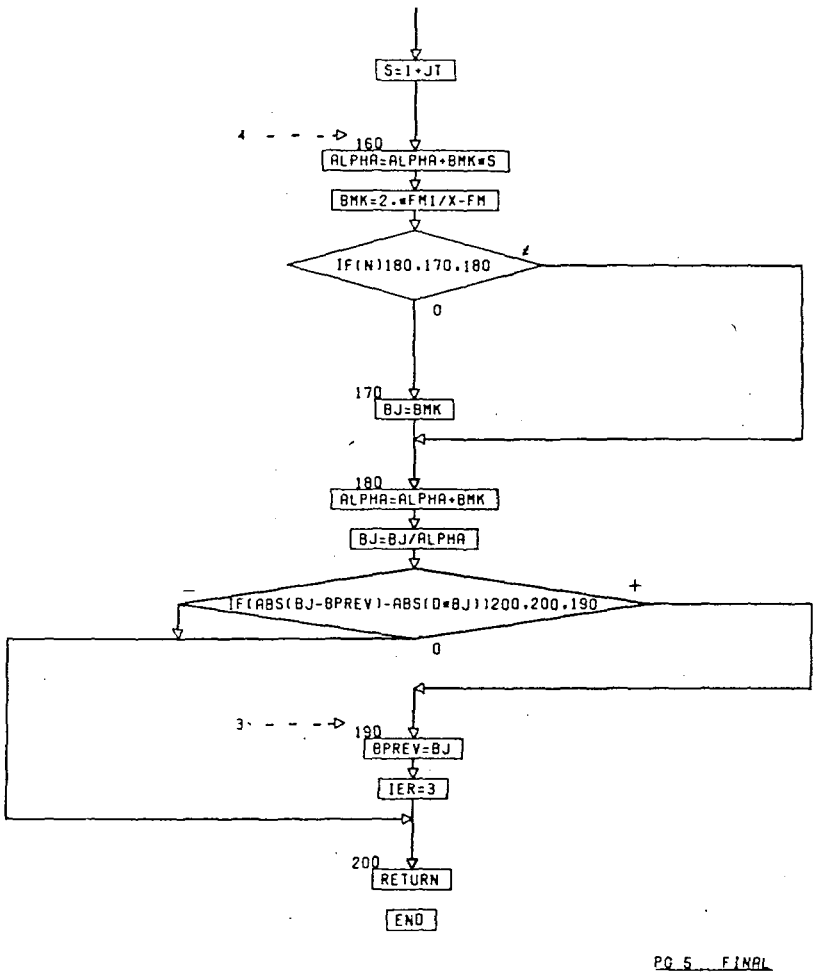

Fig. B28 (sheet 3 of 3)

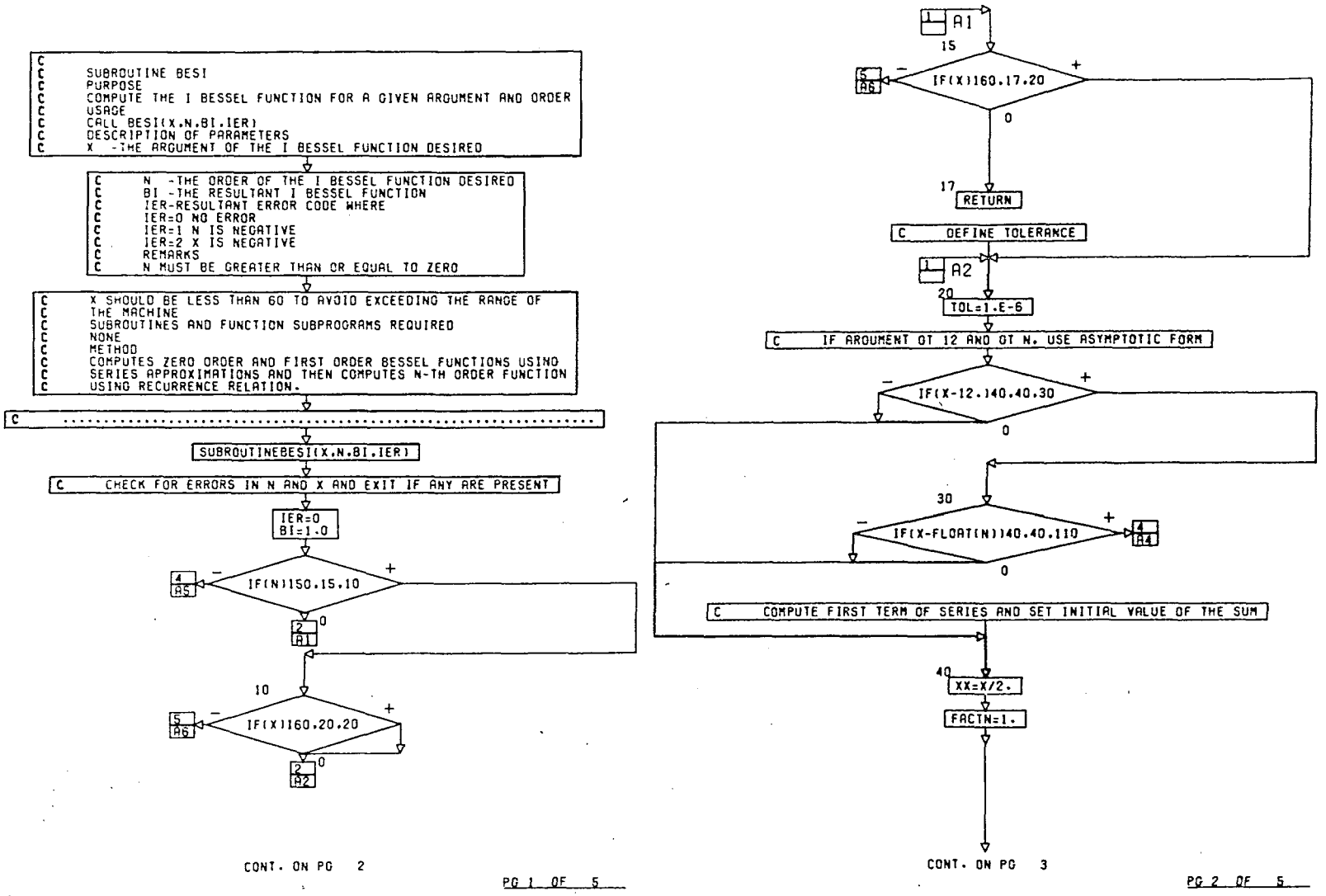

Fig. B29. Flow chart of subroutine BESI (sheet 1 of 3)

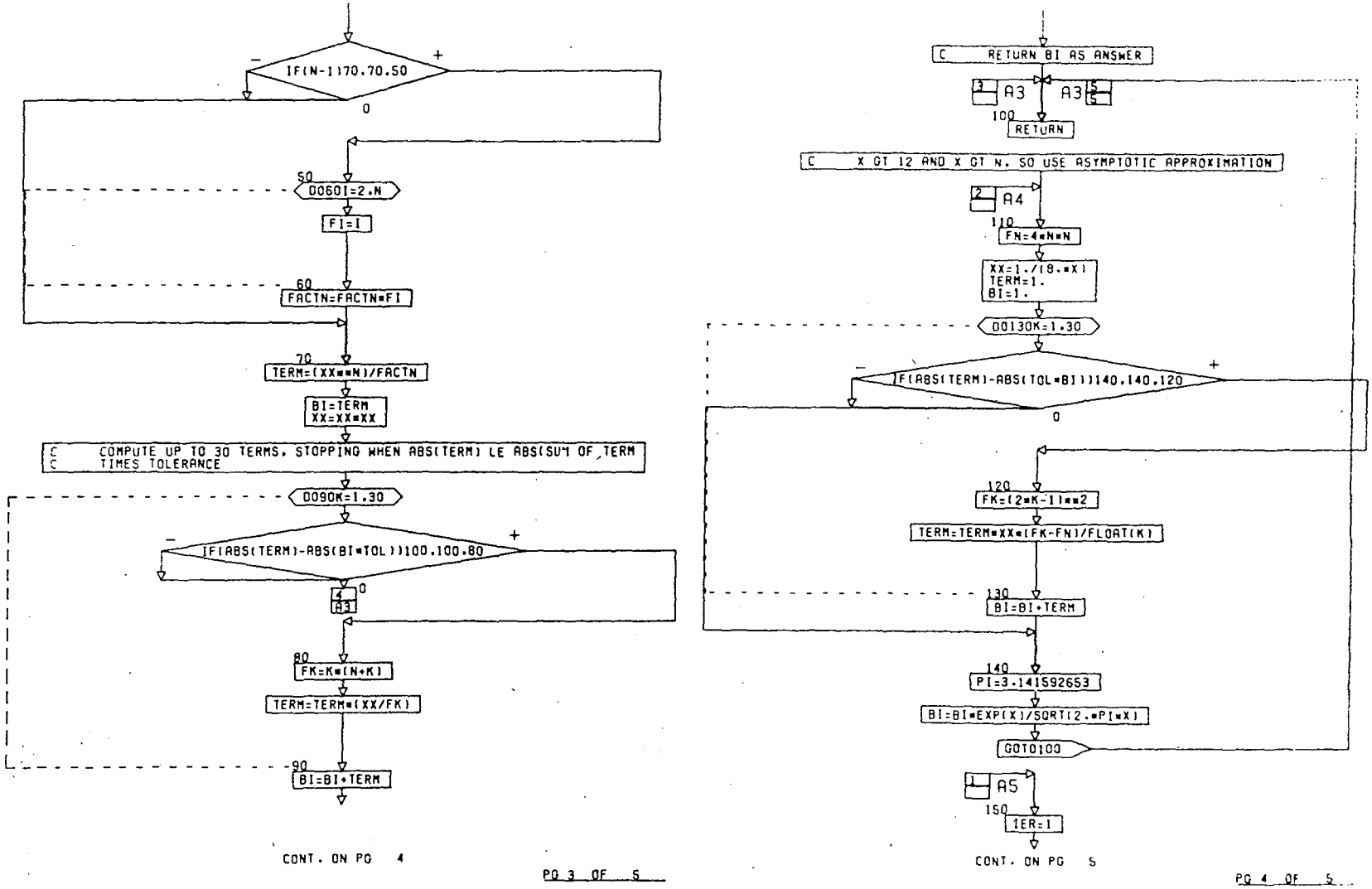

Fig. B29 (sheet 2 of 3)

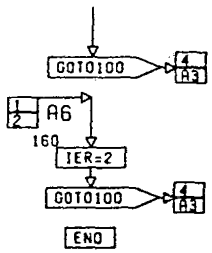

PG 5 FINAL

Fig. B29 (sheet 3 of 3)

Table B1

Input Variables

Input Record	Input Medium	Variable Name	Column(s)	Mode	Units	Description	Restriction
				Module I			
1	Card	JJ	1-10	Fixed	Count	Number of reference files to be input	Count must equal 1 through 30
		NPTS	11-20	Fixed	Count	Number of points of reference and predicted signals	Must equal 2^N where N = 1-10
2	Tape Unit 4	XLIST(J),J=1,12	1-72	Floating (12A6)	Alphanumeric characters	Identification of reference signals	
3	Tape Unit 4	Y(J),J=1,NPTS	1-72	Floating (8F9.4)	Count	Reference to predicted seismic signal	Number of Y value is power of 2
				Module II			
1	Card	NSITE(J),J=1,3	1-9	Fixed	Alphanumeric characters	Site identification	
2	Card	NTEST(J),J=1,3	1-9	Fixed	Alphanumeric characters	Test identification	
3	Card	JF	1-10	Fixed	Count	Number of reference files to be used	
		JFILE(J),J=1,JF	11-80	Fixed	Count	Reference file identification	
4	Card	HI	1-10	Floating	cm/sec megadyne	Upper limit of coupling coefficient	
		LOW	11-20	Floating	cm/sec megadyne	Lower limit of coupling coefficient	
		FRE	21-30	Floating	Hz	Maximum frequency	
		IP	31-40	Fixed	Code	Order of derivative of particle motion	
		T	41-50	Fixed	sec	Step size in Fourier analysis	
		NMODE	51-60	Fixed	Count	Number of modes	
		L	61-70	Fixed	Code	Velocity index	
5	Card	NL	1-10	Fixed	Count	Number of layers	$1 \leq N \leq 5$
		NQ	11-20	Fixed	Count	Number of matrix rows	$1 \leq NR \leq 4$
		NC	21-30	Fixed	Count	Number of matrix columns	$1 \leq NC \leq 4$
		NDBUG	31-40	Fixed	Code	Code for printing intermediate calculations	0 no printout 1 printout
6	Card	AH(J)J=2,NL+1	1-70	Floating (7F10.5)	m	Layer depth	
7	Card	AMU(J)	1-10	Floating	$n/m^2 \times 10^{-3}$	Elastic soil constant	
		ALAND(J)	11-20	Floating	$n/m^2 \times 10^{-3}$	Lamé constant	
		RHO(J) where J=1,NL	21-30	Floating	g/cm^2	Density	
8	Card	NRA RR(J) where J=1,NRA	1-10	Fixed	Count	Number of ranges	$1 \leq NRA \leq 30$
9	Card	NZ	1-10	Fixed	Count	Number of damping coefficients	$1 \leq NZ \leq 30$
		ZETA(J) where J=1,NZ	11-	Floating	m^{-1}	Wave number damping coefficients	
10	Card	DEJ	1-10	Floating	m^{-1}	Step size (real)	
		DEK	11-20	Floating	m^{-1}	Step size (imaginary)	
		Y1	21-30	Floating	m^{-1}	Wave number damping coefficient	
11	Card	X1	1-10	Floating	m^{-1}	Wave number (real)	
		FREQ	21-30	Floating	Hz	Frequency associated with wave number	

Table B2

Output Variables

Variable Name*	Description
ORIGINAL SERIES	The first 3 data points read from the input tape
FOURIER COEFFICIENTS	The first 6 coefficients in the Fourier transform file
RECONSTRUCTION ORIGINAL SERIES	The first 3 data points generated by the inverse fast Fourier transform
CMAX	Maximum value of Fourier coefficients (C_n)
CMIN	Minimum value of Fourier coefficients (C_n)
NO. HARMONIC	Number of terms generated in the Fourier analysis
AZ	Twice the average value of the time domain function
H(2)	Second value of magnitude of the product of the coupling coefficient and the transmission coefficient. (There are 512 produced)
PHI(2)	Second value of phase of the product of the coupling coefficient and the transmission coefficient. (There are 512 produced)
AVG POWER	$T^{-1}\int_0^T \lvert f(x)\rvert^2 dx$, which is equivalent to $\frac{1}{4} C_o^2 + \frac{1}{2}\sum_{n=1}^{N} C_n^2$ (N = 120 for seismic signal; N = 512 for total signal)
RMS	Root mean square of the time domain signal $\left[= (\text{AVG POWER})^{1/2}\right]$
SEISMIC INPUT	That part of the signal less than 170 Hz
TOTAL INPUT	That part of the signal less than 750 Hz
YMAX1	Maximum value of forcing function (MEGADYNES)
CMAX	Maximum value of the Fourier coefficients
YMAX	Predicted maximum amplitude in time domain
YMIN	Predicted minimum amplitude in time domain
NO. OF POINTS	Number of points in predicted signal
PERIOD SEC.	Length of period in seconds
TRIGH, TRIGM, TRIGL	Preselected threshold values
NHIGH, NMED, NLOW	Number of signals that exceed preselected threshold values

* See fig. B2.

Table B3

Program Listing

```
C      SEISMIC MODEL FOR PREDICTING SIGNALS THROUGH TERRAIN MATERIAL
C
       DIMENSION NSITE(3),NTEST(3).
       DIMENSION ZETA(5),RR(20),JFILE(30),ISEC(30)
       DIMENSION AH(5),XLIST(12)
       COMPLEX VS,VP
       COMPLEX ANU(5),ANUP(5),AMU(5),AA(5),A(5,4,4),B(2,4),
      1 D(5,4,4),C(2,4),AIA(5,4,4),AMA(5,4,8),E(5,4,4),
      2 F(2,4),FF(2,4),ALAND(5),ALFAK(5),CI,AK,
      3 BETAK(5),DEL41,DEL42,DEL43,DEL44,DELP,DELM,DELKA
       COMPLEX B1(513)
       COMPLEX VSS(5),VPP(5)
       COMMON/WCOM/EXPKFS,W(2,257)
       COMMON/YCOM/Y(1026)
       COMMON/HCOM/H(513)
       COMMON/PHICOM/PHI(513)
       COMMON/B1COM/B1
       COMMON/COND/X1,ALAND,RHO(5),Y1,DELKA,FREQ,CI,IP,VSS,VPP
       COMMON/COND1/NDBUG,L,N,FRE,NE,HI,LOW,ITEST,IBAQ,IBAW
       COMMON/CONT/NL,NR,NC,AH
       COMMON/CON2/DEJ,DEK,NNN
       COMMON/ELEM/ANU,ANUP,AMU,AA,AK
       COMMON/MATA/A
       COMMON/MATB/B
       COMMON/MATC/C
       COMMON/MATD/D
       COMMON/MATINA/AIA
       COMMON/MULT/E
       COMMON/MATF/F
       COMMON /COMAMA/AMA
       COMMON/DELT/DEL41,DEL42,DEL43,DEL44,DELP,DELM
       REAL LOW
       CALL BANS
C
C         INPUT MODE I
C
       PRINT 90
   90  FORMAT(1H1,24HE. A. BAYLOT M AND E DIV./)
       CALL DATIME(T1,T2,T3)
       PRINT 87,T1,T2
       REWIND 3
       REWIND 4
       REWIND 5
       READ 30,JJ,NPTS
       CALL SETSCT(91,1)
       DO 53 J=1,JJ
       READ(4,98)(XLIST(J1),J1=1,12)
       READ(4,99)(Y(J1),J1=1,NPTS)
       CALL SAVSCT(91,ISEC(J))
       WRITE(91,98)(XLIST(J1),J1=1,12)
```

(Continued)

Table B3 (Continued)

```
      WRITE(91,99)(Y(J1),J1=1,NPTS)
   53 CONTINUE
    1 NMD=1
      CI =(0.0,1.0)
      READ 10,(NSITE(J),J=1,3)
      CALL EOFTST(50,NFILE)
      IF(NFILE.EQ.2) GO TO 2000
C
C        INPUT MODE II
C
      READ 10,(NTEST(J),J=1,3)
      PRINT 10,(NTEST(J),J=1,3)
       PRINT 10,(NSITE(J),J=1,3)
      READ 30,JF,(JFILE(JL),JL=1,JF)
      READ 85,HI,LOW,FRE,IP,T,NMODE,L
      PRINT 86,HI,LOW,FRE,IP,NPTS,T,NMODE,L
      IP=IP-1
      READ 30, NL,NR,NC,NDBUG
      PRINT 40,NL,NR,NC
      NPL1=NL+1
      READ 35, (AH(I),I=2,NPL1)
      AH(1)=0.0
      PRINT 45
      DO 50 I= 1,NPL1
   50 PRINT 51,AH(I)
      DO 5 IN=1,NL
      READ 15,AMU(IN),ALAND(IN),RHO(IN)
      PRINT 26,AMU(IN),ALAND(IN),RHO(IN)
      VS=CSQRT(AMU(IN)/RHO(IN))
      VSS(IN)=CSQRT(RHO(IN)/(ALAND(IN)+2.0*AMU(IN)))
      VP=CSQRT((ALAND(IN)+2.0*AMU(IN))/RHO(IN))
      VPP(IN)=CSQRT(RHO(IN)/AMU(IN))
      PRINT 96,VS,VP
    5 CONTINUE
      READ 84,NRA,(RR(NF),NF=1,NRA)
      READ 84,NZ,(ZETA(NF), NF=1,NZ)
      READ 32,DEJ,DEK,Y1,XUNIT
      PRINT 42,DEJ,DEK,Y1,XUNIT
      DELKA=DEJ+DEK*CI
    7 N=0
      ITEST=1
      CALL SETSCT(92,1)
      CALL SETSCT(93,1)
      CALL SAVSCT(91,IBAW)
      CALL SAVSCT(92,IBAQ)
      CALL SAVSCT(93,IAKR)
      IF(NDBUG.EQ.1) PRINT 89,IBAW,IBAQ,IAKR
   89 FORMAT(6H IBAW=,I7,6H IBAQ=,I7,6H IAKR=,I7)
      READ(5,98)(XLIST(J1),J1=1,12)
      CALL EOFTST(5,NFILE)
```

(Continued)

Table B3 (Continued)

```
      IF(NFILE.EQ.2) GO TO 1
      PRINT 98, (XLIST(J1),J1=1,12)
    6 READ(5,33)X1,FREQ
      CALL EOFTST(5 ,NFILE)
      IF(NFILE.EQ.2) GO TO 1
      X1=X1*XUNIT
      WRITE(93,79)X1
      N=N+1
      CALL NDATA
      IF(NDBUG.EQ.1) PRINT 93,ITEST,N
   93 FORMAT(6HITEST=,I7,4H  N=,I7)
      IF(ITEST.EQ.0) GO TO 6
      REWIND 4
      NE=NE-10
      NZN=1
      NRN=1
      R=RR(NRN)
      Z=ZETA(NZN)
      LX=L
      PRINT 207,R,L,Z,NE
  207 FORMAT(6HRANGE=,F10.3,10HVEL INDEX=,I7,10HDAMP COEF=,E15.5,11HNO.
     1OF PTS=,I7)
      IF(LX.EQ.3) LX=1
  700 CALL HAN2(R,Z,LX,NE,NMD,NMODE,IAKR,IBAW,IBAQ)
      IF(NMD-NMODE)800,810,810
  800 NMD=NMD+1
      GO TO 7
  810 CONTINUE
      CALL EBFF8(JF,JFILE,ISEC,T,NPTS,NDBUG)
      IF(NRN.GE.NRA) GO TO 710
      NRN=NRN+1
  720 R=RR(NRN)
      GO TO 700
  710 IF(NZN.GE.NZ) GO TO 730
      NZN=NZN+1
      NRN=1
  750 Z=ZETA(NZN)
      GO TO 720
  730 IF(L.EQ.3.AND.LX.EQ.1) GO TO 740
      GO TO 7
  740 LX=2
      NRN=1
      NZN=1
      GO TO 750
 2000 CONTINUE
      CALL DATIME(T1,T2,T3)
      PRINT 87,T1,T2
      END FILE 3
      REWIND 3
      REWIND 4
```

(Continued)

Table B3 (Continued)

```
      REWIND 5
      CALL BANE
   10 FORMAT(3A3)
   15 FORMAT(5F10.5)
   25 FORMAT (5X,I2,5X,9E12.5)
   26 FORMAT(1X,5E12.5)
   30 FORMAT(8I10)
   32 FORMAT(4F10.5)
   35 FORMAT(7F10.5)
   36 FORMAT(I10,11A6)
   40 FORMAT(10X,14HNO. OF LAYERS=,I5,12HNO. OF ROWS=,I5,11HNO. OF COL=,
     1I5)
   42 FORMAT(10X,4HDEJ=,F10.5,5X,4HDEK=,F10.5,3HY1=,F10.5,5HUNIT=,
     1F10.5)
   43 FORMAT(10X,3HAK=,2F8.5,5HFREQ=,F10.5)
   45 FORMAT(10X,14HDEPTH OF LAYER)
   51 FORMAT(10X,8F14.5)
   79 FORMAT(4E15.5,F10.5)
   80 FORMAT(8E14.5)
   84 FORMAT(I10,7F10.4,/(8F10.4))
   85 FORMAT(3F10.2,I10,F10.0,2I10)
   86 FORMAT(30HUPPER LIMIT FOR AQ AND AW HI= ,E15.5,30H LOWER LIMIT FOR
     1AQ AND AW LW= ,E15.5,/,5HFREQ=,F10.3,4H IP=,I7,6H NPTS=,I7,
     213H TIME PERIOD=,F7.0,7H NMODE=,I7,3H L=,I7)
   87 FORMAT(26X,A8,8X,A8,/)
   96 FORMAT(3HVS=,2E20.11,4H VP=,2E20.11)
   98 FORMAT(12A6)
   33 FORMAT(2F10.0)
   99 FORMAT(6F12.4)
      END
      SUBROUTINE NDATA
      COMPLEX ANU(5),ANUP(5),AMU(5),AA(5),A(5,4,4),B(2,4),
     1 D(5,4,4),C(2,4),AIA(5,4,4),AMA(5,4,8),E(5,4,4),
     2 F(2,4),FF(2,4),ALAND(5),ALFAK(5),CI,AK,
     3 BETAK(5),DEL41,DEL42,DEL43,DEL44,DELP,DELM,ATEMP,
     4       AQ,AW,DELKA,DER,BAW,BAQ
      COMPLEX VSS(5),VPP(5)
      COMMON/COND/X1,ALAND,RHO(5),Y1,DELKA,FREQ,CI,IP,VSS,VPP
      COMMON/COND1/NDBUG,L,N,FRE,NE,HI,LOW,ITEST,IBAQ,IBAW
      COMMON/CONT/NL,NR,NC,AH
      COMMON/CON2/DEJ,DEK,NNN
      COMMON/ELEM/ANU,ANUP,AMU,AA,AK
      COMMON/MATA/A
      COMMON/MATB/B
      COMMON/MATC/C
      COMMON/MATD/D
      COMMON/MATINA/AIA
      COMMON/MULT/E
      COMMON/MATF/F
      COMMON /COMAMA/AMA
```

(Continued)

Table B3 (Continued)

```
      COMMON/DELT/DEL41,DEL42,DEL43,DEL44,DELP,DELM
        REAL LOW
      AK=(1.0,0.0)*X1-(0.0,1.0)*X1*Y1
      OM=6.283*FREQ
      DER=(OM*(0.0,1.0))**IP
      DO 10 IN =1,NL
      ALFAK(IN)=OM*VSS(IN)
      BETAK(IN)=OM*VPP(IN)
   10 CONTINUE
      NNN=0
   11 NNN=NNN+1
      DO 55 NA = 1,NL
      DO 60  I = 1,NR
      DO 60  J = 1,NC
      A(NA,I,J)=(0.0,0.0)
      D(NA,I,J)=(0.0,0.0)
      AIA(NA,I,J)=(0.0,0.0)
      AMA(NA,I,J)=(0.0,0.0)
      E(NA,I,J)=(0.0,0.0)
   60 CONTINUE
   55 CONTINUE
      DO 61 I=1,2
      DO 61 J=1,NC
      B(I,J) =(0.0,0.0)
      C(I,J) =(0.0,0.0)
      F(I,J) =(0.0,0.0)
      FF(I,J)=(0.0,0.0)
   61 CONTINUE
      I=1
      DO 64 IN=1,NL
      ANU(IN)=CSQRT(AK*AK-ALFAK(IN)*ALFAK(IN))
      ANUP(IN)=CSQRT(AK*AK-BETAK(IN)*BETAK(IN))
      AA(IN) = 2.0*AMU(IN)*ANU(IN)*ANU(IN)-ALAND(IN)*ALFAK(IN)*ALFAK(IN)
   64 CONTINUE
      CALL MATRAA
      CALL MATRBB
      CALL MATRDD
      CALL MATRCC
      CALL IVERAA
      CALL MULAAD
      CALL DELEL
      CALL NDELTA(I)
      IF(NNN-2)12,13,14
   12 AK=AK+DELKA
      GO TO 11
   13 AK=AK-2.*DELKA
      GO TO 11
C  14 ATEMP=AK*AK*2.*DELKA/(DELP-DELM) NOTE AK WAS REMOVED ON 24 APR 72
   14 AK=AK+DELKA
      ATEMP=AK*2.0*DELKA/(DELP-DELM)
```

(Continued)

Table B3 (Continued)

```
      IF(L-2) 200,210,200
  200 AW=ATEMP*(-ANU(1)*(-DEL41-DEL42)+AK*AK*(-DEL43+DEL44))
      IF(NDBUG.EQ.1) PRINT 94,AWR,HI,LOW,FRE,L,N,NE
   94 FORMAT(4E15.5,3I7)
      IF(NDBUG.EQ.1) PRINT 205,AW,AK,FREQ
      AWR=REAL(AW)
      IF(AWR.GE.HI.OR.AWR.LE.LOW.OR.AWR.EQ.0.0) GO TO 120
      AWI=AIMAG(AW)
      IF(AWI.GE.HI.OR.AWI.LE.LOW.OR.AWI.EQ.0.0) GO TO 120
      BAW    = 3.14159*FREQ*AW*DER
      IF(NDBUG.EQ.1) PRINT 208,BAW
      WRITE(91,79)BAW
      IF(L-2)66,210,210
  210 AQ=ATEMP*AK*(-DEL41+DEL42-ANUP(1)*(-DEL43-DEL44))
      IF(NDBUG.EQ.1) PRINT 206,AQ,AK,FREQ
      AQR=REAL(AQ)
      IF(AQR.GE.HI.OR.AQR.LE.LOW.OR.AQR.EQ.0.0) GO TO 100
      AQI=AIMAG(AQ)
      IF(AQI.GE.HI.OR.AQI.LE.LOW.OR.AQI.EQ.0.0) GO TO 100
      BAQ    =-3.14159*FREQ*AQ*DER
      IF(NDBUG.EQ.1) PRINT 209,BAQ
      WRITE(92,79)BAQ
   66 IF(FREQ.GE.FRE) GO TO 106
      ITEST=0
      RETURN
  106 NE=N
      ITEST=1
      RETURN
C   MOD FOR SLEWING REST OF RECORDS AFTER AQ OR AW EXCEEDS ITS LIMITS.
  120 PRINT 83,AW,FREQ
      GO TO 130
100   PRINT 82,AQ,FREQ
  130 DO 110 LL=1,512
      READ(5,81) FREQ
      CALL EOFTST(5,NFILE)
       IF(NFILE.EQ.2) GO TO 115
      IF(FREQ.GE.FRE) GO TO 115
  110 CONTINUE
  115 NE=N-1
      ITEST=1
      RETURN
   79 FORMAT(4E20.11,F10.5)
   81   FORMAT(10X,F10.5)
   82 FORMAT(3HAQ=,2E15.5,5HFREQ=,F10.5)
   83 FORMAT(3HAW=,2E15.5,5HFREQ=,F10.5)
  205 FORMAT(3HAW=,2E15.5,3HAK=,2E15.5,5HFREQ=,F10.4)
  206 FORMAT(3HAQ=,2E15.5,3HAK=,2E15.5,5HFREQ=,F10.4)
  208 FORMAT(7HBAW(K)=,2E15.5)
  209 FORMAT(7HBAQ(K)=,2E15.5)
      END
```

(Continued)

Table B3 (Continued)

```
      SUBROUTINE HAN2(R,Z,LX,NE,NMD,NMODE,IAKR,IBAW,IBAQ)
      COMPLEX BAQ,BAW,S,HA,AJ,AY
      COMPLEX B1(513),B
      COMMON/HCOM/H(513)
      COMMON/PHICOM/PHI(513)
      COMMON/B1COM/B1
      PRINT 330,R
  330 FORMAT(7H RANGE=,E15.5)
      L=LX
      NDBUG=0
      IF(NDBUG.EQ.1) PRINT 84,IBAW,IBAQ,IAKR,L,NE,NMD,NMODE,R,Z
   84 FORMAT(6H IBAW=,I7,6H IBAQ=,I7,6H IAKR=,I7,3H L=,I7,4H NE=,I7,
     1 5H NMD=,I7,7H NMODE=,I7,3H R=,E15.5,3H Z=,E15.5)
      CALL SETSCT(91,IBAW)
      CALL SETSCT(92,IBAQ)
      CALL SETSCT(93,IAKR)
      IF(NMD-1) 710,710,720
  710 DO 740 K=1,NE
      B1(K)=(0.0,0.0)
  740 CONTINUE
      NEE=NE
  720 CONTINUE
      IF(NE.GT.NEE) NE=NEE
      NEE=NE
      R=-R
      L=L-1
      XL=-1+L+L
      DO 200 N=1,NE
      K=N+1
      HA=(0.0,0.0)
C       SOLVING HANKLE FUNCTION.
      READ(93,82)AKR
      XR=AKR*R
   56 YI=XR*Z
      IF(N.EQ.1) PRINT 152,YI,AKR,XR
      AM=SQRT(XR*XR+YI*YI)
      IF(AM.GT.20.0) GO TO 400
      DO 100 J=1,4
      NR=J-L
      NS=J
      CALL BESJ(XR,NR,BJ,D,IER)
      AJ=(1.0,0.0)*BJ
      CALL BESY(XR,NR,BY,IER)
      AY=(0.0,1.0)*BY
      CALL BESI(YI,NS,BI,IER)
      HA=((0.0,1.0)**NS*(AJ-AY)*BI)*(-1)**(2*(L-J)+1)+HA
      NS=-J
      NR=L-NS
      CALL BESJ(XR,NR,BJ,D,IER)
      AJ=(1.0,0.0)*BJ
```

(Continued)

Table B3 (Continued)

```
      CALL BESY(XR,NR,BY,IER)
      AY=(0.0,1.0)*BY
      HA=HA+(0.0,1.0)**NS*(AJ-AY)*BI*(-1)**(NR+1)
  100 CONTINUE
      NR=L
      NS=0
      CALL BESJ(XR,NR,BJ,D,IER)
      AJ=(1.0,0.0)*BJ
      CALL BESY(XR,NR,BY,IER)
      AY=(0.0,1.0)*BY
      CALL BESI(YI,NS,BI,IER)
      HA=HA+(AJ-AY)*BI*XL
      GO TO 390
  400 PH1=ATAN2(YI,-XR)
      PH2=-PH1*0.5
      IF(L)360,360,370
C       S(N) NEEDS TO READ IN WHEN SURFACE IS NOT SMOOTH.
  360 PH3=-XR-0.78539+PH2
      GO TO 380
  370 PH3=-XR-2.35619+PH2
  380 HKR=SQRT(2.0/(3.14159*AM))*EXP(-YI)
      HA=(HKR*COS(PH3))*(1.0,0.0)+(HKR*SIN(PH3))*(0.0,1.0)
  390 CONTINUE
      S=(1.0,0.0)
      IF(L-1)30,40,40
   30 READ(92,79)BAW
      B=S*BAW*HA
      GO TO 50
   40 READ(92,79)BAQ
      B=S*BAQ*HA
   50 B1(N)=B1(N)+B
      IF(NMD.NE.NMODE) GO TO 200
      X1=REAL(B1(N))
      Y1=AIMAG(B1(N))
      IF(NDBUG.EQ.1) PRINT 83,N,B1(N),X1,Y1
   83 FORMAT(3H N=,I7,7H B1(N)=,2E15.5,4H X1=,E15.5,4H Y1=,E15.5)
      IF(X1.EQ.0.0.AND.Y1.EQ.0.0) GO TO 90
      H(K)=SQRT(X1*X1+Y1*Y1)
      PHI(K)=ATAN2(Y1,X1)
      GO TO 200
   90 H(K)=0.0
      PHI(K)=0.0
  200 CONTINUE
      IF(NDBUG.EQ.1) PRINT 99,(H(J),PHI(J),J=2,K)
      RETURN
   79 FORMAT(2E20.11)
   99 FORMAT(9HH AND PHI,/,(1X,2E15.5))
   82 FORMAT(E15.5)
  152 FORMAT(3HYI=,F10.5,5H AKR=,F10.5,4H XR=,F10.5)
       END
```

(Continued)

Table B3 (Continued)

```
C    THE FUNCTION OF THIS MAIN PROGRAM IS TO INPUT SEIMIC DATA
C    AND PREPARE INPUT DATA TO RUN ON FAST FOURIER ANALYSIS,
C    TO PREDICT SEISMIC SIGNALS AT GIVEN RANGES, AND TO GIVE NO. OF
C    SIGNALS ABOVE 3 GIVEN TRIGGER LEVELS,
C    AUTHORS: J. LUNDIEN AND E. BAYLOT. AUG 71,
C
C
C    INPUT VARABLES:
C
C    XLIST(K)=IDENTIFICATION DATA ON FIRST LINE. 72 CHARACTERS,
C    Y(J)=DATA FROM SEISMIC SENSOR,
C    FNS=TIME INCREMENT,  NO. OF SECONDS/NO. OF POINTS,
C    NM=NO, OF HARMONICS,
C    NPTS=NO. OF DATA POINTS,
C    DELT=SPACING BETWEEN ADJACENT DATA POINTS,
C    FACT =FACTOR USED TO OBTAIN AMPLITUDES WHEN THE DATA HAS A DISCRETE
C    SPECTRUM,
C    FN=FREQ,
C    DELW=FREQ SPACINGS IN RADIANS PER SECONDS,
C    DFILE: INPUT DATA FILE,
C    DFILE1: OUTPUT FILE OF HARMONICS, FOURIER COEF., PHASE ANGLES,
C    FT=7 HERTZ/3 DATA POINTS,
C    FR=7 HERTZ/5 DATA POINTS,
C
C    OUTPUT VARABLES:
C
C    Y2=FOURIER COEF,
C    Y2A=FACT*Y2
C    YMAX1=MAX INPUT DATA VALUE,
C    CMAX=MAX FOURIER COEF VALUE,
C    CMIN =MIN FOURIER COEF VALUE,
C    YMAX=MAX PREDICTED VALUE,
C    CA=FILTERED COEF
C    C=SQRT(A**2+B**2),  WHERE A=SINE COEF., AND B=COSINE COEF,
C    PHASE= ATAN2(-B/A) WHERE A =SINE COEF., AND B=COSINE COEF,
C
C
C***END DATA INPUT MOD***
C
      SUBROUTINE EBFF8(JF,JFILE,ISEC,T,NPTS,NDBUG)
      COMMON/WCOM/EXPKFS,W(2,257)
      COMMON/YCOM/Y(1026)
      DIMENSION JFILE(1),ISEC(1)
      DIMENSION          Y2(2,512),Y2A(2,512)
      DIMENSION XLIST(12),PHASE(513),C(513)
      EQUIVALENCE (Y,Y2)
C
C      *** DATA INPUT MOD***
C
C
```

(Continued)

Table B3 (Continued)

```
C
      JF1=1
      IF(JX.EQ.JF) GO TO 819
      JX=1
      XNPTS=NPTS
      FNS=T/XNPTS
      NM=NPTS/2
      FT=7./3.
      FR=7./5.
      NMM=NM-2
      DELT=1.0/T
      DELW=(2.*3.14159265)/(XNPTS*DELT)
      FACT=DELW*0.39894228
      CALL INTABL(NPTS)
    2 IS=JFILE(JF1)
      DO 10 J=1,NPTS
      Y(J)=0.0
   10 CONTINUE
      CALL SETSCT(91,ISEC(IS))
      READ(91,20)(XLIST(J),J=1,12)
      PRINT 20,(XLIST(J),J=1,12)
      READ(91,25),(Y(J),J=1,NPTS)
      IF(NDBUG.EQ.1) PRINT 25,(Y(J),J=1,NPTS)
      IC=0
      CMAX=0.0
      CMIN=0.0
   14 CONTINUE
      YMAX1=Y(1)
      DO 3 J=1,NPTS
      YMAX1=AMAX1(YMAX1,Y(J))
    3 CONTINUE
C
C      ***SOLVING FOURIER COEF MOD***
C
C         THE FOLLOWING SHORT PRINTOUTS ARE FOR CHECKING.
C
      PRINT50
   50 FORMAT (19H    ORIGINAL SERIES)
      PRINT 200, (Y(I),I=1,3)
  200 FORMAT(1X,5F12.6)
      CALLRFFT(Y,NPTS,DELT,NDATA,DELW)
      DO 100 J=1,NM
      Y2A(1,J)=FACT*Y2(1,J)
  100 Y2A(2,J)=FACT*Y2(2,J)
      PRINT 150
  150 FORMAT(24H    FOURIER COEFFICIENTS)
      PRINT 200,((Y2A(I,J),I=1,2),J=1,3)
      CALLINRFFT(Y,NDATA,DELW,NDATA,DELT)
      PRINT250
  250 FORMAT(35H     RECONSTRUCTION ORIGINAL SERIES)
```

(Continued)

Table B3 (Continued)

```
      PRINT 200 ,(Y(I),I=1,3)
      C(NM+1)=Y2A(2,1)
      PHASE(NM+1)=0.0
      DO 120 J=2,NM
      C(J)=SQRT(Y2A(1,J)*Y2A(1,J)+Y2A(2,J)*Y2A(2,J))
      CMAX=AMAX1(CMAX,C(J))
      CMIN=AMIN1(CMIN,C(J))
      PHASE(J)=ATAN2(-Y2A(2,J),Y2A(1,J))
  120 CONTINUE
      AZ=Y2A(1,1)
      PRINT 23,CMAX,CMIN,NM,AZ
   23 FORMAT(5HCMAX=,F10.3,5HCMIN=,F10.3,13HNO. HARMONIC=,I7,3HAZ=,
     1F10.5)
C
C     ***END FOURIER COEF MOD***
C
C
C     ***SMOOTHING FOURIER COEF. MOD***
C
      NN=NM+1
  819 CONTINUE
      CALL JLAMP3(JF,JF1,PHASE,NN)
      CALL EBJLF1(NN,DELW,DELT,AZ,C,      Y2,FNS)
      CALL INRFFT(Y,NDATA,DELW,NDATA,DELT)
      WRITE(3,21)
      WRITE(3,25)(Y(J),J=1,NPTS)
C
C
C     FINDING YMAX
C
      YMAX=Y(1)
      YMIN=Y(1)
      DO 701 J=2,NPTS
      YMAX=AMAX1(YMAX,Y(J))
      YMIN=AMIN1(YMIN,Y(J))
  701 CONTINUE
      PRINT 31,YMAX1,CMAX,YMAX
      PRINT 91,YMIN
      ADATA=NDATA*DELT
      PRINT 32,NDATA,ADATA
C
C     FINDING NUMBER OF PREDICTED VALUES ABOVE A GIVEN TRIGGER LEVEL.
C
      CALL PEAK(Y,NPTS)
      IF(JF1.EQ.JF) RETURN
      JF1=JF1+1
      GO TO 2
   15 FORMAT(8F10.2)
   20 FORMAT(12A6)
   21 FORMAT("OUTPUT2")
```

(Continued)

```
   31 FORMAT(2X,6HYMAX1=,G15.5,2X,5HCMAX=,G15.5,2X,5HYMAX=,G15.5)
   91 FORMAT(15HPREDICTED YMIN=,G15.6)
   32 FORMAT(2X,14HNO. OF POINTS=,I5,5X,12HPERIOD SEC.=,G15.5)
   25 FORMAT(6F12.4)
      END
      SUBROUTINE JLAMP3(JF,JF1,PHASE,KE)
C     THE FUNCTION OF THIS PROGRAM IS TO READ THE H'S AND THETA'S
C     FROM A FILE OUTPUT BY PROGRAM EBHAN1.
C     H=AMPLITUDE.
C     PHI=PHASE.
      COMMON/HCOM/H(513)
      COMMON/PHICOM/PHI(513)
      COMMON/COND1/NDBUG,L,N,FRE,NE,HI,LOW,ITEST,IBAQ,IBAW
      DIMENSION PHASE(1)
      NDBUG=0
      IF(JF.GT.1.AND.JF1.EQ.1) GO TO 70
      IF(JF1.GT.1)GO TO 85
   60 CONTINUE
      H(1)=0.0
      DO 100 J=2,KE
      IF(J.EQ.2),PRINT 30,H(2),PHI(2)
   30 FORMAT(5HH(2)=,E15.5,8H PHI(2)=,E15.5)
      IF(J.GT.NE) GO TO 50
      PHI(J)=PHASE(J)+PHI(J)
C     H IS MULTY BY 1000 TO GIVE 10-3 CM/SEC OUTPUT.
      H(J)=H(J)*1000.0
      GO TO 100
   50 CONTINUE
      PHI(J)=0.0
      H(J)=0.0
  100 CONTINUE
      IF(NDBUG.EQ.1) PRINT80,NE,KE,(H(J1),PHI(J1),PHASE(J1),J1=1,KE)
   80 FORMAT(3HNE=,I7,4H KE=,I7,12H PHI,PHASE,/,(6E15.5))
      RETURN
   70 CALL SAVSCT(93,IH)
      WRITE(93,25)(H(J1),PHI(J1),J1=1,512)
   25 FORMAT(6E20.11)
      GO TO 60
   85 CALL SETSCT(93,IH)
      READ(93,25)(H(J1),PHI(J1),J1=1,512)
      GO TO 60
      END
      SUBROUTINE EBJLF1(NHM,DELW,DELT,AZ,C,      Y2,FNS)
      DIMENSION C(513),            Y2(2,1)
      COMMON/HCOM/H(513)
      COMMON/PHICOM/PHI(513)
C      AZ"AVG VALUE
      HH=H(1)
      AVSP1=0.5*AZ*AZ
      AVSP2=AVSP1*HH*HH
```

(Continued)

Table B3 (Continued)

```
      AD=AZ*HH
      FACC=1./(0.39094228*DELH)
      DO 100 K=2,NHM
      XK=K-1
      CH=C(K)*H(K)
      FREQ=FNS*XK
      IF(FREQ.GE.175.0) GO TO 30
      AVSP1=AVSP1+0.5*C(K)*C(K)
      AVTP1=AVSP1
      AVSP2=AVSP2+0.5*CH*CH
      AVTP2=AVSP2
      GO TO 40
30    AVTP1=AVTP1+0.5*C(K)*C(K)
      AVTP2=AVTP2+0.5*CH*CH
40    CONTINUE
      PT=PHI(K)
      FCH=FACC*CH
      Y2(1,K)=FCH*COS(PT)
      Y2(2,K)=-FCH*SIN(PT)
100   CONTINUE
      RMS1S=SQRT(AVSP1)
      RMS2S=SQRT(AVSP2)
      RMS1T=SQRT(AVTP1)
      RMS2T=SQRT(AVTP2)
      PRINT200
200   FORMAT(31X,"SEISMIC DATA",/,18X,"AVG POWER",14X,"RMS",/,
     +17X,"10-3 CM/SEC SQ",6X,"10-3 CM/SEC")
      PRINT 210,AVSP1,RMS1S
210   FORMAT("SEISMIC INPUT",6X,G10.5,9X,G10.5)
      PRINT 220,AVTP1,RMS1T
  220 FORMAT(12HTOTAL INPUT ,8X,G10.5,9X,G10.5)
      PRINT 230,AVSP2,RMS2S
  230 FORMAT(14HSEISMIC OUTPUT,5X,G10.5,9X,G10.5)
      PRINT 240, AVTP2,RMS2T
  240 FORMAT(12HTOTAL OUTPUT,7X,G10.5,9X,G10.5)
211   FORMAT(31X,12HSEISMIC DATA,/,18X,9HAVG POWER,14X,3HRMS,/,
     +17X,14H10-3 CM/SEC SQ,6X,11H10-3 CM/SEC)
201   FORMAT(13HSEISMIC INPUT,6X,G10.5,9X,G10.5)
221   FORMAT(11HTOTAL INPUT,8X,G10.5,9X,G10.5)
231   FORMAT(14HSEISMIC OUTPUT,5X,G10.5,9X,G10.5)
241   FORMAT(12HTOTAL OUTPUT,7X,G10.5,9X,G10.5)
      Y2(1,1)=AD*FACC
      Y2(2,1)=FACC*CH
      RETURN
      END
C     PROGRAM NAME:  SUBROUTINE PEAK.
C     PROGRAM VARABLES:
C     TRIGH=SEISMIC TRIGGER LEVEL.
C
      SUBROUTINE PEAK(Y,NPTS)
```

(Continued)

```
      DIMENSION Y(1)
      TRIGH=0.0381
      TRIGM=TRIGH*2.5
      TRIGL=TRIGM*2.5
      NLOW=0
      NMED=0
      NHIGH=0
      DO 500 J=1,NPTS
      IF(Y(J)-TRIGH)500,100,100
100   NHIGH=NHIGH+1
      IF(Y(J)-TRIGM)500,200,200
200   NMED=NMED+1
      IF(Y(J)-TRIGL)500,300,300
300   NLOW=NLOW+1
500   CONTINUE
      PRINT 505,TRIGH,NHIGH
505   FORMAT(2X,7HTRIGH =,G10.5,2X,7HNHIGH =,I5)
      PRINT 506,TRIGM,NMED
506   FORMAT(2X,7HTRIGM =,G10.5,2X6HNMED =,I5)
      PRINT 507,TRIGL,NLOW
507   FORMAT(2X,7HTRIGL =,G10.5,2X,6HNLOW =,I5)
      RETURN
      END
      SUBROUTINE NDELTA(III)
C     THIS ROUTINE FORMULATES THE DETERMINANT DELTA
      DIMENSION AH(5) ,RDET(4,4),AIDET(4,4),RDET41(3,3),RDET42(3,3),
     1          RDET43(3,3),RDET44(3,3),AIDE41(3,3),AIDE42(3,3),
     2          AIDE43(3,3),AIDE44(3,3)
      COMPLEX F(2,4),C(2,4),VDELT(4,4),DEL41,DEL42,DEL43,DEL44,
     1          DELP,DELM
      COMMON/CONT/NL,NR,NC,AH
      COMMON/CON2/DEJ,DEK,NNN
      COMMON/DELT/DEL41,DEL42,DEL43,DEL44,DELP,DELM
      COMMON/MATF/F
      COMMON/MATC/C
      III=1
      DO 10 I =1,2
      DO 10 J =1,NC
      VDELT(I,J) = F(I,J)
   10 CONTINUE
      DO 20 I = 1,2
      DO 20 J = 1,NC
      VDELT(I+2,J)= C(I,J)
   20 CONTINUE
      DO 30 I = 1,NR
      DO 30 J = 1,NC
      RDET (I,J) = REAL(VDELT(I,J))
      AIDET(I,J) = AIMAG(VDELT(I,J))
   30 CONTINUE
      IF(NNN-2)140,150,160
```

(Continued)

Table B3 (Continued)

```
  140 NNRR=NR-1
      DO40 I=1,NNRR
      DO50 J=2,NC
      RDET41(I,J-1)=REAL(VDELT(I,J))
   50 AIDE41(I,J-1)=AIMAG(VDELT(I,J))
      RDET42(I,1)=REAL(VDELT(I,1))
      AIDE42(I,1)=AIMAG(VDELT(I,1))
      DO 60 J=3,NC
      RDET42(I,J-1)=REAL(VDELT(I,J))
   60 AIDE42(I,J-1)=AIMAG(VDELT(I,J))
      RDET43(I,3)=REAL(VDELT(I,4))
      AIDE43(I,3)=AIMAG(VDELT(I,4))
      DO 70 J=1,2
      RDET43(I,J)=REAL(VDELT(I,J))
   70 AIDE43(I,J)=AIMAG(VDELT(I,J))
      DO 80 J=1,NNRR
      RDET44(I,J)=REAL(VDELT(I,J))
   80 AIDE44(I,J)=AIMAG(VDELT(I,J))
   40 CONTINUE
      CALL DETER(III,NNRR,RDET41,AIDE41,DEL41)
      CALL DETER(III,NNRR,RDET42,AIDE42,DEL42)
      CALL DETER(III,NNRR,RDET43,AIDE43,DEL43)
      CALL DETER(III,NNRR,RDET44,AIDE44,DEL44)
      RETURN
  150 CALL DETER(III,NC,RDET,AIDET,DELP)
      RETURN
  160 CALL DETER(III,NC,RDET,AIDET,DELM)
      RETURN
      END
      SUBROUTINE INTABL(NPTS)
      COMMON/WCOM/EXPKFS,W(2,257)
      W(1,1)=1.0
      W(2,1)=0.0
      W(1,2)=0.0
      W(2,2)=1.0
      TR=0.
      TI=1.0
      LMAX=1
      NP=NPTS/4
      DO5 J=1,12
      KE=2**J
      IF(NP.EQ.KE) GO TO 7
    5 CONTINUE
    7 DO10 K=2,J
      TR=SQRT(.5*(TR+1))
      TI=.5*TI/TR
C     THE EFFCT OF THE PRECEDING  TWO STATEMENTS IS TO TAKE THE SQUARE ROOT
C     OF THE COMPLEX NUMBER TR+I*TI, ASSUMING TR**2+TI**I=1.0
      LMAX=LMAX+LMAX
      DO10L1=1,LMAX
```

(Continued)

Table B3 (Continued)

```
      L2=L1+LMAX
      W(1,L2)=W(1,L1)*TR-W(2,L1)*TI
      W(2,L2)=W(1,L1)*TI+W(2,L1)*TR
10    CONTINUE
      TR=SQRT(.5*(TR+1))
      W(1,NP+1)=TR
      W(2,NP+1)=.5*TI/TR
      RETURN
      END
      SUBROUTINEINRFFT(A,NPTS,DELW,NDAT,DELT)
      DIMENSIONA(2,1)
      COMMON/WCOM/EXPKFS,W(2,257)
      CALLFINDNO(NPTS,NDATA,MBITS,MBM1,NDM1)
      NDAT=NDATA
      NPTH=NDATA/2
      IF(NDATA.LT.NPTS)A(2,1)=A(1,NPTH+1)
      NPTQ=NPTH/2
      DO10K=2,NPTQ
      NPK=NPTH-K
      TEMP1R=A(1,K)+A(1,NPK+2)
      TEMP1I=A(2,K)-A(2,NPK+2)
      TEMP2R=A(2,K)+A(2,NPK+2)
      TEMP2I=A(1,NPK+2)-A(1,K)
      A(1,K)=TEMP1R
      A(2,K)=TEMP1I
      A(1,NPK+2)=TEMP2R
      A(2,NPK+2)=TEMP2I
10    CONTINUE
      WSTORR=W(1,NPTQ+1)
      WSTORI=W(2,NPTQ+1)
      DO20K=1,NPTQ,2
      CALLSWTCH1(K,KS,MBM1,KSWTCH)
      WR=W(1,K)
      WI=W(2,K)
      TEMP1R=A(1,KS+1)*WR-A(2,KS+1)*WI
      TEMP1I=A(2,KS+1)*WR+A(1,KS+1)*WI
      TEMP2R=A(1,KS+2)*WR-A(2,KS+2)*WI
      TEMP2I=A(2,KS+2)*WR+A(1,KS+2)*WI
      A(1,KS+2)=TEMP2R*WSTORR-TEMP2I*WSTORI
      A(2,KS+2)=TEMP2I*WSTORR+TEMP2R*WSTORI
      A(1,KS+1)=TEMP1R
      A(2,KS+1)=TEMP1I
20    CONTINUE
      DO30K=2,NPTQ
      NPK=NPTH-K
      TEMP1R=A(1,K)-A(2,NPK+2)
      TEMP1I=A(2,K)+A(1,NPK+2)
      TEMP2R=A(2,NPK+2)+A(1,K)
      TEMP2I=A(1,NPK+2)-A(2,K)
      A(1,K)=TEMP1R
```

(Continued)

Table B3 (Continued)

```
      A(2,K)=TEMP1I
      A(1,NPK+2)=TEMP2R
      A(2,NPK+2)=TEMP2I
30    CONTINUE
      TEMP1R=A(1,1)+A(2,1)
      TEMP1I=A(1,1)-A(2,1)
      A(1,1)=TEMP1R*2.
      A(2,1)=TEMP1I*2.
      A(1,NPTQ+1)=2.*A(1,NPTQ+1)
      A(2,NPTQ+1)=2.*A(2,NPTQ+1)
      DW=0.5*DELW
      CALLINVFFT(A,NPTH,DW,NPTH,DT)
      DELT=0.25*DT
      RETURN
      END
      SUBROUTINEFINDNO(NPTS,NDATA,MBITS,MBM1,NDM1)
      DIMENSIONITWO(15)
      DATA(ITWO(K),K=1,15)/1,2,4,8,16,32,64,128,256,512,1024,2048,4096
     *,8192,16384/
      DO10K=1,15
      IF(ITWO(K).GT.NPTS)GOTO15
10    CONTINUE
      K=16
15    NDATA=ITWO(K-1)
      MBITS=K-2
      NDM1=NDATA-1
      MBM1=MBITS-1
      RETURN
      END
      SUBROUTINEINVFFT(A,NPTS,DELW,NDATA,DELT)
      DIMENSIONA(2,1)
      DO100K=1,NPTS
      A(2,K)=-A(2,K)
100   CONTINUE
      CALLFFT(A,NPTS,DELW,NDATA,DELT)
      DO200K=1,NPTS
      A(2,K)=-A(2,K)
200   CONTINUE
      RETURN
      END
      SUBROUTINESWTCH1(J,JI,NBITS,KSWTCH)
      DIMENSIONITWO(13)
      DATA(ITWO(K),K=1,13)/4096,2048,1024,512,256,128,64,32,16,8,4,2,1/
      IK=J
      JI=0
      LBITS=14-NBITS
      DO10K=LBITS,13
      IF(IK.LT.ITWO(K))GOTO10
      L=13-K+LBITS
      JI=JI+ITWO(L)
```

(Continued)

```
      IK=JK-ITWO(K)
10    CONTINUE
      KSWTCH=0
      IF(J.GT.JI)KSWTCH=1
      RETURN
      END
      SUBROUTINEFFT(A,NPTS,DELT,NDATA,DELW)
      DIMENSIONA(1)
      COMPLEX A,W,TEMP,WSTOR
      COMMON/WCOM/EXPKFS,W(2,257)
      DATATWOPI/6.28318531/,DRT2PI/0.3989422804/
      CALLFINDNO(NPTS,I2TOM,MBITS,MBM1,NDM1)
      NDATA=I2TOM
      DELW=TWOPI/(I2TOM*DELT)
      FACT=DRT2PI*DELT
      DO216M=1,MBITS
      JJ=I2TOM
      I2TOM=I2TOM/2
      IONES=I2TOM-1
      J=0
      DO216JK=1,NDATA,JJ
      J=J+1
      JKSTOP=JK+IONES
      WSTOR=W(J)
      DO216JK1=JK,JKSTOP
      JK2=JK1+I2TOM
      TEMP=A(JK2)*WSTOR
      A(JK2)=A(JK1)-TEMP
      A(JK1)=A(JK1)+TEMP
216   CONTINUE
      NDM2=NDM1+1
      DO225JII=1,NDM2
      JI=JII-1
      CALLSWTCH1(JI,J,MBITS,KSWTCH)
      IF(KSWTCH)225,220,225
220   TEMP=A(JI+1)
      A(JI+1)=FACT*A(J+1)
      A(J+1)=FACT*TEMP
225   CONTINUE
      RETURN
      END
      SUBROUTINERFFT(A,NPTS,DELT,NDATA,DELW)
      DIMENSIONA(2,1)
      COMMON/WCOM/EXPKFS,W(2,257)
      CALLFINDNO(NPTS,NDAT,MBITS,MBM1,NDM1)
      NDATA=NDAT
      NPTH=NDAT/2
      NPTQ=NPTH/2
      CALLFFT(A,NPTH,DELT,NPTH,DW)
      DELW=0.5*DW
```

(Continued)

```
      DO10K=2,NPTQ
      NPK=NPTH-K
      TEMP1R=A(1,K)+A(1,NPK+2)
      TEMP1I=A(2,K)-A(2,NPK+2)
      TEMP2R=A(2,K)+A(2,NPK+2)
      TEMP2I=A(1,NPK+2)-A(1,K)
      A(1,K)=TEMP1R
      A(2,K)=TEMP1I
      A(1,NPK+2)=TEMP2R
      A(2,NPK+2)=TEMP2I
10    CONTINUE
      A(1,NPTQ+1)=2.*A(1,NPTQ+1)
      A(2,NPTQ+1)=2.*A(2,NPTQ+1)
      TEMP1R=A(1,1)+A(2,1)
      TEMP1I=A(1,1)-A(2,1)
      A(1,1)=TEMP1R
      A(2,1)=TEMP1I
      WSTORR=W(1,NPTQ+1)
      WSTORI=W(2,NPTQ+1)
      DO30K=1,NPTQ,2
      CALLSWTCH1(K,KS,MBM1,KSWTCH)
      WR=W(1,K)
      WI=W(2,K)
      TEMP1R=A(1,KS+1)*WR+A(2,KS+1)*WI
      TEMP1I=A(2,KS+1)*WR-A(1,KS+1)*WI
      TEMP2R=A(1,KS+2)*WR+A(2,KS+2)*WI
      TEMP2I=A(2,KS+2)*WR-A(1,KS+2)*WI
      A(1,KS+2)=TEMP2R*WSTORR+TEMP2I*WSTORI
      A(2,KS+2)=TEMP2I*WSTORR-TEMP2R*WSTORI
      A(1,KS+1)=TEMP1R
      A(2,KS+1)=TEMP1I
30    CONTINUE
      DO40K=2,NPTQ
      NPK=NPTH-K
      TEMP1R=A(1,K)-A(2,NPK+2)
      TEMP2R=A(1,K)+A(2,NPK+2)
      TEMP1I=A(2,K)+A(1,NPK+2)
      TEMP2I=A(1,NPK+2)-A(2,K)
      A(1,K)=TEMP1R
      A(2,K)=TEMP1I
      A(1,NPK+2)=TEMP2R
      A(2,NPK+2)=TEMP2I
40    CONTINUE
      RETURN
      END
      SUBROUTINE MATRAA
C     THIS ROUTINE FORMULATE THE MATRIX A
      DIMENSION AH(5)
      COMPLEX ANU(5),ANUP(5),AMU(5),AA(5),A(5,4,4),CI,AK
      COMMON/CONT/NL,NR,NC,AH
```

(Continued)

Table B3 (Continued)

```
      COMMON/MATA/A
      COMMON/ELEM/ANU,ANUP,AMU,AA,AK
      CI = (0.0,1.0)
      DO 10 I =1,NL
      A(I,1,1) =(1.0,0.0)
      A(I,1,2) =(1.0,0.0)
      A(I,1,3) =-ANUP(I)
      A(I,2,1) =-ANU(I)
      A(I,1,4) = ANUP(I)
      A(I,2,2) = ANU(I)
      A(I,2,3) = AK*AK
      A(I,2,4) = A(I,2,3)
      A(I,3,1) =-2.0*AMU(I)*ANU(I)
      A(I,3,2) =-A(I,3,1)
      A(I,3,3) = AMU(I)*(ANUP(I)*ANUP(I)* A(I,2,3))
      A(I,3,4) = A(I,3,3)
      A(I,4,1) = AA(I)
      A(I,4,2) = AA(I)
      A(I,4,3) =-2.0*AMU(I)*A(I,2,3)*ANUP(I)
      A(I,4,4) =-A(I,4,3)
   10 CONTINUE
      RETURN
      END
      SUBROUTINE MATRBB
C     THIS ROUTINE FORMULATES THE MATRIX B
      DIMENSION AH(5)
      COMPLEX ANU(5),ANUP(5),AMU(5),AA(5),B(2,4),CI,AK
      COMMON/CONT/NL,NR,NC,AH
      COMMON/MATB/B
      COMMON/ELEM/ANU,ANUP,AMU,AA,AK
      CI =(0.0,1.0)
      B(1,1) =(1.0,0.0)
      B(1,2) =(1.0,0.0)
      B(1,3) =-ANUP(NL)
      B(1,4) = ANUP(NL)
      B(2,1) =-ANU(NL)
      B(2,2) = ANU(NL)
      B(2,3) = AK*AK
      B(2,4) = B(2,3)
      RETURN
      END
      SUBROUTINE MATRCC
C     THIS ROUTINE FORMULATES THE MATRIX C
      DIMENSION AH(5)
      COMPLEX ANU(5),ANUP(5),AMU(5),AA(5),C(2,4),CI,AK
      COMMON/CONT/NL,NR,NC,AH
      COMMON/MATC/ C
      COMMON/ELEM/ANU,ANUP,AMU,AA,AK
      CI = (0.0,1.0)
      C(1,1) =-2.0*AMU(1)*ANU(1)
```

(Continued)

Table B3 (Continued)

```
      C(1,2) =-C(1,1)
      C(1,3) = AMU(1)*(ANUP(1)*ANUP(1)+AK*AK)
      C(1,4) = C(1,3)
      C(2,1) = AA(1)
      C(2,2) = AA(1)
      C(2,3) = -2.0*AMU(1)*ANUP(1)*AK*AK
      C(2,4) =-C(2,3)
      RETURN
      END
      SUBROUTINE MATRDD
C     THIS ROUTINE FORMULATES THE MATRIX D
      DIMENSION AH(5)
      COMPLEX ANU(5),ANUP(5),AMU(5),AA(5),D(5,4,4),CI,AK
      COMMON/CONT/NL,NR,NC,AH
      COMMON/MATD/ D
      COMMON/ELEM/ANU,ANUP,AMU,AA,AK
      CI =(0.0,1.0)
      DO 10 I = 1,NL
      D(I,1,1) = CEXP(-ANU(I)*(AH(I+1)-AH(I)))
      D(I,1,2) =(0.0,0.0)
      D(I,1,3) =(0.0,0.0)
      D(I,1,4) =(0.0,0.0)
      D(I,2,1) =(0.0,0.0)
      D(I,2,2) = 1.0/D(I,1,1)
      D(I,2,3) =(0.0,0.0)
      D(I,2,4) =(0.0,0.0)
      D(I,3,1) =(0.0,0.0)
      D(I,3,2) =(0.0,0.0)
      D(I,3,3) = CEXP(-ANUP(I)*(AH(I+1)-AH(I)))
      D(I,3,4) =(0.0,0.0)
      D(I,4,1) =(0.0,0.0)
      D(I,4,2) =(0.0,0.0)
      D(I,4,3) =(0.0,0.0)
      D(I,4,4) = 1.0/D(I,3,3)
   10 CONTINUE
      RETURN
      END
      SUBROUTINE MULAAD
C     THIS ROUTINE PERFORMS AA**-1*D OPERATION
      DIMENSION AH(5)
      COMPLEX A(5,4,4),AIA(5,4,4),E(5,4,4),D(5,4,4)
      COMMON/MATA/A
      COMMON/MATINA/AIA
      COMMON/MULT/ E
      COMMON/CONT/NL,NR,NC,AH
      COMMON/MATD/D
      IF(NL.EQ.1) RETURN
      NNL = NL - 1
      DO 10 NK = 1,NNL
      DO 20    I = 1,NR
```

(Continued)

Table B3 (Continued)

```
      DO 20   J = 1,NC
      E(NK,I,J) =(0.0,0.0)
      DO 30  IJ = 1,NR
   30 E(NK,I,J) = E(NK,I,J)+ AIA(NK+1,I,IJ)*A(NK,IJ,J)*D(NK,J,J)
   20 CONTINUE
   10 CONTINUE
      RETURN
      END
      SUBROUTINE DELEL
C     THIS SUBROUTINE COMPUTES THE MATRIX BN*DN*G
      DIMENSION AH(5)
      COMPLEX B(2,4),D(5,4,4),E(5,4,4),F(2,4),FF(2,4)
      COMMON/CONT/NL,NR,NC,AH
      COMMON/MATB/B
      COMMON/MATD/D
      COMMON/MULT/E
      COMMON/MATF/F
      NNL = NL - 1
      IF(NL.NE.1) GO TO 50
      DO 55 I=1,2
      DO 55 J=1,4
      F(I,J)=B(I,J)*D(1,J,J)
   55 CONTINUE
      RETURN
   50 CONTINUE
      DO 10 NK = 1,NNL
      KN = NL-NK
   70 DO 20 I = 1,2
      DO 20 J = 1,NC
      IF(NK.GT.1) GO TO 40
      F(I,J)=(0.0,0.0)
      DO30 IJ= 1,NR
   30 F(I,J)=F(I,J)+B(I,IJ)*D(NL,IJ,IJ)*E(KN,IJ,J)
      GO TO 20
   40 FF(I,J) =(0.0,0.0)
      DO 60 IJ= 1,NC
      F(I,J)  = FF(I,J) + F(I,IJ)*E(KN,IJ,J)
   60 FF(I,J) = F(I,J)
   20 CONTINUE
   10 CONTINUE
      RETURN
      END
      SUBROUTINE DETER(III,NC,RDET,AIDET,DEL)
      DIMENSION RDET(NC,1),AIDET(NC,1)
      COMPLEX DEL(1), CI
      CI = (0.0,1.0)
      D1 = 1.0
      D2 = 0.0
      I1 = 1.0
  170 I3 = I1
```

(Continued)

Table B3 (Continued)

```
      S  = ABS(RDET(I1,I1)) + ABS(AIDET(I1,I1))
      DO 100 I = I1,NC
      T  = ABS(RDET(I,I1)) + ABS(AIDET(I,I1))
      IF(S.GE.T) GO TO 100
      I3 = I
      S  = T
  100 CONTINUE
      IF(I3.EQ.I1) GO TO 110
      DO 120 J = 1,NC
      S =-RDET(I1,J)
      RDET(I1,J) = RDET(I3,J)
      RDET(I3,J) = S
      S1 = - AIDET(I1,J)
      AIDET(I1,J) = AIDET(I3,J)
      AIDET(I3,J) = S1
  120 CONTINUE
  110 I3 = I1 + 1
      DO 130 I =I3,NC
      S1 = RDET(I1,I1)*RDET(I1,I1) + AIDET(I1,I1)*AIDET(I1,I1)
      S = (RDET(I,I1)*RDET(I1,I1) + AIDET(I,I1)*AIDET(I1,I1))/S1
      AIDET(I,I1) =(RDET(I1,I1)*AIDET(I,I1)-RDET(I,I1)*AIDET(I1,I1))/S1
      RDET(I,I1) = S
  130 CONTINUE
      J2 = I1 - 1
      IF(J2.EQ.0) GO TO 140
      DO 150 J = I3,NC
      DO 150 I = 1 ,J2
      RDET(I1,J)=RDET(I1,J)-RDET(I1,I)*RDET(I,J)+AIDET(I1,I)*AIDET(I,J)
      AIDET(I1,J)=AIDET(I1,J)-AIDET(I1,I)*RDET(I,J)-RDET(I1,I)*AIDET(I,J
     1)
  150 CONTINUE
  140 J2 = I1
      I1 = I1+1
      DO 160 I = I1,NC
      DO 160 J = 1,J2
      RDET(I,I1)=RDET(I,I1)-RDET(I,J)*RDET(J,I1)+AIDET(I,J)*AIDET(J,I1)
      AIDET(I,I1)=AIDET(I,I1)-AIDET(I,J)*RDET(J,I1)-RDET(I,J)*AIDET(J,I1
     1)
  160 CONTINUE
      IF(I1.NE.NC) GO TO 170
      I3 = 1
      J2 = NC/2
      IF(NC.EQ.2*J2) GO TO 180
      I3 = 0
      D1 = RDET(NC,NC)
      D2 = AIDET(NC,NC)
  180 DO 190 I =1,J2
      J = NC - I + I3
      S = RDET(I,I)*RDET(J,J)- AIDET(I,I)*AIDET(J,J)
      S1= RDET(I,I)*AIDET(J,J)+RDET(J,J)*AIDET(I,I)
```

(Continued)

Table B3 (Continued)

```
      T = D1*S - D2*S1
      D2= D2*S + D1*S1
      D1= T
  190 CONTINUE
      DEL(III) = D1 +D2*CI
      RETURN
      END
      SUBROUTINE IVERAA
C     THIS ROUTINE FIND THE INVERSE OF MATRIX A
      DIMENSION AH(5) ,ID(8)
      COMPLEX A(5,4,4),AIA(5,4,4),AMA(5,4,8),CC,W
      COMMON/CONT/NL,NR,NC,AH
      COMMON/MATA/A
      COMMON/MATINA/AIA
      COMMON /COMAMA/AMA
      DO 10 NK= 1,NL
      DO 20 I = 1,NR
      DO 20 J = 1,NC
   20 AMA(NK,I,J) = A(NK,I,J)
      NN = NR+1
      N2 = 2*NR
      K  = 1
      DO 30 I = 1,NC
      DO 30 J =NN,N2
      AMA(NK,I,J) =(0,0,0,0)
   30 CONTINUE
      DO 35 I = 1,NC
      N3 = I+NC
       AMA(NK,I,N3)=(1,0,0,0)
   35 ID(I) = I
   40 CONTINUE
      KK = K + 1
      IS = K
      IT = K
      B  =CABS(AMA(NK,K,K))
      DO 50 I = K,NR
      DO 50 J = K,NC
      IF(CABS(AMA(NK,I,J))-B)50,50,60
   60 IS = I
      IT = J
      B  =CABS(AMA(NK,I,J))
   50 CONTINUE
      IF(IS-K) 70,70,80
   80 DO 90  J=K,N2
      CC= AMA(NK,IS,J)
      AMA(NK,IS,J) = AMA(NK,K,J)
   90 AMA(NK,K,J ) = CC
   70 CONTINUE
      IF(IT-K) 100,100,110
  110 IC = ID(K)
```

(Continued)

Table B3 (Continued)

```
      ID(K)=ID(IT)
      ID(IT)=IC
      DO 120  I=1,NR
      CC=AMA(NK,I,IT)
      AMA(NK,I,IT) = AMA(NK,I,K)
  120 AMA(NK,I,K ) = CC
  100 CONTINUE
      IF(CABS(AMA(NK,K,K)).EQ.(0.0     )) GO TO 300
  130 CONTINUE
      DO 140 J = KK,N2
      AMA(NK,K,J) = AMA(NK,K,J)/AMA(NK,K,K)
      DO 140 I = KK,NR
      W=AMA(NK,I,K)*AMA(NK,K,J)
      AMA(NK,I,J) = AMA(NK,I,J)-W
      IF(CABS(AMA(NK,I,J))-0.0001*CABS(W))150,140,140
  150 AMA(NK,I,J) =0.0
  140 CONTINUE
      K = KK
      IF(K-NR) 40,160,300
  160 IF(CABS(AMA(NK,NR,NR)).EQ.0.0) GO TO 300
      DO 170  J=NN,N2
      AMA(NK,NR,J) = AMA(NK,NR,J)/AMA(NK,NR,NR)
  170 CONTINUE
      N1 = NR - 1
      DO 180  M = 1,N1
      I = NR - M
      II= I +1
      DO 180 K =II,NR
      DO 180 J =NN,N2
  180 AMA(NK,I,J) = AMA(NK,I,J)-AMA(NK,I,K)*AMA(NK,K,J)
      DO 190 I=1,NR
      DO 190 J= 1,NC
      IF(ID(J)-I)190,195,190
  195 DO 196 K=NN,N2
      JJ=K-NR
  196 AIA(NK,I,JJ) = AMA(NK,J,K)
  190 CONTINUE
      GO TO 10
  300 PRINT 250
  250 FORMAT(20X,18HMATRIX IS SINGULAR)
   10 CONTINUE
      RETURN
      END
C
C     SUBROUTINE BESY
C
C     PURPOSE
C     COMPUTE THE Y BESSEL FUNCTION FOR A GIVEN ARGUMENT AND ORDER
C
C     USAGE
```

(Continued)

Table B3 (Continued)

```
C     CALL BESY(X,N,BY,IER)
C
C     DESCRIPTION OF PARAMETERS
C     X  -THE ARGUMENT OF THE Y BESSEL FUNCTION DESIRED
C     N  -THE ORDER OF THE Y BESSEL FUNCTION DESIRED
C     BY -THE RESULTANT Y BESSEL FUNCTION
C     IER-RESULTANT ERROR CODE WHERE
C     IER=0  NO ERROR
C     IER=1  N IS NEGATIVE
C     IER=2  X IS NEGATIVE OR ZERO
C
C     REMARKS
C     VERY SMALL VALUES OF X MAY CAUSE THE RANGE OF THE LIBRARY
C     FUNCTION ALOG TO BE EXCEEDED
C     X MUST BE GREATER THAN ZERO
C     N MUST BE GREATER THAN OR EQUAL TO ZERO
C
C     SUBROUTINES AND FUNCTION SUBPROGRAMS REQUIRED
C     NONE
C
C     METHOD
C     RECURRENCE RELATION AND POLYNOMIAL APPROXIMATION TECHNIQUE
C     AS DESCRIBED BY A.J.M.HITCHCOCK,?POLYNOMIAL APPROXIMATIONS
C     TO BESSEL FUNCTIONS OF ORDER ZERO AND ONE AND TO RELATED
C     FUNCTIONS?, M.T.A.C., V.11,1957,PP.86-88, AND G.N. WATSON,
C     ?A TREATISE ON THE THEORY OF BESSEL FUNCTIONS?, CAMBRIDGE
C     UNIVERSITY PRESS, 1958, P. 62
C
C     ..................................................................
C
      SUBROUTINEBESY(X,N,BY,IER)
C
C     CHECK FOR ERRORS IN N AND X
C
      IF(N)180,10,10
10    IER=0
      IF(X)190,190,20
20    PI=3.141592653
C
C     BRANCH IF X LESS THAN OR EQUAL 4
C
      IF(X-4.)40,40,30
C
C     COMPUTE Y0 AND Y1 FOR X GREATER THAN 4
C
30    T=4./X
      P0=.3989422793
      Q0=-.0124669441
      P1=.3989422819
      Q1=.0374008364
```

(Continued)

```
      A=T*T
      B=A
      P0=P0-.0017530620*A
      Q0=Q0+.0004564324*A
      P1=P1+.0029218256*A
      Q1=Q1-.00063904*A
      A=A*A
      P0=P0+.00017343*A
      Q0=Q0-.0000069791*A
      P1=P1-.000223203*A
      Q1=Q1+.0001064741*A
      A=A*B
      P0=P0-.0000487613*A
      Q0=Q0+.0000342468*A
      P1=P1+.0000580759*A
      Q1=Q1-.0000398708*A
      A=A*B
      P0=P0+.0000173565*A
      Q0=Q0-.0000142078*A
      P1=P1-.000020092*A
      Q1=Q1+.00001622*A
      A=A*B
      P0=P0-.0000037043*A
      Q0=Q0+.0000032312*A
      P1=P1+.0000042414*A
      Q1=Q1-.00000036594*A
      A=SQRT(2.*PI)
      B=4.*A
      P0=A*P0
      Q0=B*Q0/X
      P1=A*P1
      Q1=B*Q1/X
      A=X-PI/4.
      B=SQRT(2./(PI*X))
      Y0=B*(P0*SIN(A)+Q0*COS(A))
      Y1=B*(-P1*COS(A)+Q1*SIN(A))
      GOTO90
C
C     COMPUTE Y0 AND Y1 FOR X LESS THAN OR EQUAL TO 4
C
40    XX=X/2.
      X2=XX*XX
      T=ALOG(XX)+.5772156649
      SUM=0.
      TERM=T
      Y0=T
      DO70L=1,15
      IF(L-1)50,60,50
50    SUM=SUM+1./FLOAT(L-1)
60    FL=L
```

(Continued)

Table B3 (Continued)

```
      TS=T-SUM
      TERM=(TERM*(-X2)/FL**2)*(1.-1./(FL*TS))
70    Y0=Y0+TERM
      TERM=XX*(T-.5)
      SUM=0.
      Y1=TERM
      DO80L=2,16
      SUM=SUM+1./FLOAT(L-1)
      FL=L
      FL1=FL-1.
      TS=T-SUM
      TERM=(TERM*(-X2)/(FL1*FL))*((TS-.5/FL)/(TS+.5/FL1))
80    Y1=Y1+TERM
      PI2=2./PI
      Y0=PI2*Y0
      Y1=-PI2/X+PI2*Y1
C
C     CHECK IF ONLY Y0 OR Y1 IS DESIRED
C
90    IF(N-1)100,100,130
C
C     RETURN EITHER Y0 OR Y1 AS REQUIRED
C
100   IF(N)110,120,110
110   BY=Y1
      GOTO170
120   BY=Y0
      GOTO170
C
C     PERFORM RECURRENCE OPERATIONS TO FIND YN(X)
C
130   YA=Y0
      YB=Y1
      K=1
140   T=FLOAT(2*K)/X
      YC=T*YB-YA
      K=K+1
      IF(K-N)150,160,150
150   YA=YB
      YB=YC
      GOTO140
160   BY=YC
170   RETURN
180   IER=1
      RETURN
190   IER=2
      RETURN
      END
C
C     SUBROUTINE BESJ
```

(Continued)

Table B3 (Continued)

```
C
C       PURPOSE
C       COMPUTE THE J BESSEL FUNCTION FOR A GIVEN ARGUMENT AND ORDER
C
C       USAGE
C       CALL BESJ(X,N,BJ,D,IER)
C
C       DESCRIPTION OF PARAMETERS
C       X  -THE ARGUMENT OF THE J BESSEL FUNCTION DESIRED
C       N  -THE ORDER OF THE J BESSEL FUNCTION DESIRED
C       BJ -THE RESULTANT J BESSEL FUNCTION
C       D  -REQUIRED ACCURACY
C       IER-RESULTANT ERROR CODE WHERE
C       IER=0  NO ERROR
C       IER=1  N IS NEGATIVE
C       IER=2  X IS NEGATIVE OR ZERO
C       IER=3  REQUIRED ACCURACY NOT OBTAINED
C       IER=4  RANGE OF N COMPARED TO X NOT CORRECT (SEE REMARKS)
C
C       REMARKS
C       N MUST BE GREATER THAN OR EQUAL TO ZERO, BUT IT MUST BE
C       LESS THAN
C       20+10*X-X** 2/3   FOR X LESS THAN OR EQUAL TO 15
C       90+X/2            FOR X GREATER THAN 15
C
C       SUBROUTINES AND FUNCTION SUBPROGRAMS REQUIRED
C       NONE
C
C       METHOD
C       RECURRENCE RELATION TECHNIQUE DESCRIBED BY H. GOLDSTEIN AND
C       R.M. THALER,?RECURRENCE TECHNIQUES FOR THE CALCULATION OF
C       BESSEL FUNCTIONS?,M,T.A.C.,V.13,PP.102-108 AND I.A. STEGUN
C       AND M. ABRAMOWITZ,?GENERATION OF BESSEL FUNCTIONS ON HIGH
C       SPEED COMPUTERS?,M.T.A.C.,V.11,1957,PP.255-257
C
C       .....
C
      SUBROUTINEBESJ(X,N,BJ,D,IER)
C
      BJ=.0
      IF(N)10,20,20
10    IER=1
      RETURN
20    IF(X)30,30,31
30    IER=2
      RETURN
31    IF(X-15.)32,32,34
32    NTEST=20.+10.*X-X**2/3
      GOTO36
34    NTEST=90.+X/2.
```

(Continued)

```
36      IF(N-NTEST)40,38,38
38      IER=4
        RETURN
40      IER=0
        N1=N+1
        BPREV=.0
C
C       COMPUTE STARTING VALUE OF M
C
        IF(X-5.)50,60,60
50      MA=X+6.
        GOTO70
60      MA=1.4*X+60./X
70      MB=N+IFIX(X)/4+2
        MZERO=MAX0(MA,MB)
C
C       SET UPPER LIMIT OF M
C
        MMAX=NTEST
100     DO190M=MZERO,MMAX,3
C
C       SET F(M),F(M-1)
C
        FM1=1.0E-28
        FM=.0
        ALPHA=.0
        IF(M-(M/2)*2)120,110,120
110     JT=-1
        GOTO130
120     JT=1
130     M2=M-2
        DO160K=1,M2
        MK=M-K
        BMK=2.*FLOAT(MK)*FM1/X-FM
        FM=FM1
        FM1=BMK
        IF(MK-N-1)150,140,150
140     BJ=BMK
150     JT=-JT
        S=1+JT
160     ALPHA=ALPHA+BMK*S
        BMK=2.*FM1/X-FM
        IF(N)180,170,180
170     BJ=BMK
180     ALPHA=ALPHA+BMK
        BJ=BJ/ALPHA
        IF(ABS(BJ-BPREV)-ABS(D*BJ))200,200,190
190     BPREV=BJ
        IER=3
200     RETURN
```

(Continued)

```
      END
C
C     SUBROUTINE BESI
C
C     PURPOSE
C     COMPUTE THE I BESSEL FUNCTION FOR A GIVEN ARGUMENT AND ORDER
C
C     USAGE
C     CALL BESI(X,N,BI,IER)
C
C     DESCRIPTION OF PARAMETERS
C     X  -THE ARGUMENT OF THE I BESSEL FUNCTION DESIRED
C     N  -THE ORDER OF THE I BESSEL FUNCTION DESIRED
C     BI -THE RESULTANT I BESSEL FUNCTION
C     IER-RESULTANT ERROR CODE WHERE
C     IER=0 NO ERROR
C     IER=1 N IS NEGATIVE
C     IER=2 X IS NEGATIVE
C
C     REMARKS
C     N MUST BE GREATER THAN OR EQUAL TO ZERO
C     X SHOULD BE LESS THAN 60 TO AVOID EXCEEDING THE RANGE OF
C     THE MACHINE
C
C     SUBROUTINES AND FUNCTION SUBPROGRAMS REQUIRED
C     NONE
C
C     METHOD
C     COMPUTES ZERO ORDER AND FIRST ORDER BESSEL FUNCTIONS USING
C     SERIES APPROXIMATIONS AND THEN COMPUTES N-TH ORDER FUNCTION
C     USING RECURRENCE RELATION.
C
C     ..................................................................
C
      SUBROUTINEBESI(X,N,BI,IER)
C
C     CHECK FOR ERRORS IN N AND X AND EXIT IF ANY ARE PRESENT
C
      IER=0
      BI=1.0
      IF(N)150,15,10
10    IF(X)160,20,20
15    IF(X)160,17,20
17    RETURN
C
C     DEFINE TOLERANCE
C
20    TOL=1.E-6
C
C     IF ARGUMENT GT 12 AND GT N, USE ASYMPTOTIC FORM
```

(Continued)

Table B3 (Concluded)

```
C
      IF(X-12.)40,40,30
30    IF(X-FLOAT(N))40,40,110
C
C     COMPUTE FIRST TERM OF SERIES AND SET INITIAL VALUE OF THE SUM
C
40    XX=X/2.
      FACTN=1.
      IF(N-1)70,70,50
50    DO60I=2,N
      FI=I
60    FACTN=FACTN*FI
70    TERM=(XX**N)/FACTN
      BI=TERM
      XX=XX*XX
C
C     COMPUTE UP TO 30 TERMS, STOPPING WHEN ABS(TERM) LE ABS(SUM OF TERM
C     TIMES TOLERANCE
C
      DO90K=1,30
      IF(ABS(TERM)-ABS(BI*TOL))100,100,80
80    FK=K*(N+K)
      TERM=TERM*(XX/FK)
90    BI=BI+TERM
C
C     RETURN BI AS ANSWER
C
100   RETURN
C
C     X GT 12 AND X GT N, SO USE ASYMPTOTIC APPROXIMATION
C
110   FN=4*N*N
      XX=1./(8.*X)
      TERM=1.
      BI=1.
      DO130K=1,30
      IF(ABS(TERM)-ABS(TOL*BI))140,140,120
120   FK=(2*K-1)**2
      TERM=TERM*XX*(FK-FN)/FLOAT(K)
130   BI=BI+TERM
140   PI=3.141592653
      BI=BI*EXP(X)/SQRT(2.*PI*X)
      GOTO100
150   IER=1
      GOTO100
160   IER=2
      GOTO100
      END
```

Table B4

Listing of Subroutines

Subroutine Names	Function
DATIME*	Gives date and time of computer run
BANS*	Gives date, starting time of clock, central processor, job stack
BANE*	Gives clock time, computer storage, total INPUT-OUTPUT TIME, total central processor time
NDATA	Computes coupling coefficient (see fig. B5)
HAN2	Computes Hankle functions for each wave number at a given range (see fig. B6)
EBFF8	Conditions data for Fourier transform (see fig. B7)
EBJLF1	Computes average power, total power, root-mean-square amplitude, and A and B coefficients of predicted seismic signal (see fig. B8)
JLAMP3	Calculates phases of predicted signal (see fig. B9)
PEAK	Finds peak value of predicted signal and number of points that exceed selected threshold amplitudes (see fig. B10)
INTABL	Computes a table of factors used to compute A and B coefficients (see fig. B11)
FFT	Computes fast Fourier transform (see fig. B12)
RFFT	Computes real fast Fourier transform (see fig. B13)
SWTCH1	Determines which factor to use in Fourier analysis (see fig. B14)
FINDNO	Determines the number of data points to be analyzed (see fig. B15)
INRFFT	Computes inverse real fast Fourier transform (see fig. B16)
INVFFT	Computes inverse fast Fourier transform (see fig. B17)
DELEL	Computes multiplication of matrix BXC (see fig. B18)
IVERAA	Finds the inverse of matrix A (see fig. B19)
MATRAA	Formulates matrix A (see fig. B20)
MATRBB	Formulates matrix B (see fig. B21)
MATRCC	Formulates matrix C (see fig. B22)
MATRDD	Formulates matrix D (see fig. B23)
MULAAD	Computes multiplication of matrix AXD (see fig. B24)
NDELTA	Formulates a determinant (see fig. B25)
DETER	Solves a determinant (see fig. B26)
BESY	Computes the Y Bessel function (see fig. B27)
BESJ	Computes the J Bessel function (see fig. B28)
BESI	Computes the I Bessel function (see fig. B29)

* System routine.

APPENDIX C: RAYLEIGH WAVE DISPERSION CURVE PROGRAM

Function and Method

1. The Rayleigh wave dispersion curve program (CDSPER, and subroutines DISPER, FOLCV4, and SOLLR2) computes a theoretical dispersion curve (phase velocity versus frequency) for surface waves in a multilayered medium. It is written in FORTRAN IV and is implemented on a Honeywell G-437 time-sharing system.

2. The program computes the coordinates of 50 points along a characteristic Rayleigh wave dispersion curve whose shape and extent depend on the properties of a layered medium. For typical soil profiles, the lower and upper velocity limits of the fundamental mode are asymptotic to a velocity slightly less than the shear wave velocities of the shallowest and deepest layers of the medium, respectively. Higher order Rayleigh wave modes are generally asymptotic to the first-layer shear wave velocities only. The mathematical operations of the program are performed while incrementing the wave period; the output is converted to wave number versus frequency for use with the microseismic wave propagation model. The portion of the curve to be generated is specified to have a period within the region of 0.00133 to 0.6828 sec, or a frequency of 750 to 1.4648 Hz, respectively.

3. Referring to fig. C1, the program starts at a period T(1) with an estimated initial phase velocity C1 and increments phase velocity by DC until the curve is located (point A). The period is then incremented by DT , and 49 more points along the characteristic curve are located. An initial change in phase velocity CG must be given to find the new velocity at the second period; the program will compute this change thereafter. During each iteration, 20 attempts are made to generate the succeeding point on the curve. If the point is not located within specified limits of accuracy, the program will resign and await instructions for the next problem.

4. When this program has executed a problem successfully, the user

then uses its output as input to a spline curve-fitting program.[34*] This program is modified to generate 512 points of phase velocity versus frequency, with increments of frequency equal to 1.4648 Hz.

Input

5. The dispersion curve program is executed from a teletype. The description of the input is given in table C1, and a sample run is shown in fig. C2.

Output

6. An example of the output from program CDSPER is shown in fig. C2. The circled numbers (①-④) refer to the input record order given in table C1. The output file of phase velocity versus frequency, a portion of which is shown in table C2, is input to the spline curve-fitting program. The output file from the spline program is shown in table C3, and a plot of these points is shown in fig. C3.

Program Listing

7. A program listing of the dispersion curve program (CDSPER) is shown in table C4.

Flow Charts

8. Condensed flow charts of the Rayleigh wave dispersion program and the spline curve-fitting program are shown in figs. C4 and C5, respectively.

---

* Number refers to similarly numbered reference in Literature Cited at end of main text.

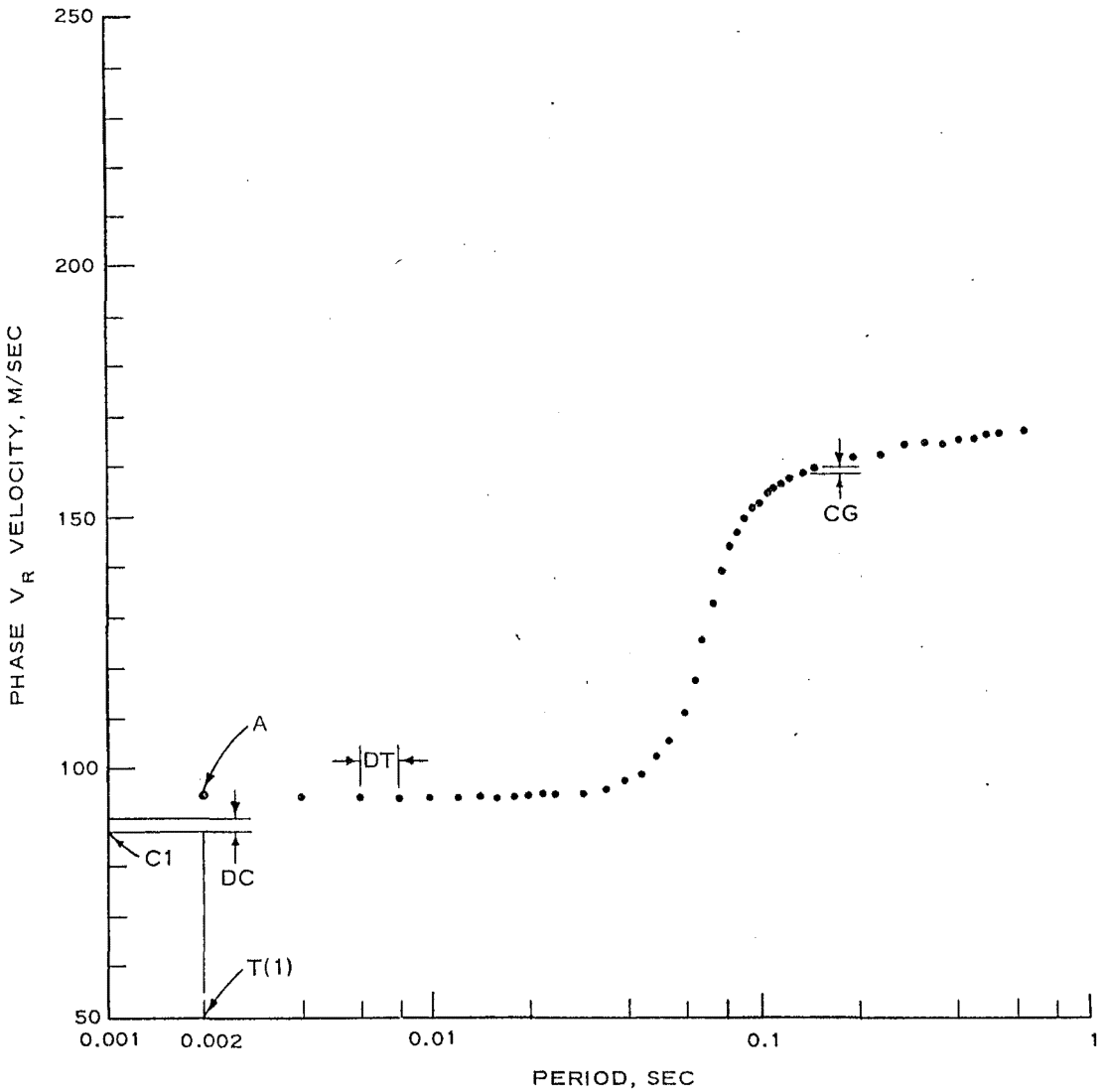

Fig. C1. Rayleigh wave phase velocity versus period for mode 1

```
READY
OLD:CDSPER

READY
RUN

CDSPER    08:55  WES  : 01/17/73.

NAME OF OBJ PROG ? CCSPER

MEDIA DATA


INPUT MODE & NO. OF LAYERS
 ? 1,2                                                    (1)

INPUT VP(1),VS(1),RH(1),H(1)
 ? 250.,100.,1.93,3.
                                                          (2)
INPUT VP(2),VS(2),RH(2)
 ? 450.,180.,2.

LAYER-1   VP:  250.  VS:  100.  RH: 1.930  H: 3.000
LAYER-2   VP:  450.  VS:  180.  RH: 2.000  H: 0.000


INPUT KK
 ? 1                                                      (3)

 INPUT FRQ,T(1),DT,C1,DC,CG
 ? 1000.,.002,.002,300.,3.,.001                           (4)


 KMAX=12
 T(1):       0.002000
 DT  :       0.002000
 C1  :     300.000000
 DC  :       3.000000
 CLB :     259.842520
 CUB :   10000.000000
 EPS :       0.00400000
 ESS :       0.00100000
 CG  :       0.00100000

      T              C            DELTA                  SLOPE
    0.002000     300.000        -.25253701E+58
    0.002000     303.000        -.48309645E+56
    0.002000     306.000        -.66952975E+54
    0.002000     309.000        -.16188621E+52
    0.002000     312.000        0.27036306E+51
 ENTER FOLCV4
    0.004000     309.645
    0.006000     309.030
    0.008000     309.643
    0.010000     309.030
    0.012000     309.645
    0.014000     309.349
    0.016000     309.379
    0.018000     309.456
    0.020000     309.587
    0.022000     309.805
    0.024000     310.129
 LEAVE FOLCV4
STOP? 1-YES 2-NO
 ? 2

   THICKNESS      ALPHA        BETA        RHO

     9.84252   820.20997   328.08399   120.48945
     0.00000  1476.37795   590.55118   124.85953

                  RAYLEIGH MODE  1

     PERIOD     PH VEL
    0.00200     309.644
    0.00400     309.337
    0.00600     309.337
    0.00800     309.337
    0.01000     309.337
    0.01200     309.340
    0.01400     309.351
    0.01600     309.383
    0.01800     309.454
    0.02000     309.586
    0.02200     309.803
    0.02400     310.128
DO YOU WANT TO TERMINATE? 1-YES 2-NO
 ? 1

INPUT C(1,1)
 ? 309.337

INPUT KK
 ? 2

 INPUT FRQ,T(1),DT,C1,DC,CG
 ? 1000.,.024,.005,310.,1.,2.


      T              C            DELTA                  SLOPE
    0.024000     310.000        -.27068453E+01
    0.024000     311.000        0.17365580E+02
 ENTER FOLCV4
    0.029000     312.135
    0.034000     313.012
    0.039000     318.093
    0.044000     324.771
    0.049000     333.880
    0.054000     346.409
    0.059000     363.344
    0.064000     385.207
    0.069000     410.833
    0.074000     435.360
    0.079000     453.518
    0.084000     468.431
    0.089000     482.851
    0.094000     492.252
    0.099000     497.344
    0.104000     501.236
    0.109000     504.676
    0.114000     507.623
    0.119000     510.107
    0.124000     512.225
    0.129000     514.052
    0.134000     515.661
    0.139000     517.094
    0.144000     518.386
    0.149000     519.563
    0.154000     520.644
 LEAVE FOLCV4
STOP? 1-YES 2-NO
 ? 2

   THICKNESS      ALPHA        BETA        RHO

     9.84252   820.20997   328.08399   120.48945
     0.00000  1476.37795   590.55118   124.85953

                  RAYLEIGH MODE  1

     PERIOD     PH VEL
    0.02400     310.135
    0.02900     311.573
    0.03400     314.226
    0.03900     318.492
    0.04400     324.854
    0.04900     333.918
    0.05400     346.443
    0.05900     363.247
    0.06400     384.722
    0.06900     409.681
    0.07400     434.581
    0.07900     455.558
    0.08400     471.261
    0.08900     482.501
    0.09400     490.591
    0.09900     496.576
    0.10400     501.155
    0.10900     504.772
    0.11400     507.715
    0.11900     510.169
    0.12400     512.260
    0.12900     514.075
    0.13400     515.674
    0.13900     517.102
    0.14400     518.391
    0.14900     519.567
    0.15400     520.646
DO YOU WANT TO TERMINATE? 1-YES 2-NO
 ? 1

INPUT KK
 ? 3

 INPUT FRQ,T(1),DT,C1,DC,CG
 ? 1000.,.154,.045,520.,1.,5.


      T              C            DELTA                  SLOPE
    0.154000     520.000        -.90007173E-03
    0.154000     521.000        0.49767527E-03
 ENTER FOLCV4
    0.199000     525.644
    0.244000     534.826
    0.289000     534.425
    0.334000     538.961
    0.379000     539.680
    0.424000     541.707
    0.469000     543.126
    0.514000     544.284
    0.559000     545.236
    0.604000     546.069
 LEAVE FOLCV4
STOP? 1-YES 2-NO
 ? 2

   THICKNESS      ALPHA        BETA        RHO

     9.84252   820.20997   328.08399   120.48945
     0.00000  1476.37795   590.55118   124.85953

                  RAYLEIGH MODE  1

     PERIOD     PH VEL
    0.15400     520.644
    0.19900     527.735
    0.24400     532.329
    0.28900     535.659
    0.33400     538.203
    0.37900     540.211
    0.42400     541.834
    0.46900     543.175
    0.51400     544.299
    0.55900     545.254
    0.60400     546.075
DO YOU WANT TO TERMINATE? 1-YES 2-NO
 ? 1

INPUT C(1,KLAST)
 ? 547.000

TYPE OUTPUT FILE NAME
 ? DDSPFB


STOP       2

RUNNING TIME:   19.8 SECS   I/O TIME :   19.0 SECS
```

Fig. C2. Sample run of the dispersion curve program (CDSPER)

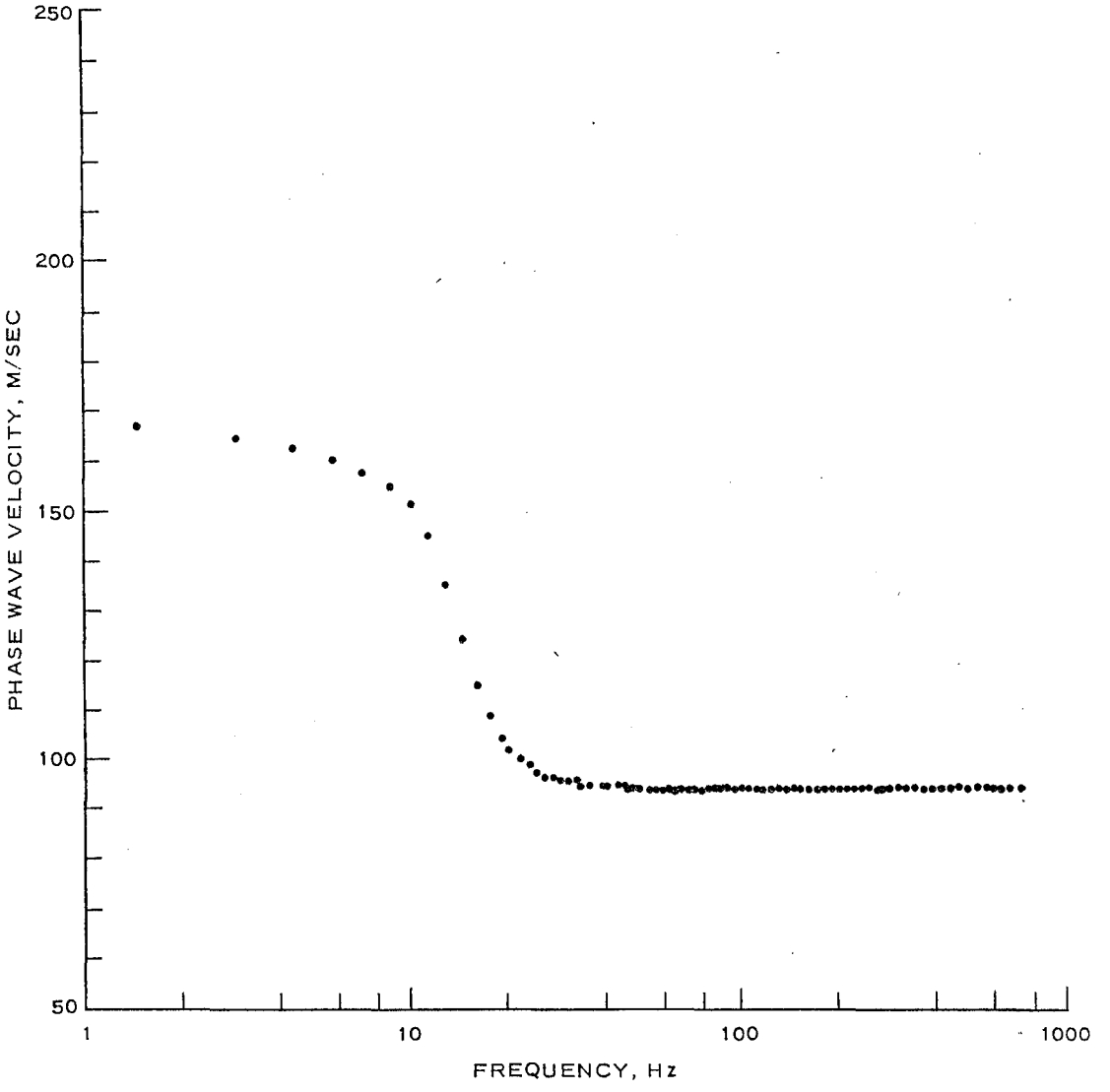

Fig. C3. Rayleigh wave phase velocity versus frequency

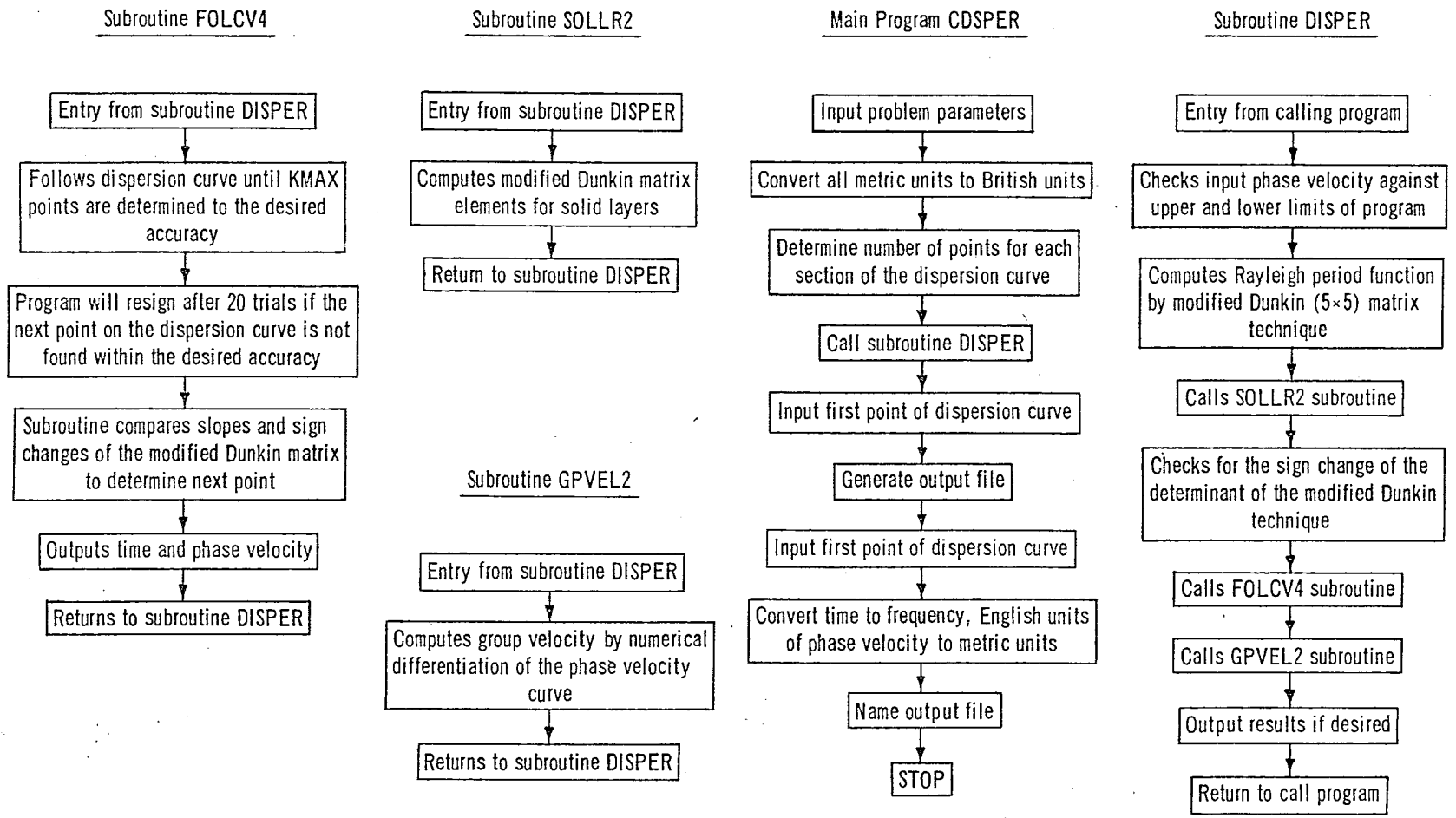

Fig. C4. Condensed flow chart of Rayleigh wave dispersion program

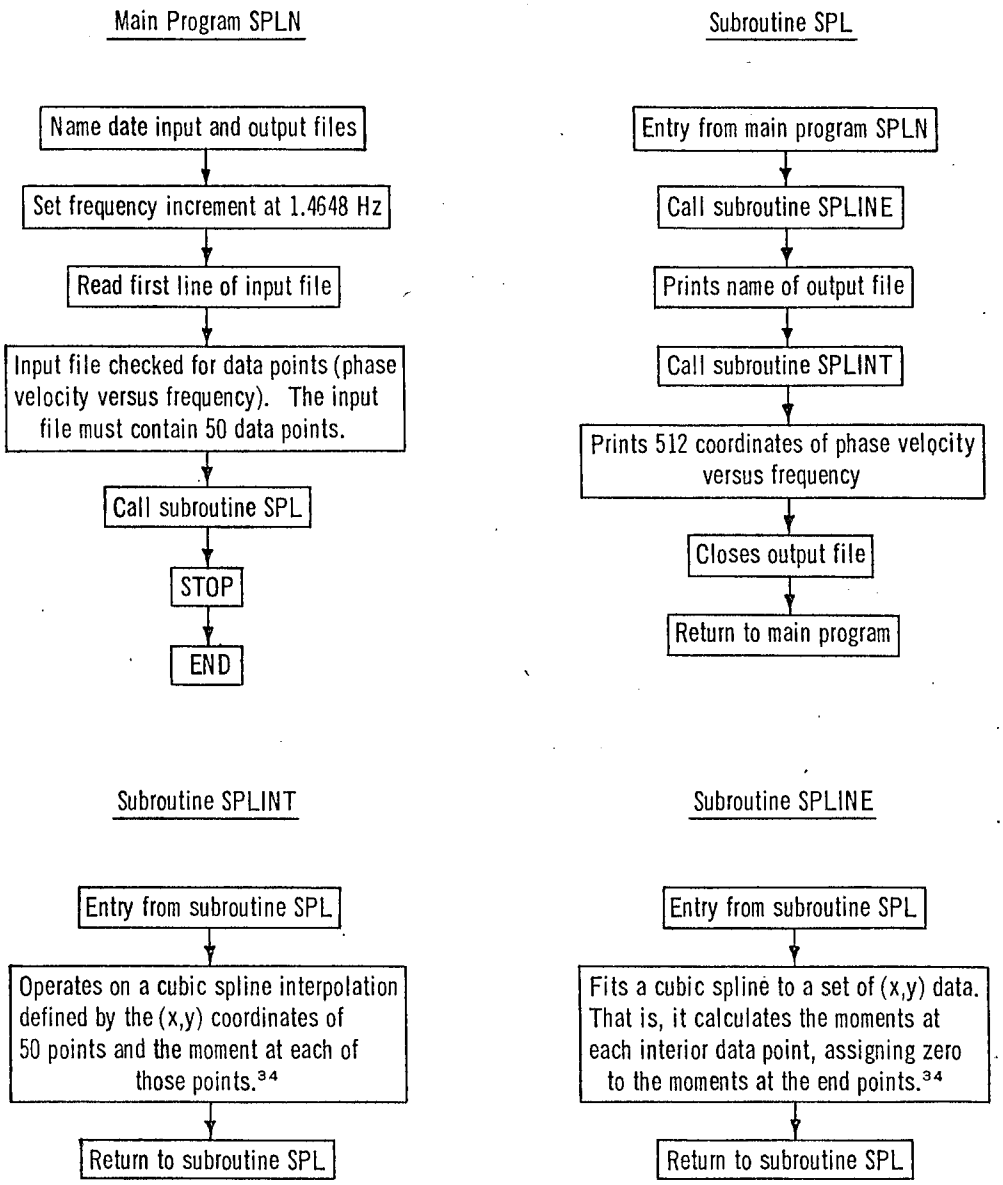

Fig. C5. Condensed flow chart of spline curve-fitting program

Table C1

Rayleigh Wave Dispersion Curve Program Input Variables (from Teletype)

Input Record	Variable Name	Column(s)	Mode	Units	Description
1	MODENO	Free field	Fixed	Count	Mode number
	MMAX	Free field	Fixed	Count	Number of layers
2*	VP	Free field	Floating	m/sec	Compression wave velocity
	VS	Free field	Floating	m/sec	Shear wave velocity
	RH	Free field	Floating	g/cm^3	Density
	H	Free field	Floating	m	Thickness of each soil layer
3	KK	Free field	Floating	Code	Code for number of values to be generated 1-12 2-27 3-11
4	FREQ	Free field	Floating	Hz	Upper frequency boundary
	T(1)	Free field	Floating	sec	Period length
	DT	Free field	Floating	ft/sec	Step size on initial Rayleigh wave velocity
	CI	Free field	Floating	ft/sec	Initial estimated Rayleigh wave velocity
	DC	Free field	Floating	ft/sec	Step size on initial Rayleigh wave velocity
	CG	Free field	Floating	ft/sec	Estimated change in initial Rayleigh wave velocity and the second value

* This input line is repeated MMAX times.

Table C2

Dispersion Curve (CDSPER) Output File (DDSPFB)

(Phase Velocity, m/sec, Versus Frequency, Hz)

Line Number	Frequency	Phase Velocity	Frequency	Phase Velocity	Frequency	Phase Velocity
00002	750.0000	94.2859	250.0000	94.2859	166.6667	94.2858
00003	125.0000	94.2858	100.0000	94.2859	83.3333	94.2867
00004	71.4286	94.2900	62.5000	94.2999	55.5556	94.3216
00005	50.0000	94.3618	45.4545	94.4278	41.6667	94.5269
00006	41.6667	94.5291	34.4828	94.9675	29.4118	95.7760
00007	25.6410	97.0763	22.7273	99.0156	20.4082	101.7782
00008	18.5185	105.5958	16.9492	110.7177	15.6250	117.2633
00009	14.4928	124.8709	13.5135	132.4602	12.6582	138.8539
00010	11.9048	143.6403	11.2360	147.0664	10.6383	149.5321
00011	10.1010	151.3564	9.6154	152.7519	9.1743	153.8546
00012	8.7719	154.7515	8.4034	155.4995	8.0645	156.1369
00013	7.7519	156.6900	7.4627	157.1775	7.1942	157.6127
00014	6.9444	158.0057	6.7114	158.3639	6.4935	158.6930
00015	6.4935	158.6923	5.0251	160.8537	4.0984	162.2538
00016	3.4602	163.2689	2.9940	164.0443	2.6385	164.6563
00017	2.3585	165.1511	2.1322	165.5597	1.9455	165.9022
00018	1.7889	166.1933	1.4648	166.7256		

Table C3

Partial Listing of Rayleigh Wave Dispersion Curve

(Output from Spline Curve-Fitting Program)

Line Number	File ID	Frequency Hz	Phase Velocity, m/sec
00001	DSPLFB		
00002		1.465	166.726
00003		2.930	164.154
00004		4.394	161.828
00005		5.859	159.275
00006		7.324	157.402
00007		8.789	154.715
00008		10.254	150.870
00009		11.719	144.671
00010		13.184	135.007
00011		14.648	123.726
00012		16.113	114.563
00013		17.578	108.381
00014		19.043	104.333
00015		20.508	101.625
00016		21.973	99.752
00017		23.437	98.426
00018		24.902	97.461
00019		26.367	96.748
00020		27.832	96.209
00021		29.297	95.803
00022		30.762	95.491
00023		32.227	95.249
00024		33.691	95.057
00025		35.156	94.897
00026		36.621	94.759
00027		38.086	94.650
00028		39.551	94.573
00029		41.016	94.533
00030		42.480	94.519
00040		57.129	94.314
00050		71.777	94.290
00100		145.019	94.286
00150		218.262	94.286
00200		291.504	94.286
00250		364.746	94.286
00300		437.988	94.286
00350		511.230	94.286
00400		584.473	94.286
00450		657.715	94.286
00500		730.957	94.286
00513		750.000	94.286

Table C4

Listing of Dispersion Curve Program (CDSPER)

CDSPER

```
100$NUM
110$LIB,COST,,,***
120$SAV
130$LIB,DISPER,F703
140 DIMENSION V(20,4),T(50),C(50,5),S(50,5),U(50),B(20,5),A(20,5,5)
150 DIMENSION VP(20),VS(20),RH(20),H(20)
160 COMMON M,MMAX,K,KMAX,DT,CS0
170 COMMONWVNO,C1,DELTA1,C2,DELTA2,C3
180 COMMON V,T,C,S
190 COMMON A,IA,U,KLAST,NTRLS,RHOC
200 COMMON CLB,CUB,EPS,ESS,CG,B
210 COMMON RSINP,SINPR,COSP,RSING,SINOK,COS0
220 COMMON DC,MODENO,IDNO
230 COMMON B1,AN,PR
240 CALL COST
250 KK=1
260 PRINT,"MEDIA DATA"
270 PRINT,$2
280 PRINT,"INPUT MODE & NO. OF LAYERS"
290 READ,MODENO,MMAX
300 H(MMAX)=0.0
310 AKP=0.4
320 PI=3.1416
330C  SOLVE FOR FREQ. AT THIS LINE NO.
340 PF3=1./0.016018
350 FPM=1./0.3048
360 IA=0
370 R=2.
380 DO 20 I=1,MMAX
390 IF(I.EQ.MMAX) PRINT 201,I,I,I
400 IF(I.EQ.MMAX) READ,VP(I),VS(I),RH(I)
410 IF(I.EQ.MMAX) GO TO 200
420 PRINT 200,I,I,I,I
425 READ,VP(I),VS(I),RH(I),H(I)
430 200FORMAT(5HINPUT,1X,"VP(",I1,"),VS(",I1,"),RH(",I1,"),H(",I1,")")
440 201 FORMAT(5HINPUT,1X,"VP(",I1,"),VS(",I1,"),RH(",I1,")")
460 V(I,1)=H(I)*FPM
470 V(I,2)=VP(I)*FPM
480 V(I,3)=VS(I)*FPM
490 V(I,4)=RH(I)*PF3
500 20 CONTINUE
510 DO 30 I=1,MMAX
520 30 PRINT 202,I,VP(I),VS(I),RH(I),H(I)
530 202FORMAT(6HLAYER-,I1,3X,"VP=",F6.0,2X,"VS=",F6.0,2X,"RH=",F6.3,
540$ 2X,"H=",F6.3)
545 C1=VS(1)*FPM*0.8
550 CLB=C1*.99
560 CUB=10000.
570 EPS=0.004
580 PRINT,$2
```

(Continued)

Table C4 (Continued)

```
CDSPEW CONTINUED

590 INDO=1
600 ESS=0.001
610 WRITE(1,60)
620 60 FORMAT("    FREQ        IN VEL  ")
630 100 CONTINUE
640 PRINT,"INPUT KK"
650 READ,KK
660 IF(KK.EQ.2) KMAX=27
670 IF(KK.EQ.3) KMAX=11
680 IF(KK.EQ.1) KMAX=12
690 PRINT," INPUT FRQ,T(1),DT,C1,DC,CC"
700 READ, FRQ,T(1),DT,C1,DC,CC
710 CALL DISPFR
720 DO 50 K=1,KLAST
730 T(K)=1.0/T(K)
740 C(K,1)=C(K,1)/FPM
750 50 CONTINUE
760 PRINT,"DO YOU WANT TO TERMINATE? 1-YES 2-NO"
770 READ,ITEST
780 IF(ITEST-1) 112,112,100
790 112 IF(KK-2) 113,114,115
800 113 PRINT,"INPUT C(1,1)"
810 READ,C(1,1)
820 T(1)=750.
830 C(1,1)=C(1,1)/FPM
840 114 WRITE(1,70) (T(K),C(K,1),K=1,KLAST)
850 GO TO 100
860 70 FORMAT(1X,6F10.4)
870 115 PRINT,"INPUT C(1,KLAST)"
880 80 FORMAT(A6)
890 READ,C(11,1)
900 C(11,1)=C(11,1)/FPM
910 T(11)=1500./1024.
920 WRITE(1,70) (T(K),C(K,1),K=1,KLAST)
930 GO TO 110
940 110 PRINT,"TYPE OUTPUT FILE NAME"
950 READ 80, DFILE1
960 CALL CLOSEF(1,DFILE1)
970 CALL COST
980 STOP 2
990 END
```

(Continued)

Table C4 (Continued)

DISPER

```
10000 SUBROUTINE DISPER
10010C      H57V
10020C  PROGRAM TO COMPUTE THEORETICAL DISPERSION CURVES (C VS. T) FOR
10030C SURFACE WAVES IN MULTILAYERED MEDIA. INITIAL ROOT IS LOCATED.
10040C SUBROUTINE FOLCV4 THEN CALLED.
10050C
10060 DIMENSIONV(20,4),T(50),C(50,5),S(50,5),U(50),B(20,5),A(20,5,5)
10070 COMMONM,MMAX,K,KMAX,DT,CSQ
10080 COMMONWVNO,C1,DELTA1,C2,DELTA2,C3
10090 COMMONV,T,C,S
10100 COMMONA,IA,U,KLAST,NTRLS,RHOC
10110 COMMONCLB,CUB,EPS,ESS,CG,B
10120 COMMONRSINP,SINPR,COSP,RSINQ,SINQR,COSQ
10125 COMMON DC,MODENO,IDNO
10130 DO14K=1,4
10140 K1=K+1
10150 DO14L=K1,5
10160 S(K,L)=0.0
10170 14C(K,L)=0.0
10180C
10310 MAX=MMAX
10320 C1B=C1
10330 DO13K=2,KMAX
10340 13T(K)=T(K-1)+DT
10350 MODE=MODENO-1
10370 IF(KMAX.NE.12) GO TO 320
10380 PRINT320,KMAX,T(1),DT,C1,DC,CLB,CUB,EPS,ESS,CG
10390 320FORMAT(6H0KMAX=I2/6H T(1)=F14.6/6H DT  =F14.6/6H C1  =F14.6/6H D
10400& =F14.6/6H CLB =F14.6/6H CUB =F14.6/6H EPS =F16.8/6H ESS =F16.8/
10410&6H CG  =F16.8)
10420 IF(EPS)338,336,338
10430 336PRINT337
10440 337FORMAT(58H0 AN ERROR WAS MADE IN SPECIFYING MORE ON THE CONTROL
10450&RD)
10460 STOP10460
10470 338CONTINUE
10480C
10490C  INITIAL ROOT SEARCH
10500 IF(C1-CLB)330,330,331
10510 330PRINT332
10520 332FORMAT(21H0 C1 IS LESS THAN CLB)
10530 GOTO99
10540 331IF(C1-CUB)335,333,333
10550 333PRINT334
10560 334FORMAT(24H0 C1 IS GREATER THAN CUB)
10570 GOTO99
10580 335CONTINUE
10590 PRINT306
10600 306FORMAT(59H0        T                C            DELTA
10610&OPE)
```

(Continued)

Table C4 (Continued)

DISPER CONTINUED

```
10620 K=1
10630 400DELTA1=DLTAR3(C1,T(1))
10640 202PRINT108,T(1),C1,DELTA1
10650 108FORMAT(1H F13.6,2X,F9.3,2X,E19.8)
10660 GOTO80
10670 81C1=C2
10680 DELTA1=DELTA2
10690 80C2=C1+DC
10700 IF(C2-CUB)312,310,310
10710 310PRINT311
10720 311FORMAT(40H PHASE VELOCITY GREATER THAN UPPER BOUND)
10730 C1=C1B
10740 DC=-DC
10750 GOTO400
10760 312IF(C2-CLB)313,313,82
10770 313PRINT314
10780 314FORMAT(37H PHASE VELOCITY LESS THAN LOWER BOUND)
10790 GOTO99
10800 82DELTA2=DLTAR3(C2,T(1))
10810 205PRINT108,T(K),C2,DELTA2
10820 IF(ABS(DELTA2-DELTA1)-ABS(DELTA2+DELTA1))81,81,110
10830 110IF(MODE)113,113,111
10840 111MODE=MODE-1
10850 GOTO81
10860C
10870C  ENTER ROOT FOLLOWING SUBROUTINE
10880 113CALLFOLCV4
10882 PRINT,"STOP? 1-YES 2-NO"
10884 READ,K15
10886 IF(K15.EQ.1) GO TO 99
10890 IF(KLAST-5)39,40,40
10900 39IF(KLAST)99,99,41
10910 41DO42K=1,KLAST
10920 42U(K)=0.0
10930 GOTO90
10940C
10950C  CALL GROUP VELOCITY SUBROUTINE
10960 40CALLGPVEL2
10970 90PRINT91,((V(M,N),N=1,4),M=1,MAX)
10980 91FORMAT(45H1  THICKNESS       ALPHA        BETA         RHO//(1H 4F2
10990&5))
11000 206PRINT92,MODENO
11010 92FORMAT(//,20X,13HRAYLEIGH MODE,I3,//,5X,6HPERIOD,5X,6HPH VEL)
11030 DO95K=1,KLAST
11040 AMDA1=T(K)*C(K,1)
11050 AMDA2=1(K)*U(K)
11060 95PRINT96,T(K),C(K,1)
11070 96FORMAT(F11.5,F11.3)
11080 99 RETURN
11100 END
```

(Continued)

Table C4 (Continued)

DISPER CONTINUED

```
11110 SUBROUTINEFOLCV4
11120C
11130C  DISPERSION CURVE IS FOLLOWED UNTIL KMAX POINTS ARE DETERMINED TO
11140C THE ACCURACY DESIRED. IF 20 TRIALS ARE INSUFFICIENT TO LOCATE A
11150C PARTICULAR POINT, PROGRAM EXITS FOLCV4.
11160C
11170 DIMENSIONV(20,4),T(50),C(50,5),S(50,5),U(50),R(20,5),A(20,5,5)
11180 COMMONM,MMAX,K,KMAX,DT,CSQ
11190 COMMONWVNO,C1,DELTA1,C2,DELTA2,C3
11200 COMMONV,T,C,S
11210 COMMONA,IA,U,KLAST,NTRLS,RHOC
11220 COMMONCLB,CUB,EPS,ESS,CG,B
11230 COMMONRSINP,SINPR,COSP,RSINQ,SINQR,COSQ
11240 PRINT401
11250 401FORMAT(13H ENTER FOLCV4)
11260 AESS=ESS
11270 K=1
11280 T1=T(K)
11290 400SLOPE=(DELTA2-DELTA1)/(C2-C1)
11300 NTRLS=0
11310 403IF(C2-C1)404,1,1
11320 404DELTAX=DELTA1
11330 CX=C1
11340 DELTA1=DELTA2
11350 C1=C2
11360 DELTA2=DELTAX
11370 C2=CX
11380C      INTERPOLATE,RETAINING DELTA1 AND DELTA2 WITH OPPOSITE SIGNS.
11390 1C3=C2-DELTA2/SLOPE
11400 IF(ABS(C1-C2)-EPS*((C1+C2)/2.0))30,30,32
11410 32IF(NTRLS-20)62,300,300
11420 62IF(ABS(C3-0.5*(C1+C2))-0.49*ABS(C1-C2))42,42,45
11430 45IF(C3-0.5*(C1+C2))145,145,146
11440 145C3=0.9*C1+0.1*C2
11450 GOTO42
11460 146C3=0.9*C2+0.1*C1
11470C      DELTA3
11480 42DELTA3=DLTAR3(C3,T1)
11490 35NTRLS=NTRLS+1
11500 IF(DELTA3)36,30,36
11510C      ARANGE
11520 36IF(SIGN(1.0,DELTA3)-SIGN(1.0,DELTA2))38,37,38
11530 37DELTA2=DELTA3
11540 C2=C3
11550 DELTAX=DELTA2
11560 CX=C2
11570 GOTO39
11580 38DELTA1=DELTA3
11590 C1=C3
11600 DELTAX=DELTA1
```

(Continued)

Table C4 (Continued)

```
DISPER CONTINUED


11610 CX=C1
11620 39SLOPE=(DELTA1-DELTA2)/(C1-C2)
11630XPRINT 103,T1,CX,DELTAX,SLOPE
11640 GOTO1
11650 30C(K,1)=C3
11660C  ROOT NO. K DETERMINED
11670C
11680 GOTO56
11690 300PRINT301
11700 301FORMAT(25H RESIGNED AFTER 20 TRIALS)
11710 58K=K-1
11720 GOTO54
11730 56S(K,1)=SLOPE
11740 50IF(K-1)51,52,51
11750 51L1=AMIN0(K,5)
11760 DO53L=2,L1
11770 C(K,L)=C(K,L-1)-C(K-1,L-1)
11780 53S(K,L)=S(K,L-1)-S(K-1,L-1)
11790 IF(K-KMAX)52,54,54
11800C      OBTAIN DELTA1 AND DELTA2 WITH OPPOSITE SIGNS.
11810 52K=K+1
11820 IF(IA)505,505,705
11830C
11840C  LAYER DROP IN EFFECT IF IA IS POSITIVE AND DT IS NEGATIVE
11850 705IF(MMAX-1)505,505,707
11860 707DEPTH=0.0
11870 MMAX2=MMAX-1
11880 500IF(DT)502,505,505
11890 502DO503I=1,MMAX2
11900 503DEPTH=DEPTH+V(I,1)
11910 X=DEPTH/(T1*C3)
11920 IF(X-3.0)505,505,504
11930 504MMAX=MMAX-1
11940 710PRINT510,MMAX
11950 510FORMAT(47H0 NO. OF LAYERS REDUCED BY ONE. MMAX NOW EQUALS I3)
11960C
11970 505T1=T(K)
11980 NTRLS=0
11990 KK=0
12000 ESS=AESS
12010 C1=C(K-1,1)+C(K-1,2)+C(K-1,3)+C(K-1,4)+C(K-1,5)
12020 IF(K-2)21,20,21
12030 20C1=C1+CC
12040 21CONTINUE
12050C      DELTA1
12060 3DELTA1=DLTAR3(C1,T1)
12070 10NTRLS=NTRLS+1
12080 PRINT100,T1,C1
12090 100FORMAT(1H F13.6,2X,F9.3)
12100 4C2=C1+ESS*C1
```

(Continued)

Table C4 (Continued)

```
DISPER CONTINUED

12110C      DELTA2 AND SLOPE
12120  7DELTA2=DLTAR3(C2,T1)
12130  11NTRLS=NTRLS+1
12140  SLOPE2=(DELTA2-DELTA1)/(C2-C1)
12150XPRINT 103,T1,C2,DELTA2,SLOPE2
12160  103FORMAT(1H F13.6,F13.7,2E19.8)
12170  121F(SIGN(1.0,DELTA1)-SIGN(1.0,DELTA2))405,120,405
12180  405SLOPE=SLOPE2
12190  GOTO403
12200  120C3=C1-ESS*C1
12210C      DELTA3 AND SLOPE
12220  121DELTA3=DLTAR3(C3,T1)
12230  124NTRLS=NTRLS+1
12240  SLOPE3=(DELTA1-DELTA3)/(C1-C3)
12250XPRINT 103,T1,C3,DELTA3,SLOPE3
12260C      COMPARING DELTA1 AND DELTA3
12270  127IF(SIGN(1.0,DELTA1)-SIGN(1.0,DELTA3))406,130,406
12280  406SLOPE=SLOPE3
12290  C2=C3
12300  DELTA2=DELTA3
12310  GOTO403
12320C      COMPARING SLOPES
12330  130IF(SIGN(1.0,SLOPE2)-SIGN(1.0,SLOPE3))131,132,131
12340  132SLOPE=0.5*(SLOPE2+SLOPE3)
12350  C2=C1-DELTA1/SLOPE
12360C      DELTA2
12370  133DELTA2=DLTAR3(C2,T1)
12380  135NTRLS=NTRLS+1
12390  SLOPE=(DELTA2-DELTA1)/(C2-C1)
12400XPRINT 103,T1,C2,DELTA2,SLOPE
12410  137IF(SIGN(1.0,DELTA1)-SIGN(1.0,DELTA2))403,139,403
12420  139C1=C2
12430  DELTA1=DELTA2
12440  IF(NTRLS-20)4,300,300
12450C      IFSLOPES ARE OPPOSITE,INCREASING ESS TENFOLD
12460  131IF(KK)160,161,160
12470  161KK=1
12480  ESS=ESS*10.0
12490  IF(NTRLS-20)162,300,300
12500  162GOTO4
12510  160C(K,1)=C1
12520  SLOPE=0.0
12530  GOTO56
12540  54KLAST=K
12550  PRINT402
12560  402FORMAT(13H LEAVE FOLCV4)
12570  RETURN
12580  END
12590  SUBROUTINEGPVEL2
12600C
```

(Continued)

DISPER CONTINUED

```
12610C  COMPUTES GROUP VELOCITY BY NUMERICAL DIFFERENTIATION OF THE PHAS
12620C VELOCITY CURVE.
12630C
12640 DIMENSIONV(20,4),T(50),C(50,5),S(50,5),U(50),B(20,5),A(20,5,5)
12650 COMMONM,MMAX,K,KMAX,DT,CSQ
12660 COMMONWVNO,C1,DELTA1,C2,DELTA2,C3
12670 COMMONV,T,C,S
12680 COMMONA,IA,U,KLAST,NTRLS,RHOC
12690 COMMONCLB,CUB,EPS,ESS,CG,B
12700 DO5020K=1,2
12710 DCDT=(C(K+1,2)-C(K+2,3)/2.0+C(K+3,4)/3.0-C(K+4,5)/4.0)/DT
12720 5020U(K)=C(K,1)/(1.0+(T(K)/C(K,1))*DCDT)
12730 K2=KLAST-2
12740 DO5030K=3,K2
12750 DCDT=((C(K,2)+C(K+1,2)-(C(K+1,4)+C(K+2,4))/6.0)/(2.0*DT)
12760 5030U(K)=C(K,1)/(1.0+(T(K)/C(K,1))*DCDT)
12770 K3=KLAST-1
12780 DO5040K=K3,KLAST
12790 DCDT=(C(K,2)+C(K,3)/2.0+C(K,4)/3.0+C(K,5)/4.0)/DT
12800 5040U(K)=C(K,1)/(1.0+(T(K)/C(K,1))*DCDT)
12810 RETURN
12820 END
12830 FUNCTIONDLTAR3(WVEL,PER)
12840C
12850C  COMPUTES RAYLEIGH PERIOD FUNCTION BY MODIFIED DUNKIN (5*5) MATRX
12860C   TECHNIQUE
12870C
12880 DIMENSIONV(20,4),T(50),C(50,5),S(50,5),U(50),B(20,5),A(20,5,5)
12890 COMMONM,MMAX,K,KMAX,DT,CSQ
12900 COMMONWVNO,C1,DELTA1,C2,DELTA2,C3
12910 COMMONV,T,C,S
12920 COMMONA,IA,U,KLAST,NTRLS,RHOC
12930 COMMONCLB,CUB,EPS,ESS,CG,B
12940 COMMONRSINP,SINPR,COSP,RSINQ,SINQR,COSQ
12950 99WVNO=.628318531E+21/(WVEL*PER)
12960 CSQ=WVEL**2
12970 M=1
12980C
12990C  TRIG(OR HYP) ARGUMENTS
13000 100ARGA=1.-CSQ/V(M,2)**2
13010 RA1=SQRT(ABS(ARGA))
13020 IF(ARGA)202,202,201
13030 201RA1=-RA1
13040 202IF(V(M,3))101,103,101
13050 101ARGB=1.-CSQ/V(M,3)**2
13060 RB1=SQRT(ABS(ARGB))
13070 IF(ARGB)204,204,203
13080 203RB1=-RB1
13090C
13100C  CALL MATRIX SUBROUTINE
```

(Continued)

Table C4 (Continued)

```
DISPER CONTINUED

13110 204CALLSOLLR2(RA1,RB1)
13120 102M=M+1
13130 IF(MMAX-M)104,100,100
13140C
13150C  LIQUID SURFACE LAYER
13160 103RB1=0.0
13170 IF(M-1)20,20,30
13180 20DO25I=1,5
13190 DO25J=1,5
13200 25A(1,I,J)=0.0
13210 PM=WVNO*RA1*V(M,1)
13220 RHOC=V(M,4)*CSQ
13230 IF(RA1)213,213,214
13240 213SINPR=(EXP(PM)-EXP(-PM))/(2.0*RA1)
13250 COSP=0.5*(EXP(PM)+EXP(-PM))
13260 GOTO215
13270 214SINPR=SIN(PM)/RA1
13280 COSP=COS(PM)
13290 215A(1,1,1)=COSP
13300 A(1,2,1)=RHOC*SINPR
13310 GOTO102
13320 30PRINT40
13330 40FORMAT(20H ILLEGAL LAYER SPECS)
13340 CALLEXIT
13350C
13360C  MATRIX MULTIPLICATION
13370C  EFFECT OF IMAGINARY ELEMENTS INCLUDED
13380 104DO108M=1,MMAX
13390 DO108I=1,5
13400 108B(M,I)=0.0
13410 DO110I=1,5
13420 110B(1,I)=A(1,I,1)
13430 M=2
13440 120DO90I=1,5
13450 DO90N=1,5
13460 IF(MMAX-M)200,200,210
13470 200IF(I-1)210,210,400
13480 210PRDT=A(M,I,N)*B(M-1,N)
13490 90B(M,I)=B(M,I)+PRDT
13500 M=M+1
13510 IF(MMAX-M)400,120,120
13520 400DLTAR3=B(MMAX,1)
13530 155RETURN
13540 END
13550 SUBROUTINESOLLR2(RA,RB)
13560C
13570C  COMPUTES MODIFIED DUNKIN MATRIX ELEMENTS FOR SOLID LAYERS
13580C
13590 DIMENSIONV(20,4),T(50),C(50,5),S(50,5),U(50),B(20,5),A(20,5,5)
13600 COMMONM,MMAX,K,KMAX,DT,CSQ
```

(Continued)

Table C4 (Continued)

```
DISPEP CONTINUED

13610  COMMONWVNO,C1,DELTA1,C2,DELTA2,C3
13620  COMMONV,T,C,S
13630  COMMONA,IA,U,KLAST,NTRLS,RHOC
13640  COMMONCLB,CUB,EPS,ESS,CG,B
13650  COMMONRSINP,SINPR,COSP,RSINQ,SINQR,COSQ
13660  G=2.*(V(M,3)**2/CSQ)
13670  G1=G-1.0
13680  IF(MMAX-M)40,52,40
13690  40RHOC=V(M,4)*CSQ
13700  PM=WVNO*RA*V(M,1)
13710  QM=WVNO*RB*V(M,1)
13720  IF(RA)213,218,214
13730  213RSINP=-RA*(.5)*(EXP(PM)-EXP(-PM))
13740  SINPR=-RSINP/(RA**2)
13750  COSP=.5*(EXP(PM)+EXP(-PM))
13760  GOTO215
13770  214RSINP=RA*SIN(PM)
13780  SINPR=RSINP/(RA**2)
13790  COSP=COS(PM)
13800  215IF(RB)216,218,217
13810  216RSINQ=-RB*(.5)*(EXP(QM)-EXP(-QM))
13820  SINQR=-RSINQ/(RB**2)
13830  COSQ=.5*(EXP(QM)+EXP(-QM))
13840  GOTO218
13850  217RSINQ=RB*SIN(QM)
13860  SINQR=RSINQ/(RB**2)
13870  COSQ=COS(QM)
13880  218RR=RSINP*RSINQ
13890  SS=SINPR*SINQR
13900  CC=COSP*COSQ
13910  A(M,1,1)=-2.*G*G1+(2.*G**2-2.*G+1.)*CC-G**2*RR-G1**2*SS
13920  A(M,2,1)=RHOC*(G1**2*SINPR*COSQ+G**2*RSINQ*COSP)
13930  A(M,3,1)=RHOC*(G*G1*(2.*G-1.)*(1.-CC)+G1**3*SS+G**3*RR)
13940  A(M,4,1)=-RHOC*(G**2*RSINP*COSQ+G1**2*SINQR*COSP)
13950  A(M,5,1)=RHOC**2*((2.*G**2*G1**2)*(1.-CC)+G1**4*SS+G**4*RR)
13960  IF(M-1)50,50,20
13970  20A(M,1,2)=-(1./RHOC)*(RSINP*COSQ+SINQR*COSP)
13980  A(M,1,3)=-(2./RHOC)*((2.*G-1.)*(1.-CC)+G1*SS+G*RR)
13990  A(M,1,4)=(1.0/RHOC)*(SINPR*COSQ+RSINQ*COSP)
14000  A(M,1,5)=(RHOC**(-2))*(2.*(1.-CC)+RR+SS)
14010  A(M,2,2)=CC
14020  A(M,2,3)=2.0*(G*RSINQ*COSP+G1*SINPR*COSQ)
14030  A(M,2,4)=SINPR*RSINQ
14040  A(M,3,2)=G1*SINQR*COSP+G*RSINP*COSQ
14050  A(M,3,3)=1.0+2.0*(2.*G*G1*(1.-CC)+G**2*RR+G1**2*SS)
14060  A(M,4,2)=RSINP*SINQR
14070  A(M,2,5)=-A(M,1,4)
14080  A(M,3,4)=A(M,2,3)*(-.5)
14090  A(M,3,5)=A(M,1,3)*0.5
14100  A(M,4,3)=A(M,3,2)*(-2.)
```

(Continued)

Table C4 (Concluded)

DISPER CONTINUED

```
14110 A(M,4,4)=A(M,2,2)
14120 A(M,4,5)=-A(M,1,2)
14130 A(M,5,2)=-A(M,4,1)
14140 A(M,5,3)=A(M,3,1)*2.0
14150 A(M,5,4)=-A(M,2,1)
14160 A(M,5,5)=A(M,1,1)
14170 50RETURN
14180 52A(M,1,1)=-2.*(V(M,3)/V(M,2))**2+(CSQ*G1**2)/(V(M,2)**2*G*RA*RB)
14190 A(M,1,2)=-(V(M,4)*V(M,2)**2*G*RB)**(-1)
14200 A(M,1,3)=-(V(M,4)*V(M,2)**2)**(-1)+G1/(V(M,4)*V(M,2)**2*G*RA*
14210*RB)
14220 A(M,1,3)=2.0*A(M,1,3)
14230 A(M,1,4)=(V(M,4)*V(M,2)**2*G*RA)**(-1)
14240 A(M,1,5)=((V(M,4)*V(M,2))**2*CSQ*G)**(-1)*(1.-(RA*RB)**(-1))
14250 GOTO50
14260 END
```

Unclassified
Security Classification

DOCUMENT CONTROL DATA - R & D

(Security classification of title, body of abstract and indexing annotation must be entered when the overall report is classified)

1. ORIGINATING ACTIVITY *(Corporate author)*
U. S. Army Engineer Waterways Experiment Station
Vicksburg, Miss.

2a. REPORT SECURITY CLASSIFICATION
Unclassified

2b. GROUP

3. REPORT TITLE

A MATHEMATICAL MODEL FOR PREDICTING MICROSEISMIC SIGNALS IN TERRAIN MATERIALS

4. DESCRIPTIVE NOTES *(Type of report and inclusive dates)*
Final report

5. AUTHOR(S) *(First name, middle initial, last name)*

Jerry R. Lundien
Hans Nikodem

6. REPORT DATE	7a. TOTAL NO. OF PAGES	7b. NO. OF REFS
June 1973	220	34

8a. CONTRACT OR GRANT NO.	9a. ORIGINATOR'S REPORT NUMBER(S)
b. PROJECT NO. 1T162112A131	Technical Report M-73-4
c. Task TM 700A-71-030	9b. OTHER REPORT NO(S) *(Any other numbers that may be assigned this report)*
d.	

10. DISTRIBUTION STATEMENT

Approved for public release; distribution unlimited.

11. SUPPLEMENTARY NOTES	12. SPONSORING MILITARY ACTIVITY
	Defense Special Projects Group and U. S. Army Materiel Command

13. ABSTRACT

The mathematical model presented herein allows the user to make predictions for the wave amplitude and frequency content of microseismic signals that would interact with a seismic intrusion detection device at the surface of the ground. These signals are propagated as a result of a force applied to the surface of a medium (stress) which in turn causes a corresponding motion to travel away from the source. Efforts were made to keep the operation of the model as general as possible such that little restriction is placed on either the source of the seismic signal or the ground media through which the signal propagates. As a result, the source signal is needed in the form of a time domain stress signal at the points of contact on the ground. The ground media can have any seismic profile that can be approximated by a layered viscoelastic structure. Examples are given of two sites to illustrate the variation in predicted signals due to multiple mode Rayleigh wave propagation, varying damping factors, varying ranges from the source, and input stress signal shapes.

DD FORM 1 NOV 68 1473 REPLACES DD FORM 1473, 1 JAN 64, WHICH IS OBSOLETE FOR ARMY USE.

Unclassified
Security Classification

14 KEY WORDS	LINK A		LINK B		LINK C	
	ROLE	WT	ROLE	WT	ROLE	WT
Mathematical models						
Microseismic waves						
Seismic detection						
Terrain						